

DEMOCRATIC AND POPULAR REPUBLIC OF ALGERIA
MINISTRY OF HIGHER EDUCATION AND SCIENTIFIC RESEARCH
KASDI MERBAH UNIVERSITY OUARGLA



Applied Sciences Division
Process Engineering Department

PhD THESIS

Improving the electroanalytical performance of electrochemical sensors for the detection of organic pollutants.

Presented by

MESKHER Hicham

In partial fulfillment of the requirements for the degree of doctor of Environmental Process Engineering

Supervisory committee:

SELLOUM Djamel	Pr.	Univ. Ouargla	Head of The Jury
ACHI Fethi	Dr.	Univ. Ouargla	Supervisor
LERARI Djahida	Pr.	CRAPC. BOUSMAIL-Tipaza	Co-Supervisor
HENNI Abdalah	Pr.	Univ. Ouargla	Examiner
BELKHALFA Hakim	Dr.	PTAPC. Ouargla	Examiner
BACHA Oussama	Dr.	Univ. Ouargla	Examiner

29 November 2022

Dedication

إذا كان لبحثي قيمة فإن هناك كثيرين ممن شاركوني في ذلك
طريق البحث العلمي كان شاقا وصعبا ولكن هناك من كانوا عوناً وسندا
المكرمان والمحمولان على الأعناق،
إلى الوالدين الجليلين
إلى الشمعة التي تنير دربنا، إلى النجمة التي تزين سماءنا
إلى الشمس التي تدفئ أرواحنا، إلى الفجوة التي تطرب بالحب قلوبنا
إلى من بها أعلو، وعليها أرتكز، إلى القلب المعطاء
أمي الحبيبة
عن فضل أمي، لن تكفي جمل الشكر، وحتى لو بلغت ملء الأرض والسماء
حفظك هلالا لنا، وجعلك ذخرا لنا، وقلبا نابضا منه نستلهم طاقتنا
إلى والدي الذي علمني خط الصواب على السطور، واقامة الدين الذي فيه النجاة من الشرور
فلو كنت حيا يا أبي لامتلأ قلبك من السرور، لكنك اليوم بين القبور
رعاك الله يا أبي في لحدك بين القبور، وسقيت ماء صافيا من جنة رب غفور
لى من بذلوا جهدا في مساعدتي وكانوا خير سند لضعفي وافتقاري إلى إخواني وأخواني
إلى الأب الروحي فارس، والسند محمد والمشجع نصر الذين
إلى الطموحة حسنية، الحنونه نورة، إلى سعيدة القوية ووسام المتألقة
إلى روح جدتي، وكل من فارقتنا من أهلي
إلى حبيب قدم، ولا زال يقدم
أصدقائي وأهلي المبدلون الذين لكن لهم كل الاحترام، الذين يُشاركونني الفرح والحزن على الدوام
أساتذتي الكرام أصحاب الفكر المستنير
إلى كل هؤلاء: أهديكم خالصة مُحمدي العلمي، الذي أسأل الله تعالى أن يتقبله خالصا

Acknowledgements

First and foremost, I would like to thank my supervisors Dr. Achi Fethi and Prof. Lerari Djahida. Dr. Achi in particular has been a constant source of support and encouragement throughout my time during this journey and I am deeply indebted to him for his guidance, understanding, patience and boundless knowledge.

I would also like to acknowledge the support I received from the Laboratory of Growth and Characterization of New Semiconductors, in particular Prof. Zouaoui Ahmed for his time, support and help. In addition, my sincere thanks to Dr. Bekhalfa Hakim for opening the physicochemical analysis center's door (P.T.A.P.C. Ouargla). A special word of thanks also goes to all the engineers and technicians who have helped me during my stay at the P.T.A.P.C. Ouargla.

Regarding my stay at P.T.A.P.C. Ouargla, I owe a big thank you to Dr. Henni Abdalah for giving me the opportunity to get in touch and to use the facilities he offered. The experience and knowledge I gained during my internship there was invaluable and I will cherish the memories both inside and outside the lab. Many thanks also should be addressed to Dr. Selloum Djamel for his support and help from the beginning till the end of my PhD. I am glad to address enormous thanking to Dr. Bacha Oussama for his support and help during my studies and the facilities he offered during the process of our thesis submission. Also, this experience would not have been as enjoyable or as memorable without my good friends and colleagues Mena Sabah and Ragdi Teqwa by my side. It is rare in life to meet such a thoughtful and kind hearted persons and I am truly honored to be able to call them both close friends. I wish them every success in the future as I wish them to defend their theses in the nearest future Insha Allah.

Thanks also to all my friends and colleagues outside of the University, who made my time here so enjoyable. A special word of thanks goes to Prof. Sohmyung Ha and Dr. Martin Peacock for their support, efforts and generosity of their time in proof reading and for their advices. Many thanks for anything they offered.

To anyone got in touch with me and helped, I would like to thank any person for providing welcome distractions and friendship when needed.

Finally, and by no means least, I would like to thank my Mum and siblings for their constant love and support. I would also like to thank another family member who played a significant role in my life, my father, RIP.

Abstract: In the present thesis, the findings are presented and discussed on the formation, characterization, optimization and catalytic performance of the synthesized nanomaterials that can be used as novel electrochemical sensors to detect organic pollutants including catechol (CC), hydroquinone (HQ) and 5-chlorophenol (5-CP). Under optimal conditions (nanomaterials volume, pH and scan rate), the CC, HQ and 5-CP were detected at the modified electrodes in a 0.1 M phosphate buffer solution (PBS), giving well defined peaks of oxidation and reduction vs. the reference electrode (SCE). The monitoring of CC, HQ and 5-CP using the modified electrodes was optimized by varying a range of factors and conditions. Using these optimized parameters, a very low limits of detection and large linear ranges were obtained for each pollutant depending on the study (the nanomaterials, the matrixes prepared and the electrodes used). A wide variety of interfering compounds were also examined to establish their effect, if any, on the determination of CC, HQ and 5-CP at the modified electrodes. The interference from several major interfering compounds, such as dopamine, glucose, caffeine acid and ascorbic acid could be effectively blocked. To evaluate the applicability of the produced sensors, each sensor was used to determine CC, HQ and 5-CP in real samples including tap water and drinking water. A very interesting recoveries were obtained giving a good indication that the sensors prepared during this study are able to be used in real sample analysis. **Keywords:** Electrochemical sensor, nanomaterials, organic pollutants, electrochemical techniques, sensitivity, selectivity.

Résumé : Dans la présente thèse, les résultats sont présentés et discutés sur la formation, la caractérisation, l'optimisation et les performances catalytiques des nanomatériaux synthétisés qui peuvent être utilisés comme nouvelles matrices de capteurs électrochimiques pour détecter les polluants organiques, notamment le catéchol (CC), l'hydroquinone (HQ) et le 5- chlorophénol (5-CP). Dans des conditions optimales (volume de nanomatériaux, pH et vitesse de balayage), le CC, le HQ et le 5-CP ont été détectés au niveau des électrodes modifiées dans une solution tampon du phosphate (PBS) 0,1 M, donnant des pics d'oxydation et de réduction bien définis par rapport à l'électrode du référence (SCE). La détermination de CC, HQ et 5-CP à l'aide des électrodes modifiées a été optimisée en faisant varier une gamme de facteurs et de conditions. Grâce à ces paramètres optimisés, des limites de détection très basses et de larges plages linéaires a été obtenues pour chaque polluant en fonction de l'étude (les nanomatériaux, les matrices préparées et les électrodes utilisées). Une grande variété de composés interférents a également été examinés pour établir leur effet, le cas échéant, sur la détermination du CC, HQ et 5-CP aux électrodes modifiées. L'interférence de plusieurs composés interférents majeurs, tels que la dopamine, le glucose, l'acide caféine et l'acide ascorbique, pourrait être efficacement bloquée. Pour évaluer l'applicabilité des capteurs produits, chaque capteur a été utilisé pour déterminer CC, HQ et 5-CP dans des échantillons réels, y compris l'eau du robinet et l'eau potable. Des récupérations très intéressantes ont été obtenues, ce qui donne une bonne indication que les capteurs préparés au cours de cette étude sont capables d'être utilisés dans l'analyse d'échantillons réels. **Mots clés :** Capteur électrochimique, nanomatériaux, polluants organiques, techniques électrochimiques, sensibilité, sélectivité.

المخلص

في هذه الأطروحة، تم عرض النتائج ومناقشتها حول انتاج ودراسة المواد النانوية المركبة وتحسين أدائها التحفيزي و التي يمكن استخدامها كمصفوفات جديدة في أجهزة الاستشعار الكهروكيميائية للكشف عن الملوثات العضوية، بما في ذلك الكاتيكول (CC) والهيدروكينون (HQ) و البنثا كلوروفينول (CP-5). في ظل الظروف المثلى (حجم وتركيز المواد النانوية، ودرجة الحموضة وسرعة المسح الكهروكيميائي)، من خلال هذه الدراسة توصلنا الى امكانية رصد كل من الكاتيكول، الهيدروكينون و البنثا كلوروفينول عند الأقطاب الكهربائية المعدلة في محلول فوسفات بتركيز 0.1 مول (PBS)، وتم فصل قمم أكسدة هذه الملوثات بكفاءة بالنسبة الى القطب كهربائي المرجع. تم تحسين رصد الكاتيكول، الهيدروكينون و البنثا كلوروفينول باستخدام الأقطاب الكهربائية المعدلة من خلال مجموعة متنوعة من العوامل والظروف. بفضل هذه العوامل المحسنة، تم الحصول على حدود كشف منخفضة جداً ونطاقات خطية واسعة لكل ملوث اعتماداً على الدراسة (المواد النانوية، المصفوفات المعدة والأقطاب الكهربائية المستخدمة). تم أيضاً فحص مجموعة متنوعة من المركبات المسببة للتداخل لتحديد تأثيرها، إن وجد، على تحديد الكاتيكول، الهيدروكينون و البنثا كلوروفينول عند الأقطاب الكهربائية المعدلة. يمكن منع تداخل العديد من المركبات الرئيسية المسببة للتدخل، مثل الدوبامين والجلوكوز وحمض الكافيين وحمض الأسكوربيك بشكل فعال. لتقييم قابلية تطبيق المستشعرات المنتجة، تم استخدام كل مستشعر لتحديد الكاتيكول، الهيدروكينون و البنثا كلوروفينول في عينات حقيقية بما في ذلك مياه الصنبور ومياه الشرب. تم الحصول على عمليات استرداد مثيرة للاهتمام للغاية، مما يعطي مؤشراً جيداً على أن المستشعرات التي تم إعدادها خلال هذه الدراسة يمكن استخدامها في تحليل عينات حقيقية. **الكلمات المفتاحية:** الحساس الكهروكيميائي، المواد النانوية، الملوثات العضوية، التقنيات الكهروكيميائية، الحساسية، الانتقائية.

Table of content

Dedication

Acknowledgements

Abstract

Figures List

Tables List

General Overview.....1

Chapter I

Electrochemical sensors for the detection of organic pollutants: An overview.

I.1. Introduction.....	6
I.2. Organic pollution in water and its effects	8
I.2.1. Effect and toxicity of CC	9
I.2.2. Effect and Toxicity of HQ.....	10
I.3. Electrochemistry and electrochemical sensing	13
I.3.1. Three-electrode system	15
I.3.2. Types of sensors	16
I.3.3. Electrochemical sensor.....	16
I.3.3.1. Background of Electrochemical Sensors	16
I.4. Analytical characteristics of electrochemical sensor	18
I.4.1. The linear range	18
I.4.2. Limit of detection (LOD)	19
I.4.3. Selectivity	19
I.4.4. Reproducibility	19
I.4.5. Stability.....	19
I.5. Electrochemical sensors preparation using conductive and semi-conductive nanomaterials..	20
I.5.1. Carbon Materials	20
I.5.1.1. Carbon nanotubes (CNTs).....	21
I.5.1.1.1. Structure and properties	22

I.5.1.1.2. Synthesis and purification.....	23
I.5.1.1.3. Carbon nanotube in electrochemical sensors	24
I.5.1.2.1.1. Synthesis of GO	25
I.5.1.2.1.2. Reduction of GO to rGO	26
I.5.1.2.2. Electrochemical sensors and rGO	26
I.5.2. Layered double hydroxide (LDH)	27
I.5.2.1. Synthesis and preparation	28
I.5.2.1.1. Urea hydrolysis	28
I.5.2.1.2. Hydrothermal synthesis.....	28
I.5.2.1.3. Ion exchange method	29
I.5.2.1.4. Co-precipitation method.....	29
I.5.2.1.5. Electrochemical synthesis of LDH on the electrode surface.....	30
I.5.2.2. LDH in electrochemical sensors	31
I.5.3. Metal organic framework MOF.....	34
I.5.3.1. Synthesis and preparation	36
I.5.3.1.1. Conventional Synthesis routes (Ca)	36
I.5.3.1.2. Microwave Synthesis (MW)	37
I.5.3.2. MOF in electrochemical sensors.....	38
I.5.4. Metals and metal oxides	40
I.5.4.1. Synthesis and preparation of Metals	42
I.5.4.2. Electrochemical sensors based on metals and metal oxides	45
I.6. Outlook, scope, and conclusions.....	47

Chapter II

Apparatus, electrochemical methods and preparation of electrodes

II.1. Introduction	71
II.2. Materials and methods.....	72
II.2.1. Reagents	72
II.2.1.1. Nanomaterial synthesis.....	72

II.2.1.1.1. Synthesis of ZnO@fMWCNTs.....	72
II.2.1.1.1.1. Synthesis of zinc oxide nanoparticles (ZnO)	72
II.2.1.1.1.2. Synthesis of functionalized multi walled carbon nanotubes (fMWCNTs)	72
II.2.1.1.1.3. Synthesis of ZnO@fMWCNTs nanocomposite.....	72
II.2.1.1.2. Preparation of NiO/rGO/fMWCNTs nano-hybrid.....	73
II.2.1.1.3. Synthesis of rGO and Fe-MOF	73
II.2.1.1.3.1. Synthesis of rGO	73
II.2.1.1.3.2. Synthesis of Fe-MOF	74
II.2.1.1.4. Synthesis of rGO-CuO and LDH.....	74
II.2.1.1.4.1. Green synthesis of the green organic-inorganic hybrid (rGO-CuO) and LDH	74
II.2.1.1.4.2. Synthesis of Ni-Co-LDH.....	75
II.2.1.2. Preparation of the modified electrodes	75
II.2.2. Instruments.....	75
II.3. Characterization techniques.....	76
II.3.1. Scanning Electron Microscopy (SEM)	76
II.3.2. X-ray diffraction (XRD) and X-ray fluorescence (XRF).....	76
II.3.3. Fourier Transform Infrared (FTIR).....	76
II.4. Experimental device for the detection of organic pollutants.....	76
II.4.1. Classic three-electrode system	77
II.4.2. The electrochemical cell	77
II.4.3. The electrodes	77
II.5. Preparation of the solutions	78
II.5.1. Buffer solution preparation	78
II.5.2. CC, HQ and 5-CP solutions preparation.....	78
II.5.3. Preparation of modified electrodes	78
II.6. Electrochemical detection.....	78
II.6.1. Cyclic voltammetry (CV)	80
II.6.2. Differential pulse voltammetry (DPV)	81
II.6.3. Square wave voltammetry (SWV)	82

II.6.4. Amperometric <i>i-t</i> curve.....	84
II.6.5. Electrochemical impedance	84
II.6.6. Comparison of the different methods for the detection of pollutants	86
II.7. Objectives	87
II.8. Conclusion.....	89

Chapter III

Results and Discussion

III. Results and discussion.....	94
III.1. FT-IR, XRD and surface morphology study of prepared nanocomposites	94
III.1.1. Physico-chemical analysis of ZnO, <i>fMWCNTs</i> and ZnO@ <i>fMWCNTs</i> nanocomposites	94
III.1.2. Physico-chemical analysis of MWCNTs, rGO, and NiO/rGO/ <i>fMWCNTs</i> nano-hybrid	97
III.1.3. Physico-chemical analysis of monometallic Fe-MOF nanosheets	100
III.1.4. Physico-chemical analysis of Ni-Co-LDH and rGO-Cu.....	103
III.2. Characterization of the electrode matrix	105
III.2.1. Electrochemical behavior of <i>fMWCNTs</i> , ZnO NPs, and ZnO@ <i>fMWCNTs</i> to catechol (CC) detection.....	105
III.2.1.1. Dosage optimization of <i>fMWCNTs</i> /ZnO@ <i>fMWCNTs</i>	106
III.2.1.2. Electrochemical behavior of CC at <i>fMWCNTs</i> /ZnO@ <i>fMWCNTs</i> /GCE.....	107
III.2.2. Electrochemical characterization of NiO/rGO/ <i>fMWCNTs</i> , rGO/ <i>fMWCNTs</i> , and <i>fMWCNTs</i>	109
III.2.2.1. Optimization of NiO/rGO/ <i>fMWCNTs</i> modification amount.....	110
III.2.2.2. Simultaneous electrochemical behavior of NiO/rGO/ <i>fMWCNTs</i> /Pt toward CC and HQ	111
III.2.3. Electrochemical behavior of rGO, Fe-MOF and rGO/Fe-MOF to 5-chlorophenol (5-CP) detection.....	112
III.2.4. Electrochemical characterization of Ni-Co-LDH, rGO-CuO and Ni-Co-LDH/rGO-CuO	113

III.3. Effect of scan rate and pH value.....	114
III.3.1. Effect of scan rate and pH on fMWCNTs/ZnO@fMWCNTs/GCE.....	114
III.3.2. Effect of scan rate and pH on NiO/rGO/fMWCNTs/Pt.....	116
III.3.3. Effect of scan rate on rGO/Fe-MOF/AuE.....	119
III.3.4. Effect of scan rate on Ni-Co-LDH/rGO-CuO/AuE.....	121
III.4. Electrochemical detection of the organic pollutant.....	122
III.4.1. Electrochemical detection of CC using fMWCNTs/ZnO@fMWCNTs/GCE.....	122
III.4.2. Simultaneous detection of CC and HQ using NiO/rGO/fMWCNTs/Pt.....	123
III.4.3. Electrochemical detection of 5-CP using rGO/Fe-MOF/AuE.....	126
III.4.3.1. ANN modeling of the sensor.....	127
III.4.3.1.1. Data analysis of 5-CP using ANN.....	127
III.4.4. Electrochemical detection of 5-CP using Ni-Co-LDH/rGO-Cu/AuE.....	133
III.5. Analytical performance of the fabricated sensors.....	134
III.5.1. Analytical performance of fMWCNTs/ZnO@fMWCNTs/GCE.....	134
III.5.1.1. Selectivity, stability, repeatability, and reproducibility of fMWCNTs/ZnO@fMWCNTs/GCE.....	134
III.5.1.2. Practicality of fMWCNTs/ZnO@fMWCNTs/GCE.....	136
III.5.2. Electroanalytical performance of NiO/rGO/fMWCNTs/Pt.....	137
III.5.2.1. Stability Anti-interference and reproducibility of NiO/rGO/fMWCNTs/Pt.....	137
III.5.2.2. Practicality of NiO/rGO/fMWCNTs/Pt.....	139
III.5.3. Electroanalytical performance of rGO/MOF/AuE.....	140
III.5.3.1. Reproducibility and repeatability of the rGO/MOF/AuE.....	140
III.5.4. Electroanalytical performance of Ni-Co-LDH/rGO-CuO/AuE.....	141
III.5.4.1. Stability of Ni-Co-LDH/rGO-CuO/AuE.....	141
III.6. Conclusion.....	142
General conclusion and future prospective.....	144

Figures list

Figure I.1. A typical schematic presentation of a three-electrode system.....	14
Figure I.2. Graphs of potential vs. time for some voltammetry techniques to produce a signal...	15
Figure I.3. The fabrication process of the sensor and the catalytic mechanism for the oxidation of catechol and hydroquinone.....	17
Figure I.4. Illustration of the nanoscale relative to biologically active molecules, and examples of nanomaterials of relevance for biomedical and bio sensing applications.	20
Figure I.5. Schematic of an individual (A) SWCNTs and (B) MWCNTs.	22
Figure I.6. The structure of Graphene, Graphene Oxide and Reduced Graphen Oxide	25
Figure I.7. Flow chart of the synthesis mechanism of Fe ₃ O ₄ @CuAl NSs	30
Figure I.8. Schematic illustration of the fabrication mechanism of CuO@MnAl NSs.	30
Figure I.9. Key characteristics of LDH modified electrodes.	31
Figure I.10. Schematic representation of important reported MOFs which are known for high gas storage properties.	35
Figure I.11. Schematic representation of different structures of noble metal-metal oxide nanocomposite.....	42
Figure I.12. Schematic Illustration of the Hydrothermal Synthesis of Fe ₃ O ₄ –PEI NPs and the Subsequent Functionalization of the Fe ₃ O ₄ –PEI NPs	44
Figure I.13. Vapor-Liquid-Solid (VLS) method for vapor-phase synthesis of metal nanowires..	44
Figure II.1. Diagram of the experimental device used for the electrochemical measurements. ...	77
Figure II.2. Electrochemical detection of pollutants by different type of electrocatalysts.	79
Figure II.3. Different mechanisms of the electrochemical analysis including CV (A-C), DPV (D), SWV (E-G), I-T (H) and impedance methods	79
Figure III.1. FTIR spectra of ZnO@fMWCNTs, fMWCNTs and ZnO nanocomposites.	95
Figure III.2. XRD fragments and (b) XRF of synthesized nanocomposites ZnO@fMWCNTs. .	95
Figure III.3. SEM analysis of A) ZnO NPs, B) fMWCNTs, and C) ZnO@fMWCNTs.	96
Figure III.4. SEM analysis of (a) fMWCNTs, (b) rGO and, (c) NiO/rGO/fMWCNTs.	98
Figure III.5. Fourier transform infrared spectroscopy spectra of fMWCNTs, rGO/fMWCNTs and NiO/rGO/fMWCNTs nanocomposites.....	98
Figure III.6. XRD fragments and (b) XRF of the synthesized nanocomposites.....	99
Figure III.7. XRD fragments of the synthesized Fe-MOF.....	108

Figure III.8. XRF patterns of the synthesized Fe-MOF.....	101
Figure III.9. The SEM images of rGO (A), (B), (C), homogeneous distribution of the organometallic particles in the synthesized framework (D), three-dimensional shape of the MOF (E), and porous structure of the synthesized MOF (F).....	102
Figure III.10. FTIR spectra of (a) GO and rGO-CuO and, (b) Ni-Co-LDH composites.....	104
Figure III.11. SEM analysis of (a, b) Ni-Co-LDH and (c, d) rGO-CuO nanocomposites.	104
Figure III.12. CV responses of the bare GCE and the modified electrodes.	105
Figure III.13. Dosage effect of fMWCNTs/ZnO@fMWCNTs (μL) in presence of 1 mM CC in 0.1M PBS at Sweep rate 100 mV/s.	114
Figure III.14. (a) CVs and (b) EIS for the bare GCE (blue curve) and fMWCNTs/ZnO@fMWCNTs/GCE (red curve) in a 0.1 M PBS solution (pH 7.5) with 100 mM CC at a sweep rate of 0.1 V/s	107
Figure III.15. CV responses of three different modified and bare Pt electrodes in the presence of 5 mM CC in 0.1 M PBS (pH 7.5) at a scan rate of 100 mV/s.....	110
Figure III.16. Effect of dosage of NiO/rGO/fMWCNTs (3mg/ml) in 0.1 M PBS (pH 7) contains 5 mM catechol with sweep rate of 0.1 V/s.	111
Figure III.17. (a) CV and (b) EIS results of NiO/rGO/fMWCNTs/Pt and a bare Pt electrode. A 0.1 M PBS (pH 7) with 100- μM CC and 100- μM of HQ, and a scan rate of 100 mV/s are used.	111
Figure III.18. CVs of 5 mM 5-CP at different modified gold electrodes (AuEs) in the 0.1-M PBS at scan rate of 50 mV/s.....	111
Figure III.19. CVs of 5 mM ferri-ferrocyanide at different modified AuE in the presence of 0.1 M PBS (pH 7) at sweep rate of 0.1 V/s.	114
Figure III.20. (a) CVs obtained for CC at fMWCNTs/ZnO@fMWCNTs/GCE in the presence of varied pH; (b) Plot of E_{pa} versus pH; (c) Graph of I_{pa} versus pH.....	114
Figure III.21. Effect of (a) scan rate of 100 μM CC at fMWCNTs/ZnO@fMWCNTs/GCE, plots of peak current versus (b) scan rates and (c) (scan rates) ^{1/2} for CC in 0.1M PBS.....	115
Figure III.22. (a) Cyclic voltammetry curves obtained for catechol and hydroquinone (100 μM) at NiO/rGO/fMWCNTs/Pt in the presence of varied pH; (b) Graph of oxidation current versus pH; (c) Plot of oxidation potential versus pH.	117

Figure III.23. (a) Cyclic voltammetry curves obtained for catechol and hydroquinone (100 μM) in 0.1 M PBS (pH 7) at NiO/rGO/fMWCNTs/Pt in the presence of varied scan rate; b) Plot of oxidation current(Catechol) (d) and oxidation current(hydroquinone) (c) versus scan rate $^{1/2}$...	118
Figure III.24. Effect of CV scan rate on 100 μM 5-CP in 0.1 M PBS at rGO/Fe-MOF/GE. The scan rates: 10, 30, 50, and 100 mV/s.....	120
Figure III.25. Plots of peak current versus scan rates (a), (scan rates) $^{1/2}$ (b) (10–100 mV/s), and relationship between E and $\ln(v)$ (c) for 100 μM 5-CP.	120
Figure III.26. Effect of scan rate range from 20 to 80 mV/s of 50 μM 5-CP in 0.1 M PBS at Ni-Co-LDH/rGO-CuO/AuE. (b) Current (μA) versus Scan rate $^{1/2}$ (mV/s).....	121
Figure III.27. (a) CVs of fMWCNTs/ZnO@fMWCNTs/GCE for various concentrations (10–1000 μM CC) in a 0.1 M PBS at a sweep rate of 0.1 V/s. (b) Ipa versus CC concentration.	122
Figure III.28. (a) CVs obtained for various concentrations of CC and HQ in 0.1 M PBS (pH 7) at NiO/rGO/fMWCNTs/Pt; (b) Ipa versus CC concentration; (c) Ipa versus HQ concentration. ...	125
Figure III.29. (A) SWV of rGO/Fe-MOF/GE for various concentrations (50–200 μM 5-CP) in a 0.1M PBS at a sweep rate of 0.05 V/s. (B) Ipa versus 5-CP concentration.	126
Figure III.30. ANN architecture for estimation of 5-CP concentrations.	127
Figure III.31. Mean squared error (MSE) over the trained epochs of the ANN. The learning rate (LR) was set to 10%.	128
Figure III.32. Correlation factor (R) for the training, validation, testing, and all data of the developed ANN.....	130
Figure III.33. (A) ANN prediction error; (B), (C) Comparison between the real values (green color) and the predicted ones (red color) obtained by the developed ANN.....	131
Figure III.34. (a) CVs of Ni-Co-LDH/rGO-Cu/AuE for various concentrations (1–50 μM 5-CP) in a 0.1 M PBS at a sweep rate of 0.1 V/s. B) Ipa versus 5-CP concentration.	133
Figure III.35. (a) CV results at a scan rate of 100 mV/s for fMWCNTs/ZnO@fMWCNTs/GCE in 0.1 M PBS solution with hydroquinone (HQ), penta-chlorophenol (p-Ch-ph) and phenol (ph). The CC concentration is varied from 50 to 200 μM while concentrations of the others are kept at 50 mM. (b) The percentage current change (%) of each interference.....	134
Figure III.36. Stability of 50 CVs gotten for 100 μM CC at fMWCNTs/ ZnO@fMWCNTs/GCE with sweep rate of 0.1 V/s, respectively.....	135

Figure III.37. (a) CVs gotten for 100 μM CC at 8 different fMWCNTs/ZnO@fMWCNTs/GCE with sweep rate of 0.1 V/s. (b) The percentage current change (%) of each modified GCE.	136
Figure III.38. (a) 10 repeated CVs gotten for 100 μM CC at fMWCNTs/ZnO@fMWCNTs/GCE with sweep rate of 0.1 V/s. (b) The percentage current change (%) of each experiment.	136
Figure III.39. CV curves at a sweep rate of 0.1 V/s for CC for tap water samples with three different CC concentrations (10, 50, and 100 μM).	137
Figure III.40. Stability of 50 cyclic voltammetry curves gotten for 100 μM catechol and 10 μM hydroquinone at NiO/rGO/fMWCNTs/Pt with sweep rate of 0.1 V/s.	138
Figure III.41. DPV curves at NiO/rGO/fMWCNTs/Pt with constant HQ concentration and varied CC concentrations in 0.1 M PBS (pH = 7.0).	138
Figure III.42. (a) 10 repeated cyclic voltammetry curves gotten for 100 μM catechol at fMWCNTs/ZnO@fMWCNTs/Pt with sweep rate of 0.1 V/s. (b) and (c) the percentage of current change (%) of catechol and hydroquinone, respectively.	139
Figure III.43. CV curves at a sweep rate of 0.1 V/s for CC and HQ in tap water samples with three different concentrations of CC and HQ (10, 50, and 100 μM).	140
Figure III.44. (a) Reproducibility test for 5 rGO/MOF/AuE in the presence of 200 μM of 5-CP. (b). Repeatability test for 5 rGO/MOF/AuE in the presence of 200 μM of 5-CP.	140
Figure III.45. Stability of 20 CVs gotten for 50 μM 5-CP at Ni-Co-LDH/rGO-CuO/AuE with sweep rate of 0.1 V/s.	141

Tables list

Table I.1. Some of the physicochemical properties of CC and HQ.	12
Table I.2. Summary and comparison of the most important synthesis procedures for CNTs.....	23
Table I.3. Comparison with state-of-the-art catechol sensors based on carbon nanotubes.....	24
Table I.4. Comparison with state-of-the-art catechol sensors based on reduced graphene oxide.	27
Table I.5. Comparison with state-of-the-art electrochemical sensors based on LDH.....	34
Table I.6. Comparison with state-of-the-art electrochemical sensors based on MOFs.....	40
Table I.7. Comparison with state-of-the-art electrochemical sensors based on metals and metal oxides nanoparticles.	47
Table II.1. The advantages and disadvantages of different analysis methods.	86
Table III.1. Comparison with state-of-the-art synthesis methods of NiO, rGO, and fMWCNTs.	100
Table III.2. Heterogeneous rate constant for CC at fMWCNTs/ZnO@fMWCNTs/GCE.....	116
Table III.3. Comparison with state-of-the-art catechol sensors based on carbon nanotubes.....	123
Table III.4. Comparison with state-of-the-art CC and HQ sensors based on rGO.	124
Table III.5. Comparison with state-of-the-art phenol-compound sensors based on MOFs.	127
Table III.6. Structure, architecture and settings of the best found model for the 5-CP prediction.	128
Table III.7. Comparison between the real and estimated 5-CP concentrations using the developed ANN	131
Table III.8. Recoveries of CC in a local tap water sample at fMWCNTs/ZnO@fMWCNTs/GCE.	137
Table III.9. Recoveries of CC and HQ in a local tap water sample at NiO/rGO/fMWCNTs/Pt.	140

General Overview

Catechol, hydroquinone and pentachlorophenol are isomers of phenolic compounds widely used in a variety of sectors including textiles and paints, plastics, petroleum refineries, cosmetics, antioxidants, pesticides, pharmaceuticals and photography. Phenolic chemicals are extremely dangerous to human health. Furthermore, the US Environmental Protection Agency and the European Union consider them to be environmental pollutants even in very low amounts. A high dose of hydroquinone (eg, 1 g or more) may cause fatigue, headache, edema, nausea, dermatitis, eczema and possibly death from respiratory failure in the patient. To detect pollution caused by organic compounds, there is an urgent need for sensitive, easy and fast analytical methods to monitor this type of pollution both quantitatively and qualitatively. From here, physicochemical analyzers were used to monitor and detect these pollutants such as catechol, hydroquinone and pentachlorophenol. Although these analytical methods have shown arguably positive results, they have many shortcomings. Some are expensive or require staff training because these analytical tools require complex processes. Others require a long sensing and response time, have low sensitivity and specificity, or require a sample preprocessing. On the other hand, electrochemical sensors are one of the most promising and widely used methods for detecting this type of pollution due to its outstanding characteristics such as simplicity, short analysis time, wide linear range, high selectivity, high sensitivity, and low cost. Based on this principle and due to the extraordinary mechanical properties and unique electrical properties of carbon-based materials such as carbon nanotubes and graphene with other nanomaterials such as metals and conductive polymers, it has stimulated extensive research activities all over the world since its discovery to develop its uses in the field of electrochemical sensing.

Through this research, we used the modified electrodes repeatedly in the electrochemical analysis to detect the aforementioned phenolic compounds in a sensitive and selective manner. We found that the electrodes made of glass carbon provide several advantages compared to other electrodes, including biocompatibility with test samples and rapid technology. It is simple to produce from cheap materials and easy to modify with nanomaterials developed and produced in this research. Through this study we concluded that this type of electrode has a repeatable and renewable surface with little residual current during the analysis. This type of electrode is also

characterized by cheap production cost, porous surfaces and, once modified, can be used to reduce active area blockage in electrochemical sensor electrodes when working with phenolic compounds. Through this research we found that the main benefits of using these electrodes modified with nanoparticles increase the active area efficiency of the modified electrode, the enhanced sensitivity and selectivity, and the effective mass transfer via the mediated electron transfer between the electrically studied materials during reactions in solution. Carbon-based nanomaterials (such as carbon nanotubes, graphene oxide, and reference graphene oxide), metals, metal oxides, polymers and printed polymers which are nanoparticles with chemical properties and physical and electrical components distinct from other materials. These features enable them to be employed in a variety of analytical fields, including the manufacture of new and effective sensors. The above-mentioned nanoparticles have been frequently used to modify the electrodes used in the sensitive and selective detection of catechol, hydroquinone as well as pentachlorophenol and other phenolic compounds using electrochemical analytical procedures. Through this paper, we study the electrochemical performance of new sensors made of multi-walled carbon nanotubes, reference graphene oxide, double-layer hydroxide, metal oxide nanoparticles, partially printed polymers, and study their applications in sensor systems to detect pollution from organic compounds such as catechol, hydroquinone. and pentachlorophenol.

The first chapter of this thesis is a general introduction to the latest methods for the production of multiwalled carbon nanotubes, reference graphene oxide, double-layered hydroxide, metal oxide nanoparticles and molecularly printed polymers and their applications in sensing systems for the detection of catechol, hydroquinone and pentachlorophenol. This chapter also briefly talks about electrochemistry and electrochemical sensors. It also briefly describes the synthesis and preparation of these materials, followed by applications in electrochemical sensors.

The second chapter presents the materials and tools used in this research and also includes the objectives that motivated this work. This chapter describes the preparation steps of the nanocomposite as well as physicochemical characterization by infrared spectroscopy, scanning electron microscopy, X-ray scanning as well as electrochemical characterization such as resistance measurements to confirm the conductivity of the nanocomposite. This

nanocomposite was applied after optimizing the experimental parameters such as the optimum pH value, the appropriate applied potential and the scanning speed required to perform the electrochemical measurements. In summary, this chapter aims to reveal, in the first part, the operating protocols and experimental devices used in the preparation and employment of the electrode surfaces studied in the framework of this thesis. The second part of this chapter is devoted to the different characterization techniques applied. Finally, we presented the electrochemical techniques adopted to study the interaction of detailed electrodes with respect to the targeted analyses.

Chapter 3 describes the study of the properties of multi-walled carbon nanotubes, reference graphene oxide, double-layered hydroxide, metal oxide nanoparticles and molecularly printed polymers to enhance electronic transport to electrochemical sensing systems. Modifications of conventional electrode surfaces and responses to detection of catechol, hydroquinone and pentachlorophenol were studied. The third chapter summarizes and finally discusses the scientific findings and conclusions related to this thesis while giving future perspectives for research in this field at the same time. It was concluded from the simultaneous detection of catechol and hydroquinone that the electrode modified using multiwalled carbon nanotubes and reference graphene oxide exhibits high electrical activity. The modified electrode provides higher selectivity in voltammetric measurements for catechol and hydroquinone. The use of a combination of electrostatic interactions is a new aspect that allows for a more rational design of analytical strategies that could find applications in neuroscience. However, these studies in this direction are currently underway.

The nanocomposite hybrid of reference graphene oxide and double-layered hydroxide provided sufficient reactive sites and electrocatalytic activity toward the detection of pentachlorophenol as an electrochemical sensor. This made the proposed sensor perform well with excellent sensitivity and very low detection of very low concentrations of the latter. Then, based on this compound, an electrochemical sensing platform with excellent sensitivity and potential applicability was built. As a result of the research, the proposed sensor component may open up new avenues for the design and production of other highly sensitive sensor systems for different applications in the future for monitoring pentachlorophenol in water.

This study showed that the electrodes modifications with the composite nanomaterials developed in this research in most cases improved their electrochemical performance while recording a lower analysis period and a wide linear range. using unmodified electrodes. The demonstrated ability of the materials studied in this study to enhance electron transfer between these pollutants and the electrode surface indicates an attractive electrocatalytic nanomaterial for the development of novel electrochemical sensors.

Through this study, we recommend researchers specialized in this field that the future applications of the developed nanomaterials, including carbon nanotubes, graphene, metal oxides and the rest of the previously mentioned nanomaterials require further developments in the following directions:

- Improving the electrochemical response (sensitivity, detection limit, stability, etc.) to catechol, hydroquinone as well as pentachlorophenol as well as other phenolic compounds and working more on the applicability of the sensors in real samples.
- Development of carbon-based electrochemical sensors, as these devices will provide many advantages such as low cost, quick response and simple preparation. New alternatives for the production and development of carbon nanotubes with other polymeric matrices will be studied with interest in 3D printing technology for carbon nanotube-based conducting electrodes.
- Focus in the near future on the application of prepared sensors mentioned in action in a lab-on-a-chip system to assess electrochemical response to improve sensitivity and operational stability using minimum sample size and work on their application in medicine and environmental studies.

Chapter I

**Electrochemical sensors for the detection of organic
pollutants: An overview**

I.1. Introduction

The determination and examination of organic pollution (carbon-based compounds) with analogous chemical properties is an interesting topic in analytical chemistry [1]. This topic is interested in the analyzing of the amount or the kind of the chemical compounds including organic pollutants [2,3].

Hence, the electroanalytical aspect of the chemical compounds is devoted to the detection and study of organic/inorganic pollutants having comparable electrochemical characteristics. Catechol (CC) and Hydroquinone (HQ) are phenolic compound isomers that are widely employed in a variety of sectors including textiles, paints, plastics, petroleum refineries, cosmetics, antioxidants, insecticides, medicines, and photography [4-7]. Phenolic chemicals are extremely hazardous to human health [6,8]. Furthermore, United States Environmental Protection Agency and the European Union consider them to be environmental contaminants even at extremely low quantities. A high dose of hydroquinone (e.g., 1 gram or more) might induce weariness, headache, edema, nausea, internal organs, dermatitis, eczema, collapse, and potentially death from respiratory failure in the patient [9-11].

DM de Oliveira et al. (2010) studied the toxic properties stimulated by catechol using human glioblastoma GL-15 cells to get more data about its toxic effects on the human central nervous system. In addition, they reported that it can reduce the glutathione amount and prompted the cell death principally by apoptosis [12]. They also point out that it lowers glutathione levels and induces cell death predominantly through apoptosis. Furthermore, because catechol and hydroquinone have similar structures and properties, they exist concurrently and interact with each other via environmental recognition samples. As a result, breakthroughs in sensitive and quick diagnostic procedures are required for their concurrent analysis. Capillary electrophoresis, gas chromatography, and liquid chromatography are more prevalent procedures that need an isolation step. Electrochemical techniques have the advantages of being simple to operate with precision equipment and saving time, and depending on the features of the isomers of dihydroxybenzene, electrochemical processes may be appropriate alternatives, as many reports have been referenced in the literature [13-15].

To detect CC effectively, sensitive, easy and fast analytical methods for quantitative and qualitative CC monitoring are strongly needed [16]. Hence, various analytical methods for detecting CC have been developed and applied over the years, including gas chromatography/mass spectrometry [17], chemiluminescence [18] synchronous fluorescence [19], electrochemical methods [20], high-performance liquid chromatography (HPLC) [21]. Although these analytical methods exhibited effective detection of CC, they involve many disadvantages. Some of them are expensive [17,18] or need training personnel because these analytical tools require complicated processes [19]. Others require too long sensing and response time [21], have low sensitivity and specificity or need a sample of pretreatment [22]. One of the most promising and widely used methods for CC detection is electrochemical sensing due to its prominent characteristics including simplicity, short analysis time, wide linear range, high selectivity, high sensitivity, and low cost [23].

Modified electrodes have been frequently employed in electrochemical analysis for sensitive and selective compound detection [23]. Glassy carbon electrodes (GCE) offers—various benefits over conventional solid electrodes, including biocompatibility with test samples and a quick and simple technique of production from inexpensive materials [24]. They have a repeatable and renewable surface with little residual current during analysis. GCE also has a cheap production cost, porous surfaces, and once it is modified, it may be utilized to reduce fouling in electrochemical sensor electrodes when working with phenolic compounds such as CC and HQ [25,26]. However, the GCE modified with nanomaterials has lately gained prominence. Increase the electrochemical characteristics of the substances under consideration. The key benefits of utilizing modified GCE with nanoparticles on large electrodes or unmodified GCE include effective surface area, enhanced sensitivity and selectivity, and efficient mass transfer via electron transfer mediation between electrically active species during reactions in solution [27,28]. Carbon-based nanomaterials (such as carbon nanotubes (CNTs), graphene oxide (GOs), and reduced graphene oxide (rGO)), metals, metal oxides, polymers, and printed polymers are nanoparticles with chemical characteristics, distinctive physical, and electrical components that distinguish them from bulk materials. These distinct features enable them to be employed in a variety of analytical procedures, including the fabrication of new and better sensors. Similar to electrolysis sensors. The nanoparticles cited below

have been frequently employed to modify electrodes used in the sensitive and selective detection of CC and HQ and other phenolic compounds using analytical procedures [29,30].

To resume, the use of nanostructured materials in these electrodes is suggested. Significant increases in compound electrochemical behavior due to high effective surface, stimulating action, and mass transfer. Carbon-based nanomaterials (such as CNTs, GOs, and rGOs), metal oxides, metals, polymers, and printed polymer nanoparticles are all nanoparticles that are utilized to perform the electrocatalytic activity of the electrodes due to their superior electrochemical characteristics. They are employed to improve the detection limit, offer a large electroactive surface area, a catalytic action, high electromagnetic activity, attractive electron transport, sensitivity, and chemical stability [31]. The nanomaterials discussed above have a conductivity effect, which makes them excellent for improving electron transport between analytes and electrodes [32]. These nanoparticles have a wide range of applications, including biomaterials, bioseparation, biomedical and bioengineering applications, and food analysis [33,34].

The purpose of this chapter is to investigate the electrochemical behavior of various phenolic compounds (**Figure I.1**). Hence, an overview about the advanced methods and technical challenges made for preparing a novel electrochemical sensor for monitoring organic compounds with high analytical performances was presented.

I.2. Organic pollution in water and its effects

Industrial development has caused a huge increase in the release of potentially toxic compounds into the atmosphere, water bodies, and soils. In the last decades, environmental pollutants have been directly connected to the increase in human diseases, particularly those involved with the immune system. The contribution of benzene and its metabolites to this issue is well recognized, making them a public health problem. Catechol (CC) and Hydroquinone (HQ), the major benzene metabolites, are ubiquitous chemicals in the environment due to their widespread application in human and industrial activities. They can be used as a developing agent in photography, dye intermediate, stabilizer in paints, varnishes oils, and motor fuels. In addition, hydroquinone has been used as an antioxidant in the rubber and food industry. From 1950s to 2001 CC and HQ were applied in the commercially available cosmetic skin lightening formulations in European Union countries and since 1960s they were both commercially available as a medical

product. They are also present in cosmetic formulations of products for coating finger nails and hair dyes [4-7].

On the other hand, CC and HQ can be components of high molecular aromatic compounds (e.g., resin), an intermediate, or appear as a degradation product generated by the transformation of aromatic compounds. Advanced oxidation processes (APOs) of aromatic compounds, particularly of phenol, yield several benzene derivatives, such as hydroquinone, catechol, and resorcinol, as intermediate metabolites of their transformation. The formation of HQ and CC and (and p -benzoquinone at early stages of phenol oxidation increases the toxicity of phenol wastewaters, showing that these compounds were more toxic and less degradable than the original pollutant [35, 36].

I.2.1. Effect and toxicity of CC

Catechol (1,2-dihydroxybenzene) is used in a variety of applications such as a reagent for photography, dyeing fur, rubber and plastic production and in the pharmaceutical industry [37]. Substituted catechols, especially chlorinated and methylated catechols, are by-products in pulp and oil mills [38]. Catechol is an intermediary product from the degradation of aromatic compounds and lignin by microorganism [39]. In humans and mammals catechols can occur as metabolites in the degradation of benzene or estrogens or as endogenous compounds, such as neurotransmitter and their precursors [adrenaline, noradrenaline, dopamine and L-DOPA (L-3,4-dihydroxyphenylalanine) [40,41].

Additionally, catechols can be taken up in the form of tobacco smoke (as catechol, catechol semiquinones and polymerized catechols) [42] or as food components (e.g. catechol, dopamine, caffeic acid, tea catechin) [43]. The toxicity of catechols for microorganisms has been demonstrated in the past years [44,45], and has been suggested to be the reason for the difficulties in cultivating microorganisms on benzene, toluene or chlorobenzene [55,46]. Despite the fact that catechols are ubiquitous, and their toxicity has been observed in a variety of organisms the modes of action causing the toxicity are hardly understood. In the following review, an overview about the chemical properties of catechols is given, which is required to understand their possible toxic modes of action. The molecular modes of action found for catecholic compounds are summarized and discussed, subsequently. Because basic toxic processes in the context of catechol toxicity are

similar in different cell types, ranging from microorganisms to mammals, the information from reactions in different cell types is integrated.

Several studies additionally indicated the toxicity of CC for water flea, zebra fish, trout, rabbit, cat, rat, and mouse and for human cell lines [51,47]. As mentioned earlier, CC is strongly irritating to the eyes, skin, and respiratory tract, and it has been proven to cause DNA damage, vascular collapse, coma, and death. However, these compounds are considered as the primary pollutants in wastewater due to their high toxicity, high oxygen demand, and low biodegradability [9 ,48].

1.2.2. Effect and Toxicity of HQ

Hydroquinone is an aromatic compound consisting of the benzene ring and two –OH groups at *para* position. It is available in the form of white crystals, but industrial use grades may be light grey or light tan. Contact with air and light causes oxidation and darkening of color. Hydroquinone is soluble in water, methanol, and ether. However, it has less solubility in water than the other two dihydroxybenzenes, which means hydroquinone has less affinity towards hydrophilic solvents. Its octanol/water partition value is also less than that of catechol and resorcinol (Table 1). Hydroquinone can occur naturally in many plant foods, as glucose conjugate, namely, arbutin, for example, in the wheat, pears, coffee, onion, tea and red wine [49,50].

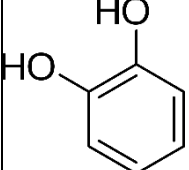
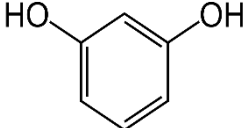
Dihydroxybenzene and quinones are recognized to induce oxidative stress as well as to nonspecifically bind both DNA and protein [49]. Hydroquinone can form complexes with various di- and trivalent metal ions, such as copper and iron. In the case of copper, the complex formed increased H₂O₂ production by hydroquinone and enhances its autooxidation to benzoquinone [51]. Hydroquinone can be originated during phenol [58] or benzene biotransformation [52]. The benzene is first metabolized by liver cytochrome P-450 monooxygenase to phenol. Further hydroxylation of phenol by cytochrome P- 450 monooxygenase or by human peroxidase resulted in the formation of mainly hydroquinone, which accumulates in the bone marrow [53].

Hydroquinone can also be produced through three chemical processes, involving oxidation, reduction, and alkylation reactions. Firstly, it can be generated by oxidation of phenol; secondly, the oxidation of aniline with manganese dioxide in acidic conditions, followed by reduction with iron dust in aqueous medium; finally, the alkylation of benzene with propylene to originate the *para*-di-isopropylbenzene isomer, besides other isomers, which is oxidized and produces the

corresponding dihydroperoxide, that is subsequently treated with an acid to originate hydroquinone [54,46].

It is known that phenolic compounds are extremely toxic for aquatic organisms at the concentration level of part-per-million and most of them can influence the organoleptic properties of shellfish and fish at part-per-billion level [55]. Studies on *Photobacterium phosphoreum* showed that hydroquinone is one hundred and one thousand times more toxic than catechol and resorcinol, respectively [56]. Meanwhile, it was reported that hydroquinone was the less toxic dihydroxybenzene to the grampositive bacteria *Bacillus subtilis*; however, it was shown that hydroquinone and catechol mixture exerts a synergistic joint action while the other mixtures have an additive actions [57]. The toxic effect of phenolic compounds on soil microbial activity has been evaluated, showing hydroquinone as the most toxic dihydroxybenzene [44]. The number of cultivable microorganisms decreased with increasing concentration of phenolic compounds. Table below highlights key feature properties of CC and HQ.

Table I.1. Some of the physicochemical properties of CC and HQ. Reproduced from Elsevier [54].

<i>Parameters</i>	<i>CC</i>	<i>HQ</i>
Chemical structure	 <chem>Oc1ccccc1O</chem> $C_6H_6O_2$	 <chem>Oc1ccc(O)cc1</chem> $C_6H_4(OH)_2$
Other names	Pyrocatechol, 1,2-benzenedio, 1,2- dihydroxybenzene.	<i>p</i> -Benzenediol, 1,4-Benzenediol, dihydroxtbenzene, 1,4-dihydroxybenzene, Quinol.
λ_{max} (nm)	275	289
Boiling point (°C) at 101.3 KPa	245.5	287
Density (g/cm³)	1.344	1.3
Molecular weight (MW. g/mol)	110.11	110.159
Water solubility (g/l) at 25 °C	430	59
Molecular size (nm)	0.55 x 0.55	-
pKa	9.25, 13	9.9-11.6
Dipole moment (Debye: D)	2.620	0.0
Polarity/Polarizability parameter (n:cm³)	11.89+- 0.5*10 ⁻²⁴	0.21+-0.02
Hydrogen-bonding donor parameter (a_s)	0.85	-
Hydrogen-bondign acceptor parameter (B_m)	0.58	-

I.3. Electrochemistry and electrochemical sensing

Electrochemistry is a field of chemistry that deals with the interaction of electrical and chemical processes [58]. For hundreds of years, scientists have been working on the electrochemical techniques [59,60]. More sensitive and precise micro- or nano-electrodes have been created and fabricated as a result of the advancement of nanotechnology, bringing the electrochemical technique back to the platform for point-of-care testing [61,62]. Just before, gas-liquid chromatography, mass spectrometry, nuclear magnetic resonance (NMR), infrared (IR) spectroscopy, and flame element analysis were well-known as examples of laboratory analytical procedures [63,64]. They are classified as destructive (e.g., mass spectrometry, flame analysis) or non-destructive (e.g., infrared spectroscopy, electron microscopy, etc.) based on whether the sample is destroyed as a result of the processing phase. These techniques are commercially available, extremely sensitive and accurate, and may be used for a wide range of studies. They are, however, time-consuming and expensive to conduct, need specialized training, and, in some circumstances, significant sample preparation. The equipment used also necessitates a high level of maintenance in order to remain operational and, in most cases, must be used in a clean lab environment [17,22].

Electrochemical techniques, on the other hand, are gaining popularity in the field of analytical chemistry. These techniques provide the same sensitivity at a cheaper cost, with fewer complicated operating processes and faster on-site detection [65,66]. For organic pollution detection, many electrochemical systems have been developed. Nanomaterials, in particular, have provided numerous benefits in this field due to their unique electrical, chemical, and mechanical characteristics [67,68]. As a result, several electrochemical sensors based on nanoparticles have been developed for organic pollution detection [67,69].

Voltammetry techniques are the most frequently used electrochemical techniques in the detection of organic pollution ions. Voltammetry is a broad term that encompasses all electrochemical systems that rely on measurements of dependent potential current [70-72].

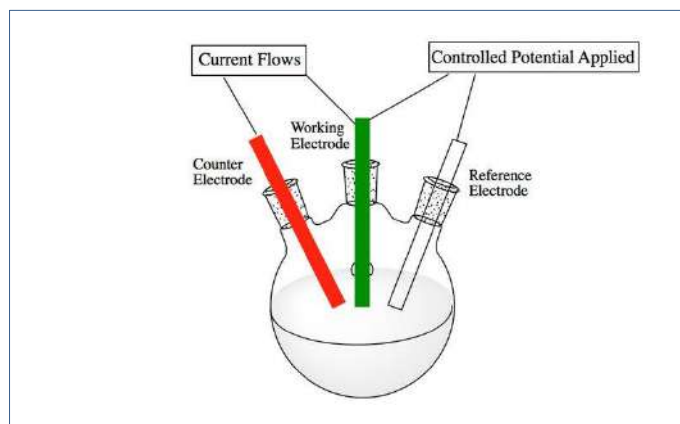


Figure I.1. A typical schematic presentation of a three-electrode system. Reproduced from MDPI [73].

The measurement of a cyclic voltmeter (CV) consists of linearly scanning the voltage in one direction and then inverting the potential of a working electrode. To put it another way, it contains one or more triangular potential waveforms [70]. The basic principle underlying the measurement of a pulse voltmeter is the use of a voltage signal pulse. Different varieties of pulse voltimeters exist by varying the form and amplitude of the pulses [71]. Differential pulse voltammetry (DPV) works by superimposing constant-size pulses on a linear potential slope [74]. When a symmetric square wave waveform is overlaid on a base tray voltage and delivered to the working electrode, square wave voltage (SWV) is measured [75]. A cut-off voltmeter, more precisely an anodic voltmeter (ASV), works in two stages. The first step is to oxidize the organic pollution molecule and generate electrons that will be transported on the electrode surface. The pickling stage is the second step, in which the pollution molecule will be reduced. Following the two stages, various variables, such as electrode material, scan rate, matrix material and its concentration, pH of the studied sample are known to impact the analysis [69,76]

Figure I.2 depicts how the possibility for CV, LSV, DPV and SWV to create a signal evolves over time. The combination of several of these approaches improves sensitivity and detection limitations. Differential pulse anode voltimeters (DPASV), square wave anode scanning voltimeters (SWASV), and linear scanning anode voltimeters are included in the kits (SWASV).

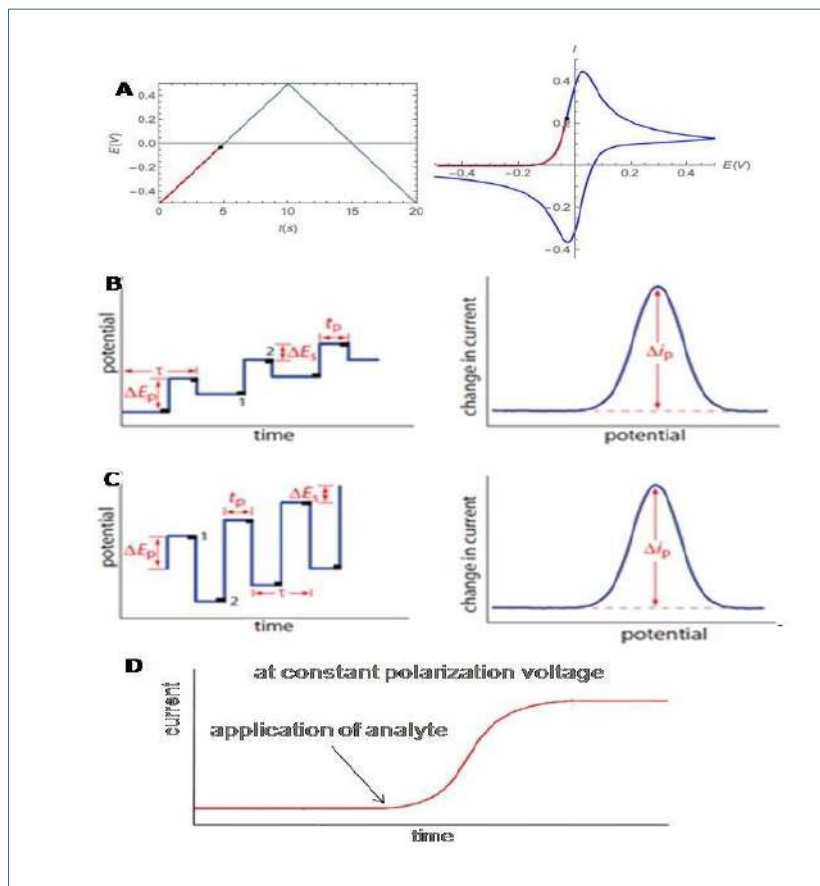


Figure I.2. Electrochemical techniques - parameters and characteristic voltammograms: A) cyclic voltammetry, B) differential pulse voltammetry, C) square-wave voltammetry and D) amperometry. Reproduced from scindeks [77].

I.3.1. Three-electrode system

A working electrode, a counter electrode, and a reference electrode are often used in a three-electrode electrochemical setup. Between the working and reference electrodes, a voltage is supplied, and the current is measured between the working and meter electrodes [78]. The electrochemical reaction occurs with the transport of electrons at the working electrode. The working electrode material is generally chosen to be redox sensitive. The reference electrode maintains a constant voltage and current over time. Normal hydrogen electrode (NHE), saturated calomel electrode (SCE), and silver-silver chloride electrode are examples of standard reference electrodes [79,80]. There are certain disadvantages to this sort of bipolar system. Current flowing via the reference electrode depolarizes over time, resulting in a steady drift potential. Because such a tiny voltage difference between the working and reference electrodes can lead to significant measurement error, the three-electrode method is currently utilized by adding a counter electrode

that can assist pass the bulk of the current to assure the reference electrode's steady potential [78]. The counter electrode is frequently made of gold or platinum, which is difficult to polarize. The meter electrode is generally the biggest, which aids in current conductivity.

I.3.2. Types of sensors

The use of chemical sensors is a very interesting topic in environmental monitoring [67, 69 ,81]. A sensor typically consists of three components: a sensing element that responds to a certain analysis (target chemical type); a transducer element that transforms this response into a quantifiable signal; and lastly, a measurement element that records the sensor's [82].

Electrochemical sensors are less versatile (they are unique to a single analyzer) than in vitro analytical methods, but they have the benefit of being extremely portable and capable of providing quick (if not real-time) detection of pollution and other target compounds in situ. They also have basic designs that need little or no sample preparation, are simple to install and use, and are yet reasonably priced. However, they are typically restricted in that they are less accurate and more vulnerable to false positives due to chemical species interference from the laboratory analytical process. Depending on the recognition element used to detect the target analyte, portable chemical sensors are classified into three types: biosensors [83], electrochemical sensors [67], and biomimetic sensors [84].

I.3.3. Electrochemical sensor

Electrochemical sensors make use of an identifying element known as a matrix, which can be MIPs [85], MOFs [86], carbon compounds [87], or metal oxides nanoparticles (NPs) [88]. Natural recognition elements attach to a specific chemical molecule with great precision [82,89] and are then converted into a quantifiable outcome.

I.3.3.1. Background of Electrochemical Sensors

As can be seen in **figure I.3**, an electrochemical sensor includes: a) the identification of elements related to analysis; b) the transducer where a specific reaction occurs interface with recognition elements and results in the appearance of a signal; and c) an electronic system that converts the electronic signal into a meaningful parameter describing the running process. A human operator interface was used to study and show the final data. The following requirements must be met by a high-performance electrochemical sensor for the non-specialized market:

- For the objectives of analysis, the elements of recognition must be highly specific. It is stable under normal storage settings and exhibits acceptable variations between tests.
- The reaction must be unaffected by physical factors such as convection, pH, and temperature.
- The response must be timely, accurate, repeatable, clear, and written on the proper focus range. Untreated samples, such as human blood or urine, must be able to be measured.
- The entire sensor should be low-cost, compact, tiny, portable, and simple to install.

Nanomaterials that function as chemical catalysts are used in the sensor array or sensor recognition element. Its porous structure conducts electricity and serves as an electron transfer agent. The matrix components' electrocatalytic activity allows them to convert the target analyte into a product molecule and transmit the generated electrons to the sensor surface and then to the transducer [90,91]. Nanomaterials such as MIPs [85], MOFs [101], carbon compounds [87], or metal oxides nanoparticles (NPs) [88]. must be immobilized and bonded to the surface of a working electrode such as glassy carbon (GCE) electrodes, platinum (Pt) electrodes, and gold (GE) electrodes to alter this interaction. A detecting capability is provided to the working electrode, allowing electrochemical measurements (CV, DPV, SWV, etc.) to be done within the framework of an electrochemical half-cell holding the sample to detect the reduction or oxidation of any analyte.

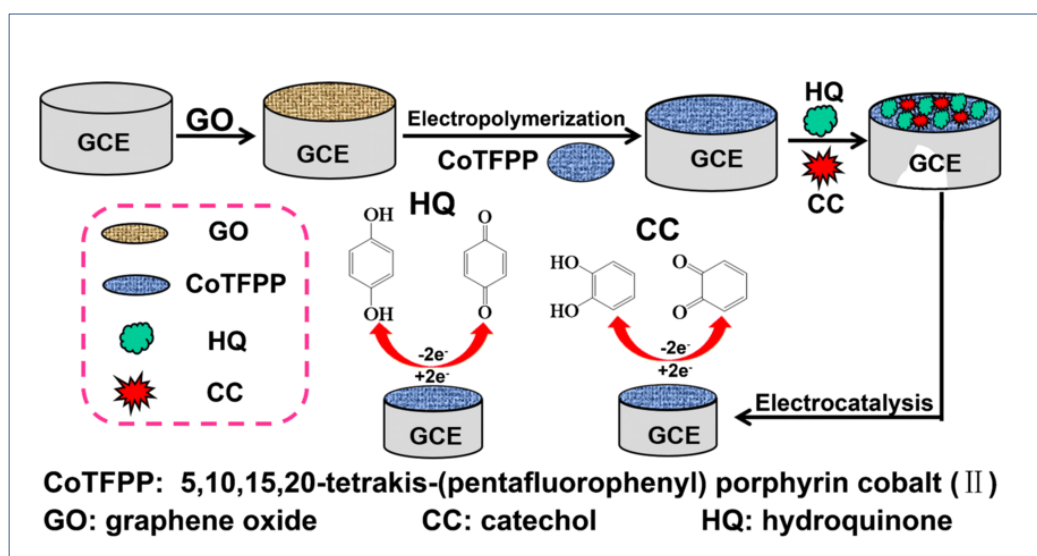


Figure I.3. The fabrication process of the sensor and the catalytic mechanism for the oxidation of catechol and hydroquinone. Reproduced from Springer [92].

It was created for this purpose, which is an important element of electrochemical sensor design. Choosing an electrochemical detection approach that allows for easy, quick, and precise measurements of the reaction of interest [87,93]. Typically, in electrochemical detection, the investigated reaction produces either a detectable current (amperometric)[94], a measurable potential or charge buildup (potentiometric) [95], or a measurable change in the conductive characteristics of a medium (conductivity measurement) between the electrodes [96]. When an electric field is produced between two electrodes immersed in electrolyte solution, current flow is created by migration of ions with opposing charges. Among the three major electrochemical methods, this conversion is the least sensitive. It is hard to differentiate between two ions because conductivity is cumulative. Furthermore, if the ion concentration is too high, it might cause injury to others. The voltage measurement is determined by the difference in output potentials. Activity is transmitted across a membrane put between two solutions with different kinds of charges. Voltage sensors are well suited to detecting low concentrations in tiny volumes. Because it has no chemical effect on the sample, sample volume. Amperometry measures the current generated by the oxidation or reduction of a sample's electrically active species [94,97]. Since then, this has been the most commonly utilized method. An analyte's inherent characteristic is its oxidation or reduction potential. In general, if the current is measured at a constant voltage, it is referred to as measuring the current; if the current is measured within a regulated potential range, it is referred to as Voltmeter measurement.

I.4. Analytical characteristics of electrochemical sensor

Any electrochemical sensor has certain static and dynamic attributes. Optimization of these parameters affects the performance of the sensor [98]

I.4.1. The linear range

Linearity expresses the precision of the response to a group of measurements at different concentrations, where the slope of linearity is the sensitivity of the sensor. linearity good resolution is required because most biosensor applications require not only detection of the analyte, but also measurement of analyte concentrations over a wide operating range [116,99].

I.4.2. Limit of detection (LOD)

It is defined as the smallest concentration of the analyte to be detected by the sensor. To calculate the limit of detection (LOD), the researchers conventionally use the formula ($LOD = 3S / N$) to distinguish the signal (S: calculated by the standard deviation SD of the calibration curve) from the noise of the device (N: Noise) [100].

I.4.3. Selectivity

Selectivity is an important characteristic to consider when choosing a biometric sensor receptor. The receptor can detect a specific target analyte molecule in a sample. It consists of a mixture of spices and unwanted contaminants. To construct a sensor, selectivity is the main consideration when choosing bioreceptors [101,102].

Sensitivity and selectivity are two additional key elements of electrochemical sensor development [66,103]. What differs an electrochemical biosensor from a sensor is the immobilization of a biomolecule in the recognition element of the sensor [104]. Immobilization of biomolecules on the working electrode surface such as enzyme [105] and DNA [106] are very efficient approach to enhance current responses and interfaces with a highly precise binding affinity for the targeted analyte [107-109].

I.4.4.4. Reproducibility

Reproducibility is the ability of a sensor to generate identical responses for a reproducible experimental setup [110]. It is characterized by precision (similar output when the sample is measured more than once) and precision (the ability of the sensor to generate an average value closer to the actual value when measuring the sample every time). It is the ability of a sensor to produce identical results whenever they are similar. The sample has been measured more than once (44).

I.4.4.5. Stability

Stability is the degree to which environmental disturbances are detected in and around the detection system. This is the most important feature in applications where the biosensor requires long incubation steps or continuous monitoring. The response of transducers and electronics can be temperature sensitive, which can affect the stability of the biosensor. Therefore, proper adjustment of the electronics is necessary to ensure a stable response of the sensor [111].

I.5. Electrochemical sensors preparation using conductive and semi-conductive nanomaterials

A few years ago, the uses of nanotechnology appeared far-fetched. However, with the discovery of new nanomaterials with novel characteristics, nanoscience research has grown dramatically, and as a result, nanotechnology applications and products have just lately begun to appear. However, nanotechnology applications are starting to emerge, and more research is needed to create novel discoveries and uses for these sorts of materials [112 -114].

As highlighted in **figure I.4**, nanostructured materials with characteristics smaller than 100 nm in particle size, layer thickness, or form are gaining prominence in nanotechnology [115,116]. The science and technology of nanomaterials and devices, as well as their applications in functionally categorized materials, molecular electronics, nanocomputers, sensors, actuators, and molecular machines, are all included in the topic of nanotechnology [66 ,103].

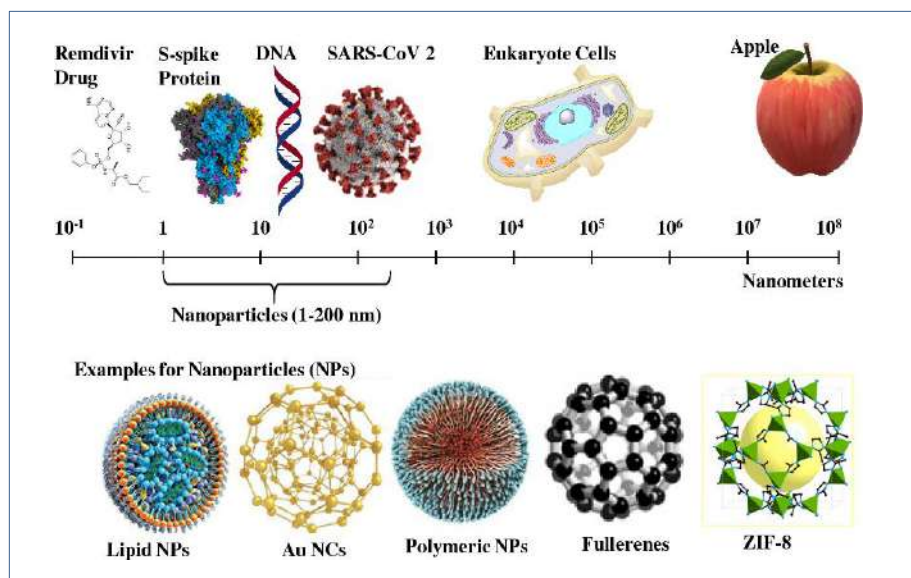


Figure I.4. Illustration of the nanoscale relative to biologically active molecules, and examples of nanomaterials of relevance for biomedical and bio sensing applications. Reproduced from Springer [117].

I.5.1. Carbon Materials

The discovery of atomic-level micro-materials such as fullerenes in the mid-1980s and carbon nanotubes (CNTs) in 1991, as well as graphene, resulted in a significant advancement in nanotechnology [118]. Other materials, including as metal-organic frameworks [119], metals and metal oxides NPs [88], and MIPs [120], have since been developed for application in nanotechnology advancements. Because of the remarkable characteristics of these materials, an

intriguing new field of study in nanoscience and nanotechnology has emerged. Furthermore, new characteristics have been identified, and prospective applications for this material are frequently proposed.

Carbon nanoparticles, polymers, and metal oxides study now spans numerous fields, with the objective of better understanding and utilizing these interesting materials. Other areas of research have been devoted to fundamental sciences in order to change the structure and surface of these nanomaterials. These materials characteristics have opened new vistas in chemistry, physics, engineering, medicine, and materials science [121,103].

I.5.1.1. Carbon nanotubes (CNTs)

The discovery of fullerenes at Buckminster Fuller in 1985 marked the beginning of a new era in carbon chemistry and the development of novel materials. Sumi Ijima of Japan discovered carbon nanotubes (CNTs) in 1991 [118]

Carbon nanotubes have gotten a lot of interest since they were discovered because of their field emission and electron transport capabilities, as well as their superior mechanical and chemical properties. As a result, there is a rising possibility for carbon nanotubes to be used as field-emitting devices [122], nano-transistors [123], microscopy tips [124], or components of composite materials [125].

Single-walled carbon nanotubes (SWCNT) and multi-walled carbon nanotubes (MWCNT) are the two kinds of carbon nanotubes [126]. As can be seen in **figure I.5**, SWCNTs are cylindrical nanostructures formed by rolling a single sheet of graphite into a tube. As a consequence, SWCNTs can be compared to molecular threads, with each atom on the surface [127,128]. MWCNTs are made up of a collection of such nanotubes that are piled concentrically like tree trunk rings. The figure below presents single walled carbon nanotube (SWCNT) and multi walled carbon nanotube (MWCNT) [129].

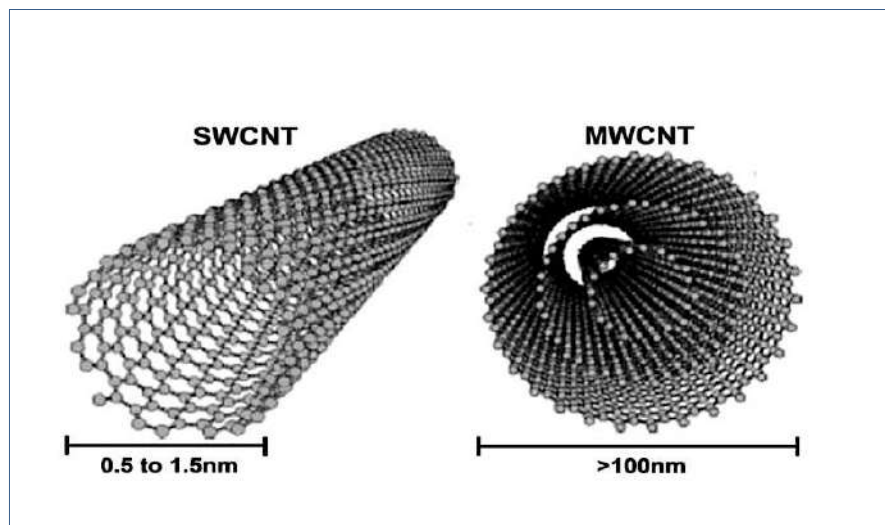


Figure I.5. Schematic of an individual (A) SWCNTs and (B) MWCNTs. Reproduced from Scielo [129].

Carbon nanotubes are one of the most common nanotechnology construction materials. Carbon nanotubes look to be an outstanding material, with tensile strength 100 times that of steel, thermal conductivity greater than the finest diamond, and electrical conductivity equivalent to copper but with much higher current carrying capacity. Much more crucial.

I.5.1.1.1. Structure and properties

Some properties of CNTs are stated below.

- ❖ **Electricity:** The structural characteristics of the nanotube reveal how twisted it is. Carbon nanotubes have the property of being extremely conductive and hence metallic. Its conductivity has been demonstrated to be a function of its symmetry, degree of torsion, and diameter [130,131].
- ❖ **Mechanical:** The tiny diameter of carbon nanotubes has a large effect on mechanical characteristics when compared to graphite fibers of typical micron size. The ability to connect high elasticity and strength with high toughness, which is not present in graphite fibers, is perhaps the most noteworthy consequence. These characteristics of carbon nanotubes open the way for the creation of a new generation of high-performance composites. The nanotube as a whole is highly flexible because to its length [158,132].
- ❖ **Chemical:** The large specific surface area and sp^2 -rehybridization enable particle adsorption, doping, and charge transfer on nanotubes, as well as electronic property modification [133].
- ❖ **Thermal and thermoelectric:** The heat conductivity of nanotubes is quite high. As a

result, nanotube reinforcements in polymeric materials are predicted to improve the thermal and thermomechanical characteristics of these compounds substantially [134].

I.5.1.1.2. Synthesis and purification

Arc vacuum, laser ablation, and chemical vapor deposition (CVD) are three well-established techniques for constructing carbon nanotubes (**Table I.2**).

However, in order for carbon nanotubes to be employed in new technologies, these highly crystalline materials must be mass-produced at a reasonable cost on a huge scale. CVD catalytic technology, namely the floating catalyst technique, is the best way for producing high number of carbon nanotubes in this context. This approach is more regulated and cost-effective than arc unloading and other procedures [135-139].

Table I.2. Summary and comparison of the most important synthesis procedures for CNTs.

Synthesis method	Principle	SWCNTs or MWCNTs	Reference
Arc-discharge	Carbon atoms are produced via an arc discharge between two electrodes at temperatures exceeding 3000°C. Nanotubes (Fe, Co, or Ni) form when appropriate catalyst metal particles are present.	Both	[135] [136]
Laser-ablation	Carbon nanotubes are created utilizing laser ablation technique, which involves irradiating a graphite rod with stimuli heated to 1,000°C or more with a pulsed laser.	SWCNTs	[137]
Chemical Vapor Deposition (CVD)	Metal nanoparticles (Co or Fe) increase the breakdown of the gaseous source of hydrocarbons at high temperatures (500-1000 ° C) (ethylene or acetylene). Carbon has a poor solubility in some metals at high temperatures, causing it to precipitate and form nanotubes.	Both	[138] [139]

I.5.1.1.3. Carbon nanotube in electrochemical sensors

As highlighted in **table I.3**, Carbon nanotubes have an extremely high electrical, thermal, and mechanical conductivity. It opens up a slew of new opportunities in materials research, electronics, chemical processing, energy management, and a variety of other fields [87,140, 133].

Table I.3. Comparison with state-of-the-art catechol sensors based on carbon nanotubes.

Sensing interface	Pollutant	Linear range (μM)	LOD (μM)	Reference
Lac/MWCNTsCOOH/AuNPsSDBS/PEDOT/GCE	CC	11.99 – 94.11	12.26	[141]
GCE/MWCNT@CADE	CC	0 – 1000	-	[142]
Co ₃ O ₄ /MWCNTs/GCE	CC	10 – 700	8.5	[143]
MWCNTs@reduced graphene oxide nanoribbon/GCE	CC	15 – 1101	1.73	[144]
PDEA-PS/C ₆₀ MWCNT/GCE	CC	4 – 135	1.45	[145]
c-MWCNTs/PDAd(b-CDe)/c-MWCNT/GCE	CC	0.25 – 4000	0.04	[29]
Gr-CDP-MWCNTs/GCE	CC	0.1 – 27.2	0.03	[30]
Modified CPE (RGO-MWNTs)	HQ	1-120	0.3	[51]
Modified GCE [Cu(Sal- β -Ala)(3, 5-DMPz) ₂]/SWCNTs	HQ	8-391	1.46	[146]
MWCNTs@RGONR/GCE	HQ	15-921	3.89	[144]

I.5.1.2. Graphene

Graphene is an atomically thin two-dimensional (2D) honeycomb sheet of sp² carbon atoms [147,148] (**figure I.6**). It has been demonstrated to have several desired qualities, including strong mechanical strength [149,132], electrical conductivity [150], and molecular barrier capabilities [151]. As a result of these factors, several research attempts have been made to combine graphene into various nanomaterials and nanocomposites such as carbon nanotubes, polymers, metals, and metal oxides to manufacture and develop electrochemical sensors and biosensors [152-154].

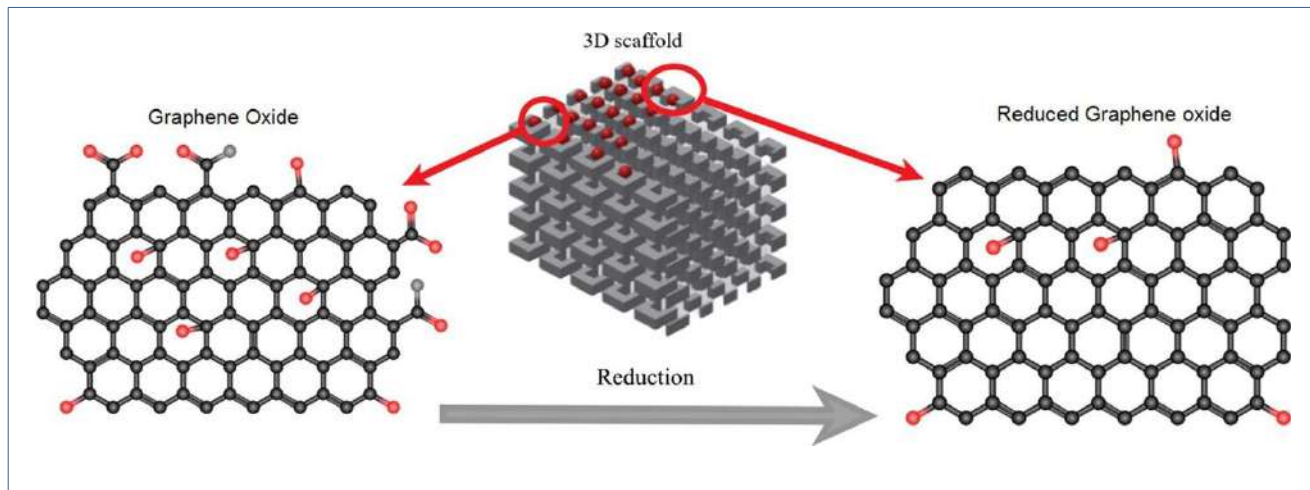


Figure I.6. The structure of Graphene, Graphene Oxide and Reduced Graphen Oxide. Reproduced from Science direct [176].

I.5.1.2.1. Synthesis and preparation

When it comes to the production of graphene and its derivatives, the intended structure and characteristics are heavily influenced by the size, shape, and functional groups linked to the material's surface [155]. The ideal structure is a single-atom sp^2 monolayer graphene with minimum imperfections, which is a completely hybridized carbon structure. However, because to the ease with which graphene sheets may be stacked, a multilayer graphene structure will be created. As previously stated, installing such structures from the ground up has proven difficult for industrial purposes [156]. As a result, it is easier to generate the highly oxidized form of graphene, GO, with sp^2 and sp^3 carbons containing abundant oxygen groups, which upon reduction (rGO) can remove most of the oxygen groups and sp^3 carbon to generate a more “graphene-like” material with significantly improved properties. The top-down method may then be used to control GO and rGO to create quantum dots of both GOQD and rGQD [157].

I.5.1.2.1.1. Synthesis of GO

Bottom-up procedures, in which single carbon molecules are utilized to produce pure graphene, and “top-down” methods, in which layers of graphene derivatives are removed from a layer, are the two primary types of GO synthesis. Graphite is a common carbon source [158,159]. Bottom-up synthesis (for example, chemical vapor deposition, epitaxial growth on silicon carbide wafers, and so on) is time-consuming and has scaling issues [160,161]. As a result, top-down techniques that produce GO and/or rGO first are more common for producing graphene derivatives,

particularly for usage in nanocomposites materials. Brodie [162], Staudenmaier [163], Hummers, and Offeman [164] are generally credited with the first synthesis of GO, both of which are produced from graphite oxide by oxidizing graphite using distinct methods. To make the two original techniques safer, Hummers and Offeman modified them by using KMnO_4 as an oxidant (rather than KClO_3 , which generates hazardous ClO_2 gas) and adding sodium nitrate (to create nitric acid on site rather than using nitric acid as a solvent). Because the Hummers technique is more safe and scalable, it is generally used (or, in most cases, somewhat modified) to construct GO [162,165].

I.5.1.2.1.2. Reduction of GO to rGO

Extensive research has been conducted to remove functional oxygen groups from GO in order to generate materials with characteristics as near to pure graphene as feasible [166,167]. This reduction can be accomplished by a variety of methods, ranging from thermal to chemical to electrochemical, each of which results in variations in morphology, electrical characteristics, and so on [166,168]. The final product's C/O ratio, selectivity in eliminating one kind of oxygen group (hydroxyl vs. carboxylic acid vs. epoxy, etc.), and healing of surface defects are all important design variables for GO reduction. Oxidation, selection of green reducing agents, and preservation or enhancement of the required physical and chemical properties of GO (mechanical resistance, conductivity, optical properties, solubility/dispersion of nanosheets, and so on).

I.5.1.2.2. Electrochemical sensors and RGO

As previously stated, when encapsulated in carbon nanomaterials and/or metal-based arrays, rGO exhibits excellent electrical conductivity characteristics. It is not unexpected, then, that this rGO has good operability in the presence of electrical catalysts [169,170]. Recently, the combination of nanomaterials with electrochemical sensing platforms has shown to be a strong analytical technique for detecting phenolic compounds [170,153] (**table I.4**).

Table I.4. Comparison with state-of-the-art catechol sensors based on reduced graphene oxide

Modified electrode	Linear range (μM)		Detection limit (μM)		Reference
	CC	HQ	CC	HQ	
CNCs-rGO	1–400	1-300	0.4	0.87	[171]
Au-PdNF/rGO	2.5-100	1.6-10	0.8	0.5	[172]
P-rGO	5-120	5-90	0.18	0.08	[173]
AgNP/MWCNT	20-260	2.5-260	0.2	0.16	[174]
rGO	1-200	6-200	0.1	0.2	[176]
rGO-MWCNTs	5.5-540	8-391	1.8	2.6	[177]
rGO/Fe ₃ O ₄ /AuNPs	0.05–550	0.1–500	0.02	0.17	[178]
NiO/rGO/fMWCNTs	10-300	10-300	0.019	0.040	[13]

I.5.2. Layered double hydroxide (LDH)

Layered double hydroxides (LDHs) are two-dimensional nanostructured materials with unique physicochemical properties. They are the enthralling class of inorganic materials with adjustable chemical composition and structures. They are also identified as hydrotalcite or anionic clays. By composition, they consist of positively charged layers of metal hydroxides with charge-balancing anions and some water molecules situated in between the layers. They are denoted by the general formula $[\text{M}^{2+}_{1-x}\text{M}^{3+}_x(\text{OH})_2]_x^+ (\text{An}^{x/n-})_x \cdot m\text{H}_2\text{O}$, where M^{2+} and M^{3+} are di- and trivalent metal cations and An^- is the interlayer guest ions with n - valence [179,180]. From the structural point of view, LDHs have resemblance with brucite, $\text{Mg}(\text{OH})_2$, in which Mg^{2+} is surrounded by six OH^- ions and the resulting octahedral structures are connected to each other forming an infinite two-dimensional layer. Brucite layers get positively charged by replacing some divalent ions with trivalent ions. This positive charge is then balanced or neutralized by localizing anions in the interlayer spaces. Water molecules are also intercalated in the interlayer spaces stabilizing the structure of resulting LDHs. The stability of LDH structure comes from electrostatic interaction and hydrogen bonding between the layer and interlayer contents. The structures of LDHs are amenable to desired fine-tuning by changing the divalent and trivalent ions and intercalated anions. The selected di and trivalent ions should have their radii not

significantly different from those of Mg^{2+} and Al^{3+} . LDHs are characterized by the unique features of being low-cost, nontoxic, high surface area, two-dimensional structure, replaceable intercalated anions, positively charged surface and tunable internal and external architecture [181]. Their unique applications emerge from their highly porous structure, large anion exchange capacities, and water resistant structures. LDHs have been extensively used in catalysis [182], flame retardants [183], fuel cells [184], drug delivery [185], analytical extractions [186], and in many other areas [187].

I.5.2.1. Synthesis and preparation

Layered double hydroxide based electrochemical sensors fabrication is facile and their miniaturization in the laboratory is easy. Numerous methods are being used for the synthesis of the LDH including sol-gel method, urea hydrolysis, hydrothermal synthesis and the co-precipitation.

I.5.2.1.1. Urea hydrolysis

LDH with large crystallites, homogeneous distribution of particle size and with high crystallinity could be achieved using urea hydrolysis [188]. Urea considered as attractive precipitation agent for several metal ions as their hydroxide due to controllable hydrolysis rate using temperature and high-water solubility. One of the major drawbacks of the Urea hydrolysis as only the carbonate containing LDH could be prepared. The carbonate is continuously being generated due to the decomposition of the urea. It put a severe limit to get a wide variety of the LDH for varied applicability. R. Xu et al. synthesized 3D hierarchical flower-like Mg–Al-LDHs using urea for electrochemical sensor development and applied for the sensing of Cd(II) [189]. Similarly, a biosensor was developed consist of bi-protein/layered double hydroxide (LDH) ultra thin film for catechol. The LDH for the fabrication of the biosensor was synthesized by urea method under hydrothermal treatment [190]. In some reports, synthesized LDH was vigorously agitated in formamide under a N_2 flow at room temperature for several hours. The formamide allows to swell and exfoliate the LDH particles and it is a facile method to get LDH single nanosheets without provision of heat or refluxing treatment [219,191].

I.5.2.1.2. Hydrothermal synthesis

Hydrothermal method is generally used when co-precipitation or ion exchange method is not feasible for synthesis of the desired LDH and especially in a situation where organic guest species

of low affinity are required to intercalate in the LDH layers [192]. Yang et al [193], proposed a facile hydrothermal strategy is adopted to synthesize the composite of NiCo-layered double hydroxide(NiCo-LDH) with biomass carbon while another group prepared a novel Zn-Mg-based LDHs over a copper substrate by using a hydrothermal method. The work reported Two types of Zn-Mg-based LDH coating are prepared based on hydrothermal reaction time [194].

I.5.2.1.3. Ion exchange method

Ion exchange is another method through which the LDH could be prepared. The ion exchange method is preferred over co-precipitation where the divalent or trivalent metal cations or the anions involved are unstable in alkaline solution. The ion exchange method is promising when there is more feasibility of the direct reaction between metal ions and the guest anions. This method could be used to replace the interlayer anions with guest anions to achieve desired characteristic LDH. J. Dong replaced the interlayer's anions of the LDH by EDTA²⁻ anion to attained EDTA-LDHs composites for ultra-trace level determination of Pb (II) [195]. Mg–Al–thioglycolic acid (TGA) LDH nanoparticles were also synthesized by anion exchange method. The method consisted of two steps; synthesis of LDH and then incorporation of TGA through anion exchange reaction [196].

I.5.2.1.4. Co-precipitation method

For most of the LDH and LDH-hybrid modified electrochemical sensors, LDH was synthesized using Co-precipitation method [220,197,198]. For instance, a co-precipitation method was used to synthesize Fe/Mg/Ni ternary LDHs which were later used for fabrication of modified electrode [199]. Generally, the hydrothermal assisted co-precipitation was used for the synthesis of the desired LDH [200]. M. Asif et al. synthesized core-shell Fe₃O₄@CuAl LDH NSs using a facile hydrothermal and co-precipitation method, and it was drop cast on GCE [201]. The schematic is given below in **figure I.7**. Similarly, CuO@MnAl NSs were prepared by facile co-precipitation and hydrothermal routes. The synthesis protocol is given in **figure I.8**.

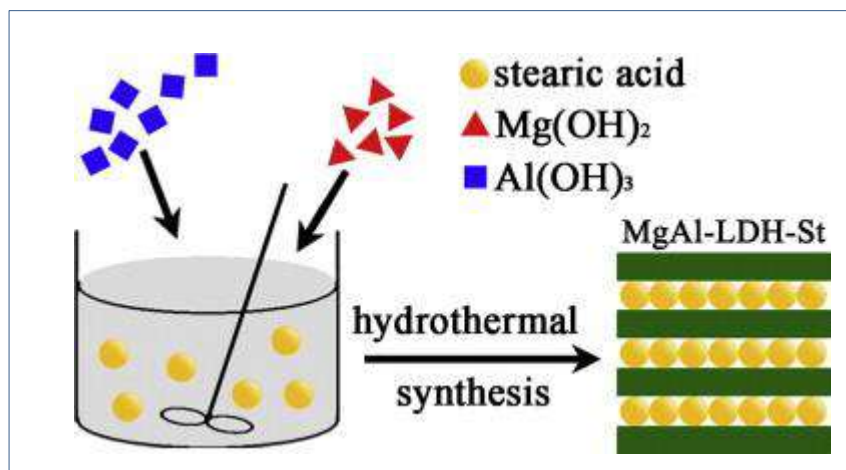


Figure I.7. Flow chart of the synthesis mechanism of MgAl-LDH-St. Reproduced from Science Direct [201].

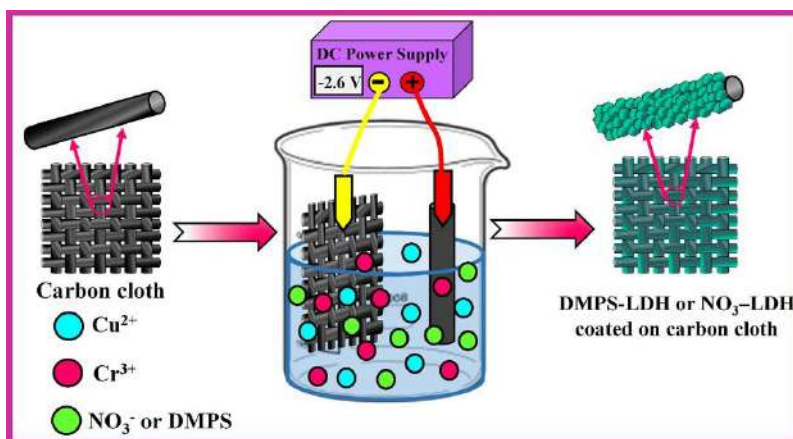


Figure I.8. Schematic illustration of the fabrication mechanism of Cu Cr-layered double hydroxide nanosheet intercalated with 2,3-dimercaptopropane sulfonate (DMPS-LDH). Reproduced from Elsevier [218].

I.5.2.1.5. Electrochemical synthesis of LDH on the electrode surface

In this method, LDH is electrochemically synthesized on the bare or previously modified electrode surface [202] [203]. This is accomplished through dipping the electrode into a solution containing LDH precursors of known concentration. For example, LDH was synthesized over GNs modified electrode via dipping of exfoliated GO/GCE into an 0.3 M KNO₃ solution comprising 22.5 mM Ni(NO₃)₂ and 7.5 mM Al(NO₃)₂, and then cycling the potential between 0.1 and -1.4V (versus SCE)

at a scan rate of 50 mV/s for 8 cycles [232]. Similarly, some other methods have been reported for electrosynthesis of LDHs on different electrode surfaces [204 ,205].

I.5.2.2. LDH in electrochemical sensors

Several studies have shown that LDHs are emerging materials for chemical modification of electrode surfaces (**figure I.9**). Generally, in trace and ultra-trace analysis, such materials allow analytes to confine into a minimal volume near the electrode during preconcentration step leading to low limits of detection (LODs). LDHs can improve sensitivity and selectivity of detection as they allow to immobilize electrocatalytic reagents [206].

LDHs in electrochemical sensing play one or more of the following roles.

- Electrocatalysts.*
- Adsorbents for stripping analysis.*
- A surface for immobilization of other modifiers or biomolecules.*



Figure I.9. Key characteristics of LDH modified electrodes.

J. Dong et al. fabricated a highly sensitive carbon paste electrode for the detection of the Pb based on the EDTA/Mg/Al/LDH. EDTA [H₄Y] is a well-recognized chelating agent. It forms stable complexes with the heavy metals. In LDH, the EDTA is intercalated by anion exchange method. EDTA can easily replace the anions of the interlayer of the LDH when pH is maintained from 4 to 6 due to its presence in form of anion [H₂Y]²⁻. The fabricated electrode is suitable for the stripping analysis of different metal cations. Modified electrode displayed an excellent

electrocatalytic activity and sensitivity for the sensing of ultra-trace level Pb in the tap water and demonstrated very low limit of detection 0.95 ng/L. Apart from this, the developed method was also validated by ICP-AES [195]. Isa et al. successfully used Zn/Al-LDH-MPP/SWCNT/PE for the determination of Hg (II) in various samples. In this method, the synergistic effect of the SWCNT and the LDH has been used to enhance the sensitivity of the electrode. The SWCNTs have excellent conductivity, fast response time and a wide working range while LDH has an excellent ion exchange capability. The developed sensor exhibited superb detection limit of 1 nM. The regeneration of the surface could be attained by mechanical polishing and does not need for various cleaning agents [207].

The sensitivity and the selectivity of the electrochemical sensor for the determination of the Hg (II) can also be improved by introducing the chelating agent. Thiol group demonstrates an excellent chelating capability for the Hg (II). The thiol group eSH form the mercaptides by interacting with the metal ions [208]. K. Asadpour-Zeynali and Roghayeh Amini incorporated thioglycolic acid (TGA) in the interlayers of the Mg–Al LDH. TGA was intercalated into the LDH using anion exchange method. The developed electrochemical sensor was applied for the trace level quantification of Hg (II). The response of the Mg–Al–TGA LDH/GCE towards Hg (II) was influenced by the pH change. The maximum response was attained at pH 4. At higher pH, the response was decreased due to the hydrolysis of the metal ions and at lower pH due to LDH instability. TGA in LDH is playing great role for accumulation of Hg (II) due to the strong chelating capability thiol group for the Hg (II). The chelating behavior is one of the factors that improve the sensitivity of the Mg–Al–TGA LDH/GCE and helps to achieve very low limit of detection 0.8 nM [196].

Due to its increasing use in different applications and concerns about toxicity, it is imperative to monitor H₂O₂ levels in various environmental compartments. CoAl LDH/MWCNTs nanocomposite modified CPE was used for determination of H₂O₂. Cobalt species in the composite catalyzed the electrooxidation reaction, and CoAl-LDH enhanced the electro-reduction process while MWCNTs have shown the significant electrocatalytic effect on both the electro-reduction and electrooxidation of hydrogen peroxide. The applicability of the proposed sensor was tested in river and wastewater, and very good recoveries were obtained [209]. Silver was electrodeposited on LDH-modified GCE to fabricate a sensor for H₂O₂ detection. LDH

provided a stable matrix for electrodeposition of Ag structures. The porous structure of the Ag nanodendrites provided a large surface area for the electrochemical reactions and enhanced the sensitivity of the sensor. The LOD was 2.2 μM . The sensor was used to determine H_2O_2 in spiked milk samples, and outstanding recoveries were obtained [200]. LDH modified electrodes have been fabricated for the sensitive, selective and low-cost detection of various pesticides. S. Khan et al. used zinc and vanadium for the formation of LDH on the silver electrode. The i-v curve was attained at different concentrations of thiourea. The current was increased as the concentration of the thiourea increased. The change in current due to the addition of thiourea could be explained by the adsorption of atmospheric oxygen on the LDH prior to analysis. The LDH attained positive charge due to the transfer of electrons to oxygen and formed Oads^- . The potential barrier increased at grain boundaries and the transducer conductance decreased. Oads^- could decrease the potential barrier at grain boundaries by releasing the trapped electrons to LDH conduction band. The conductance of the sensor increased as the energy released by the decomposition of the adsorbed molecule is sufficient for transfer of an electron to the conduction band. Thiourea reacts with negative charged adsorbed oxygen and facilitates the transfer of electrons to the conduction band. The linear range was observed from 10 to 500 μM for thiourea [210]. Similarly, pentachlorophenol is also included in priority pollutants list by USEPA. At a large scale, the pentachlorophenol is being used as bactericide, disinfectant and the wood preservative. The territorial and the aquatic ecosystem is badly contaminated due to large scale use of pentachlorophenol. S. Yuan developed a bi-functional sensor which could simultaneously analyze the copper ions and the pentachlorophenol. For this purpose, the multilayers films of the humic acid and the Mg–Al-LDH were developed on the ITO electrode using a layer-by-layer methodology. The layer-by-layer assembly is facilitated by electrostatic attraction of the negatively charged humic acid and positively charged LDH. The combined properties of humic acid and Mg–Al-LDH facilitate the fast charge transfer, enrichment of the target analytes and simultaneous sensing. Very low limit of detection 0.4 nM and 2 nM was attained using (LDH/HA)/ITO for pentachlorophenol and copper ions, respectively [211]. Similarly, the simultaneous determination of catechol and hydroquinone in the presence of resorcinol was done by fabricating a dihydroxybenzene sensor. The Zn/Al layered double hydroxide film sensor was developed by direct electrochemical deposition of the divalent Zn and trivalent Al on the surface of the glassy carbon electrode. The developed sensor exhibited good capability to cope with potential interferences in the presence of targeted analytes

[212]. M. Shen et al. synthesized hierarchical NiAl/LDHs using room temperature ionic liquid 1-butyl-3-methylimidazolium tetrafluoroborate as a soft template. The hierarchical NiAl/LDHs could provide more exposure to the electroactive site, huge surface area, fast charge transfers and better stability. The fabricated sensor with H-NiAl/LDHs exhibited a great electroactivity for the electrooxidation of hydroquinone and catechol by shortening the diffusion path and facilitating with mass transport channels and easing the electron transfer. The limit of detection 3 nM was observed for the hydroquinone and catechol [213]. **Table I.5** represents recent electrochemical sensors based on LDH as sensing platform.

Table I.5. Comparison with state-of-the-art electrochemical sensors based on LDH.

Sensing interface	Pollutant	Linear range (μM)	LOD (μM)	Reference
Co-Al-SDBS HT/GCE	2-chlorophenol	0.005–0.5 μM	0.002 μM	[197]
(LDH/HA)8/ITO	Cu(II), pentachlorophenol	3–320 nM,	2.0 nM,	[211]
Mg-Al-SDS/GCE	Bisphenol A	0.008–2.808 μM	2.0 nM,	[214]
CHT/[Zn3-Al-Cl]/PPO/GCE	CC	3.6 nM–40 μM	0.36 nM	[215]
HeNiAl/LDHs	CC/HQ	0.6 μM –6 mM	0.1 μM	[213]
LDH/HB/LDH/HRP) ₂ UTF	CC	6–170 μM	5 μM	[190]
LDH-PCNT/GCE	CC	10–200 μM	0.27 μM	[216]

I.5.3. Metal organic framework MOF

Metal organic framework (MOF) are a developing class of porous nanostructures formed by ions/metal groups and membership connections, with promising applications in gas absorption, rejection, stimulation, energy storage, chemical sensors, cancer therapy, and medicines [217-219].

Delivery Particularly considering its wide selective surface space, multi-chemical activities, changeable pore size, and close relationships with essential molecules.; plus, apparent interactions, including π - π stacking, hydrogen bonding, and electrostatic force, can be formed between the functional groups (-NH₂ or -COOH) in MOFs linkers and probe biomolecules, making MOFs an

excellent platforms for biomolecules and drug delivery systems in the environment or medicine applications [220,221].

More precisely, as shown in **figure I.10**, metal organic frameworks (MOFs) are a kind of crystal porosity composed of inorganic metal centers and organic bridge connections [222]. Because of its high surface area, numerous and customizable pores, and chemical resistance, it has been widely used in heterogeneous stimulation, absorption, medication administration, power storage, and sensors [218,219].

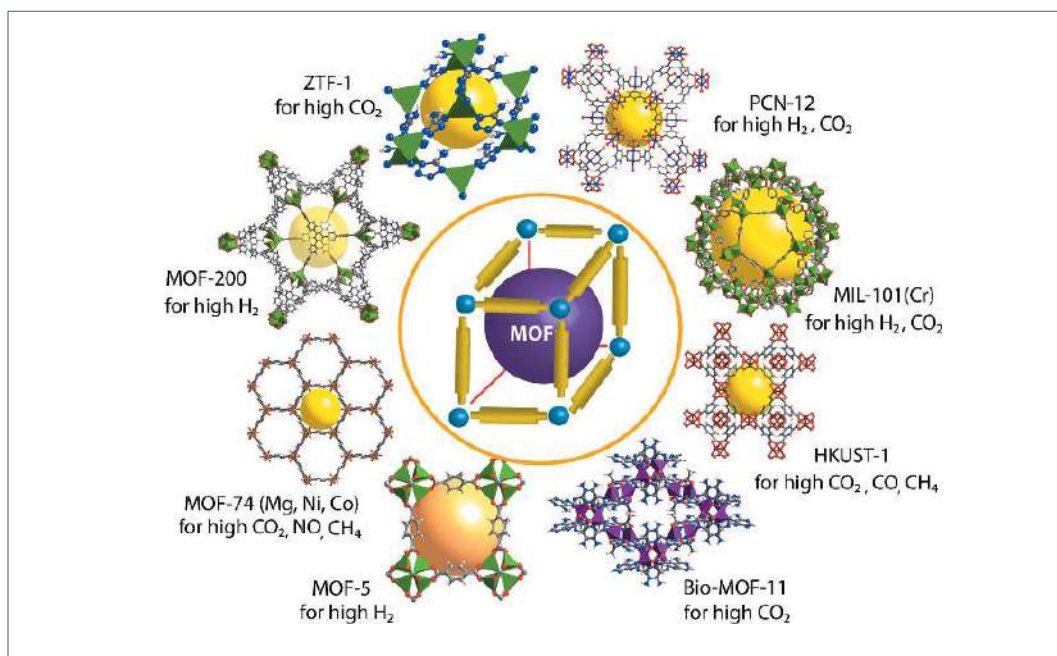


Figure I.10. Schematic representation of important reported MOFs which are known for high gas storage properties. Reproduced from wiley [223].

Metal organic reinforcements have piqued the interest of numerous researchers during the last two decades as novel functional materials. These novel hybrid porous materials are created by combining organic and aggregate connections that include metals or contractual metals. Almost any metal, as well as a wide range of organic species, may be utilized to construct adhesion frames, resulting in a wide range of organic metal tires with varying topologies and properties [224]. Hence, metal organic frameworks have the capacity to adapt during their chemically changed state due to the presence of functional groups in organic dependency. The capacity to create pores and their functions by selecting organic connectivity, functional group, metals, and activation technique distinguishes mineral organic frameworks from other solids

I.5.3.1. Synthesis and preparation

Because of the potential of customizing its structure dependent on its uses, it has been clearly focused on the synthesis of metal organic frameworks during the last decade. There are several ways for producing metal organic frameworks, including conventional, aided microwave, sonochemical, and chemical [225,226]. The primary difference between these methods is the type of the power input, which will be discussed in the following sections.

I.5.3.1.1. Conventional Synthesis routes (Ca)

It should be mentioned that the conventional method of assembling metal organic frameworks is the most popular. The needed energy is delivered into the system via typical heating sources. Because temperature is crucial in chemical processes, this path differs from the tract of heat solvent interactions (hydrothermal) and maximal thermal. While heat reactions take place in the CSS reactor (which is generally closed by baggage) under self-contained pressure, the temperature of the reaction must be higher than the solvent boiling point [227]. Typically, the temperature range for enlarging metal organic frameworks extends from ambient temperature to around 250 ° C. Because of the simplicity of installation, most metal organic frameworks are produced using heat solvents. As previously stated, this interaction often happens via the format link between organic and mineral salt in the solvent under the aforementioned circumstances, with the end result taking the shape of crystal or powder. Although temperature is an important component in most combinations, only few of the known metal organic frameworks, notably HKUST-1, MOF-5, MOF-177, MOF-74, and ZIF-8, were produced at ambient temperature [228].

The aspect associated with such interactions is that the sediment happens in a short period of time, which is sometimes referred to as direct sedimentation reaction; as a result, there will be a considerable decrease in interaction time [229]. In instance, ZIF-8 has superior chemical stability when compared to other compounds [230]. In general, the organic frameworks are significantly affected by the temperature of interaction, so that metal organic frameworks with different properties, such as different surface spaces and crystallization, can be obtained at different temperatures, whereas intensive metal organic frameworks are generally obtained at high interaction temperatures [231]. Furthermore, not only does high synthesis affect crystallization, but it also increases interaction rates, particularly when more interactive ions are employed [232]. As a

result of the long reaction time and significant energy consumption, other techniques of synthesis were developed.

Furthermore, different approaches can only diminish interaction. Save time and energy while simultaneously having a significant impact on particle formation, dispersion, and size. Pores, which have a significant impact on the properties of metal organic frameworks. In terms of gas separation and storage, the size of holes influences the distribution of guest molecules as well as the adsorption properties of porous materials such as metal organic frames. Because of these objectives, other artificial means such as microwave-assisted tracks, sonocular chemical corridors, mechanical and electrical systems have been used.

I.5.3.1.2. Microwave Synthesis (MW)

Microwave irradiation is a well-known method for creating materials [233]. This technique is based on the interaction of mobile electric charge with electromagnetic radiation. Electrons or ions in solids, as well as the presence of polar solvent and molecules / ions in solution, can offer electric shipment. As a result, the power supply and heating are generated in a solid form and a solution on the basis of the aforementioned discriminating mechanism. In the case of a solid article, the power is generated as a machine to compensate for the electrical resistance of the solid object Materials. The power supply is created in the solution by aligning the particles / ions when exposed to an electromagnetic field, the direction of which is constantly changing. where, For the best final product, a suitable frequency is required to create a suitable collision between The reagents contribute to increasing kinetic energy and temperature reaction Furthermore, due to the possibility of interaction between raw materials and megawatic radiation [234], the selection of selective power inputs and appropriate solvents is required and must be taken into account.

The synthesis reaction takes place in a microwave oven, and the interaction conditions must be met. It is specifically regulated in terms of temperature and pressure. Be reactionary for organic frameworks. It was finished at temperatures exceeding 100 ° C in less than an hour, which is faster than traditional procedures. The MW advised on how to raise the syrup rate while keeping the crystalline size low (mainly in the nanoscale). This artificial road is an excellent heating energy Effective technique due to its high reaction speed, short reaction time, and the interaction between the detector and radiation. As a result, the synthesis reaction can also take place at a rapid rate of

heating. Many studies reported the advantages of using microwave synthesis of MOF [235,236]. These studies confirmed that microwave irradiation reduces the time of reaction considerably, suggesting the effectiveness of this methodology in the synthesis of metal-organic frameworks. It is noteworthy that microwave assisted synthesis produces monocrystals suitable for X-ray diffraction studies, reducing reaction time and with higher yield than the classical hydrothermal procedures. To construct metal organic frameworks, other routes are available, including electrochemical, mechanochemical, and Ultrasound-mediated chemical interactions.

I.5.3.2. MOF in electrochemical sensors

Because of the structure of the macro / total porosity, high connector, and wide surface area, the composite of the organic metal works (MOFs) are becoming more attractive in the field of electrochemical senses [237]. However, the rational design of metal-metallic metal frameworks is still in its early stages for electrochemical vital sensors, and more significantly, there were a few metallic metal organic frameworks to detect phenolic compounds [27,28]. When employed in electrochemical vital sensors, nickel and copper-based organic frameworks, in particular, have good stability, stimulation, and low fascination activity, as well as a low vital conflict [238].

A series of nanoscale MOFs, such as Ni-MOFs and Cu-MOFs, have been reported to be efficient electrocatalysts for detecting analytes [239,241]. Compared with their bulk analogues, the nano-MOFs based electrochemical sensors showed significantly improved sensitivities and greatly decreased detection limits, even down to Nm or pM concentrations. Liu group [231] also investigated the influence of the nanostructure and particle size of Cu-BTC MOFs on the electrochemical response of sensors for detecting glucose. However, the decrease in the particle size may to a large extent result in serious aggregation during the electrode preparation process, which may in turn reduce the number of exposed active sites. To solve this problem, Liu et al. prepared monolayer-oriented Cu-BTC nanocube arrays via a facile interfacial emulsion synthesis method and further integrated these arrays in a flexible amino-functionalized graphene paper (NH₂-GP) electrode for both the static and dynamic measurement of lactate and glucose in human sweat [232].

MOF-based materials with core-shell heterostructures have been reported to have a good selectivity for detecting analytes. For instance, Yanng et al. [233] prepared a

core-shell heterostructure of Cu_xO NPs@ZIF-8 via the direct calcination of $\text{Cu}_3(\text{BTC})_2$ @ZIF-8 composites by considering the different thermostability of the two MOFs. The small Cu_xO NPs cores derived from $\text{Cu}_3(\text{BTC})_2$ were uniformly dispersed inside the ZIF-8 shell, which allows only small sized H_2O_2 molecules to pass through, while larger molecules are blocked. As a result, the fabricated electrochemical H_2O_2 sensor displayed a high selectivity towards interferents including uric acid, dopamine, amino acid, ascorbic acid, etc. Meanwhile, Cu_xO NPs without protecting MOFs suffered from serious interference effect. Although noble MNPs@MOFs were also widely reported for use in electrochemical sensor applications, noble MNP-based electrochemical sensors usually work best at high potentials, leading the electrochemical sensors to exhibit a poor selectivity.

Various methods have been employed to prepare MOF/MNP composites, most of which involve loading the MNPs on the as prepared MOF surfaces, forming surface attached structures, or encapsulating the as-prepared MNPs into MOF cages/channels, forming a totally surrounded structure [242]. For instance, Ma et al. [243] reported the attachment of AuNPs on metalmetalloporphyrin frameworks (Au NPs/MMPF-6(Fe)) via electrostatic adsorption. Due to the strong synergistic catalysis effects, enlarged active surface area, and high conductivity, the AuNPs/MMPF-6(Fe) composite could ultra-sensitively detect hydroxylamine at concentrations as low as nanomolar levels in real pharmaceutical and water samples. Likewise, Li et al. prepared composite by decorating Ag NP surfaced with MIL-101 MOFs to detect tryptophan [244]. In similar work, Ce-MOF/CNTs nanocomposites were prepared by a simple method and post-treated with $\text{NaOH}/\text{H}_2\text{O}_2$ mixed solution was prepared by Huang et al., [69]. The electrochemical behaviors of nanocomposite were also investigated on electrochemical work station. By utilization of the good electrical conductivity of CNT, the two-valence of Ce and the high surface area of MOF, the nanocomposites were used to fabricate the electrochemical sensor for the simultaneous electrochemical detection of hydroquinone (HQ) and catechol (CC). Compared to the Ce-MOF/CNTs/GCE, the post-treated Ce-MOF (TV)/CNTs/GCE exhibited two well-defined peaks for the electrochemical oxidation of HQ and CC. The linear ranges responding to HQ and CC are 10 ~ 100 μM and 5 ~ 50 μM respectively. Another work published by Dand et al, AuNPs-NH₂/Cu-MOF/GCE exhibits itself as a highly sensitive and selective electrochemical enzyme-free sensor for H_2O_2 detection. A quantitative detection to H_2O_2 can be found with a wide linear response

toward H₂O₂ concentrations ranging 5–850 μM, its limit of detection (LOD) is as low as 1.2 μM with a high sensitivity of 1.71 μA/cm²·μM. AuNPs-NH₂/Cu-MOF/GCE sensor has been applied to determine H₂O₂ effectively in human cervical cancer cells by adding the ascorbic acid as the stimulant. Our work presented a AuNPs-NH₂/Cu-MOF/GCE composite electrode which is a promising enzyme-free electrochemical sensor for quantitative H₂O₂ detection in human cervical cancer cells [245].

Table I.6. Comparison with state-of-the-art electrochemical sensors based on MOFs.

Modified electrode	Linear range (μM)		Detection limit (μM)		Reference
	CC	HQ	CC	HQ	
Ce-MOF(TV)/CNTs/GCE	10-100	10-50	2.05	2.05	[69]
TiO ₂ /C900/GCE	5-10	5-10	1.24	2.05	[246]
MOF-ERGO-5 / G	0.1-566	0.1-476	0.1	0.1	[247]
ZIF-8@rGO-0.02/GCE	10-70	10-70	0.47	0.37	[248]
Cu-MOF	0.2–184.5 (H ₂ O ₂)		0.067 mM		[249]
Ni-MOF	Nitrobenzene 0.25–1.5 mM;		NA		[250]
Cu-MOF	Histidine 0.1-200 μM		25nm		[251]
Cu-MOF	ASCORBIC ACID 0-4MM		14.97		

I.5.4. Metals and metal oxides

In the realm of electrochemical detection, nanoparticles, particularly metallic nanoparticles, provide several benefits. Nanoparticles, because to their tiny size, can enhance the surface area of the electrode utilized. Furthermore, metallic nanoparticles can speed up electron transport and enhance the sensitivity of the electrodes employed [252, 253]. In this section, we will discuss how different forms of metal nanoparticles may be used in electrochemical sensors.

Metal oxide nanoparticles have been the focus of extensive research in electrochemical detection in recent years. Varied techniques were used to produce different sizes, stability, and morphology. Because of these variations, they exhibit distinct electrical and photochemical characteristics, resulting in diverse applications [251]. Porous metals and porous metal oxides are examples of porous and nanostructured materials. They offer numerous exceptional properties (for

example, their unique pore structure, huge apparent surface area, and high electrical conductivity) that make them an amazingly attractive candidate for a wide range of essential applications (such as energy storage, detection and catalysis). Different metal oxides, particularly transition metal oxides, have been utilized to modify electrodes for the detection of various analytes, including heavy metals. Although virtually all transition metals have been utilized to manufacture these oxides, only a handful have been employed to detect organic pollutants [254] .

Many inorganic and organic components are found in porous materials, including carbon, metals, metal oxides, inorganic and organic hybrid materials, and polymers. Porous materials are classified as microporous (pore size 2 nm), porous (2 nm pore size 50 nm), and microporous (pore size [50 nm]) by the International Union of Pure and Applied Chemistry (IUPAC) [255]. Porous materials have pores with a diameter of less than 100 nanometers. Porous nanometals/metal oxide-based materials produced by dispersing them have garnered extensive interest in various domains such as energy storage, sensing, and catalysis due to their high-order networks and excellent pore size distributions. Excellent electrical stimulation, for example, can, on the one hand, extend the active region accessible to reactive molecules; on the other hand, it can boost electron mobility in solid ligands due to their metallic porosity frameworks [256].

Furthermore, additional significant uses of large porous materials have been investigated, ranging from sensing to energy storage systems [257]. Various strategies for adapting porous architectures and rational design of porous metal/metal oxide materials have been developed during the last decade. The physicochemical performance and fundamental information of these effectively manufactured metal/metal oxide nanomaterials allowed for a systematic experimental investigation, which led to the creation of numerous functional devices, such as microsensors and ultra-thin supercapacitors [258,259]. The field of application of nano-metals/metal oxide-based materials is now undergoing an exciting development with growing success. It is necessary to provide timely updates of such type of advanced materials, including in the essential properties and new applications. This study summarizes major applications such as supercapacitors, lithium-ion batteries, energy storage, detection, electrocatalysis, and photocatalysis [253,252]. This will be useful for research on nanoscale metals and metal oxides, and it may lead to more sophisticated functional materials in associated sectors.

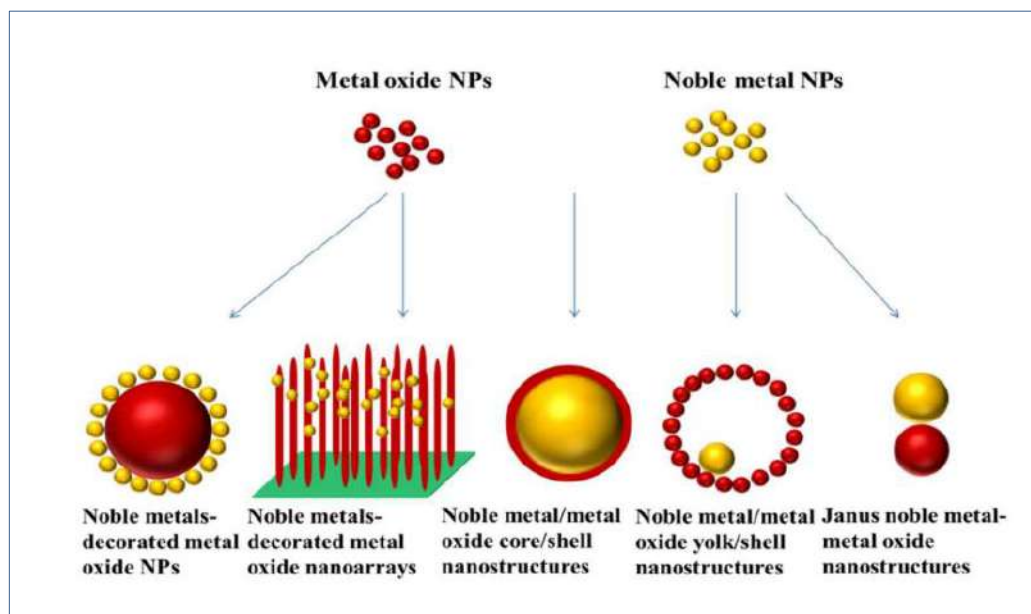


Figure I.11. Schematic representation of different structures of noble metal-metal oxide nanocomposite. Reproduced from Royal society of chemistry [260].

I.5.4.1. Synthesis and preparation of Metals

Metal manufacturing from mineral compounds has been a major human activity since time immemorial, and minerals have played an important part in building the modern world as it is now [261]. The chemical reduction of many minerals results in the formation of many minerals [262]. Their specific oxides and reduction technique are determined by the relative stability of the metal oxides and the oxides of the reducing agent employed. Transition metal and actinide stable oxides require reduction with strong reducing agents such as lithium, sodium, calcium, or magnesium and even plants extracts [263, 264] .

Metallic thermal reduction does not pose such issues; however direct one-step reduction is frequently problematic due to oxygen contamination of the metal result. often enjoy Metal oxides must be converted to specific halides before being chemically reduced with alkaline earth metals to produce metals with low oxygen pollution [265]. Metal oxides are also difficult to electrolyze conventionally due to their limited solubility in electrolyte melting, high working temperature, strong metal affinity for oxygen, and other factors [266]. These metal manufacturing methods create huge volumes of toxic gases, such as fluorine or chlorine, salts, and used trash, all of which require extra treatment to avoid pollution of the environment [267]. In the recent past, there has been much discussion regarding the electrochemical process of molten salt in which a solid metal is produced. At very low oxygen levels, oxides can be directly reduced to related metals or alloys

[268]. The patented process's simplicity and the predicted claims Capable of generating metals or alloys more effectively and inexpensively than existing traditional techniques, the novel technology has sparked global research efforts to extract various metals/alloys from their respective oxides.

Up to now, the control of the size, shape and structure of MONCs have been achieved by various synthetic methods. Vapor phase growth is always carried out in a thermal furnace. It is necessary to regulate the reaction between oxygen gas and metal vapor source. In order to achieve it, various methods have been developed to control the aspect ratio, diameter and specific surface area of the product. It mainly involves thermal chemical vapor deposition (CVD) and metal–organic chemical vapor deposition (MOCVD), etc. [269,270] (**figure I.12**) . Meanwhile, the mechanism could be classified as vapor–solid (VS) and vapor–liquid–solid (VLS) [271,272] (**figure I.13**). Generally, metal nanoparticles are used as the nucleation seeds, which have essential influences on the growth direction and diameter of products in VLS process. In the beginning, catalysts are molten into liquid alloy droplets which also contain source metal. When the alloy droplets achieve supersaturated, source metal start to precipitate and form metal oxide under the oxygen flow. In general, the as–synthesized metal oxides preferentially grow along particular orientation, which lead to the formation of 1D nanostructures. So far, the preparation of metal oxide nanowires, such as ZnO [273] and TiO₂ [274], have been achieved by means of VLS mechanism. From what have been discussed above, VLS process belongs to catalyst–assisted growth, while VS process belongs to catalyst–free growth. In the course of VS process, the reactants are first heated to form vapor under high temperature and directly condensed on the substrate, on which seed crystals will take shape and be served as the nucleation sites located. Facilitate directional growth followed will minimize the surface energy of product. Electrochemical deposition has been successfully applied to fabricate metal oxide nanostructures. It exhibits many advantages during synthesis process. Take the preparation of ZnO [275] for example, making use of appropriate electrolyte, ZnO have been successfully prepared. Meanwhile, researchers also try to introduce the template into electrochemical deposition method. A gel comprising of sol particles is essential for sol–gel process [276,277].

Back in the 1970s, hydrothermal process was firstly employed to synthesize crystalline structures. The reactants are placed in a closed vessel with water as a reaction medium. The reaction is conducted under high temperature and pressure conditions. Hydrothermal process can accelerate

the reactions between ions and promote the hydrolysis reaction. Ultimately, the growth and self-assembly of crystals will be achieved in solution. The advantages of the method involve low cost, mild reaction conditions and controlling the device easily. By changing the experimental parameters (temperature, pressure, time, the reaction medium, etc.), the morphology, structure and properties of the product can be well regulated. In order to improve the hydrothermal process, surfactants are introduced to the system. Surfactant-promoted process has been demonstrated to be an effective method to fabricate metal oxide with a variety of morphologies. The system is always composed of three phases: oil phase, surfactant phase and aqueous phase. In the course of process, surfactants can confine the growth of product.



Figure I.11. Schematic Illustration of the Hydrothermal Synthesis of ZnO nanosheets. Reproduced from MDPI [278].

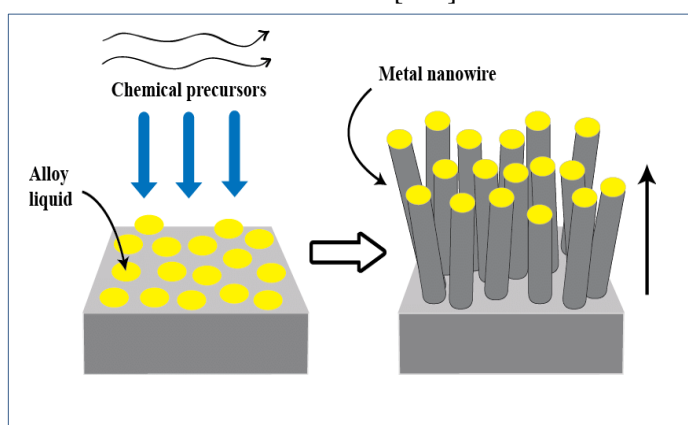


Figure I.13. Vapor-Liquid-Solid (VLS) method for vapor-phase synthesis of metal nanowires. Reproduced from Research gate [279].

I.5.4.2. Electrochemical sensors based on metals and metal oxides

Metal and metal oxide based electrochemical sensors are attracting more studies for sophisticated applications in the biomedical, environmental, and security industries because to their high sensitivity, compact size, and low cost [246,280]. In recent years then, novel nanostructures based on metal oxides have been proposed as detecting materials to increase their detection characteristics. Detection of hazardous compounds, toxic molecules, viruses and even cancer in real samples such as water, food, human body, industrial sites, or industrial wastewater are just a few examples of situations where using metal and metal oxide based sensors and biosensors for a sensitive, rapid and selective detection of the target analyte is critical [280,246,281]. Indeed, quick and precise detection is critical in light of practical applications in domains such as medical diagnosis, environmental monitoring and hazardous compounds detection.

Pan et al. have prepared hierarchical hybrid films of MnO₂ nanoparticles/multi-walled fullerene nanotubes–graphene (MNPs/ MWFNTs–GS) via a simple wetchemical method for the detection of H₂O₂. Studies revealed that MWFNTs can further enhance the conductivity and catalytic performance of MNPs/GS by providing extra electron/ ion transfer paths and inhibiting the aggregation of GS and MNPs [282]. f-MWCNT/MnO₂/GCE modified film provides a good platform for the determination of ferulic acid and the synergistic effects of CNTs and the metal oxide nanocomposites could improve the electrode conductivity [283]. For the detection of catechin, a Pt/MnO₂/f-MWCNT/GCE modified electrode was developed by the electrochemical treatment of the f-MWCNT coated GCE. This electrode was able to determine catechin from real samples like red wine, black tea, and green tea and have a good linear range and low limit of detection [284]. Molecularly imprinted polymer modified electrochemical sensor based on manganese oxide nanoparticles were also studied. The synthesized MnO₂/GO/CuO nanocomposites were reinforced by poly vinyl acetate molecularly imprinted polymer of glucose which coated on copper wire surface was used as the working electrode. This sensor exhibited linear range from 0.55 to 4.4 mM and the detection limit was 53 μM [285].

Copper oxide nanoparticles integrated with carbonaceous materials like graphene [286], carbon nanotubes [287], mesoporous carbons [288] and carbon nanofibers [289] can improve the performance of the sensor by enhancing the charge transfer between support matrices and analytes. In the case of imprinted polymer-based sensors, CuO nanoparticles were used to enhance the

number of imprinted sites of the electrode and thereby improving the selectivity and sensitivity of the electrochemical sensor [290]. Cu_xO NPs@ZIF-8 composite derived from core-shell metal-organic frameworks were synthesized by Yang et al. and found that well dispersed Cu_xO NPs possessed good crystalline structure and the encapsulated Cu_xO NPs presented good electrocatalysis for H₂O₂ oxidation [291].

Molecularly imprinted polymer-based sensor for 4-nitrophenol was described using ZnO nanoparticles/multiwall carbon nanotubes-chitosan nanocomposite. This was coated onto an ITO electrode and then imprinted sol-gel solution was electrodeposited onto the modified electrode to construct the sensor. The developed nanocomposites have porous electrodeposition imprinted film with abundant selective binding sites and functional monolayer with electrochemical catalytic activities [292]. Roy et al, presented a novel imprinted polymer-based sensor for the detection, removal, and destruction of *Escherichia coli* bacteria on the surface of Ag-ZnO bimetallic nanoparticle and graphene oxide nanocomposite. This nanocomposite provided a platform for imprinting of bacteria as well as participated in their laser-light induced photo killing. The MIP-modified glass plate is able to remove 98% of bacteria in a single analysis [293]. Nickel nanoparticles incorporated ZnO sensors possessed strong electrocatalytic ability towards the sensing of glucose, dopamine and uric acid [294]. A sensor for electrochemical monitoring of nucleic acid hybridization related to the Hepatitis B Virus (HBV) contains, ZnO NPs enriched with poly (vinylferrocenium) (PVF⁺) modified single-use graphite electrodes.[295].

Electrodeposited cobalt oxide has been a promising material for FAD immobilization with excellent catalytic activity for nitrite reduction over a linear range of 1–30 μM and limit of detection of 0.20 μM [296]. Single crystal and vertically aligned cobalt oxide (Co₃O₄) nanowalls coated on GCE via conductive silver paint were used for the electrocatalytic oxidation and reduction of hydrogen peroxide in 0.01 M pH 7.4 phosphate buffer medium up to 10 mM concentration of H₂O₂ [297].

Table I.7. Comparison with state-of-the-art electrochemical sensors based on metals and metal oxides nanoparticles.

Modified electrode	Linear range (μM)		Detection limit (μM)		Reference
	CC	HQ	CC	HQ	
MgO/GO/MCPE	-	-	0.45	0.37	[7]
AuNPs/Fe ₃ O ₄ -APTES-GO/GCE	-	-	0.8	1.1	[298]
AuNPs@MoS ₂ -rGO-AuNPs/GCE	1-145	3-137	0.95	0.04	[299]
Ag/MWCNT/GCE	3-160	0.1-40	0.2	0.16	[174]
NiO/MWCNT/GCE	20-260	2.5-260	0.015	0.039	[300]
Au-PdNF/rGO/GCE	7.4-56	7.4-56	0.8	0.5	[172]

I.6. Outlook, scope, and conclusions

Design and fabrication of electrochemical sensors for organic pollutant (CC, HQ and 5-CP) is an active area of research that has drawn the interest of scientific communities due to the high toxicity of these pollutants. In the present work, several types of electrochemical sensors for CC, HQ and 5-CP detection were developed based on advanced materials namely CNTs, MOFs, LDHs, graphene, metals and metal oxides NPs. These systems are offering new opportunities with advantages such as high sensitivity and selectivity, rapid response, and cost efficiency.

Electrochemical techniques coupled with the use of nanomaterials are useful for the development of electrochemical sensors capable of sensitive monitoring of CC, HQ and 5-CP with fast-responses. A combination of nanomaterials offers a high degree of specificity and makes the sensing formats attractive for the design and fabrication of integrated detection systems. In the present thesis, the use of nanostructured materials in the development of sensors has led to an increase in sensitivity, sensibility, and reproducibility, which confirms the benefits of nanomaterials combinations.

Nanomaterial based sensors provide a new and powerful paradigm in terms of novel and augmented functionality that encompasses a wide variety of applications in clinical diagnostics and biological research. The rapid and precise real-time detection of analytes requires that electrochemical sensors be endowed with low energy consumption, rapid response time, enhanced selectivity, sensitivity and swift recoverability (refreshability). Each of these parameters will undoubtedly undergo further improvements and refinements in the future due to advances in nanomaterials synthesis,

processing, integration and testing techniques. It is anticipated that nanomaterials will play an unprecedented role in the future development of advanced diagnostics.

Based on the results obtained in the present thesis, we highly emphasize the following points to readers:

- Because of their multiple unique properties, CNTs, MOFs, LDHs, graphene, metals and metal oxides NPs provide significant advantages. Outstanding mechanical strength, huge surface area, excellent electrical conductance, electrochemical stability in aqueous and non-aqueous samples, and high thermal conductivity. Because of their extraordinary characteristics, they are ideal materials for ultrasensitive nanoscale sensors and biosensors.
- The development of appropriate methods for tackling the challenges connected with the quick and sensitive detection of organic pollutant in aqueous environments is now underway in scientific research including materials science platforms. However, the path "from laboratory to reality" is difficult and must be improved by inventing new gadgets based on nanomaterials such as CNTs, MOFs, LDHs, graphene metals and metal oxides NPs, which are inexpensive to manufacture and have the fewest negative environmental consequences. However, the cost of preparation, as well as the stability and biocompatibility of these nanomaterial, must be considered, and better control over their properties is necessary.
- Researchers must explore the potential for synergistic effects of CNTs, MOFs, LDHs, graphene with other nanomaterials, in particular metals and metal oxides and its biocompatibility with biological components. Such combinations can promote performance and speed up the biosensor response to organic pollutant and even viral diagnosis including SARS-CoV-2.

In conclusion, the field of carbon nanomaterial-based sensors is growing quickly with the invention of many new carbon nanomaterials taking into consideration their synergetic effect with metals and metal oxides NPs. Carbon nanomaterials have many advantages for electrochemistry including fast electron transfer rates, high aspect ratios, and resistance to fouling. While many new materials are still being developed, future studies will likely help narrow down which are the most effective for mediating electron transfer. Newer methods that allow growth of carbon nanomaterials directly on the electrode

substrate or fabrication of electrodes solely from CNTs for example might be helpful for making sensors of pure carbon nanomaterials.

However, combinations of carbon nanomaterials, polymers, and metal particles will also continue to be popular because of the synergistic effects of combining materials. In the future, advances in fundamental knowledge of new nanomaterials along with a focus on practical applications in real-world systems will drive the field and lead to breakthroughs in sensing and biosensing technology.

References

- [1] K. Scida, P. W. Stege, G. Haby, G. A. Messina, and C. D. García, “Recent applications of carbon-based nanomaterials in analytical chemistry: Critical review,” *Anal. Chim. Acta*, vol. 691, no. 1–2, pp. 6–17, Apr. 2011, doi: 10.1016/j.aca.2011.02.025.
- [2] T. Huang, X. Tang, K. Luo, Y. Wu, X. Hou, and S. Tang, “An overview of graphene-based nanoadsorbent materials for environmental contaminants detection,” *TrAC Trends Anal. Chem.*, vol. 139, p. 116255, Jun. 2021, doi: 10.1016/j.trac.2021.116255.
- [3] M. Farré, S. Pérez, C. Gonçalves, M. F. Alpendurada, and D. Barceló, “Green analytical chemistry in the determination of organic pollutants in the aquatic environment,” *TrAC Trends Anal. Chem.*, vol. 29, no. 11, pp. 1347–1362, Dec. 2010, doi: 10.1016/j.trac.2010.07.016.
- [4] X. Yuan *et al.*, “A rapid and simple strategy for discrimination and detection of catechol and hydroquinone by fluorescent silicon nanoparticles,” *Microchem. J.*, vol. 158, p. 105263, Nov. 2020, doi: 10.1016/j.microc.2020.105263.
- [5] C. Maraveas, I. S. Bayer, and T. Bartzanas, “Recent Advances in Antioxidant Polymers: From Sustainable and Natural Monomers to Synthesis and Applications,” *Polymers*, vol. 13, no. 15, p. 2465, Jul. 2021, doi: 10.3390/polym13152465.
- [6] H. Soltani, A. Pardakhty, and S. Ahmadzadeh, “Determination of hydroquinone in food and pharmaceutical samples using a voltammetric based sensor employing NiO nanoparticle and ionic liquids,” *J. Mol. Liq.*, vol. 219, pp. 63–67, Jul. 2016, doi: 10.1016/j.molliq.2016.03.014.
- [7] K. Chetankumar, B. E. K. Swamy, and T. S. S. K. Naik, “A reliable electrochemical sensor for detection of catechol and hydroquinone at MgO/GO modified carbon paste electrode,” *J. Mater. Sci. Mater. Electron.*, vol. 31, no. 22, pp. 19728–19740, Nov. 2020, doi: 10.1007/s10854-020-04498-x.
- [8] T. S. Sunil Kumar Naik and B. E. Kumara Swamy, “Modification of carbon paste electrode by electrochemical polymerization of neutral red and its catalytic capability towards the simultaneous determination of catechol and hydroquinone: A voltammetric study,” *J. Electroanal. Chem.*, vol. 804, pp. 78–86, Nov. 2017, doi: 10.1016/j.jelechem.2017.08.047.
- [9] K. Ahmad, P. Kumar, and S. M. Mobin, “Hydrothermally Grown SnO₂ Flowers as Efficient Electrode Modifier for Simultaneous Detection of Catechol and Hydroquinone,” *J. Electrochem. Soc.*, vol. 166, no. 15, pp. B1577–B1584, 2019, doi: 10.1149/2.0871915jes.
- [10] K. V. Harisha, B. E. Kumara Swamy, and E. E. Ebenso, “Poly (glycine) modified carbon paste electrode for simultaneous determination of catechol and hydroquinone: A voltammetric study,” *J. Electroanal. Chem.*, vol. 823, pp. 730–736, Aug. 2018, doi: 10.1016/j.jelechem.2018.07.021.
- [11] S. Su, S. Chen, and C. Fan, “Recent advances in two-dimensional nanomaterials-based electrochemical sensors for environmental analysis,” *Green Energy Environ.*, vol. 3, no. 2, pp. 97–106, Apr. 2018, doi: 10.1016/j.gee.2017.08.005.
- [12] D. de Oliveira *et al.*, “Catechol cytotoxicity in vitro: Induction of glioblastoma cell death by apoptosis,” *Hum. Exp. Toxicol.*, vol. 29, no. 3, pp. 199–212, Mar. 2010, doi: 10.1177/0960327109360364.
- [13] H. Meskher, F. Achi, A. Zouaoui, S. Ha, M. Peacock, and H. Belkhalifa, “Simultaneous and Selective Electrochemical Determination of Catechol and Hydroquinone on A Nickel Oxide (NiO) Reduced Graphene Oxide (rGO) Doped Multiwalled Carbon Nanotube (fMWCNT) Modified Platinum Electrode,” *Anal. Lett.*, vol. 55, no. 9, pp. 1466–1481, Jun. 2022, doi: 10.1080/00032719.2021.2008951.

- [14] N. Ben Messaoud, A. Ait Lahcen, C. Dridi, and A. Amine, "Ultrasound assisted magnetic imprinted polymer combined sensor based on carbon black and gold nanoparticles for selective and sensitive electrochemical detection of Bisphenol A," *Sens. Actuators B Chem.*, vol. 276, pp. 304–312, Dec. 2018, doi: 10.1016/j.snb.2018.08.092.
- [15] M. Wang *et al.*, "Bimetallic metal–organic framework derived FeO/TiO₂ embedded in mesoporous carbon nanocomposite for the sensitive electrochemical detection of 4-nitrophenol," *Sens. Actuators B Chem.*, vol. 281, pp. 1063–1072, Feb. 2019, doi: 10.1016/j.snb.2018.11.083.
- [16] W. Long *et al.*, "Preparation of nitrogen-doped hollow carbon spheres for sensitive catechol electrochemical sensing," *Fuller. Nanotub. Carbon Nanostructures*, vol. 26, no. 12, pp. 856–862, Dec. 2018, doi: 10.1080/1536383X.2018.1512973.
- [17] S. C. Moldoveanu and M. Kiser, "Gas chromatography/mass spectrometry versus liquid chromatography/fluorescence detection in the analysis of phenols in mainstream cigarette smoke," *J. Chromatogr. A*, vol. 1141, no. 1, pp. 90–97, Feb. 2007, doi: 10.1016/j.chroma.2006.11.100.
- [18] L. Gámiz-Gracia, A. M. García-Campaña, J. F. Huertas-Pérez, and F. J. Lara, "Chemiluminescence detection in liquid chromatography: Applications to clinical, pharmaceutical, environmental and food analysis—A review," *Anal. Chim. Acta*, vol. 640, no. 1–2, pp. 7–28, Apr. 2009, doi: 10.1016/j.aca.2009.03.017.
- [19] M. F. Pistonesi, M. S. Di Nezio, M. E. Centurión, M. E. Palomeque, A. G. Lista, and B. S. Fernández Band, "Determination of phenol, resorcinol and hydroquinone in air samples by synchronous fluorescence using partial least-squares (PLS)," *Talanta*, vol. 69, no. 5, pp. 1265–1268, Jul. 2006, doi: 10.1016/j.talanta.2005.12.050.
- [20] J. Du *et al.*, "An electrochemical sensor based on the three-dimensional functionalized graphene for simultaneous determination of hydroquinone and catechol," *J. Electroanal. Chem.*, vol. 722–723, pp. 38–45, May 2014, doi: 10.1016/j.jelechem.2014.02.024.
- [21] J.-Q. Qiao *et al.*, "Determination of catalytic oxidation products of phenol by RP-HPLC," *Res. Chem. Intermed.*, vol. 38, no. 2, pp. 549–558, Feb. 2012, doi: 10.1007/s11164-011-0370-3.
- [22] G. Marrubini, E. Calleri, T. Coccini, A. F. Castoldi, and L. Manzo, "Direct Analysis of Phenol, Catechol and Hydroquinone in Human Urine by Coupled-Column HPLC with Fluorimetric Detection," *Chromatographia*, vol. 62, no. 1–2, pp. 25–31, Jul. 2005, doi: 10.1365/s10337-005-0570-3.
- [23] H. Karimi-Maleh, F. Karimi, M. Alizadeh, and A. L. Sanati, "Electrochemical Sensors, a Bright Future in the Fabrication of Portable Kits in Analytical Systems," *Chem. Rec.*, vol. 20, no. 7, pp. 682–692, Jul. 2020, doi: 10.1002/tcr.201900092.
- [24] W. E. Van der Linden and J. W. Dieker, "Glassy carbon as electrode material in electro-analytical chemistry," *Anal. Chim. Acta*, vol. 119, no. 1, pp. 1–24, Sep. 1980, doi: 10.1016/S0003-2670(00)00025-8.
- [25] M. Hicham, A. Fethi, S. Ha, and B. Khaldoun, "Antifouling double layers of functionalized-multi-walled carbon nanotubes coated ZnO for sensitive and selective electrochemical detection of catechol," *Fuller. Nanotub. Carbon Nanostructures*, vol. 30, no. 3, pp. 334–347, Mar. 2022, doi: 10.1080/1536383X.2021.1940150.
- [26] K. K. Masibi *et al.*, "Electrochemical Detection of Endosulfan Using an AONP-PANI-SWCNT Modified Glassy Carbon Electrode," *Materials*, vol. 14, no. 4, p. 723, Feb. 2021, doi: 10.3390/ma14040723.
- [27] S. S. Ming *et al.*, "Aluminium MOF fabricated electrochemical sensor for the ultra-sensitive detection of hydroquinone in water samples," *J. Electroanal. Chem.*, vol. 883, p. 115067, Feb. 2021, doi: 10.1016/j.jelechem.2021.115067.
- [28] X. Huang, D. Huang, J. Chen, R. Ye, Q. Lin, and S. Chen, "Fabrication of novel electrochemical sensor based on bimetallic Ce-Ni-MOF for sensitive detection of bisphenol A," *Anal. Bioanal. Chem.*, vol. 412, no. 4, pp. 849–860, Feb. 2020, doi: 10.1007/s00216-019-02282-3.

- [29] Y. Wang, X. Liu, S. Liu, Y. Zhang, and F. Chang, "Multilayered Chemically Modified Electrode Based on Carbon Nanotubes Conglutinated by Polydopamine: A New Strategy for the Electrochemical Signal Enhancement for the Determination of Catechol," *Anal. Lett.*, vol. 53, no. 7, pp. 1061–1074, May 2020, doi: 10.1080/00032719.2019.1695810.
- [30] X. Huang, X. Deng, W. Qi, and D. Wu, "Simultaneous Detection of Hydroquinone and Catechol Using Platinum Nanoparticles Decorated Graphene/Poly-Cyclodextrin/Multiwalled Carbon Nanotubes (MWCNTs) Nanocomposite Based Biosensor," *J. Nanosci. Nanotechnol.*, vol. 18, no. 12, pp. 8118–8123, Dec. 2018, doi: 10.1166/jnn.2018.16295.
- [31] A. Bensana and F. Achi, "Analytical performance of functional nanostructured biointerfaces for sensing phenolic compounds," *Colloids Surf. B Biointerfaces*, vol. 196, p. 111344, Dec. 2020, doi: 10.1016/j.colsurfb.2020.111344.
- [32] A. Fethi, "Novel materials for electrochemical sensing platforms," *Sens. Int.*, vol. 1, p. 100035, 2020, doi: 10.1016/j.sintl.2020.100035.
- [33] A. Ayub and Z. A. Raza, "Arsenic removal approaches: A focus on chitosan biosorption to conserve the water sources," *Int. J. Biol. Macromol.*, vol. 192, pp. 1196–1216, Dec. 2021, doi: 10.1016/j.ijbiomac.2021.10.050.
- [34] F. Garkani Nejad, S. Tajik, H. Beitollahi, and I. Sheikhshoae, "Magnetic nanomaterials based electrochemical (bio)sensors for food analysis," *Talanta*, vol. 228, p. 122075, Jun. 2021, doi: 10.1016/j.talanta.2020.122075.
- [35] H. Truong, S. Lomnicki, and B. Dellinger, "Mechanisms of molecular product and persistent radical formation from the pyrolysis of hydroquinone," *Chemosphere*, vol. 71, no. 1, pp. 107–113, Mar. 2008, doi: 10.1016/j.chemosphere.2007.10.007.
- [36] Z. Sun *et al.*, "Persistent Free Radicals from Low-Molecular-Weight Organic Compounds Enhance Cross-Coupling Reactions and Toxicity of Anthracene on Amorphous Silica Surfaces under Light," *Environ. Sci. Technol.*, vol. 55, no. 6, pp. 3716–3726, Mar. 2021, doi: 10.1021/acs.est.0c07472.
- [37] P. Nagaraja, R. A. Vasantha, and K. R. Sunitha, "A new sensitive and selective spectrophotometric method for the determination of catechol derivatives and its pharmaceutical preparations," *J. Pharm. Biomed. Anal.*, vol. 25, no. 3–4, pp. 417–424, Jun. 2001, doi: 10.1016/S0731-7085(00)00504-5.
- [38] R. Capasso, A. Evidente, L. Schivo, G. Orru, M. A. Marcialis, and G. Cristinzio, "Antibacterial polyphenols from olive oil mill waste waters," *J. Appl. Bacteriol.*, vol. 79, no. 4, pp. 393–398, Oct. 1995, doi: 10.1111/j.1365-2672.1995.tb03153.x.
- [39] R. Zhang, J. Wang, S. Milligan, and Y. Yan, "Microbial utilization of lignin-derived aromatics *via* a synthetic catechol *meta* -cleavage pathway," *Green Chem.*, vol. 23, no. 20, pp. 8238–8250, 2021, doi: 10.1039/D1GC02347K.
- [40] E. L. Cavalieri and E. G. Rogan, "Unbalanced metabolism of endogenous estrogens in the etiology and prevention of human cancer," *J. Steroid Biochem. Mol. Biol.*, vol. 125, no. 3–5, pp. 169–180, Jul. 2011, doi: 10.1016/j.jsbmb.2011.03.008.
- [41] N. Schweigert, A. J. B. Zehnder, and R. I. L. Eggen, "Chemical properties of catechols and their molecular modes of toxic action in cells, from microorganisms to mammals. Minireview," *Environ. Microbiol.*, vol. 3, no. 2, pp. 81–91, Feb. 2001, doi: 10.1046/j.1462-2920.2001.00176.x.
- [42] J. D. Mold, M. P. Peyton, R. E. Means, and T. B. Walker, "Determination of catechol in cigarette smoke," *The Analyst*, vol. 91, no. 1080, p. 189, 1966, doi: 10.1039/an9669100189.
- [43] L. Zhao, B. Lv, H. Yuan, Z. Zhou, and D. Xiao, "A Sensitive Chemiluminescence Method for Determination of Hydroquinone and Catechol," *Sensors*, vol. 7, no. 4, pp. 578–588, Apr. 2007, doi: 10.3390/s7040578.

- [44] X. Chen, X. Hu, Q. Lu, Y. Yang, S. Linghu, and X. Zhang, "Study on the differences in sludge toxicity and microbial community structure caused by catechol, resorcinol and hydroquinone with metagenomic analysis," *J. Environ. Manage.*, vol. 302, p. 114027, Jan. 2022, doi: 10.1016/j.jenvman.2021.114027.
- [45] X. Wei *et al.*, "Deciphering the Changes of Sludge Toxicity and the Succession of Dominant Bacteria During the Process of Catechol Degradation by Acclimated Sludge," *Waste Biomass Valorization*, Apr. 2022, doi: 10.1007/s12649-022-01774-1.
- [46] P. Alviz-Gazitua, R. E. Durán, F. A. Millacura, F. Cárdenas, L. A. Rojas, and M. Seeger, "Cupriavidus metallidurans CH34 Possesses Aromatic Catabolic Versatility and Degrades Benzene in the Presence of Mercury and Cadmium," *Microorganisms*, vol. 10, no. 2, p. 484, Feb. 2022, doi: 10.3390/microorganisms10020484.
- [47] N. Schweigert, R. W. Hunziker, B. I. Escher, and R. I. L. Eggen, "Acute toxicity of (chloro-)catechols and (chloro-)catechol-copper combinations in *Escherichia coli* corresponds to their membrane toxicity in vitro," *Environ. Toxicol. Chem.*, vol. 20, no. 2, pp. 239–247, Feb. 2001, doi: 10.1002/etc.5620200203.
- [48] A. J. S. Ahammad *et al.*, "Cost-Effective Electrochemical Sensor Based on Carbon Nanotube Modified-Pencil Electrode for the Simultaneous Determination of Hydroquinone and Catechol," *J. Electrochem. Soc.*, vol. 165, no. 9, pp. B390–B397, 2018, doi: 10.1149/2.1341809jes.
- [49] F. J. Enguita and A. L. Leitão, "Hydroquinone: Environmental Pollution, Toxicity, and Microbial Answers," *BioMed Res. Int.*, vol. 2013, pp. 1–14, 2013, doi: 10.1155/2013/542168.
- [50] P. J. Deisinger, "HUMAN EXPOSURE TO NATURALLY OCCURRING HYDROQUINONE," *J. Toxicol. Environ. Health*, vol. 47, no. 1, pp. 31–46, Jan. 1996, doi: 10.1080/009841096161915.
- [51] C. Sarkar, P. K. Mitra, S. Saha, C. Nayak, and R. Chakraborty, "Effect of Copper-Hydroquinone Complex on Oxidative Stress-Related Parameters in Human Erythrocytes (In Vitro)," *Toxicol. Mech. Methods*, vol. 19, no. 2, pp. 86–93, Feb. 2009, doi: 10.1080/15376510802164683.
- [52] P. Mandani, K. Desai, and H. Highland, "Cytotoxic Effects of Benzene Metabolites on Human Sperm Function: An *In Vitro* Study," *ISRN Toxicol.*, vol. 2013, pp. 1–6, Dec. 2013, doi: 10.1155/2013/397524.
- [53] V. V. Subrahmanyam, P. Kolachana, and M. T. Smith, "Hydroxylation of Phenol to Hydroquinone Catalyzed by A Human Myeloperoxidase-Superoxide Complex: Possible Implications In Benzene-Induced Myelotoxicity," *Free Radic. Res. Commun.*, vol. 15, no. 5, pp. 285–296, Jan. 1991, doi: 10.3109/10715769109105224.
- [54] S. Suresh, V. C. Srivastava, and I. M. Mishra, "Adsorption of catechol, resorcinol, hydroquinone, and their derivatives: a review," *Int. J. Energy Environ. Eng.*, vol. 3, no. 1, p. 32, 2012, doi: 10.1186/2251-6832-3-32.
- [55] R. Guerra, "Ecotoxicological and chemical evaluation of phenolic compounds in industrial effluents," *Chemosphere*, vol. 44, no. 8, pp. 1737–1747, Sep. 2001, doi: 10.1016/S0045-6535(00)00562-2.
- [56] K. L. E. Kaiser and V. S. Palabrica, "Photobacterium phosphoreum Toxicity Data Index," *Water Qual. Res. J.*, vol. 26, no. 3, pp. 361–431, Aug. 1991, doi: 10.2166/wqrj.1991.017.
- [57] H. Chen *et al.*, "Toxicity of three phenolic compounds and their mixtures on the gram-positive bacteria *Bacillus subtilis* in the aquatic environment," *Sci. Total Environ.*, vol. 408, no. 5, pp. 1043–1049, Feb. 2010, doi: 10.1016/j.scitotenv.2009.11.051.
- [58] M. Bekmezci, E. E. Altuner, V. Erduran, R. Bayat, I. Isik, and F. Şen, "Fundamentals of electrochemistry," in *Nanomaterials for Direct Alcohol Fuel Cells*, Elsevier, 2021, pp. 1–15. doi: 10.1016/B978-0-12-821713-9.00023-8.
- [59] Y. Zhou, H. Yin, W.-W. Zhao, and S. Ai, "Electrochemical, electrochemiluminescent and photoelectrochemical bioanalysis of epigenetic modifiers: A comprehensive review," *Coord. Chem. Rev.*, vol. 424, p. 213519, Dec. 2020, doi: 10.1016/j.ccr.2020.213519.

- [60] R. Ding, Y. H. Cheong, A. Ahamed, and G. Lisak, "Heavy Metals Detection with Paper-Based Electrochemical Sensors," *Anal. Chem.*, vol. 93, no. 4, pp. 1880–1888, Feb. 2021, doi: 10.1021/acs.analchem.0c04247.
- [61] S. Marinesco, "Micro- and nano-electrodes for neurotransmitter monitoring," *Curr. Opin. Electrochem.*, vol. 29, p. 100746, Oct. 2021, doi: 10.1016/j.coelec.2021.100746.
- [62] Y. Liu, J. Du, M. Wang, J. Zhang, C. Liu, and X. Li, "Recent Progress in Quantitatively Monitoring Vesicular Neurotransmitter Release and Storage With Micro/Nanoelectrodes," *Front. Chem.*, vol. 8, p. 591311, Jan. 2021, doi: 10.3389/fchem.2020.591311.
- [63] A. Sudhakar, S. K. Chakraborty, N. K. Mahanti, and C. Varghese, "Advanced techniques in edible oil authentication: A systematic review and critical analysis," *Crit. Rev. Food Sci. Nutr.*, pp. 1–29, Aug. 2021, doi: 10.1080/10408398.2021.1956424.
- [64] M. Schledorn *et al.*, "Protein NMR Spectroscopy at 150 kHz Magic-Angle Spinning Continues To Improve Resolution and Mass Sensitivity," *ChemBioChem*, vol. 21, no. 17, pp. 2540–2548, Sep. 2020, doi: 10.1002/cbic.202000341.
- [65] Z. Jahromi, E. Mirzaei, A. Savardashtaki, M. Afzali, and Z. Afzali, "A rapid and selective electrochemical sensor based on electrospun carbon nanofibers for tramadol detection," *Microchem. J.*, vol. 157, p. 104942, Sep. 2020, doi: 10.1016/j.microc.2020.104942.
- [66] S. Motia, B. Bouchikhi, E. Llobet, and N. El Bari, "Synthesis and characterization of a highly sensitive and selective electrochemical sensor based on molecularly imprinted polymer with gold nanoparticles modified screen-printed electrode for glycerol determination in wastewater," *Talanta*, vol. 216, p. 120953, Aug. 2020, doi: 10.1016/j.talanta.2020.120953.
- [67] T. Ören Varol, O. Hakli, and U. Anik, "Graphene oxide–porphyrin composite nanostructure included electrochemical sensor for catechol detection," *New J. Chem.*, vol. 45, no. 3, pp. 1734–1742, 2021, doi: 10.1039/D0NJ05475E.
- [68] T. A. Saleh, "Nanomaterials: Classification, properties, and environmental toxicities," *Environ. Technol. Innov.*, vol. 20, p. 101067, Nov. 2020, doi: 10.1016/j.eti.2020.101067.
- [69] H. Huang, Y. Chen, Z. Chen, J. Chen, Y. Hu, and J.-J. Zhu, "Electrochemical sensor based on Ce-MOF/carbon nanotube composite for the simultaneous discrimination of hydroquinone and catechol," *J. Hazard. Mater.*, vol. 416, p. 125895, Aug. 2021, doi: 10.1016/j.jhazmat.2021.125895.
- [70] H.-W. Wang, C. Bringans, A. J. R. Hickey, J. A. Windsor, P. A. Kilmartin, and A. R. J. Phillips, "Cyclic Voltammetry in Biological Samples: A Systematic Review of Methods and Techniques Applicable to Clinical Settings," *Signals*, vol. 2, no. 1, pp. 138–158, Mar. 2021, doi: 10.3390/signals2010012.
- [71] F. Crespi, "Differential Pulse Voltammetry: Evolution of an In Vivo Methodology and New Chemical Entries, A Short Review," *J. New Dev. Chem.*, vol. 2, no. 4, pp. 20–28, Apr. 2020, doi: 10.14302/issn.2377-2549.jndc-20-3298.
- [72] H. H. Çelik *et al.*, "The synthesis of a novel DDPHC diazonium salt: Investigation of its usability in the determination of phenol and chlorophenols using CV, SWV and DPV techniques," *Inorg. Chem. Commun.*, vol. 116, p. 107893, Jun. 2020, doi: 10.1016/j.inoche.2020.107893.
- [73] K. Dujeanic-Stephane *et al.*, "The Effect of Modifications of Activated Carbon Materials on the Capacitive Performance: Surface, Microstructure, and Wettability," *J. Compos. Sci.*, vol. 5, no. 3, p. 66, Feb. 2021, doi: 10.3390/jcs5030066.
- [74] Â. Vilas-Boas, P. Valderrama, N. Fontes, D. Geraldo, and F. Bento, "Evaluation of total polyphenol content of wines by means of voltammetric techniques: Cyclic voltammetry vs differential pulse voltammetry," *Food Chem.*, vol. 276, pp. 719–725, Mar. 2019, doi: 10.1016/j.foodchem.2018.10.078.

- [75] M. Lovrić, “Square-Wave Voltammetry,” in *Electroanalytical Methods*, F. Scholz, A. M. Bond, R. G. Compton, D. A. Fiedler, G. Inzelt, H. Kahlert, Š. Komorsky-Lovrić, H. Lohse, M. Lovrić, F. Marken, A. Neudeck, U. Retter, F. Scholz, and Z. Stojek, Eds. Berlin, Heidelberg: Springer Berlin Heidelberg, 2010, pp. 121–145. doi: 10.1007/978-3-642-02915-8_6.
- [76] A. A. Avan and H. Filik, “Simultaneous electrochemical sensing of dihydroxybenzene isomers at multi-walled carbon nanotubes aerogel/gold nanoparticles modified graphene screen-printed electrode,” *J. Electroanal. Chem.*, vol. 878, p. 114682, Dec. 2020, doi: 10.1016/j.jelechem.2020.114682.
- [77] S. Sawan, R. Maalouf, A. Errachid, and N. Jaffrezic-Renault, “Metal and metal oxide nanoparticles in the voltammetric detection of heavy metals: A review,” *TrAC Trends Anal. Chem.*, vol. 131, p. 116014, Oct. 2020, doi: 10.1016/j.trac.2020.116014.
- [78] W. Choi, H.-C. Shin, J. M. Kim, J.-Y. Choi, and W.-S. Yoon, “Modeling and Applications of Electrochemical Impedance Spectroscopy (EIS) for Lithium-ion Batteries,” *J. Electrochem. Sci. Technol.*, vol. 11, no. 1, pp. 1–13, Feb. 2020, doi: 10.33961/jecst.2019.00528.
- [79] J. Yin, L. Qi, and H. Wang, “Antifreezing Ag/AgCl reference electrodes: Fabrication and applications,” *J. Electroanal. Chem.*, vol. 666, pp. 25–31, Feb. 2012, doi: 10.1016/j.jelechem.2011.11.021.
- [80] J. Ghilane, P. Hapiot, and A. J. Bard, “Metal/Polypyrrole Quasi-Reference Electrode for Voltammetry in Nonaqueous and Aqueous Solutions,” *Anal. Chem.*, vol. 78, no. 19, pp. 6868–6872, Oct. 2006, doi: 10.1021/ac060818o.
- [81] B. Pejčić, P. Eadington, and A. Ross, “Environmental Monitoring of Hydrocarbons: A Chemical Sensor Perspective,” *Environ. Sci. Technol.*, vol. 41, no. 18, pp. 6333–6342, Sep. 2007, doi: 10.1021/es0704535.
- [82] N. Hashemi Goradel *et al.*, “Biosensors for the Detection of Environmental and Urban Pollutions,” *J. Cell. Biochem.*, vol. 119, no. 1, pp. 207–212, Jan. 2018, doi: 10.1002/jcb.26030.
- [83] B. Purohit, P. R. Vernekar, N. P. Shetti, and P. Chandra, “Biosensor nanoengineering: Design, operation, and implementation for biomolecular analysis,” *Sens. Int.*, vol. 1, p. 100040, 2020, doi: 10.1016/j.sintl.2020.100040.
- [84] D. Wang *et al.*, “Biomimetic, biocompatible and robust silk Fibroin-MXene film with stable 3D cross-link structure for flexible pressure sensors,” *Nano Energy*, vol. 78, p. 105252, Dec. 2020, doi: 10.1016/j.nanoen.2020.105252.
- [85] Q. Zhou *et al.*, “Electrochemical sensor based on corncob biochar layer supported chitosan-MIPs for determination of dibutyl phthalate (DBP),” *J. Electroanal. Chem.*, vol. 897, p. 115549, Sep. 2021, doi: 10.1016/j.jelechem.2021.115549.
- [86] C. Ye *et al.*, “Study on the properties and reaction mechanism of polypyrrole@norfloxacin molecularly imprinted electrochemical sensor based on three-dimensional CoFe-MOFs/AuNPs,” *Electrochimica Acta*, vol. 379, p. 138174, May 2021, doi: 10.1016/j.electacta.2021.138174.
- [87] Z. Bai *et al.*, “Construction of an ultra-sensitive electrochemical sensor based on polyoxometalates decorated with CNTs and AuCo nanoparticles for the voltammetric simultaneous determination of dopamine and uric acid,” *Microchim. Acta*, vol. 187, no. 8, p. 483, Aug. 2020, doi: 10.1007/s00604-020-04446-w.
- [88] G. Fadillah, W. P. Wicaksono, I. Fatimah, and T. A. Saleh, “A sensitive electrochemical sensor based on functionalized graphene oxide/SnO₂ for the determination of eugenol,” *Microchem. J.*, vol. 159, p. 105353, Dec. 2020, doi: 10.1016/j.microc.2020.105353.
- [89] J. Upan *et al.*, “A simple label-free electrochemical sensor for sensitive detection of alpha-fetoprotein based on specific aptamer immobilized platinum nanoparticles/carboxylated-graphene oxide,” *Sci. Rep.*, vol. 11, no. 1, p. 13969, Dec. 2021, doi: 10.1038/s41598-021-93399-y.

- [90] E. Sehit and Z. Altintas, "Significance of nanomaterials in electrochemical glucose sensors: An updated review (2016-2020)," *Biosens. Bioelectron.*, vol. 159, p. 112165, Jul. 2020, doi: 10.1016/j.bios.2020.112165.
- [91] H. Filik and A. A. Avan, "Review on applications of carbon nanomaterials for simultaneous electrochemical sensing of environmental contaminant dihydroxybenzene isomers," *Arab. J. Chem.*, vol. 13, no. 7, pp. 6092–6105, Jul. 2020, doi: 10.1016/j.arabjc.2020.05.009.
- [92] D.-L. Huang *et al.*, "Synergistic effect of a cobalt fluoroporphyrin and graphene oxide on the simultaneous voltammetric determination of catechol and hydroquinone," *Microchim. Acta*, vol. 186, no. 6, p. 381, Jun. 2019, doi: 10.1007/s00604-019-3417-6.
- [93] S. Guo *et al.*, "A facile and sensitive electrochemical sensor for non-enzymatic glucose detection based on three-dimensional flexible polyurethane sponge decorated with nickel hydroxide," *Anal. Chim. Acta*, vol. 1109, pp. 130–139, May 2020, doi: 10.1016/j.aca.2020.02.037.
- [94] Cosimino. Malitesta, Francesco. Palmisano, Luisa. Torsi, and P. Giorgio. Zambonin, "Glucose fast-response amperometric sensor based on glucose oxidase immobilized in an electropolymerized poly(o-phenylenediamine) film," *Anal. Chem.*, vol. 62, no. 24, pp. 2735–2740, Dec. 1990, doi: 10.1021/ac00223a016.
- [95] A. Bratov, N. Abramova, and A. Ipatov, "Recent trends in potentiometric sensor arrays—A review," *Anal. Chim. Acta*, vol. 678, no. 2, pp. 149–159, Sep. 2010, doi: 10.1016/j.aca.2010.08.035.
- [96] Y. He, "Rapid thermal conductivity measurement with a hot disk sensor," *Thermochim. Acta*, vol. 436, no. 1–2, pp. 130–134, Oct. 2005, doi: 10.1016/j.tca.2005.07.003.
- [97] L. R. Jordan, P. C. Hauser, and G. A. Dawson, "Amperometric Sensor for Monitoring Ethylene," *Anal. Chem.*, vol. 69, no. 4, pp. 558–562, Feb. 1997, doi: 10.1021/ac9610117.
- [98] M. Stoytcheva, R. Zlatev, Z. Velkova, B. Valdez, and M. Ovalle, "Analytical Characteristics of Electrochemical Biosensors:," *Port. Electrochimica Acta*, vol. 27, no. 3, pp. 353–362, 2009, doi: 10.4152/pea.200903353.
- [99] E. Desimoni and B. Brunetti, "Presenting Analytical Performances of Electrochemical Sensors. Some Suggestions," *Electroanalysis*, vol. 25, no. 7, pp. 1645–1651, Jul. 2013, doi: 10.1002/elan.201300150.
- [100] J. Leuermann *et al.*, "Optimizing the Limit of Detection of Waveguide-Based Interferometric Biosensor Devices," *Sensors*, vol. 19, no. 17, p. 3671, Aug. 2019, doi: 10.3390/s19173671.
- [101] G. Korotcenkov and B. K. Cho, "Engineering approaches for the improvement of conductometric gas sensor parameters," *Sens. Actuators B Chem.*, vol. 188, pp. 709–728, Nov. 2013, doi: 10.1016/j.snb.2013.07.101.
- [102] L. Zipser, "Selectivity of sensor systems," *Sens. Actuators Phys.*, vol. 37–38, pp. 286–289, Jun. 1993, doi: 10.1016/0924-4247(93)80048-L.
- [103] L. Yuan *et al.*, "Fabrication of highly sensitive and selective electrochemical sensor by using optimized molecularly imprinted polymers on multi-walled carbon nanotubes for metronidazole measurement," *Sens. Actuators B Chem.*, vol. 206, pp. 647–652, Jan. 2015, doi: 10.1016/j.snb.2014.10.019.
- [104] M. Bilgi, E. M. Sahin, and E. Ayranci, "Sensor and biosensor application of a new redox mediator: Rosmarinic acid modified screen-printed carbon electrode for electrochemical determination of NADH and ethanol," *J. Electroanal. Chem.*, vol. 813, pp. 67–74, Mar. 2018, doi: 10.1016/j.jelechem.2018.02.012.
- [105] Y. Wee, S. Park, Y. H. Kwon, Y. Ju, K.-M. Yeon, and J. Kim, "Tyrosinase-immobilized CNT based biosensor for highly-sensitive detection of phenolic compounds," *Biosens. Bioelectron.*, vol. 132, pp. 279–285, May 2019, doi: 10.1016/j.bios.2019.03.008.

- [106] T. D. Tran, P. T. Nguyen, T. N. Le, and M. I. Kim, "DNA-copper hybrid nanoflowers as efficient laccase mimics for colorimetric detection of phenolic compounds in paper microfluidic devices," *Biosens. Bioelectron.*, vol. 182, p. 113187, Jun. 2021, doi: 10.1016/j.bios.2021.113187.
- [107] B. Kapan, S. Kurbanoglu, E. N. Esenturk, S. Soylemez, and L. Toppare, "Electrochemical catechol biosensor based on β -cyclodextrin capped gold nanoparticles and inhibition effect of ibuprofen," *Process Biochem.*, vol. 108, pp. 80–89, Sep. 2021, doi: 10.1016/j.procbio.2021.06.004.
- [108] S. G. Chavan *et al.*, "Dimeric-serotonin bivalent ligands induced gold nanoparticle aggregation for highly sensitive and selective serotonin biosensor," *Biosens. Bioelectron.*, vol. 191, p. 113447, Nov. 2021, doi: 10.1016/j.bios.2021.113447.
- [109] T. Hyun Chung, M. N. A. Meshref, and B. Ranjan Dhar, "A review and roadmap for developing microbial electrochemical cell-based biosensors for recalcitrant environmental contaminants, emphasis on aromatic compounds," *Chem. Eng. J.*, vol. 424, p. 130245, Nov. 2021, doi: 10.1016/j.cej.2021.130245.
- [110] D. R. Thévenot, K. Toth, R. A. Durst, and G. S. Wilson, "Electrochemical biosensors: recommended definitions and classification|International Union of Pure and Applied Chemistry: Physical Chemistry Division, Commission I.7 (Biophysical Chemistry); Analytical Chemistry Division, Commission V.5 (Electroanalytical Chemistry).1," *Biosens. Bioelectron.*, vol. 16, no. 1–2, pp. 121–131, Jan. 2001, doi: 10.1016/S0956-5663(01)00115-4.
- [111] D. S. Silvester, "Recent advances in the use of ionic liquids for electrochemical sensing," *The Analyst*, vol. 136, no. 23, p. 4871, 2011, doi: 10.1039/c1an15699c.
- [112] F. Deng, X.-B. Luo, L. Ding, and S.-L. Luo, "Application of Nanomaterials and Nanotechnology in the Reutilization of Metal Ion From Wastewater," in *Nanomaterials for the Removal of Pollutants and Resource Reutilization*, Elsevier, 2019, pp. 149–178. doi: 10.1016/B978-0-12-814837-2.00005-6.
- [113] M. Nasrollahzadeh, M. Sajjadi, G. J. Soufi, S. Irvani, and R. S. Varma, "Nanomaterials and Nanotechnology-Associated Innovations against Viral Infections with a Focus on Coronaviruses," *Nanomaterials*, vol. 10, no. 6, p. 1072, May 2020, doi: 10.3390/nano10061072.
- [114] E. Inshakova and A. Inshakova, "Nanomaterials and nanotechnology: prospects for technological re-equipment in the power engineering industry," *IOP Conf. Ser. Mater. Sci. Eng.*, vol. 709, no. 3, p. 033020, Jan. 2020, doi: 10.1088/1757-899X/709/3/033020.
- [115] K. Pathakoti, M. Manubolu, and H.-M. Hwang, "Nanostructures: Current uses and future applications in food science," *J. Food Drug Anal.*, vol. 25, no. 2, pp. 245–253, Apr. 2017, doi: 10.1016/j.jfda.2017.02.004.
- [116] M. Kulkarni *et al.*, "Titanium nanostructures for biomedical applications," *Nanotechnology*, vol. 26, no. 6, p. 062002, Feb. 2015, doi: 10.1088/0957-4484/26/6/062002.
- [117] H. N. Abdelhamid and G. Badr, "Nanobiotechnology as a platform for the diagnosis of COVID-19: a review," *Nanotechnol. Environ. Eng.*, vol. 6, no. 1, p. 19, May 2021, doi: 10.1007/s41204-021-00109-0.
- [118] Z. Zhu, L. Garcia-Gancedo, A. J. Flewitt, H. Xie, F. Moussy, and W. I. Milne, "A Critical Review of Glucose Biosensors Based on Carbon Nanomaterials: Carbon Nanotubes and Graphene," *Sensors*, vol. 12, no. 5, pp. 5996–6022, May 2012, doi: 10.3390/s120505996.
- [119] F. N. Al-Rowaili, A. Jamal, M. S. Ba Shammakh, and A. Rana, "A Review on Recent Advances for Electrochemical Reduction of Carbon Dioxide to Methanol Using Metal–Organic Framework (MOF) and Non-MOF Catalysts: Challenges and Future Prospects," *ACS Sustain. Chem. Eng.*, vol. 6, no. 12, pp. 15895–15914, Dec. 2018, doi: 10.1021/acssuschemeng.8b03843.

- [120] E. Roy, S. Patra, A. Tiwari, R. Madhuri, and P. K. Sharma, "Introduction of selectivity and specificity to graphene using an inimitable combination of molecular imprinting and nanotechnology," *Biosens. Bioelectron.*, vol. 89, pp. 234–248, Mar. 2017, doi: 10.1016/j.bios.2016.02.056.
- [121] E. Roy, S. Patra, A. Tiwari, R. Madhuri, and P. K. Sharma, "Introduction of selectivity and specificity to graphene using an inimitable combination of molecular imprinting and nanotechnology," *Biosens. Bioelectron.*, vol. 89, pp. 234–248, Mar. 2017, doi: 10.1016/j.bios.2016.02.056.
- [122] N. Sinha, D. Roy Mahapatra, Y. Sun, J. T. W. Yeow, R. V. N. Melnik, and D. A. Jaffray, "Electromechanical interactions in a carbon nanotube based thin film field emitting diode," *Nanotechnology*, vol. 19, no. 2, p. 025701, Jan. 2008, doi: 10.1088/0957-4484/19/02/025701.
- [123] J.-H. Lee, Y. K. Jeong, J. A. Peters, G.-H. Nam, S. Jin, and J.-H. Kim, "In Situ Fabrication of Nano Transistors by Selective Deposition of a Gate Dielectric around Carbon Nanotubes," *ACS Appl. Mater. Interfaces*, vol. 7, no. 43, pp. 24094–24102, Nov. 2015, doi: 10.1021/acsami.5b07137.
- [124] D. Ju, Y. Zhang, R. Li, S. Liu, L. Li, and H. Chen, "Mechanism-Independent Manipulation of Single-Wall Carbon Nanotubes with Atomic Force Microscopy Tip," *Nanomaterials*, vol. 10, no. 8, p. 1494, Jul. 2020, doi: 10.3390/nano10081494.
- [125] K. Lota, I. Acznik, A. Sierczynska, and G. Lota, "Enhancing the performance of polypyrrole composites as electrode materials for supercapacitors by carbon nanotubes additives," *J. Appl. Polym. Sci.*, vol. 137, no. 28, p. 48867, Jul. 2020, doi: 10.1002/app.48867.
- [126] O. Farshad *et al.*, "Spermatotoxic Effects of Single-Walled and Multi-Walled Carbon Nanotubes on Male Mice," *Front. Vet. Sci.*, vol. 7, p. 591558, Dec. 2020, doi: 10.3389/fvets.2020.591558.
- [127] A. Hussain *et al.*, "Scalable growth of single-walled carbon nanotubes with a highly uniform structure," *Nanoscale*, vol. 12, no. 23, pp. 12263–12267, 2020, doi: 10.1039/D0NR01919D.
- [128] S. O. Mirabootalebi, "A new method for preparing buckypaper by pressing a mixture of multi-walled carbon nanotubes and amorphous carbon," *Adv. Compos. Hybrid Mater.*, vol. 3, no. 3, pp. 336–343, Sep. 2020, doi: 10.1007/s42114-020-00167-z.
- [129] B. Ribeiro, E. C. Botelho, M. L. Costa, and C. F. Bandeira, "Carbon nanotube buckypaper reinforced polymer composites: a review," *Polímeros*, vol. 27, no. 3, pp. 247–255, Sep. 2017, doi: 10.1590/0104-1428.03916.
- [130] M. R. Watt and R. A. Gerhardt, "Factors that Affect Network Formation in Carbon Nanotube Composites and their Resultant Electrical Properties," *J. Compos. Sci.*, vol. 4, no. 3, p. 100, Jul. 2020, doi: 10.3390/jcs4030100.
- [131] S. Fu, X. Chen, and P. Liu, "Preparation of CNTs/Cu composites with good electrical conductivity and excellent mechanical properties," *Mater. Sci. Eng. A*, vol. 771, p. 138656, Jan. 2020, doi: 10.1016/j.msea.2019.138656.
- [132] A. Kumar, K. Sharma, and A. R. Dixit, "A review on the mechanical properties of polymer composites reinforced by carbon nanotubes and graphene," *Carbon Lett.*, vol. 31, no. 2, pp. 149–165, Apr. 2021, doi: 10.1007/s42823-020-00161-x.
- [133] S. K. Soni, B. Thomas, and V. R. Kar, "A Comprehensive Review on CNTs and CNT-Reinforced Composites: Syntheses, Characteristics and Applications," *Mater. Today Commun.*, vol. 25, p. 101546, Dec. 2020, doi: 10.1016/j.mtcomm.2020.101546.
- [134] C. Guo *et al.*, "Mechanical and thermal properties of multiwalled carbon-nanotube-reinforced Al₂O₃ nanocomposites," *Ceram. Int.*, vol. 46, no. 11, pp. 17449–17460, Aug. 2020, doi: 10.1016/j.ceramint.2020.04.039.
- [135] R. Kuchi *et al.*, "Optimization of FeNi/SWCNT composites by a simple co-arc discharge process to improve microwave absorption performance," *J. Alloys Compd.*, vol. 852, p. 156712, Jan. 2021, doi: 10.1016/j.jallcom.2020.156712.

- [136] S. K. Chaudhary and K. K. Singh, "Complex Phenomenal Growth of Multi-walled Carbon Nanotubes in Conventional Arc Discharge Process," *Trans. Indian Inst. Met.*, vol. 74, no. 8, pp. 2043–2048, Aug. 2021, doi: 10.1007/s12666-021-02316-4.
- [137] F. S. Alamro, A. M. Mostafa, K. A. A. Abu Al-Ola, H. A. Ahmed, and A. Toghan, "Synthesis of Ag Nanoparticles-Decorated CNTs via Laser Ablation Method for the Enhancement the Photocatalytic Removal of Naphthalene from Water," *Nanomaterials*, vol. 11, no. 8, p. 2142, Aug. 2021, doi: 10.3390/nano11082142.
- [138] E. A. Mwafy, "Eco-friendly approach for the synthesis of MWCNTs from waste tires via chemical vapor deposition," *Environ. Nanotechnol. Monit. Manag.*, vol. 14, p. 100342, Dec. 2020, doi: 10.1016/j.enmm.2020.100342.
- [139] Y. Tian *et al.*, "CNTs synthesized with polyoxometalate-based metal–organic compounds as catalyst precursors *via* the CVD method and their adsorption performance towards organic dyes," *New J. Chem.*, vol. 44, no. 14, pp. 5508–5512, 2020, doi: 10.1039/C9NJ06331E.
- [140] H. Sabeeh *et al.*, "Self-Supporting Design of NiS/CNTs Nanohybrid for Advanced Electrochemical Energy Storage Applications," *J. Clust. Sci.*, Jul. 2021, doi: 10.1007/s10876-021-02138-w.
- [141] X. Jiaojiao, W. Pengyun, Z. Bin, and A. I. Onyinye, "Enhancing electrochemical sensing for catechol by biomimetic oxidase covalently functionalized graphene oxide," *Bioprocess Biosyst. Eng.*, vol. 44, no. 2, pp. 343–353, Feb. 2021, doi: 10.1007/s00449-020-02446-x.
- [142] M. Gandhi, D. Rajagopal, and A. Senthil Kumar, "Facile Electrochemical Demethylation of 2-Methoxyphenol to Surface-Confined Catechol on the MWCNT and Its Efficient Electrocatalytic Hydrazine Oxidation and Sensing Applications," *ACS Omega*, vol. 5, no. 26, pp. 16208–16219, Jul. 2020, doi: 10.1021/acsomega.0c01846.
- [143] Y. Song, M. Zhao, X. Wang, H. Qu, Y. Liu, and S. Chen, "Simultaneous electrochemical determination of catechol and hydroquinone in seawater using Co₃O₄/MWCNTs/GCE," *Mater. Chem. Phys.*, vol. 234, pp. 217–223, Aug. 2019, doi: 10.1016/j.matchemphys.2019.05.071.
- [144] S. Yang *et al.*, "An Ultrasensitive Electrochemical Sensor Based on Multiwalled Carbon Nanotube@Reduced Graphene Oxide Nanoribbon Composite for Simultaneous Determination of Hydroquinone, Catechol and Resorcinol," *J. Electrochem. Soc.*, vol. 166, no. 6, pp. B547–B553, 2019, doi: 10.1149/2.0011908jes.
- [145] C. Chen, P. Zhao, C. Li, Y. Xie, and J. Fei, "Highly Sensitive Temperature-responsive Sensor Based on PS-PDEA-PS/C₆₀-MWCNTs for Reversible Switch Detection of Catechol," *Electroanalysis*, vol. 31, no. 5, pp. 913–921, May 2019, doi: 10.1002/elan.201800769.
- [146] L. Alshahrani *et al.*, "The Simultaneous Electrochemical Detection of Catechol and Hydroquinone with [Cu(Sal-β-Ala)(3,5-DMPz)₂]/SWCNTs/GCE," *Sensors*, vol. 14, no. 12, pp. 22274–22284, Nov. 2014, doi: 10.3390/s14122274.
- [147] W. Zhang, C. Chai, Q. Fan, Y. Song, and Y. Yang, "A novel two-dimensional sp²-sp³ hybridized carbon nanostructure with a negative in-plane Poisson ratio and high electron mobility," *Comput. Mater. Sci.*, vol. 185, p. 109904, Dec. 2020, doi: 10.1016/j.commatsci.2020.109904.
- [148] W. Zhang, C. Chai, Q. Fan, Y. Song, and Y. Yang, "PBCF-Graphene: A 2D Sp² Hybridized Honeycomb Carbon Allotrope with a Direct Band Gap," *ChemNanoMat*, vol. 6, no. 1, pp. 139–147, Jan. 2020, doi: 10.1002/cnma.201900645.
- [149] Ö. Güler and N. Bağcı, "A short review on mechanical properties of graphene reinforced metal matrix composites," *J. Mater. Res. Technol.*, vol. 9, no. 3, pp. 6808–6833, May 2020, doi: 10.1016/j.jmrt.2020.01.077.
- [150] Z. Said, M. A. Abdelkareem, H. Rezk, A. M. Nassef, and H. Z. Atwany, "Stability, thermophysical and electrical properties of synthesized carbon nanofiber and reduced-graphene oxide-based nanofluids and their hybrid along with fuzzy modeling approach," *Powder Technol.*, vol. 364, pp. 795–809, Mar. 2020, doi: 10.1016/j.powtec.2020.02.026.

- [151] H.-D. Huang *et al.*, “Improved barrier properties of poly(lactic acid) with randomly dispersed graphene oxide nanosheets,” *J. Membr. Sci.*, vol. 464, pp. 110–118, Aug. 2014, doi: 10.1016/j.memsci.2014.04.009.
- [152] X. Niu *et al.*, “Fabrication of an electrochemical chiral sensor via an integrated polysaccharides/3D nitrogen-doped graphene-CNT frame,” *Bioelectrochemistry*, vol. 131, p. 107396, Feb. 2020, doi: 10.1016/j.bioelechem.2019.107396.
- [153] N. Ruecha, N. Rodthongkum, D. M. Cate, J. Volckens, O. Chailapakul, and C. S. Henry, “Sensitive electrochemical sensor using a graphene–polyaniline nanocomposite for simultaneous detection of Zn(II), Cd(II), and Pb(II),” *Anal. Chim. Acta*, vol. 874, pp. 40–48, May 2015, doi: 10.1016/j.aca.2015.02.064.
- [154] S. Zhang, B.-Q. Li, and J.-B. Zheng, “An electrochemical sensor for the sensitive determination of nitrites based on Pt–PANI–graphene nanocomposites,” *Anal. Methods*, vol. 7, no. 19, pp. 8366–8372, 2015, doi: 10.1039/C5AY01710F.
- [155] S. Sajjad, S. A. Khan Leghari, and A. Iqbal, “Study of Graphene Oxide Structural Features for Catalytic, Antibacterial, Gas Sensing, and Metals Decontamination Environmental Applications,” *ACS Appl. Mater. Interfaces*, vol. 9, no. 50, pp. 43393–43414, Dec. 2017, doi: 10.1021/acsami.7b08232.
- [156] M. Tahriri *et al.*, “Graphene and its derivatives: Opportunities and challenges in dentistry,” *Mater. Sci. Eng. C*, vol. 102, pp. 171–185, Sep. 2019, doi: 10.1016/j.msec.2019.04.051.
- [157] B. A. Al Jahdaly, M. F. Elsadek, B. M. Ahmed, M. F. Farahat, M. M. Taher, and A. M. Khalil, “Outstanding Graphene Quantum Dots from Carbon Source for Biomedical and Corrosion Inhibition Applications: A Review,” *Sustainability*, vol. 13, no. 4, p. 2127, Feb. 2021, doi: 10.3390/su13042127.
- [158] H. Yan *et al.*, “Bottom-up precise synthesis of stable platinum dimers on graphene,” *Nat. Commun.*, vol. 8, no. 1, p. 1070, Dec. 2017, doi: 10.1038/s41467-017-01259-z.
- [159] T. Wang, Z. Wang, R. V. Salvatierra, E. McHugh, and J. M. Tour, “Top-down synthesis of graphene nanoribbons using different sources of carbon nanotubes,” *Carbon*, vol. 158, pp. 615–623, Mar. 2020, doi: 10.1016/j.carbon.2019.11.033.
- [160] W. Chen, G. Lv, W. Hu, D. Li, S. Chen, and Z. Dai, “Synthesis and applications of graphene quantum dots: a review,” *Nanotechnol. Rev.*, vol. 7, no. 2, pp. 157–185, Apr. 2018, doi: 10.1515/ntrev-2017-0199.
- [161] J. Cai *et al.*, “Atomically precise bottom-up fabrication of graphene nanoribbons,” *Nature*, vol. 466, no. 7305, pp. 470–473, Jul. 2010, doi: 10.1038/nature09211.
- [162] P. P. Brisebois and M. Siaj, “Harvesting graphene oxide – years 1859 to 2019: a review of its structure, synthesis, properties and exfoliation,” *J. Mater. Chem. C*, vol. 8, no. 5, pp. 1517–1547, 2020, doi: 10.1039/C9TC03251G.
- [163] A. Adetayo and D. Runsewe, “Synthesis and Fabrication of Graphene and Graphene Oxide: A Review,” *Open J. Compos. Mater.*, vol. 09, no. 02, pp. 207–229, 2019, doi: 10.4236/ojcm.2019.92012.
- [164] N. I. Zaaba, K. L. Foo, U. Hashim, S. J. Tan, W.-W. Liu, and C. H. Voon, “Synthesis of Graphene Oxide using Modified Hummers Method: Solvent Influence,” *Procedia Eng.*, vol. 184, pp. 469–477, 2017, doi: 10.1016/j.proeng.2017.04.118.
- [165] J. Chen, B. Yao, C. Li, and G. Shi, “An improved Hummers method for eco-friendly synthesis of graphene oxide,” *Carbon*, vol. 64, pp. 225–229, Nov. 2013, doi: 10.1016/j.carbon.2013.07.055.
- [166] S. Y. Toh, K. S. Loh, S. K. Kamarudin, and W. R. W. Daud, “Graphene production via electrochemical reduction of graphene oxide: Synthesis and characterisation,” *Chem. Eng. J.*, vol. 251, pp. 422–434, Sep. 2014, doi: 10.1016/j.cej.2014.04.004.

- [167] V. Agarwal and P. B. Zetterlund, "Strategies for reduction of graphene oxide – A comprehensive review," *Chem. Eng. J.*, vol. 405, p. 127018, Feb. 2021, doi: 10.1016/j.cej.2020.127018.
- [168] S. N. Alam, N. Sharma, and L. Kumar, "Synthesis of Graphene Oxide (GO) by Modified Hummers Method and Its Thermal Reduction to Obtain Reduced Graphene Oxide (rGO)*," *Graphene*, vol. 06, no. 01, pp. 1–18, 2017, doi: 10.4236/graphene.2017.61001.
- [169] B. Patella *et al.*, "Electrochemical sensor based on rGO/Au nanoparticles for monitoring H₂O₂ released by human macrophages," *Sens. Actuators B Chem.*, vol. 327, p. 128901, Jan. 2021, doi: 10.1016/j.snb.2020.128901.
- [170] T.-Y. Huang, J.-H. Huang, H.-Y. Wei, K.-C. Ho, and C.-W. Chu, "rGO/SWCNT composites as novel electrode materials for electrochemical biosensing," *Biosens. Bioelectron.*, vol. 43, pp. 173–179, May 2013, doi: 10.1016/j.bios.2012.10.047.
- [171] Y. H. Huang *et al.*, "One-pot hydrothermal synthesis carbon nanocages-reduced graphene oxide composites for simultaneous electrochemical detection of catechol and hydroquinone," *Sens. Actuators B Chem.*, vol. 212, pp. 165–173, Jun. 2015, doi: 10.1016/j.snb.2015.02.013.
- [172] Y. Chen *et al.*, "Ultrasensitive and simultaneous detection of hydroquinone, catechol and resorcinol based on the electrochemical co-reduction prepared Au-Pd nanoflower/reduced graphene oxide nanocomposite," *Electrochimica Acta*, vol. 231, pp. 677–685, Mar. 2017, doi: 10.1016/j.electacta.2017.02.060.
- [173] H. Zhang, X. Bo, and L. Guo, "Electrochemical preparation of porous graphene and its electrochemical application in the simultaneous determination of hydroquinone, catechol, and resorcinol," *Sens. Actuators B Chem.*, vol. 220, pp. 919–926, Dec. 2015, doi: 10.1016/j.snb.2015.06.035.
- [174] L. A. Goulart, R. Gonçalves, A. A. Correa, E. C. Pereira, and L. H. Mascaro, "Synergic effect of silver nanoparticles and carbon nanotubes on the simultaneous voltammetric determination of hydroquinone, catechol, bisphenol A and phenol," *Microchim. Acta*, vol. 185, no. 1, p. 12, Jan. 2018, doi: 10.1007/s00604-017-2540-5.
- [175] H. Yin *et al.*, "Electrochemical behavior of catechol, resorcinol and hydroquinone at graphene–chitosan composite film modified glassy carbon electrode and their simultaneous determination in water samples," *Electrochimica Acta*, vol. 56, no. 6, pp. 2748–2753, Feb. 2011, doi: 10.1016/j.electacta.2010.12.060.
- [176] L. Chen, Y. Tang, K. Wang, C. Liu, and S. Luo, "Direct electrodeposition of reduced graphene oxide on glassy carbon electrode and its electrochemical application," *Electrochem. Commun.*, vol. 13, no. 2, pp. 133–137, Feb. 2011, doi: 10.1016/j.elecom.2010.11.033.
- [177] F. Hu, S. Chen, C. Wang, R. Yuan, D. Yuan, and C. Wang, "Study on the application of reduced graphene oxide and multiwall carbon nanotubes hybrid materials for simultaneous determination of catechol, hydroquinone, p-cresol and nitrite," *Anal. Chim. Acta*, vol. 724, pp. 40–46, Apr. 2012, doi: 10.1016/j.aca.2012.02.037.
- [178] F.-Y. Kong *et al.*, "Voltammetric simultaneous determination of catechol and hydroquinone using a glassy carbon electrode modified with a ternary hybrid material composed of reduced graphene oxide, magnetite nanoparticles and gold nanoparticles," *Microchim. Acta*, vol. 186, no. 3, p. 177, Mar. 2019, doi: 10.1007/s00604-019-3273-4.
- [179] H. Sohrabi *et al.*, "Electrochemical layered double hydroxide (LDH)-based biosensors for pesticides detection in food and environment samples: A review of status and prospects," *Food Chem. Toxicol.*, vol. 164, p. 113010, Jun. 2022, doi: 10.1016/j.fct.2022.113010.
- [180] C. Zhang, X. Liang, Y. Lu, H. Li, and X. Xu, "Performance of CuAl-LDH/Gr Nanocomposite-Based Electrochemical Sensor with Regard to Trace Glyphosate Detection in Water," *Sensors*, vol. 20, no. 15, p. 4146, Jul. 2020, doi: 10.3390/s20154146.
- [181] M. Sajid and C. Basheer, "Layered double hydroxides: Emerging sorbent materials for analytical extractions," *TrAC Trends Anal. Chem.*, vol. 75, pp. 174–182, Jan. 2016, doi: 10.1016/j.trac.2015.06.010.

- [182] S. He, Z. An, M. Wei, D. G. Evans, and X. Duan, "Layered double hydroxide-based catalysts: nanostructure design and catalytic performance," *Chem. Commun.*, vol. 49, no. 53, p. 5912, 2013, doi: 10.1039/c3cc42137f.
- [183] E. N. Kalali, X. Wang, and D.-Y. Wang, "Functionalized layered double hydroxide-based epoxy nanocomposites with improved flame retardancy and mechanical properties," *J. Mater. Chem. A*, vol. 3, no. 13, pp. 6819–6826, 2015, doi: 10.1039/C5TA00010F.
- [184] I. Nicotera *et al.*, "Composite polymer electrolyte membranes based on Mg–Al layered double hydroxide (LDH) platelets for H₂/air-fed fuel cells," *Solid State Ion.*, vol. 276, pp. 40–46, Aug. 2015, doi: 10.1016/j.ssi.2015.03.037.
- [185] L. Li, W. Gu, J. Chen, W. Chen, and Z. P. Xu, "Co-delivery of siRNAs and anti-cancer drugs using layered double hydroxide nanoparticles," *Biomaterials*, vol. 35, no. 10, pp. 3331–3339, Mar. 2014, doi: 10.1016/j.biomaterials.2013.12.095.
- [186] C. Li, M. Wei, D. G. Evans, and X. Duan, "Layered Double Hydroxide-based Nanomaterials as Highly Efficient Catalysts and Adsorbents," *Small*, vol. 10, no. 22, pp. 4469–4486, Nov. 2014, doi: 10.1002/sml.201401464.
- [187] D. Chaillot, S. Bennici, and J. Brendlé, "Layered double hydroxides and LDH-derived materials in chosen environmental applications: a review," *Environ. Sci. Pollut. Res.*, vol. 28, no. 19, pp. 24375–24405, May 2021, doi: 10.1007/s11356-020-08498-6.
- [188] A. Inayat, M. Klumpp, and W. Schwieger, "The urea method for the direct synthesis of ZnAl layered double hydroxides with nitrate as the interlayer anion," *Appl. Clay Sci.*, vol. 51, no. 4, pp. 452–459, Mar. 2011, doi: 10.1016/j.clay.2011.01.008.
- [189] R.-X. Xu, X.-Y. Yu, C. Gao, J.-H. Liu, R. G. Compton, and X.-J. Huang, "Enhancing selectivity in stripping voltammetry by different adsorption behaviors: the use of nanostructured Mg–Al-layered double hydroxides to detect Cd(ii)," *The Analyst*, vol. 138, no. 6, p. 1812, 2013, doi: 10.1039/c3an36271j.
- [190] X. Kong, X. Rao, J. Han, M. Wei, and X. Duan, "Layer-by-layer assembly of bi-protein/layered double hydroxide ultrathin film and its electrocatalytic behavior for catechol," *Biosens. Bioelectron.*, vol. 26, no. 2, pp. 549–554, Oct. 2010, doi: 10.1016/j.bios.2010.07.045.
- [191] X. Chen, C. Fu, Y. Wang, W. Yang, and D. G. Evans, "Direct electrochemistry and electrocatalysis based on a film of horseradish peroxidase intercalated into Ni–Al layered double hydroxide nanosheets," *Biosens. Bioelectron.*, vol. 24, no. 3, pp. 356–361, Nov. 2008, doi: 10.1016/j.bios.2008.04.007.
- [192] K.-H. Goh, T.-T. Lim, and Z. Dong, "Application of layered double hydroxides for removal of oxyanions: A review," *Water Res.*, vol. 42, no. 6–7, pp. 1343–1368, Mar. 2008, doi: 10.1016/j.watres.2007.10.043.
- [193] F. Yang, J. Chu, Y. Cheng, J. Gong, X. Wang, and S. Xiong, "Hydrothermal Synthesis of NiCo-layered Double Hydroxide Nanosheets Decorated on Biomass Carbon Skeleton for High Performance Supercapacitor," *Chem. Res. Chin. Univ.*, vol. 37, no. 3, pp. 772–777, Jun. 2021, doi: 10.1007/s40242-020-0333-6.
- [194] Nikhil, G. Ji, and R. Prakash, "Hydrothermal synthesis of Zn-Mg-based layered double hydroxide coatings for the corrosion protection of copper in chloride and hydroxide media," *Int. J. Miner. Metall. Mater.*, vol. 28, no. 12, pp. 1991–2000, Dec. 2021, doi: 10.1007/s12613-020-2122-0.
- [195] J. Dong, Q. Fang, H. He, Y. Zhang, J. Xu, and Y. Sun, "Electrochemical sensor based on EDTA intercalated into layered double hydroxides of magnesium and aluminum for ultra trace level detection of lead (II)," *Microchim. Acta*, vol. 182, no. 3–4, pp. 653–659, Feb. 2015, doi: 10.1007/s00604-014-1369-4.
- [196] K. Asadpour-Zeynali and R. Amini, "A novel voltammetric sensor for mercury(II) based on mercaptocarboxylic acid intercalated layered double hydroxide nanoparticles modified electrode," *Sens. Actuators B Chem.*, vol. 246, pp. 961–968, Jul. 2017, doi: 10.1016/j.snb.2017.02.141.

- [197] L. Fernández, I. Ledezma, C. Borrás, L. A. Martínez, and H. Carrero, "Horseradish peroxidase modified electrode based on a film of Co–Al layered double hydroxide modified with sodium dodecylbenzenesulfonate for determination of 2-chlorophenol," *Sens. Actuators B Chem.*, vol. 182, pp. 625–632, Jun. 2013, doi: 10.1016/j.snb.2013.02.109.
- [198] T. Zhan, Y. Song, X. Li, and W. Hou, "Electrochemical sensor for bisphenol A based on ionic liquid functionalized Zn–Al layered double hydroxide modified electrode," *Mater. Sci. Eng. C*, vol. 64, pp. 354–361, Jul. 2016, doi: 10.1016/j.msec.2016.03.093.
- [199] S.-S. Li, M. Jiang, T.-J. Jiang, J.-H. Liu, Z. Guo, and X.-J. Huang, "Competitive adsorption behavior toward metal ions on nano-Fe/Mg/Ni ternary layered double hydroxide proved by XPS: Evidence of selective and sensitive detection of Pb(II)," *J. Hazard. Mater.*, vol. 338, pp. 1–10, Sep. 2017, doi: 10.1016/j.jhazmat.2017.05.017.
- [200] Z. Yang, W. W. Tjiu, W. Fan, and T. Liu, "Electrodepositing Ag nanodendrites on layered double hydroxides modified glassy carbon electrode: Novel hierarchical structure for hydrogen peroxide detection," *Electrochimica Acta*, vol. 90, pp. 400–407, Feb. 2013, doi: 10.1016/j.electacta.2012.12.038.
- [201] M. Asif *et al.*, "Core-shell iron oxide-layered double hydroxide: High electrochemical sensing performance of H₂O₂ biomarker in live cancer cells with plasma therapeutics," *Biosens. Bioelectron.*, vol. 97, pp. 352–359, Nov. 2017, doi: 10.1016/j.bios.2017.05.057.
- [202] M. Asif *et al.*, "Metal oxide intercalated layered double hydroxide nanosphere: With enhanced electrocatalytic activity towards H₂O₂ for biological applications," *Sens. Actuators B Chem.*, vol. 239, pp. 243–252, Feb. 2017, doi: 10.1016/j.snb.2016.08.010.
- [203] H. Liang, X. Miao, and J. Gong, "One-step fabrication of layered double hydroxides/graphene hybrid as solid-phase extraction for stripping voltammetric detection of methyl parathion," *Electrochem. Commun.*, vol. 20, pp. 149–152, Jul. 2012, doi: 10.1016/j.elecom.2012.04.010.
- [204] M. S. Yarger, E. M. P. Steinmiller, and K.-S. Choi, "Electrochemical Synthesis of Zn–Al Layered Double Hydroxide (LDH) Films," *Inorg. Chem.*, vol. 47, no. 13, pp. 5859–5865, Jul. 2008, doi: 10.1021/ic800193j.
- [205] K. Nejati and K. Asadpour-Zeynali, "Electrochemical synthesis of nickel–iron layered double hydroxide: Application as a novel modified electrode in electrocatalytic reduction of metronidazole," *Mater. Sci. Eng. C*, vol. 35, pp. 179–184, Feb. 2014, doi: 10.1016/j.msec.2013.11.003.
- [206] N. Baig and M. Sajid, "Applications of layered double hydroxides based electrochemical sensors for determination of environmental pollutants: A review," *Trends Environ. Anal. Chem.*, vol. 16, pp. 1–15, Oct. 2017, doi: 10.1016/j.teac.2017.10.003.
- [207] I. M. Isa, S. N. M. Sharif, N. Hashim, and S. A. Ghani, "Amperometric determination of nanomolar mercury(II) by layered double nanocomposite of zinc/aluminium hydroxide-3(4-methoxyphenyl)propionate modified single-walled carbon nanotube paste electrode," *Ionics*, vol. 21, no. 10, pp. 2949–2958, Oct. 2015, doi: 10.1007/s11581-015-1466-3.
- [208] H. Nakayama, S. Hiram, and M. Tshako, "Selective adsorption of mercury ion by mercaptocarboxylic acid intercalated Mg–Al layered double hydroxide," *J. Colloid Interface Sci.*, vol. 315, no. 1, pp. 177–183, Nov. 2007, doi: 10.1016/j.jcis.2007.06.036.
- [209] H. Heli, J. Pishahang, and H. B. Amiri, "Synthesis of hexagonal CoAl-layered double hydroxide nanoshales/carbon nanotubes composite for the non-enzymatic detection of hydrogen peroxide," *J. Electroanal. Chem.*, vol. 768, pp. 134–144, May 2016, doi: 10.1016/j.jelechem.2016.01.042.
- [210] S. B. Khan, A. M. Asiri, K. Akhtar, and M. A. Rub, "Development of electrochemical sensor based on layered double hydroxide as a marker of environmental toxin," *J. Ind. Eng. Chem.*, vol. 30, pp. 234–238, Oct. 2015, doi: 10.1016/j.jiec.2015.05.027.

- [211] S. Yuan, D. Peng, X. Hu, and J. Gong, "Bifunctional sensor of pentachlorophenol and copper ions based on nanostructured hybrid films of humic acid and exfoliated layered double hydroxide via a facile layer-by-layer assembly," *Anal. Chim. Acta*, vol. 785, pp. 34–42, Jun. 2013, doi: 10.1016/j.aca.2013.04.050.
- [212] M. Li *et al.*, "Sensitive and Facile Determination of Catechol and Hydroquinone Simultaneously Under Coexistence of Resorcinol with a Zn/Al Layered Double Hydroxide Film Modified Glassy Carbon Electrode," *Electroanalysis*, vol. 21, no. 13, pp. 1521–1526, Jul. 2009, doi: 10.1002/elan.200804573.
- [213] M. Shen, Z. Zhang, and Y. Ding, "Synthesizing NiAl-layered double hydroxide microspheres with hierarchical structure and electrochemical detection of hydroquinone and catechol," *Microchem. J.*, vol. 124, pp. 209–214, Jan. 2016, doi: 10.1016/j.microc.2015.08.011.
- [214] H. Yin, Y. Zhou, L. Cui, X. Liu, S. Ai, and L. Zhu, "Electrochemical oxidation behavior of bisphenol A at surfactant/layered double hydroxide modified glassy carbon electrode and its determination," *J. Solid State Electrochem.*, vol. 15, no. 1, pp. 167–173, Jan. 2011, doi: 10.1007/s10008-010-1089-6.
- [215] E. Han, D. Shan, H. Xue, and S. Cosnier, "Hybrid Material Based on Chitosan and Layered Double Hydroxides: Characterization and Application to the Design of Amperometric Phenol Biosensor," *Biomacromolecules*, vol. 8, no. 3, pp. 971–975, Mar. 2007, doi: 10.1021/bm060897d.
- [216] P. Bai, G. Fan, and F. Li, "Novel Zn–Al layered double hydroxide/carbon nanotube nanocomposite for electrochemical determination of catechol and hydroquinone," *Mater. Lett.*, vol. 65, no. 15–16, pp. 2330–2332, Aug. 2011, doi: 10.1016/j.matlet.2011.05.038.
- [217] M. Ali, E. Pervaiz, T. Noor, O. Rabi, R. Zahra, and M. Yang, "Recent advancements in MOF- based catalysts for applications in electrochemical and photoelectrochemical water splitting: A review," *Int. J. Energy Res.*, vol. 45, no. 2, pp. 1190–1226, Feb. 2021, doi: 10.1002/er.5807.
- [218] C. Candia-Onfray, S. Rojas, M. V. B. Zanoni, and R. Salazar, "An updated review of metal–organic framework materials in photo(electro)catalytic applications: From CO₂ reduction to wastewater treatments," *Curr. Opin. Electrochem.*, vol. 26, p. 100669, Apr. 2021, doi: 10.1016/j.coelec.2020.100669.
- [219] A. Amini, S. Kazemi, and V. Safarifard, "Metal-organic framework-based nanocomposites for sensing applications – A review," *Polyhedron*, vol. 177, p. 114260, Feb. 2020, doi: 10.1016/j.poly.2019.114260.
- [220] L. He *et al.*, "Recent progress in nanoscale metal-organic frameworks for drug release and cancer therapy," *Nanomed.*, vol. 14, no. 10, pp. 1343–1365, May 2019, doi: 10.2217/nnm-2018-0347.
- [221] Y. Cao, X. Mi, X. Li, and B. Wang, "Defect Engineering in Metal–Organic Frameworks as Futuristic Options for Purification of Pollutants in an Aqueous Environment," *Front. Chem.*, vol. 9, p. 673738, Aug. 2021, doi: 10.3389/fchem.2021.673738.
- [222] Y. Wen, X. Wu, and Q. Zhu, "The Structures of Metal–Organic Frameworks," in *Advanced Structural Chemistry*, 1st ed., R. Cao, Ed. Wiley, 2021, pp. 342–389. doi: 10.1002/9783527831753.ch6c.
- [223] C. Dey, T. Kundu, B. P. Biswal, A. Mallick, and R. Banerjee, "Crystalline metal-organic frameworks (MOFs): synthesis, structure and function," *Acta Crystallogr. Sect. B Struct. Sci. Cryst. Eng. Mater.*, vol. 70, no. 1, pp. 3–10, Feb. 2014, doi: 10.1107/S2052520613029557.
- [224] L. J. Wang *et al.*, "Synthesis and Characterization of Metal–Organic Framework-74 Containing 2, 4, 6, 8, and 10 Different Metals," *Inorg. Chem.*, vol. 53, no. 12, pp. 5881–5883, Jun. 2014, doi: 10.1021/ic500434a.
- [225] E. A. Flügel, A. Ranft, F. Haase, and B. V. Lotsch, "Synthetic routes toward MOF nanomorphologies," *J. Mater. Chem.*, vol. 22, no. 20, p. 10119, 2012, doi: 10.1039/c2jm15675j.
- [226] Y.-R. Lee, J. Kim, and W.-S. Ahn, "Synthesis of metal-organic frameworks: A mini review," *Korean J. Chem. Eng.*, vol. 30, no. 9, pp. 1667–1680, Sep. 2013, doi: 10.1007/s11814-013-0140-6.

- [227] W. Kleist, M. Maciejewski, and A. Baiker, "MOF-5 based mixed-linker metal-organic frameworks: Synthesis, thermal stability and catalytic application," *Thermochim. Acta*, vol. 499, no. 1–2, pp. 71–78, Feb. 2010, doi: 10.1016/j.tca.2009.11.004.
- [228] D. J. Tranchemontagne, J. R. Hunt, and O. M. Yaghi, "Room temperature synthesis of metal-organic frameworks: MOF-5, MOF-74, MOF-177, MOF-199, and IRMOF-0," *Tetrahedron*, vol. 64, no. 36, pp. 8553–8557, Sep. 2008, doi: 10.1016/j.tet.2008.06.036.
- [229] Q. Wu, C. Zhang, K. Sun, and H.-L. Jiang, "Microwave-Assisted Synthesis and Photocatalytic Performance of a Soluble Porphyrinic MOF," *Acta Chim. Sin.*, vol. 78, no. 7, p. 688, 2020, doi: 10.6023/A20050141.
- [230] H. Zhang, M. Zhao, and Y. S. Lin, "Stability of ZIF-8 in water under ambient conditions," *Microporous Mesoporous Mater.*, vol. 279, pp. 201–210, May 2019, doi: 10.1016/j.micromeso.2018.12.035.
- [231] H. Jiang, Q. Wang, H. Wang, Y. Chen, and M. Zhang, "Temperature effect on the morphology and catalytic performance of Co-MOF-74 in low-temperature NH₃-SCR process," *Catal. Commun.*, vol. 80, pp. 24–27, May 2016, doi: 10.1016/j.catcom.2016.03.013.
- [232] N. Nijem *et al.*, "Interaction of Molecular Hydrogen with Microporous Metal Organic Framework Materials at Room Temperature," *J. Am. Chem. Soc.*, vol. 132, no. 5, pp. 1654–1664, Feb. 2010, doi: 10.1021/ja908817n.
- [233] A. Benedetto and A. Calvi, "A pilot study on microwave heating for production and recycling of road pavement materials," *Constr. Build. Mater.*, vol. 44, pp. 351–359, Jul. 2013, doi: 10.1016/j.conbuildmat.2013.02.082.
- [234] N. A. Pivovarov, "Use of Wave Effect in Processing of the Hydrocarbonic Raw Material (Review)," *Pet. Chem.*, vol. 59, no. 6, pp. 559–569, Jun. 2019, doi: 10.1134/S0965544119060148.
- [235] P. Amo-Ochoa, G. Givaja, P. J. S. Miguel, O. Castillo, and F. Zamora, "Microwave assisted hydrothermal synthesis of a novel CuI-sulfate-pyrazine MOF," *Inorg. Chem. Commun.*, vol. 10, no. 8, pp. 921–924, Aug. 2007, doi: 10.1016/j.inoche.2007.04.024.
- [236] J. Klinowski, F. A. Almeida Paz, P. Silva, and J. Rocha, "Microwave-Assisted Synthesis of Metal-Organic Frameworks," *Dalton Trans*, vol. 40, no. 2, pp. 321–330, 2011, doi: 10.1039/C0DT00708K.
- [237] Y. Liu, Y. Zhang, J. Chen, and H. Pang, "Copper metal-organic framework nanocrystal for plane effect nonenzymatic electro-catalytic activity of glucose," *Nanoscale*, vol. 6, no. 19, pp. 10989–10994, 2014, doi: 10.1039/C4NR03396E.
- [238] Z. Li *et al.*, "An electrochemical sensor for bacterial lipopolysaccharide detection based on dual functional Cu²⁺-modified metal-organic framework nanoparticles," *Microchim. Acta*, vol. 187, no. 7, p. 415, Jul. 2020, doi: 10.1007/s00604-020-04364-x.
- [239] P. Arul and S. A. John, "Size controlled synthesis of Ni-MOF using polyvinylpyrrolidone: New electrode material for the trace level determination of nitrobenzene," *J. Electroanal. Chem.*, vol. 829, pp. 168–176, Nov. 2018, doi: 10.1016/j.jelechem.2018.10.014.
- [240] X. Gao *et al.*, "Surface functionalization of carbon cloth with cobalt-porphyrin-based metal organic framework for enhanced electrochemical sensing," *Carbon*, vol. 148, pp. 64–71, Jul. 2019, doi: 10.1016/j.carbon.2019.03.040.
- [241] N. S. Lopa *et al.*, "A chemically and electrochemically stable, redox-active and highly sensitive metal azolate framework for non-enzymatic electrochemical detection of glucose," *J. Electroanal. Chem.*, vol. 840, pp. 263–271, May 2019, doi: 10.1016/j.jelechem.2019.03.081.
- [242] B. Li, J. Ma, and P. Cheng, "Integration of Metal Nanoparticles into Metal-Organic Frameworks for Composite Catalysts: Design and Synthetic Strategy," *Small*, vol. 15, no. 32, p. 1804849, Aug. 2019, doi: 10.1002/sml.201804849.

- [243] Y. Wang, L. Wang, H. Chen, X. Hu, and S. Ma, "Fabrication of Highly Sensitive and Stable Hydroxylamine Electrochemical Sensor Based on Gold Nanoparticles and Metal–Metalloporphyrin Framework Modified Electrode," *ACS Appl. Mater. Interfaces*, vol. 8, no. 28, pp. 18173–18181, Jul. 2016, doi: 10.1021/acsami.6b04819.
- [244] Z. Peng, Z. Jiang, X. Huang, and Y. Li, "A novel electrochemical sensor of tryptophan based on silver nanoparticles/metal–organic framework composite modified glassy carbon electrode," *RSC Adv.*, vol. 6, no. 17, pp. 13742–13748, 2016, doi: 10.1039/C5RA25251B.
- [245] W. Dang, Y. Sun, H. Jiao, L. Xu, and M. Lin, "AuNPs-NH₂/Cu-MOF modified glassy carbon electrode as enzyme-free electrochemical sensor detecting H₂O₂," *J. Electroanal. Chem.*, vol. 856, p. 113592, Jan. 2020, doi: 10.1016/j.jelechem.2019.113592.
- [246] Z. Wang *et al.*, "MOF-derived binary mixed carbon/metal oxide porous materials for constructing simultaneous determination of hydroquinone and catechol sensor," *J. Solid State Electrochem.*, vol. 23, no. 1, pp. 81–89, Jan. 2019, doi: 10.1007/s10008-018-4111-z.
- [247] H. Chen, X. Wu, C. Lao, Y. Li, Q. Yuan, and W. Gan, "MOF derived porous carbon modified rGO for simultaneous determination of hydroquinone and catechol," *J. Electroanal. Chem.*, vol. 835, pp. 254–261, Feb. 2019, doi: 10.1016/j.jelechem.2019.01.027.
- [248] Y. Zhou, C. Li, Y. Hao, B. Ye, and M. Xu, "Oriented growth of cross-linked metal-organic framework film on graphene surface for non-enzymatic electrochemical sensor of hydrogen peroxide in disinfectant," *Talanta*, vol. 188, pp. 282–287, Oct. 2018, doi: 10.1016/j.talanta.2018.05.078.
- [249] X.-Q. Wu *et al.*, "Metal–organic framework biosensor with high stability and selectivity in a bio-mimic environment," *Chem. Commun.*, vol. 51, no. 44, pp. 9161–9164, 2015, doi: 10.1039/C5CC02113H.
- [250] Y. Hua *et al.*, "Highly selective and reproducible electroanalysis for histidine in blood with turn-on responses at a potential approaching zero using tetrahedral copper metal organic frameworks," *Chem. Commun.*, vol. 55, no. 9, pp. 1271–1274, 2019, doi: 10.1039/C8CC09562K.
- [251] W. Ling *et al.*, "Materials and Techniques for Implantable Nutrient Sensing Using Flexible Sensors Integrated with Metal–Organic Frameworks," *Adv. Mater.*, vol. 30, no. 23, p. 1800917, Jun. 2018, doi: 10.1002/adma.201800917.
- [252] D. Yu, Y. Zeng, Y. Qi, T. Zhou, and G. Shi, "A novel electrochemical sensor for determination of dopamine based on AuNPs@SiO₂ core-shell imprinted composite," *Biosens. Bioelectron.*, vol. 38, no. 1, pp. 270–277, Oct. 2012, doi: 10.1016/j.bios.2012.05.045.
- [253] N. P. Shetti, S. J. Malode, D. Ilager, K. Raghava Reddy, S. S. Shukla, and T. M. Aminabhavi, "A Novel Electrochemical Sensor for Detection of Molinate Using ZnO Nanoparticles Loaded Carbon Electrode," *Electroanalysis*, vol. 31, no. 6, pp. 1040–1049, Jun. 2019, doi: 10.1002/elan.201800775.
- [254] L. A. Alshahrani, L. Liu, P. Sathishkumar, J. Nan, and F. L. Gu, "Copper oxide and carbon nano-fragments modified glassy carbon electrode as selective electrochemical sensor for simultaneous determination of catechol and hydroquinone in real-life water samples," *J. Electroanal. Chem.*, vol. 815, pp. 68–75, Apr. 2018, doi: 10.1016/j.jelechem.2018.03.004.
- [255] X. Wang, X. Bu, and P. Feng, "Porous Inorganic Materials," in *Encyclopedia of Inorganic and Bioinorganic Chemistry*, R. A. Scott, Ed. Chichester, UK: John Wiley & Sons, Ltd, 2011, p. eibc0264. doi: 10.1002/9781119951438.eibc0264.
- [256] H. Huwe and M. Fröba, "Synthesis and characterization of transition metal and metal oxide nanoparticles inside mesoporous carbon CMK-3," *Carbon*, vol. 45, no. 2, pp. 304–314, Feb. 2007, doi: 10.1016/j.carbon.2006.09.021.
- [257] J. M. George, A. Antony, and B. Mathew, "Metal oxide nanoparticles in electrochemical sensing and biosensing: a review," *Microchim. Acta*, vol. 185, no. 7, p. 358, Jul. 2018, doi: 10.1007/s00604-018-2894-3.

- [258] B. Panchapakesan, D. L. DeVoe, M. R. Widmaier, R. Cavicchi, and S. Semancik, "Nanoparticle engineering and control of tin oxide microstructures for chemical microsensor applications," *Nanotechnology*, vol. 12, no. 3, pp. 336–349, Sep. 2001, doi: 10.1088/0957-4484/12/3/323.
- [259] A. Mirzaei, K. Janghorban, B. Hashemi, and G. Neri, "Metal-core@metal oxide-shell nanomaterials for gas-sensing applications: a review," *J. Nanoparticle Res.*, vol. 17, no. 9, p. 371, Sep. 2015, doi: 10.1007/s11051-015-3164-5.
- [260] X. Liu *et al.*, "Noble metal–metal oxide nano hybrids with tailored nanostructures for efficient solar energy conversion, photocatalysis and environmental remediation," *Energy Environ. Sci.*, vol. 10, no. 2, pp. 402–434, 2017, doi: 10.1039/C6EE02265K.
- [261] Y. Ren, Z. Ma, and P. G. Bruce, "Ordered mesoporous metal oxides: synthesis and applications," *Chem. Soc. Rev.*, vol. 41, no. 14, p. 4909, 2012, doi: 10.1039/c2cs35086f.
- [262] X. Hu *et al.*, "Molten salt-promoted Ni–Fe/Al₂O₃ catalyst for methane decomposition," *Int. J. Hydrog. Energy*, vol. 45, no. 7, pp. 4244–4253, Feb. 2020, doi: 10.1016/j.ijhydene.2019.11.209.
- [263] M. A. Hayward, M. A. Green, M. J. Rosseinsky, and J. Sloan, "Sodium Hydride as a Powerful Reducing Agent for Topotactic Oxide Deintercalation: Synthesis and Characterization of the Nickel(I) Oxide LaNiO₂," *J. Am. Chem. Soc.*, vol. 121, no. 38, pp. 8843–8854, Sep. 1999, doi: 10.1021/ja991573i.
- [264] "Psidium Guajava Leave Extract as Reducing Agent for Synthesis of Zinc Oxide Nanoparticles and its Application to Impart Multifunctional Properties for Cellulosic Fabrics," *Biointerface Res. Appl. Chem.*, vol. 11, no. 5, pp. 13535–13556, Feb. 2021, doi: 10.33263/BRIAC115.1353513556.
- [265] A. V. Nikam, B. L. V. Prasad, and A. A. Kulkarni, "Wet chemical synthesis of metal oxide nanoparticles: a review," *CrystEngComm*, vol. 20, no. 35, pp. 5091–5107, 2018, doi: 10.1039/C8CE00487K.
- [266] A. Allanore, "Features and Challenges of Molten Oxide Electrolytes for Metal Extraction," *J. Electrochem. Soc.*, vol. 162, no. 1, pp. E13–E22, 2015, doi: 10.1149/2.0451501jes.
- [267] R. O. Wright and A. Baccarelli, "Metals and Neurotoxicology," *J. Nutr.*, vol. 137, no. 12, pp. 2809–2813, Dec. 2007, doi: 10.1093/jn/137.12.2809.
- [268] K. S. Mohandas, "Direct electrochemical conversion of metal oxides to metal by molten salt electrolysis: a review," *Miner. Process. Extr. Metall.*, vol. 122, no. 4, pp. 195–212, Dec. 2013, doi: 10.1179/0371955313Z.00000000069.
- [269] C. Young, J. Wang, J. Kim, Y. Sugahara, J. Henzie, and Y. Yamauchi, "Controlled Chemical Vapor Deposition for Synthesis of Nanowire Arrays of Metal–Organic Frameworks and Their Thermal Conversion to Carbon/Metal Oxide Hybrid Materials," *Chem. Mater.*, vol. 30, no. 10, pp. 3379–3386, May 2018, doi: 10.1021/acs.chemmater.8b00836.
- [270] R. John, A. Ashokreddy, C. Vijayan, and T. Pradeep, "Single- and few-layer graphene growth on stainless steel substrates by direct thermal chemical vapor deposition," *Nanotechnology*, vol. 22, no. 16, p. 165701, Apr. 2011, doi: 10.1088/0957-4484/22/16/165701.
- [271] N. Kaur, E. Comini, D. Zappa, N. Poli, and G. Sberveglieri, "Nickel oxide nanowires: vapor liquid solid synthesis and integration into a gas sensing device," *Nanotechnology*, vol. 27, no. 20, p. 205701, May 2016, doi: 10.1088/0957-4484/27/20/205701.
- [272] H. K. Yu and J.-L. Lee, "Growth mechanism of metal-oxide nanowires synthesized by electron beam evaporation: A self-catalytic vapor-liquid-solid process," *Sci. Rep.*, vol. 4, no. 1, p. 6589, May 2015, doi: 10.1038/srep06589.

- [273] S. Shafiei, A. Nourbakhsh, B. Ganjipour, M. Zahedifar, and G. Vakili-Nezhaad, "Diameter optimization of VLS-synthesized ZnO nanowires, using statistical design of experiment," *Nanotechnology*, vol. 18, no. 35, p. 355708, Sep. 2007, doi: 10.1088/0957-4484/18/35/355708.
- [274] J. L. Gumaste, S. K. Singh, P. K. Sahoo, and R. K. Galgali, "Synthesis of TiC Fibres from TiO₂ Containing Raw Materials by Vapour-Liquid-Solid (V-L-S) Growth Method," *Trans. Indian Ceram. Soc.*, vol. 62, no. 2, pp. 97–99, Apr. 2003, doi: 10.1080/0371750X.2003.11012084.
- [275] M. Starowicz and B. Stypuła, "Electrochemical Synthesis of ZnO Nanoparticles," *Eur. J. Inorg. Chem.*, vol. 2008, no. 6, pp. 869–872, Feb. 2008, doi: 10.1002/ejic.200700989.
- [276] M. N. Kamalasanan and S. Chandra, "Sol-gel synthesis of ZnO thin films," *Thin Solid Films*, vol. 288, no. 1–2, pp. 112–115, Nov. 1996, doi: 10.1016/S0040-6090(96)08864-5.
- [277] R. Sui and P. Charpentier, "Synthesis of Metal Oxide Nanostructures by Direct Sol–Gel Chemistry in Supercritical Fluids," *Chem. Rev.*, vol. 112, no. 6, pp. 3057–3082, Jun. 2012, doi: 10.1021/cr2000465.
- [278] H. Cai *et al.*, "Facile Hydrothermal Synthesis and Surface Functionalization of Polyethyleneimine-Coated Iron Oxide Nanoparticles for Biomedical Applications," *ACS Appl. Mater. Interfaces*, vol. 5, no. 5, pp. 1722–1731, Mar. 2013, doi: 10.1021/am302883m.
- [279] S. Narayanan, "Metal-Polymer Hybrid Materials For Transparent Conductors," 2014, doi: 10.13140/RG.2.1.3957.7682.
- [280] X. Zhou, H. Pu, and D.-W. Sun, "DNA functionalized metal and metal oxide nanoparticles: principles and recent advances in food safety detection," *Crit. Rev. Food Sci. Nutr.*, vol. 61, no. 14, pp. 2277–2296, Aug. 2021, doi: 10.1080/10408398.2020.1809343.
- [281] H. Abunahla *et al.*, "MOMSense: Metal-Oxide-Metal Elementary Glucose Sensor," *Sci. Rep.*, vol. 9, no. 1, p. 5524, Dec. 2019, doi: 10.1038/s41598-019-41892-w.
- [282] Y. Pan, Z. Hou, W. Yi, W. Zhu, F. Zeng, and Y.-N. Liu, "Hierarchical hybrid film of MnO₂ nanoparticles/multi-walled fullerene nanotubes–graphene for highly selective sensing of hydrogen peroxide," *Talanta*, vol. 141, pp. 86–91, Aug. 2015, doi: 10.1016/j.talanta.2015.03.059.
- [283] A. T. E. Vilian and S.-M. Chen, "Preparation of carbon nanotubes decorated with manganese dioxide nanoparticles for electrochemical determination of ferulic acid," *Microchim. Acta*, vol. 182, no. 5–6, pp. 1103–1111, Apr. 2015, doi: 10.1007/s00604-014-1431-2.
- [284] A. T. Ezhil Vilian *et al.*, "Facile synthesis of MnO₂/carbon nanotubes decorated with a nanocomposite of Pt nanoparticles as a new platform for the electrochemical detection of catechin in red wine and green tea samples," *J. Mater. Chem. B*, vol. 3, no. 30, pp. 6285–6292, 2015, doi: 10.1039/C5TB00508F.
- [285] M. M. Farid, L. Goudini, F. Piri, A. Zamani, and F. Saadati, "Molecular imprinting method for fabricating novel glucose sensor: Polyvinyl acetate electrode reinforced by MnO₂/CuO loaded on graphene oxide nanoparticles," *Food Chem.*, vol. 194, pp. 61–67, Mar. 2016, doi: 10.1016/j.foodchem.2015.07.128.
- [286] Y.-W. Hsu, T.-K. Hsu, C.-L. Sun, Y.-T. Nien, N.-W. Pu, and M.-D. Ger, "Synthesis of CuO/graphene nanocomposites for nonenzymatic electrochemical glucose biosensor applications," *Electrochimica Acta*, vol. 82, pp. 152–157, Nov. 2012, doi: 10.1016/j.electacta.2012.03.094.
- [287] J. Yang, L.-C. Jiang, W.-D. Zhang, and S. Gunasekaran, "A highly sensitive non-enzymatic glucose sensor based on a simple two-step electrodeposition of cupric oxide (CuO) nanoparticles onto multi-walled carbon nanotube arrays," *Talanta*, vol. 82, no. 1, pp. 25–33, Jun. 2010, doi: 10.1016/j.talanta.2010.03.047.

- [288] J. Zhang *et al.*, “Serum immunoglobulin A/C3 ratio predicts progression of immunoglobulin A nephropathy: Serum IgA/C3 Ratio and IgA Nephropathy,” *Nephrology*, vol. 18, no. 2, pp. 125–131, Feb. 2013, doi: 10.1111/nep.12010.
- [289] J. Zhang, C. Bai, and Y. Song, “MIOTIC study: a prospective, multicenter, randomized study to evaluate the long-term efficacy of mobile phone-based Internet of Things in the management of patients with stable COPD,” *Int. J. Chron. Obstruct. Pulmon. Dis.*, p. 433, Sep. 2013, doi: 10.2147/COPD.S50205.
- [290] B. Li *et al.*, “Highly selective and sensitive determination of dopamine by the novel molecularly imprinted poly(nicotinamide)/CuO nanoparticles modified electrode,” *Biosens. Bioelectron.*, vol. 67, pp. 121–128, May 2015, doi: 10.1016/j.bios.2014.07.053.
- [291] J. Yang, H. Ye, F. Zhao, and B. Zeng, “A Novel Cu_xO Nanoparticles@ZIF-8 Composite Derived from Core–Shell Metal–Organic Frameworks for Highly Selective Electrochemical Sensing of Hydrogen Peroxide,” *ACS Appl. Mater. Interfaces*, vol. 8, no. 31, pp. 20407–20414, Aug. 2016, doi: 10.1021/acsami.6b06436.
- [292] Y. Hu, Z. Zhang, H. Zhang, L. Luo, and S. Yao, “Sensitive and selective imprinted electrochemical sensor for p-nitrophenol based on ZnO nanoparticles/carbon nanotubes doped chitosan film,” *Thin Solid Films*, vol. 520, no. 16, pp. 5314–5321, Jun. 2012, doi: 10.1016/j.tsf.2011.11.083.
- [293] E. Roy, S. Patra, A. Tiwari, R. Madhuri, and P. K. Sharma, “RETRACTED: Single cell imprinting on the surface of Ag–ZnO bimetallic nanoparticle modified graphene oxide sheets for targeted detection, removal and photothermal killing of E. Coli,” *Biosens. Bioelectron.*, vol. 89, pp. 620–626, Mar. 2017, doi: 10.1016/j.bios.2015.12.085.
- [294] Y. Yang, Y. Wang, X. Bao, and H. Li, “Electrochemical deposition of Ni nanoparticles decorated ZnO hexagonal prisms as an effective platform for non-enzymatic detection of glucose,” *J. Electroanal. Chem.*, vol. 775, pp. 163–170, Aug. 2016, doi: 10.1016/j.jelechem.2016.04.041.
- [295] T. Yumak, F. Kuralay, M. Muti, A. Sinag, A. Erdem, and S. Abaci, “Preparation and characterization of zinc oxide nanoparticles and their sensor applications for electrochemical monitoring of nucleic acid hybridization,” *Colloids Surf. B Biointerfaces*, vol. 86, no. 2, pp. 397–403, Sep. 2011, doi: 10.1016/j.colsurfb.2011.04.030.
- [296] A. Salimi, R. Hallaj, H. Mamkhezri, and S. M. T. Hosaini, “Electrochemical properties and electrocatalytic activity of FAD immobilized onto cobalt oxide nanoparticles: Application to nitrite detection,” *J. Electroanal. Chem.*, vol. 619–620, pp. 31–38, Jul. 2008, doi: 10.1016/j.jelechem.2008.03.003.
- [297] W. Jia *et al.*, “Electrocatalytic oxidation and reduction of H₂O₂ on vertically aligned Co₃O₄ nanowalls electrode: Toward H₂O₂ detection,” *J. Electroanal. Chem.*, vol. 625, no. 1, pp. 27–32, Jan. 2009, doi: 10.1016/j.jelechem.2008.09.020.
- [298] S. Erogul, S. Z. Bas, M. Ozmen, and S. Yildiz, “A new electrochemical sensor based on Fe₃O₄ functionalized graphene oxide-gold nanoparticle composite film for simultaneous determination of catechol and hydroquinone,” *Electrochimica Acta*, vol. 186, pp. 302–313, Dec. 2015, doi: 10.1016/j.electacta.2015.10.174.
- [299] G. Ma, H. Xu, M. Wu, L. Wang, J. Wu, and F. Xu, “A hybrid composed of MoS₂, reduced graphene oxide and gold nanoparticles for voltammetric determination of hydroquinone, catechol, and resorcinol,” *Microchim. Acta*, vol. 186, no. 11, p. 689, Nov. 2019, doi: 10.1007/s00604-019-3771-4.
- [300] L. A. Goulart and L. H. Mascaro, “GC electrode modified with carbon nanotubes and NiO for the simultaneous determination of bisphenol A, hydroquinone and catechol,” *Electrochimica Acta*, vol. 196, pp. 48–55, Apr. 2016, doi: 10.1016/j.electacta.2016.02.174.

Chapter II

**Apparatus, electrochemical methods
and preparation of electrodes**

II.1. Introduction

Carbon-based materials for the preparation of electrochemical sensors are widely used because of their low cost, their wide availability, and their biocompatibility and also their ability to create a very favorable microenvironment for the electrochemical system (reaction-diffusion) of electroactive species [1-3]. For example, the use of graphite, carbon nanotubes (CNT) or even graphene with its two forms (oxidized or reduced) is very successful and many scientific articles have discussed the performance of the use of carbon-based materials on the response analytics of electrochemical sensors [4-6].

The catalytic properties of carbon-based nanocomposites are considerably improved by the combination of noble materials such as zinc oxide (ZnO) [7] or manganese oxide (MgO) [4]. In the present thesis, different electrochemical sensors were prepared for the detection of the organic pollutants like catechol (CC), hydroquinone (HQ) and pentachlorophenol (5-CP) using metal organic framework (MOF) and layered double hydroxide (LDH).

The present chapter describes the experimental methods for the preparation of new nanocomposites as high electrocatalysts for sensing applications. The prepared nanocomposites were characterized by Fourier transform infrared spectroscopy (FTIR) and scanning electron microscopy (SEM). The electrochemical characterization was also carried out such as impedance measurements to confirm the conductivity and the electrocatalytic behavior of the synthesized nanocomposite. The application of this nanocomposite is carried out after the optimization of the experimental parameters such as the optimal value of the pH, the adequate potential applied and the scanning speed necessary to perform the electrochemical measurements.

To summarize, this chapter aims to expose, in a first part, the operating protocols and the experimental devices used for the preparation and the functionalization of the sensing surfaces of the electrodes studied within the framework of this thesis. The second part of the chapter will be devoted to the different characterization techniques implemented. Finally, we present the electrochemical techniques adopted for the study of the reactivity of the elaborated electrodes with respect to the targeted analytes.

II.2. Materials and methods

II.2.1. Reagents

Monosodium and disodium phosphate, Catechol (CC), Hydroquinone (HQ), phenol (ph), p-chlorophenol (5-CP), graphite, Multi walled carbon nanotubes (MWCNTs), and other chemicals including ethanol, sulfuric acid (H_2SO_4), nitric acid (HNO_3), zinc nitrate ($(\text{ZnNO}_3)_2$), iron chloride (FeCl_3) and sodium hydroxide (NaOH) and alumina slurry are obtained from Sigma-Aldrich. All chemicals used in this work were analytical grade, and all the solutions were prepared using deionized water (DW).

II.2.1.1. Nanomaterial synthesis

II.2.1.1.1. Synthesis of ZnO@fMWCNTs

II.2.1.1.1.1. Synthesis of zinc oxide nanoparticles (ZnO)

To synthesize zinc oxide nanoparticles, 20 ml of sodium hydroxide (NaOH) solution (0.9 M) was prepared and heated at $55\text{ }^\circ\text{C}$ under stirring. Then, 10 ml of zinc nitrate ($\text{Zn}(\text{NO}_3)_2$) solution (0.45 M) was added to the NaOH solution slowly for 45 minutes. The mixture was heated at $55\text{ }^\circ\text{C}$ for 2 hours while being stirred. When zinc oxide nanoparticles were formed as white precipitation in the solution, they were collected, washed twice with deionized water, and then dried at $50\text{ }^\circ\text{C}$ for four hours.

II.2.1.1.1.2. Synthesis of functionalized multi walled carbon nanotubes (fMWCNTs)

To functionalize MWCNTs, 1 g of MWCNTs was added to a mixture of 53 ml of nitric acid (99%) and 33 ml of sulfuric acid (65%) under stirring for 15 minutes. The final mixture was refluxed and stirred for 1 hour at room temperature. Then, the solution was filtered to collect pure functionalized multi-walled carbon nanotubes. The obtained mass was washed with deionized water several times till pH 7 was reached. And then, it was dried at $80\text{ }^\circ\text{C}$ for 2 hours.

II.2.1.1.1.3. Synthesis of ZnO@fMWCNTs nanocomposite

For the synthesis of ZnO@fMWCNTs nanocomposite, 10 mg of fMWCNTs was added to 20 ml of ethanol, and ultrasonication of the mixture was undertaken for 30 minutes. Afterward, 10 mg of ZnO was introduced to the solution. Then, after another 30 minutes of ultrasonication, dark green precipitation occurred in the solution. The obtained mass was gathered, filtered, and washed numerous times with deionized water and ethanol. And then, it was dried at $90\text{ }^\circ\text{C}$ for three hours.

II.2.1.1.2. Preparation of NiO/rGO/fMWCNTs nano-hybrid

Typical MWCNTs were dissolved in H₂SO₄/HNO₃ solution (3:1 v/v) [17], and the solution is sonicated to obtain carboxylated MWCNTs. These were subsequently washed with ethanol and water to bring the pH to 7.0 and wash impurities and salts. GO was obtained by the Hammer Method [18].

The carboxylated MWCNTs (5.5 mg/mL) were dispersed in a phosphate buffer solution (PBS) (pH 8.5), and were sonicated for 15 minutes to ensure the MWCNTs purity once more. Subsequently, 5 mg of GO was added to the solution. The obtained mixture was then added to a NiCl₂ solution (10 mM). A reduction process was next used applied to form rGO and NiO. Later, 20 ml of NaOH was carefully added to the mixture at 85 °C for one hour. Then, the solution turned black indicating that GO was successfully reduced. To ensure completion of the reaction, the final mixture is kept under magnetic stirring for an additional hour.

The solid material was collected by centrifugation, then washed 3 times with ethanol and water. Finally, the collected NiO/rGO/fMWCNTs was vacuum dried at 60 °C for 12 hours.

II.2.1.1.3. Synthesis of rGO and Fe-MOF

II.2.1.1.3.1. Synthesis of rGO

Graphene oxide (GO) was prepared using Hummer's process [36]. In an ice bath, 1 g of graphite was added to 25 ml of sulfuric. And the mixture was kept under stirring. 3 g of potassium permanganate (KMnO₄) were added carefully with stirring and cooling so that the temperature did not exceed 0 °C. Afterward, the mixture was kept under stirring for 3 hours at 49 °C. Here, 50 ml of distilled water was added. To reduce the excess potassium permanganate, 100 ml of distilled water and 5 ml of hydrogen peroxide were added to the final mixture. Then, a change in color from black to brown indicated the reduction of potassium permanganate and the formation of GO. Next, the GO was separated from the liquid phase by centrifugation, then washed until a pH value of 6.0. The final product was obtained after drying for 12 hours at 60 C°.

To reduce GO, two solutions were prepared. The first one was obtained by dissolving 43 mg of NaOH in 43 ml of distilled water while the second solution consisted of 1 mg/ml of GO. Next, GO was carefully dropped onto the NaOH solution after heating for 3 minutes. The final mixture was

kept under stirring for 30 minutes at 90°C until the appearance of a black color indicating the formation of GO. To recover the rGO, the solution was filtered three times. The resulting mass was washed with distilled water and ethanol. This washing was carried out to clean the rGO from the amount which is not reduced and also to remove the excess of the reducing agent in order to neutralize the pH up to the value 7. The final mass obtained was dried for 12 hours at 60.

II.2.1.1.3.2. Synthesis of Fe-MOF

To prepare an iron metal-organic framework (Fe-MOF), a mass of 0.7 g of FeCl₂ was dissolved in 50 ml of ethanol. The solution was kept under stirring for 15 minutes. On the other hand, another solution with 0.5 g of benzoic acid in 50 ml of ethanol was prepared and added carefully to the FeCl₂ solution under stirring for 15 minutes. Then, a yellow-colored precipitate was formed after 30 minutes. To recover the product, the solution was filtered three times. The mass of the product obtained is washed twice with ethanol to clean the impurities and remove the salts. The final mass obtained was dried overnight in an oven at 60 °C.

II.2.1.1.4. Synthesis of rGO-CuO and LDH

II.2.1.1.4.1. Green synthesis of the green organic-inorganic hybrid (rGO-CuO) and LDH

The organic-inorganic hybrid namely rGO-CuO was produced utilizing the aqueous extract Artemisia. The plant was collected from an arid region in Ouargla city-Algeria. Following identification, fresh Artemisia leaves were washed multiple times with tap water, then distilled water, to eliminate any dust particles. After drying, the plant leaves were crushed into a fine powder. Leaf extract was made by combining 30 g of fine plant powder with 100 ml of purified water and heating it at 60 C° for around 10 minutes. After that, it was left at room temperature for 24 hours. The leaf extract was filtered and kept at 4 °C for further research.

To make rGO-CuO, 30 mg of GO was mixed with 50 ml of CuSO₄ (10 mM) 160 mg. The brownie blue solution was combined with 20 ml of aqueous extract of Artemisia leaves at room temperature for 35 minutes at 80°C. The solution's hue shifted to dark, confirming the bio-reduction of GO and copper ions. The acquired quantity was washed three times with distilled water to eliminate contaminants until the pH value reached 7, and the finished product was dried at a temperature of 25°C for 72 hours.

II.2.1.1.4.2. Synthesis of Ni-Co-LDH

The synthesis of Ni-Co-LDH is carried out as follows: two separate solutions of $\text{Co}(\text{NO}_3)_2 \cdot 6\text{H}_2\text{O}$ and $\text{Ni}(\text{NO}_3)_2 \cdot 6\text{H}_2\text{O}$ are prepared by dissolving 0.145 g of $\text{Co}(\text{NO}_3)_2 \cdot 6\text{H}_2\text{O}$ with 0.118 g $\text{Ni}(\text{NO}_3)_2 \cdot 6\text{H}_2\text{O}$ in 50 mL of deionized water, dissolve $6\text{H}_2\text{O}$. Each solution's pH was adjusted to 10 by adding NaOH (0.1 M) sparingly. Finally, the two solutions, $\text{Ni}(\text{NO}_3)_2$ and $\text{Co}(\text{NO}_3)_2$, were gently put into a 100 ml beaker and stirred for 16 hours at $90\text{ }^\circ\text{C}$. To eliminate salts and contaminants while maintaining a pH of 7, the bulk was washed numerous times with water and ethanol. Finally, the material produced was dried at $80\text{ }^\circ\text{C}$ for 24 hours.

II.2.1.2. Preparation of the modified electrodes

Before and after any experiment, the bare electrode was primarily burnished using Alumina powder ($50\text{ nm Al}_2\text{O}_3$) in a circular motion to clean its surface. Afterward, the electrode surface was moved smoothly while drawing number eight shape to avoid creating grooves in the active surface of the electrode. This surface was then cleaned with deionized water to wash it from any trace of Al_2O_3 or any other nanomaterials. On the other hand, 15 mg of each synthesized nonmaterial was dispersed in 5 ml of ethanol by ultrasonication to obtain 3 mg/ml homogeneous colloidal solutions. Finally, a micro-volume of each suspension solvent was lowered on the bare electrode surface and kept at room temperature to manufacture modified electrodes.

II.2.2. Instruments

The synthesized nanoparticles and nanocomposites were confirmed and characterized by Fourier transform infrared spectroscopy (FT-IR) (Agilent 670 FT-IR), X-ray diffraction (XRD), and X-ray fluorescence (XRF) (Olympus BTX-716). Their surface morphology was observed using field emission scanning electron microscopy (SEM) (Zeiss Ultra-55).

The electrochemical analyzes were carried out by two different Potentiostats namely Voltalab 301 PGZ and Biologic SP300 with a three-electrodes system, a platinum wire as counter-electrode, a platinum electrode (Pt), a gold electrode (AuE) and a glassy carbon electrode (GCE) were all used as working electrodes and, and a calomel saturated electrode (SCE) as reference electrode. The cyclic voltammetry (CV) technique is used to characterize the nanomaterials synthesized and also to optimize the sensing platform, to study the effect of pH and the operational stability of the sensor. To evaluate the selectivity of the prepared sensors, both of amperometry (Amp) and CV techniques were used. The electrochemical impedance spectroscopic (EIS) method was used to confirm the

electrical conductivity of the modified electrodes. Also, the square wave voltammetry (SWV) and the difference pulse voltammetry (DPV) were used for the determination of the organic pollutants.

II.3. Characterization techniques

It is essential to understand a material to characterize it, and to analyze its properties. There are many materials characterization techniques that rely on different basic physical principles. We present below the characterization techniques that we used during our work.

II.3.1. Scanning Electron Microscopy (SEM)

In order to examine the microstructure of the synthesized nanomaterials, we used scanning electron microscopy (SEM). The SEM images were taken using a ZEISS Ultra-55 type microscope. This technique allows to visualize the surface topography of the deposited films down to micrometric details, as well as to have an estimate of the evolution of their roughness during the different stages of preparation and functionalization of the modified electrodes.

II.3.2. X-ray diffraction (XRD) and X-ray fluorescence (XRF)

XRD analysis was used to characterize the crystallographic structure and the degree of crystallinity of the synthesized nanomaterials, we used a diffractometer of the Olympus BTX-716. Data acquisition was performed by the Absolute Scan measurement program with $K\alpha$ copper radiation ($\lambda = 1.54 \text{ \AA}$). While XRF which is a non-destructive analytical technique used to determine the elemental composition of the synthesized materials. XRF analyzers determine the chemistry of a sample by measuring the fluorescent (or secondary) X-ray emitted from a sample when it is excited by a primary X-ray source

II.3.3. Fourier Transform Infrared (FTIR)

The FTIR analysis uses the mathematical process (Fourier transform) to transfer the raw data into the actual spectrum. FTIR method is used to obtain the infrared spectrum of transmission or absorption of the synthesized materials. In the present thesis, Agilent 670 FT-IR has been used.

II.4. Experimental device for the detection of organic pollutants

As mentioned in the previous section, the electrochemical study of the prepared sensors was carried out at the Laboratory for the Development and Promotion of Saharan Resources at Kasdi Merbah Ouargla University using a Voltalab 40 (PGZ 301), controlled by a microcomputer (Voltmaster 04 Software). Similar works were conducted in the Growth and Characterization of New

Semiconductors Laboratory at Ferhat Abbas University using Biologic SP300 potentiostat controlled by a microcomputer (EC Lab).

Both potentiostats use the classic three-electrode system shown in **Figure II.1**.

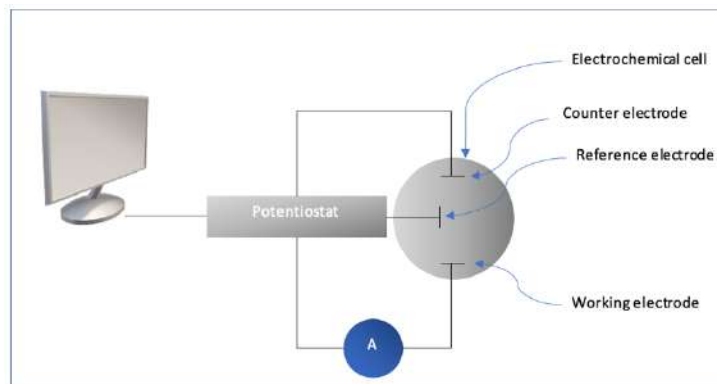


Figure II.1. Diagram of the experimental device used for the electrochemical measurements.

II.4.1. Classic three-electrode system

In all the experiments, the assembly with three electrodes were used: a reference electrode, a counter (auxiliary) and a working electrode.

II.4.2. The electrochemical cell

The cell used is made of glass (thermostatic), volume sufficient for the concentration of electroactive species to remain constant during manipulation. The latter is equipped with a double wall and a cover with 4 holes to pass the three electrodes and the degassing tube.

II.4.3. The electrodes

- In the present thesis, three different working electrodes were used: A gold (AuE), a Platinum (Pt) and a glassy carbon electrode (GCE).

It is interesting to note that the preparation of these working electrodes plays a very important role in the results obtained (the layout of the curves, the quality of the deposits). At first, the electrode surface is washed with deionized water and then ethanol. Just after, the surface of each working electrode was polished with alumina slurry and then washed again with deionized water and dried at room temperature.

- For all experiments presented in the present research, a platine electrode was used as counter electrode.

- The measurement conducted in the present work were all taken against the saturated calomel electrode (SCE) in potassium chloride KCl, constituted by the calomel system. Its potential with respect to the normal hydrogen electrode is equal to +0.2444 V at 25°C.

II.5. Preparation of the solutions

II.5.1. Buffer solution preparation

Phosphate buffer solutions (PBS) with different pH values were prepared using monosodium (NaH_2PO_4) and disodium (Na_2HPO_4) phosphate.

II.5.2. CC, HQ and 5-CP solutions preparation

For each pollutant, a solution of 5 mM was prepared through dissolving of the determined mass of each pollutant in 30 ml of distilled water in a bottle of 100 ml. The bottle then was ultra-sonicated for 10 minutes to homogenize the solution. After that, through dilution process, we prepared other solutions depending on the case study.

II.5.3. Preparation of modified electrodes

For each study, the working electrodes were polished in a circular motion by an alumina slurry (0.3 μm) to clean the surface. To avoid creating grooves on the surface, eight shape movements were made while polishing the surface and the electrode was cleaned thoroughly with deionized water. The clean electrode was dried in air. For comparison of the modified working electrode with bare electrode, different colloidal solutions (3 mg/ml) of synthesized nanomaterials were prepared using ethanol. For each modification, 3 ml of the colloidal solution were drop casted on the surface of the electrode to promote the electro-catalytic activity of the bare electrode. Lastly, before its usage, each modified electrode was dried in air.

II.6. Electrochemical detection

Electrochemical method is widely used in the detection of environmental pollutants, in which the working electrode is the core of the electrochemical sensor. The key to electrochemical signal amplification lies in the interface design between target molecules and electrodes, and the construction of efficient interface electron transmission. Many electrochemical platforms have been constructed for different electrochemical methods in related research. These electrochemical platforms include carbon-based materials (graphene oxide (GO), carbon nanotubes (CNTs) and carbon black (CB)), metal organic frameworks (MOFs), conductive polymers including molecularly imprinted polymers (MIPs), metals and metal oxides NPs as shown in **Fig. II.2**.

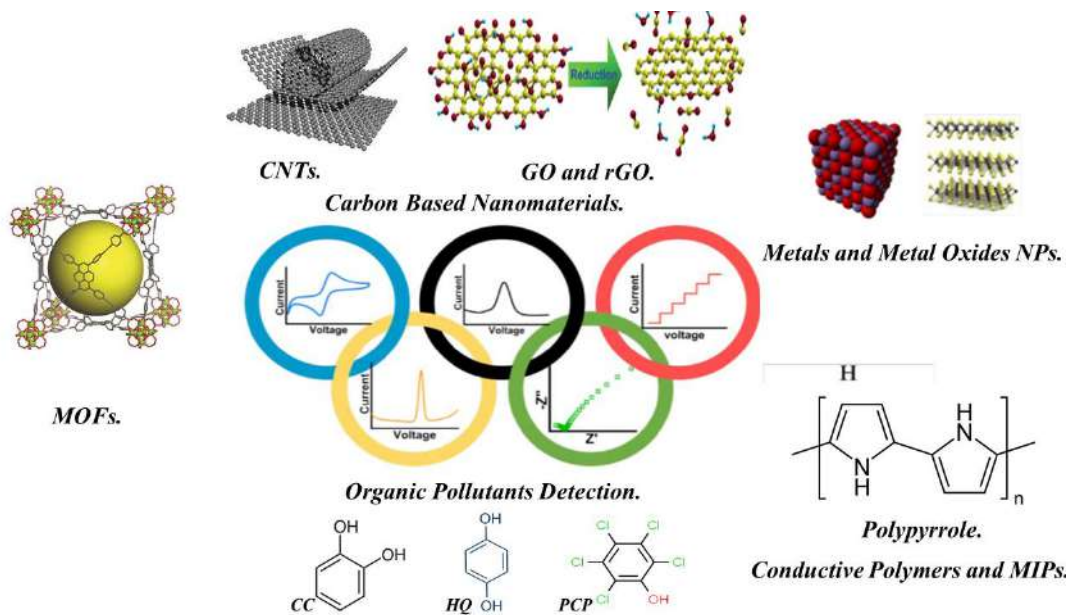


Figure II.2. Electrochemical detection of pollutants by different type of electrocatalysts.

Most of environmental pollutants have a certain redox potential. When a voltage is applied, the target will undergo a redox reaction at a certain voltage, thereby generating a current signal (Faraday current). This current signal will change with the concentration of the substance, which can help to complete the electrochemical detection of the target. The detection mechanism of different analytical methods (**Fig. II.3**) will be introduced.

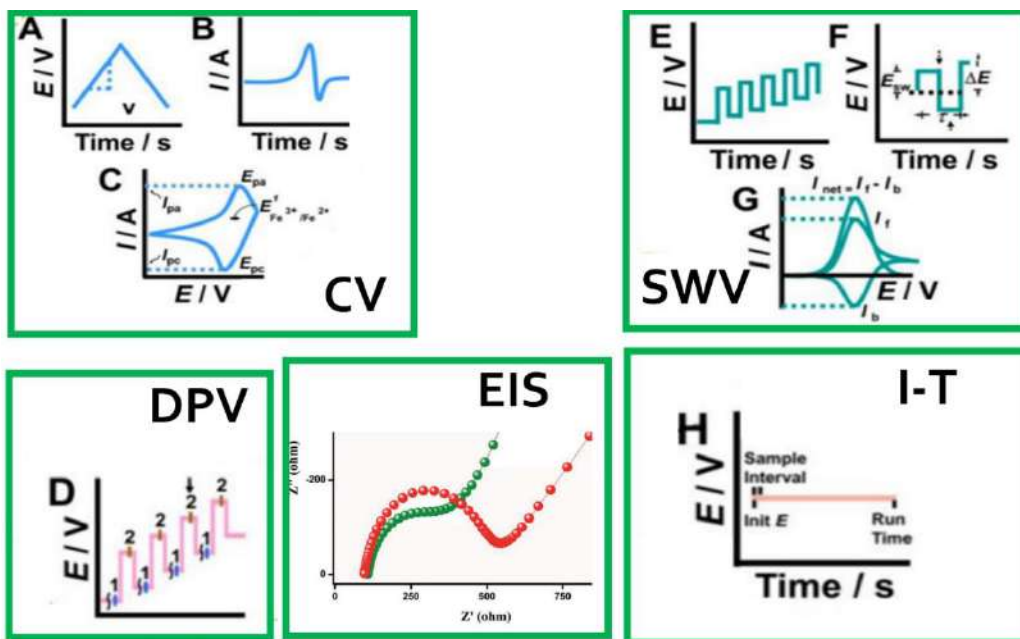


Figure II.3. Different mechanisms of the electrochemical analysis including CV (A-C), DPV (D), SWV (E-G), I-T (H) and impedance methods.

II.6.1. Cyclic voltammetry (CV)

Cyclic voltammetry refers that a linear scanning voltage is applied on an electrode to scan at a constant rate. When the current signal reaches the set termination potential, it returns to the set starting potential in the opposite direction [8]. The CV curve is scanned from the initial potential (E_1) to the final potential (E_2), and then returns to the initial potential (E_1) (Fig.II.3A). During the scanning process, the relationship between CV current and time is shown in Fig.II.3B. The experimental result of CV is shown in Fig.II.3C. When the scanning speed is constant, the voltage is increased from E_1 to E_2 . At first, only the background current can be observed. As the voltage increases, the electrochemical oxidation reaction occurs on the electrode surface, and the current gradually increases to a maximum and then decreases. The maximum current is called the peak current, which corresponds to the anodizing process (I_{pa}). The corresponding point becomes the oxidation potential (E_{pa}). Then, the potential reaches E_2 and decreases to E_1 . In this process, the electrode surface undergoes electrochemical reduction and the negative maximum current appears. The corresponding currents and potentials are called reduction current (I_{pc}) and reduction potential (E_{pc}), respectively [9,10].

Cyclic voltammetry method has been widely used in electrochemical analysis and detection. Firstly, the CV method can be used for electrochemical characterization to judge the quality of electrode preparation [11]. Secondly, CV method is used for qualitative analysis of targets. Thirdly, CV method can be used to judge the reaction mechanism of the electrode surface through the relationship between different sweep speeds and the peak current of the corresponding CV curve [12].

If the peak current is proportional to the sweep speed, reaction on electrode surface is adsorption control, while the peak current is proportional to the square root of the sweep speed, it is diffusion control. Generally, its application is mainly five aspects. (i) It can be used to judge the reversibility of the electrode. CV includes anodic oxidation and cathodic reduction processes. Therefore, the reversibility of the reaction of the electrode substance on the electrode surface can be judged from the peak height and symmetry of the oxidation peak and the reduction peak [13], (ii) It can be used to judge the electrode reaction mechanism. The CV method can be used to study the adsorption phenomenon of electrodes, the products of electrochemical reactions, and the mechanism of redox reactions of electroactive materials [14]. (iii) It can be used for qualitative analysis of multiple

substances. The oxidation-reduction potential of each substance is different, therefore, the CV method can be used for qualitative analysis [15]. (iv) It can be used to indicate the control process of the electrode surface. The control process of the electrode surface includes adsorption control and diffusion control processes [12]. (v) It can also be used to determine the roughness of the electrode surface, that is, to calculate the electrochemically active surface area (ECSA) [16].

II.6.2. Differential pulse voltammetry (DPV)

Pulse voltammetry is the most commonly used technology in electrochemical analysis. After applying the pulse voltage, the electrode is charged to generate a corresponding charging current, and then the charging current will quickly decay to zero; the applied pulse voltage can make the target to produce electrode response, which generates electrolytic current (Faraday current) during the reaction. The Faraday current is controlled by the diffusion of the reactive substrate of the electrode, which decays slowly with the reaction of the reactive substrate on the electrode. Nevertheless, the decay speed of the electrolytic current is much slower than that of the charging current. Therefore, the current is sampled at the late stage of the applied pulse voltage, and the measured current is almost equivalent to the electrolytic current. Differential pulse voltammetry is based on a stepped electric potential and a fixed amplitude pulse as the excitation signal. Each jump in potential occurs immediately before the drop of mercury (such as point 1 in **Fig.II.3D**) and at the end of the pulse life (such as point 2 in **Fig.II.3D**), and the current is sampled twice at these two points (I_1 and I_2). Moreover, the difference ($\Delta I = I_2 - I_1$) of these two currents is taken as the y-axis, and applied voltage is taken as the x-axis. There is a current peak in the resulting DPV curve, and the height of the peak is proportional to the concentration of the analyte. The relationship between current and concentration can be expressed as the following equations:

$$I_p = n \cdot F \cdot c \cdot \sqrt{\frac{D}{t}} \cdot \left(\frac{1 - \partial}{1 + \partial} \right) \quad (\text{II.1})$$

$$\partial = \exp \left(\frac{2RT}{nF\Delta\Phi} \right) \quad (\text{II.2})$$

where n is the number of electrons involved in the reaction, F is the Faraday constant, c is the concentration of the substance, D is the diffusion coefficient, t is the time interval between point 1 and point 2, R is the ideal gas constant (joules per kelvin per

mole), T is the temperature in kelvin, and $\Delta\Phi$ in the pulse amplitude. When the pulse amplitude is large, the maximum value of the quotient of $\frac{1-\theta}{1+\theta}$ is “1” [8].

The current peaks of different substances correspond to different voltages, and they can be distinguished by the peak potential. Therefore, the DPV method can be used for both qualitative and quantitative analysis.

Although CV shows promising advantage in electrochemical research, it is rarely used for quantitative analysis due its low sensitivity. As mentioned earlier, the DPV method has excellent advantages in quantitative analysis [12,17]. An electrochemical sensor based on Au/reduced graphene oxide (RGO) modified GCE was successfully prepared for simultaneous detection of ascorbic acid (AA), dopamine (DA) and uric acid (UA) by DPV method [18]. In addition, the DPV method was also used to detect emerging organic pollutants, such as bisphenol A (BPA), tetrabromobisphenol A (TBBPA), heavy metals, EDCs, pesticide, P5-CPs and so on [19-22]. For example, hierarchical Ce-MOF modified with cetyltrimethylammonium bromide (CTAB) was applied to detect BPA by DPV method. This designed sensor has a wide linear range from 5.0×10^{-9} to 5.0×10^{-5} M and a low detection limit of 2.0×10^{-9} M [8]. The DPV method can perform qualitative and quantitative detection of substances so that it can be used to analyze complex samples. Moreover, it has the advantages of low background current, high detection sensitivity, and lower detection limit. DPV method also supports low concentration of electrolyte, which is beneficial for the detection of trace substances.

II.6.3. Square wave voltammetry (SWV)

In the electrochemical analysis of nanomaterials, SWV is an advanced technology developed by Kalousek commutator and Barker square wave polarography [23,24]. The excitation signal applied at the working electrode is a superposition of a symmetrical square wave and a stepped voltage, and the forward pulse voltage of the square wave coincides with the step voltage. The basic characteristics of pulse voltage and step potential application, the volt-ampere curve of the SWV reaction mechanism is shown in **Fig.II.3E-G**. In the process of SWV reaction, the square wave pulse voltage and the ramp-like step potential are used to modulate the potential (**Fig.II.2E**). As shown in **Fig.II.2F**, the applied period by the potential modulation mainly includes the height of the pulse voltage (E_{sw}) and the pulse frequency (f , defined as $f=1/t$), where t is the applied time for one period. The application time of a single pulse voltage is defined as t_p , then the entire cycle

is $A=2t_p$, and the application frequency of the entire cycle is $f=1/2t_p$. At the same, the applied frequency (f) is also important [25,26].

Different from DPV, the pulse voltage in the application period of SWV consists of two parts: forward pulse voltage (E_f) and reverse pulse voltage (E_b), which are defined by the direction of the step potential (**Fig.II.2F**). Therefore, during the pulse voltage cycle, the electrode reactions are performed on the anode and the cathode, respectively. In each square wave cycle, the current is sampled twice, including the one when the forward pulse voltage ends and the other when the reverse pulse voltage ends. The application of a reverse pulse voltage will cause a reverse reaction of the product obtained by the forward pulse voltage, due to the larger amplitude of the square wave. Therefore, the relationship between the forward pulse voltage and the reverse pulse voltage and their corresponding currents can be shown from **Fig.II.2G**. As the pulse voltage increases from low to high, a peak current will appear at a specific position for a target substance, and the peak current here includes forward current (I_f) and reverse current (I_b). The net current (I_{net}) of SWV is obtained by subtracting the reverse current from the forward current, and plotting it against the basic step voltage. The peak curve of the net current is symmetrical about the redox center, and peak current is directly proportional to the concentration [26,27].

Square wave voltammetry has become a pioneer in electrochemical analysis methods due to its excellent sensitivity and short analysis time. Hence, it is always used to quantitatively analyze environmental pollutants such as heavy metal ions, biomolecules, drugs and so on [28-30]. For example, a graphene-based electrode was used to detect acetaminophen by using SWV method [28]. This graphene-based sensor showed a good performance for detecting paracetamol with a detection limit of 3.2×10^{-8} M and a wide linear ranging from 1.0×10^{-7} to 2.0×10^{-5} M. Zhang's group used GO deposition of Ag nanoparticles for the detection of Pb^{2+} [29]. The sensor exhibited excellent electrochemical performance for Pb^{2+} with a wide linear range from 1.0×10^{-10} to 1.0×10^{-5} M and a detection limit of 8.0×10^{-11} M. The SWV has several advantages. As mentioned earlier, the net current of SWV is the difference between the forward current and the reverse current. This leads to the reduced background current charged at the electrode, and extremely high sensitivity. Normally, the detection limit by using SWV can be at nano-scale even lower.

Compared with other pulse voltammetry, the biggest advantage of SWV is that it can control the response time by controlling the frequency. Therefore, SWV can utilize faster scanning speed,

shorter analysis time. A SWV curve can even be completed in seconds. Generally, SWV has high selectivity and ultra-short analysis time, which has the potential in a fast and high-resolution detection of actual sample sensors.

II.6.4. Amperometric *i-t* curve

Amperometric *i-t* curve is commonly used as a means of electrochemical detection. A constant potential is applied to the substance to be measured, which will undergo an oxidation or reduction reaction, and then Faraday current is formed. The current passes through the electrode and transmits the signal to the electrochemical workstation. The magnitude of the current will be proportional to the concentration of the substance. Thus, the electrochemical detection of the substance can be completed. **Fig.II.2H** shows the applied potential of the amperometric *i-t* curve. An initial potential and run time should be selected for electrochemical test. The potential remains at the initial value, and a sample is taken every certain time interval.

Amperometric *i-t* curve is also applied for the detection of some biological molecules and antigenic organisms [31-33]. For example, Zhu et al. reported that Au/MnO was used to detect H₂O₂ by using amperometric *i-t* curves. The sensor displayed high electrochemical performance for the detection of H₂O₂ with a detection limit of 8.0×10^{-9} M. Jiang's group used 2D g-C₃N₄/CuO as the sensor to detect DA [31]. The 2D g-C₃N₄/CuO sensor exhibited high sensitivity for DA detection with linear range of 2.0×10^{-9} to 7.1×10^{-5} M with a detection limit of 1.0×10^{-10} M. Although amperometric *i-t* curve has high sensitivity, short analysis time and strong continuity, it can only be applied to quantitative analysis. Amperometric *i-t* curve is not suitable for qualitative analysis owing to its poor selectivity, instead, it is often to combine with the other electrochemical methods.

II.6.5. Electrochemical impedance

Electrochemical impedance method plays a significant role in electrochemical test. The principle of electrochemical impedance is described following. A small amplitude sine wave potential (or current) is used as a perturbation signal to cause the electrode system to produce an approximately linear response. At this time, the impedance spectrum of the electrode system over a wide frequency range is measured to study the electrode system [34,35]. The electrochemical impedance spectrum is represented by Nyquist plot. The semicircle diameter in the Nyquist plot represents the transmission resistance (*R*_{ct}) of the electrode surface, which reflects the electron transporting ability of the electrode surface. A small *R*_{ct} value can be observed in a solution system, which can

be attributed to the free electron transfer directly from the solution to the electrode. Meanwhile, the electrodes are polarized by a small amplitude symmetrical alternating current. The changes in the surface state of the electrode are not observed owing to its short cycle duration accompanied with high frequencies. The cathodic process and the anodic process occur alternately on the electrode surface, thereby avoiding the cumulative development of electrode surface polarization and the greater impact on the system. Consequently, the electrochemical impedance method has stronger stability than other electrochemical methods.

Electrochemical impedance has been used to judge material modification, electro-catalytic activity, equivalent circuits, and electrodeposition, although it is rarely used in the field of sensors. Recently, some scientists have been devoted to the search of impedance sensors for the detection of environmental pollutants, such as antibiotics, EDCs, heavy metal ions, and biological antigens [36]. For instance, Merkoci's group reported molecularly imprinted membrane modified magnetite nanoparticles to detect sulfonamide by using impedance [36]. As the concentration of sulfonamide gradually increases, sulfonamide is gradually captured by vacancies on the molecularly imprinted membrane, which hinders the transfer of electrons on the electrode surface and increases the semicircle diameter of the Nyquist plot. The relationship between the transmission resistance (R_{ct}) of the electrode surface and the concentration of sulfonamide. With the concentration increasing, the value of R_{ct} increases logarithmically. The detection of sulfonamide by impedance exhibited a wide linear range from 1.0×10^{-10} to 1.0×10^{-2} M and a low detection limit of 1.0×10^{-12} M. Huang et al. used azo dye-modified Au electrode to detect $\text{Cr}^{(VI)}$ [37]. An interlayer complex can be formed by the combination of crown ethers and $\text{Cr}^{(VI)}$, hindering the transport of electrons on the electrode surface. It exhibited a detection limit of 1.4×10^{-3} ppb and the linear range of $1.0 - 1.0 \times 10^2$ ppb for the detection of $\text{Cr}^{(VI)}$ at $\text{pH} = 5.0$. Electrochemical impedance sensor is an emerging electrochemical sensor in recent years, which can be used to detect a variety of environmental pollutants. However, the poor selectivity of the impedance sensor limits its application. Therefore, the impedance sensor always needs to be used with molecular imprinting technology, or modified some substances that specifically recognize the target on the surface of the electrode, including enzymes, and specific antigens, etc [36,37].

II.6.6. Comparison of the different methods for the detection of pollutants

It's known that the detection limit is the most valuable value to evaluate the performance of sensor. In general, the detection rules of pollutants by different detection methods can be summarized as the following three points. (i) In the electrochemical detection of pollutants, the DPV method is the most widely used among the other electrochemical methods. As mentioned earlier, the literature on DPV methods is the most extensive for ten common pollutants. (ii) In the application of pollutant detection methods, the sensitivity of the impedance method and the photocurrent method is generally the highest, and the detection limit can reach picomolar level. These may be due to the extremely high sensitivity brought by the transient electron transfer of the impedance sensor and the improvement of the electrochemical signal under light conditions by the photocurrent method. (iii) For the detection of pesticides, the DPV method is the most widely used. And the amperometric *i-t* curve method is the most widely used for the detection of H₂O₂.

Environmental pollutants in water have attracted more and more attention owing to their serious harmfulness. Electrochemical and photo-electrochemical technology can provide a platform for detecting environmental pollutants in water, including EDCs, heavy metals, P5-CPs, pesticide and pathogenic microorganisms. Electrochemical and photo-electrochemical detection have high sensitivity, good stability and reproducibility, and fast analysis time. **Table 1** summarizes the advantages and the disadvantages of each electrochemical technique.

Table II.1. The advantages and disadvantages of different analysis methods.

	Methods	Advantage	Disadvantage
Electrochemical detection	CV	<ol style="list-style-type: none"> 1. Judgment of the reversibility of redox reaction; 2. Judgment of reaction mechanism; 3. Qualitative analysis; 4. Judgement of electrode surface control process; 5. Calculation of the electrochemical active surface area (ECSA). 	Due to its low sensitivity, CV is rarely used for trace quantitative analysis.
	DPV/SWV	<ol style="list-style-type: none"> 1. Qualitative and quantitative analysis of trace substances; 2. Low background current; 3. Low detection limit; 4. High sensitivity; 5. Fast analysis time. 	-
	Amperometric <i>i-t</i>	<ol style="list-style-type: none"> 1. High sensitivity; 2. Low detection limit; 3. Quantitative analysis; 4. Fast analysis time; 	I-T cannot perform qualitative analysis of multiple substances

	5. Continuity.	
Impedance	1. Higher sensitivity than other electrochemical methods; 2. Low detection limit 3. Quantitative analysis; 4. Fast analysis time.	Poor selectivity

II.7. Objectives

The primary goal of this work is to investigate the electrocatalytic behavior of carbon nanomaterials such as carbon nanotubes (CNTs) and reduced graphene oxide (rGO) in conjunction with metal oxide nanoparticles (NPs) such as copper oxide (CuO), zinc oxide, and nickel oxide (NiO). Metal organic framework (MOF) and Layer double hydroxide (LDH) have been investigated as newly manufactured nano-composites also. Simultaneously, this work aims to build innovative electrochemical sensors based on changes of electrode surfaces with these nanomaterials, using various alternatives of these nanomaterials and nanocomposites integration into sensing systems for organic pollution detection. The work related to organic pollution detection such as catechol (CC), hydroquinone (HQ) and penta-chlorophenol (5-CP) detection.

The detailed particular objectives are:

1. Evaluate the advantages of using carbon nanomaterials and metal oxides electrode modifiers in relation to the electrocatalytic properties beside the general analytical improvements achieved by the sensor. The evaluation of the ability of these materials to promote the electron-transfer reaction would be the key point for the development of new electrochemical sensors.

1.1. Study the catalytic effects of CNTs integrated onto a conventional glassy carbon electrode with interest for CC detection. Study the effect of using double layers of CNTs to reduce the sensor shortage due to fouling phenomenon.

1.2. Study a novel matrix design based on rGO doped with CNTs to ensure better mechanical/robustness properties of the sensor membrane. Additionally, NiO as a matrix-stabilizer and electron transfer booster with future promises for sensors applications to detect CC and HQ simultaneously will also be studied.

1.3. Evaluate and compare the CNTs and rGO efficiency for electrochemical oxidation

of CC and HQ. Compare them with other carbon materials (i.e. carbon nanofibers and carbon microparticles) used as modifiers of conventional electrodes such as glassy carbon and gold.

1.4. Study the effect of CNTs in combination with zinc oxide matrix to detect CC. As ZnO enhances the diffusion electron through its cavities the objective is to study if the dispersed CNTs onto the electrode in presence of ZnO facilitate the CC recognition and the electron transfer.

1.5. Compare the modified electrode for CC and HQ detection with a glassy carbon electrode without modifications so as to verify the contribution of CNTs, ZnO and NiO and rGO in the improved electrochemical detection.

2. Evaluate the advantages of using MOF and LDH as electrode modifiers in relation to the electrocatalytic properties beside the general analytical improvements achieved by the sensor. The evaluation of the ability of these nano-composites to promote the electron-transfer reaction would be the key point for the development of new electrochemical sensors.

2.1. Develop an LDH/rGO-CuO sensor based on a novel two steps procedures. Evaluate if this procedure ensures a production of conductive LDH and its synergic effect with the organic-inorganic nanohybrid rGO-CuO. Evaluate if the use of LDH as the conductive part of the composite ensures better detection matrix and a faster electron transfer rates toward 5-CP oxidation

2.2. Develop a sensor based on a MOF to detect 5-CP in aqueous environment. Evaluate if the use of FeO₃ along with MOF improve matrix sensitivity toward 5-CP oxidation

2.3. Develop, evaluate and validate an artificial neural network (ANN) using MATALB software of the prepared MOF sensor. Evaluate the validity of the predicted results of the developed ANN.

II.8. Conclusion

In this chapter, we presented the experimental techniques used during this work to develop and characterize our modified electrodes, as well as the operating protocols and the experimental conditions which allowed a good reproducibility of the results. In the following chapter, we present the results obtained concerning the characterization (morphological and structural) of the deposited matrix for each sensor and the study of the electrochemical reactivity of these sensors for the detection of the targeted species namely CC, HQ and 5-CP.

References

- [1] S. Miserere, S. Ledru, N. Ruillé, S. Griveau, M. Boujtita, and F. Bedioui, “Biocompatible carbon-based screen-printed electrodes for the electrochemical detection of nitric oxide,” *Electrochem. Commun.*, vol. 8, no. 2, pp. 238–244, Feb. 2006, doi: 10.1016/j.elecom.2005.11.016.
- [2] J. R. Camargo *et al.*, “Development of conductive inks for electrochemical sensors and biosensors,” *Microchem. J.*, vol. 164, p. 105998, May 2021, doi: 10.1016/j.microc.2021.105998.
- [3] M. D. Angione *et al.*, “Carbon based materials for electronic bio-sensing,” *Mater. Today*, vol. 14, no. 9, pp. 424–433, Sep. 2011, doi: 10.1016/S1369-7021(11)70187-0.
- [4] X.-Y. Lu *et al.*, “Facile synthesis of TiO₂-ZnO-rGO nanocomposites for highly sensitive simultaneous determination of hydroquinone and catechol,” *Microchem. J.*, vol. 166, p. 106246, Jul. 2021, doi: 10.1016/j.microc.2021.106246.
- [5] K. Chetankumar, B. E. K. Swamy, and T. S. S. K. Naik, “A reliable electrochemical sensor for detection of catechol and hydroquinone at MgO/GO modified carbon paste electrode,” *J. Mater. Sci. Mater. Electron.*, vol. 31, no. 22, pp. 19728–19740, Nov. 2020, doi: 10.1007/s10854-020-04498-x.
- [6] H. S. Han, J.-M. You, H. Seol, H. Jeong, and S. Jeon, “Electrochemical sensor for hydroquinone and catechol based on electrochemically reduced GO–terthiophene–CNT,” *Sens. Actuators B Chem.*, vol. 194, pp. 460–469, Apr. 2014, doi: 10.1016/j.snb.2014.01.006.
- [7] Z. Panahi, L. Custer, and J. M. Halpern, “Recent advances in non-enzymatic electrochemical detection of hydrophobic metabolites in biofluids,” *Sens. Actuators Rep.*, vol. 3, p. 100051, Nov. 2021, doi: 10.1016/j.snr.2021.100051.
- [8] Z. Li and M. Zhu, “Detection of pollutants in water bodies: electrochemical detection or photo-electrochemical detection?,” *Chem. Commun.*, vol. 56, no. 93, pp. 14541–14552, 2020, doi: 10.1039/D0CC05709F.
- [9] F. Harnisch and S. Freguia, “A Basic Tutorial on Cyclic Voltammetry for the Investigation of Electroactive Microbial Biofilms,” *Chem. - Asian J.*, vol. 7, no. 3, pp. 466–475, Mar. 2012, doi: 10.1002/asia.201100740.
- [10] F. Joao *et al.*, “Reassessing the interpretation of oxidation–reduction potential in male infertility,” *Reprod. Fertil.*, vol. 3, no. 2, pp. 67–76, Apr. 2022, doi: 10.1530/RAF-21-0005.
- [11] W. Zhang *et al.*, “Novel nanostructured MIL-101(Cr)/XC-72 modified electrode sensor: A highly sensitive and selective determination of chloramphenicol,” *Sens. Actuators B Chem.*, vol. 247, pp. 756–764, Aug. 2017, doi: 10.1016/j.snb.2017.03.104.
- [12] X. Zhang, Y.-C. Zhang, and L.-X. Ma, “One-pot facile fabrication of graphene-zinc oxide composite and its enhanced sensitivity for simultaneous electrochemical detection of ascorbic acid, dopamine and uric acid,” *Sens. Actuators B Chem.*, vol. 227, pp. 488–496, May 2016, doi: 10.1016/j.snb.2015.12.073.
- [13] A. U. Alam, Y. Qin, M. M. R. Howlader, N.-X. Hu, and M. J. Deen, “Electrochemical sensing of acetaminophen using multi-walled carbon nanotube and β -cyclodextrin,” *Sens. Actuators B Chem.*, vol. 254, pp. 896–909, Jan. 2018, doi: 10.1016/j.snb.2017.07.127.
- [14] N. R. Devi, T. H. V. Kumar, and A. K. Sundramoorthy, “Electrochemically Exfoliated Carbon Quantum Dots Modified Electrodes for Detection of Dopamine Neurotransmitter,” *J. Electrochem. Soc.*, vol. 165, no. 12, pp. G3112–G3119, 2018, doi: 10.1149/2.0191812jes.
- [15] J. Du *et al.*, “Novel graphene flowers modified carbon fibers for simultaneous determination of ascorbic acid, dopamine and uric acid,” *Biosens. Bioelectron.*, vol. 53, pp. 220–224, Mar. 2014, doi: 10.1016/j.bios.2013.09.064.

- [16] Y. Li *et al.*, "A novel electrochemical biomimetic sensor based on poly(Cu-AMT) with reduced graphene oxide for ultrasensitive detection of dopamine," *Talanta*, vol. 162, pp. 80–89, Jan. 2017, doi: 10.1016/j.talanta.2016.10.016.
- [17] C. Wang, X. Shao, Q. Liu, Q. Qu, G. Yang, and X. Hu, "Differential pulse voltammetric determination of nimesulide in pharmaceutical formulation and human serum at glassy carbon electrode modified by cysteic acid/CNTs based on electrochemical oxidation of l-cysteine," *J. Pharm. Biomed. Anal.*, vol. 42, no. 2, pp. 237–244, Sep. 2006, doi: 10.1016/j.jpba.2006.03.038.
- [18] C. Wang *et al.*, "A facile electrochemical sensor based on reduced graphene oxide and Au nanoplates modified glassy carbon electrode for simultaneous detection of ascorbic acid, dopamine and uric acid," *Sens. Actuators B Chem.*, vol. 204, pp. 302–309, Dec. 2014, doi: 10.1016/j.snb.2014.07.077.
- [19] A. Ehsani, M. Esfahaniha, P. Khodaei kahriz, R. Safari, and H. Parsimehr, "Functionalized graphene oxide aerogel as a high efficient material for electrochemical sensing of organic pollutant," *Surf. Interfaces*, vol. 22, p. 100817, Feb. 2021, doi: 10.1016/j.surfin.2020.100817.
- [20] G. Zhu, L. Wu, X. Zhang, W. Liu, X. Zhang, and J. Chen, "A New Dual-Signalling Electrochemical Sensing Strategy Based on Competitive Host-Guest Interaction of a β -Cyclodextrin/Poly(*N*-acetylaniline)/Graphene-Modified Electrode: Sensitive Electrochemical Determination of Organic Pollutants," *Chem. - Eur. J.*, vol. 19, no. 20, pp. 6368–6373, May 2013, doi: 10.1002/chem.201204635.
- [21] M. Zahran, Z. Khalifa, M. A.-H. Zahran, and M. Abdel Azzem, "Recent advances in silver nanoparticle-based electrochemical sensors for determining organic pollutants in water: a review," *Mater. Adv.*, vol. 2, no. 22, pp. 7350–7365, 2021, doi: 10.1039/D1MA00769F.
- [22] A. Shah, M. Akhtar, S. Aftab, A. H. Shah, and H.-B. Kraatz, "Gold copper alloy nanoparticles (Au-Cu NPs) modified electrode as an enhanced electrochemical sensing platform for the detection of persistent toxic organic pollutants," *Electrochimica Acta*, vol. 241, pp. 281–290, Jul. 2017, doi: 10.1016/j.electacta.2017.04.166.
- [23] G. C. Barker and I. L. Jenkins, "Square-wave polarography," *The Analyst*, vol. 117, no. 12, p. R1, 1992, doi: 10.1039/an99217000r1.
- [24] G. C. Barker, "Square wave polarography and some related techniques," *Anal. Chim. Acta*, vol. 18, pp. 118–131, 1958, doi: 10.1016/S0003-2670(00)87111-1.
- [25] Louis. Ramaley and M. S. Krause, "Theory of square wave voltammetry," *Anal. Chem.*, vol. 41, no. 11, pp. 1362–1365, Sep. 1969, doi: 10.1021/ac60280a005.
- [26] M. Hicham, A. Fethi, S. Ha, and B. Khaldoun, "Antifouling double layers of functionalized-multi-walled carbon nanotubes coated ZnO for sensitive and selective electrochemical detection of catechol," *Fuller. Nanotub. Carbon Nanostructures*, vol. 30, no. 3, pp. 334–347, Mar. 2022, doi: 10.1080/1536383X.2021.1940150.
- [27] W. C. Barrette and D. T. Sawyer, "Determination of dissolved hydrogen and effects of media and electrode materials on the electrochemical oxidation of molecular hydrogen," *Anal. Chem.*, vol. 56, no. 4, pp. 653–657, Apr. 1984, doi: 10.1021/ac00268a015.
- [28] X. Kang, J. Wang, H. Wu, J. Liu, I. A. Aksay, and Y. Lin, "A graphene-based electrochemical sensor for sensitive detection of paracetamol," *Talanta*, vol. 81, no. 3, pp. 754–759, May 2010, doi: 10.1016/j.talanta.2010.01.009.
- [29] S. Tang *et al.*, "Label free electrochemical sensor for Pb²⁺ based on graphene oxide mediated deposition of silver nanoparticles," *Electrochimica Acta*, vol. 187, pp. 286–292, Jan. 2016, doi: 10.1016/j.electacta.2015.11.040.
- [30] S. Gao *et al.*, "Highly Efficient and Exceptionally Durable CO₂ Photoreduction to Methanol over Freestanding Defective Single-Unit-Cell Bismuth Vanadate Layers," *J. Am. Chem. Soc.*, vol. 139, no. 9, pp. 3438–3445, Mar. 2017, doi: 10.1021/jacs.6b11263.

- [31] J. Zou *et al.*, “An ultra-sensitive electrochemical sensor based on 2D g-C₃N₄/CuO nanocomposites for dopamine detection,” *Carbon*, vol. 130, pp. 652–663, Apr. 2018, doi: 10.1016/j.carbon.2018.01.008.
- [32] S. Yu, H. Li, G. Li, L. Niu, W. Liu, and X. Di, “Reduced graphene oxide-supported gold dendrite for electrochemical sensing of acetaminophen,” *Talanta*, vol. 184, pp. 244–250, Jul. 2018, doi: 10.1016/j.talanta.2018.03.011.
- [33] Y. Yang *et al.*, “A novel label-free electrochemical immunosensor based on functionalized nitrogen-doped graphene quantum dots for carcinoembryonic antigen detection,” *Biosens. Bioelectron.*, vol. 90, pp. 31–38, Apr. 2017, doi: 10.1016/j.bios.2016.11.029.
- [34] Q.-A. Huang, R. Hui, B. Wang, and J. Zhang, “A review of AC impedance modeling and validation in SOFC diagnosis,” *Electrochimica Acta*, vol. 52, no. 28, pp. 8144–8164, Nov. 2007, doi: 10.1016/j.electacta.2007.05.071.
- [35] S. M. Rezaei Niya and M. Hoorfar, “Study of proton exchange membrane fuel cells using electrochemical impedance spectroscopy technique – A review,” *J. Power Sources*, vol. 240, pp. 281–293, Oct. 2013, doi: 10.1016/j.jpowsour.2013.04.011.
- [36] A. Zamora-Gálvez, A. Ait-Lahcen, L. A. Mercante, E. Morales-Narváez, A. Amine, and A. Merkoçi, “Molecularly Imprinted Polymer-Decorated Magnetite Nanoparticles for Selective Sulfonamide Detection,” *Anal. Chem.*, vol. 88, no. 7, pp. 3578–3584, Apr. 2016, doi: 10.1021/acs.analchem.5b04092.
- [37] J. Wei, Z. Guo, X. Chen, D.-D. Han, X.-K. Wang, and X.-J. Huang, “Ultrasensitive and Ultraspecific Impedimetric Detection of Cr(VI) Using Crown Ethers as High-Affinity Targeting Receptors,” *Anal. Chem.*, vol. 87, no. 3, pp. 1991–1998, Feb. 2015, doi: 10.1021/ac504449v.

Chapter III

Results and Discussion.

III. Results and discussion

III.1. FT-IR, XRD and surface morphology study of prepared nanocomposites

III.1.1. Physico-chemical analysis of ZnO, *fMWCNTs* and ZnO@*fMWCNTs* nanocomposites

The chemical structures of ZnO, *fMWCNTs* and ZnO@*fMWCNTs* nanocomposites were characterized by FT-IR spectrometry. The resulting spectra are shown in **Figure III.1**. As can be seen, there is an intense band at 560 cm^{-1} , exhibiting a stretching vibration of zinc and oxygen represented in the synthesized ZnO NPs. Several weak peaks around 900 cm^{-1} clearly denote the Zn-OH stretching vibrations. The band at 3400 cm^{-1} coincides with the bending and stretching of the vibration (OH). All the peaks mentioned here confirm that ZnO NPs were purely synthesized with no impurities [1]. The FT-IR spectrum of *fMWCNTs* shown in **Figure III.1** has broad peaks around 3510 cm^{-1} owing to the absorption of the OH (hydroxyl) group. The appearance of the fine peaks at 1720 , and 1182 cm^{-1} corresponds to the C=O and C-N absorption bands, respectively [2].

The asymmetric methyl stretching band at 2960 cm^{-1} and asymmetric/symmetric methylene stretching bands between 2950 and 2800 cm^{-1} are observed, respectively [3]. The peak located at 1360 cm^{-1} was originated from the bending vibration of CH in the methyl group. These results confirm the formation of *fMWCNTs*. The ZnO@*fMWCNTs* FT-IR spectrum has similar peaks with the *fMWCNTs* spectrum at 3650 cm^{-1} , 2970 cm^{-1} , 1620 cm^{-1} , 1400 cm^{-1} , 1360 cm^{-1} and 1200 cm^{-1} . Besides, the band at 560 and 500 cm^{-1} were attributed to the stretching mode of ZnO while the Zn-OH stretching vibrations appear at 880 cm^{-1} . It is noticeable that there are shifted bands between the FT-IR spectra of *fMWCNTs* and ZnO@*fMWCNTs*. These could be caused by an interaction between ZnO NPs and *fMWCNTs*. Hence, it can be confirmed that ZnO@*fMWCNTs* were successfully synthesized and ZnO NPs were successfully anchored onto the *fMWCNTs*. On the other hand, the adsorption peak around 2400 cm^{-1} may due to the presence of the CO_2 in the studied samples.

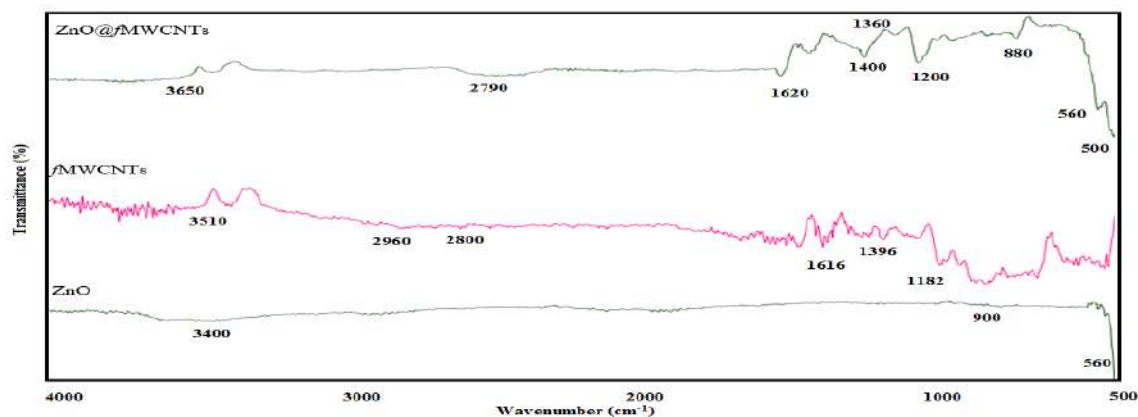


Figure III.1. FTIR spectra of ZnO@fMWCNTs, fMWCNTs and ZnO nanocomposites.

XRD patterns of ZnO@fMWCNTs nanocomposites were obtained using an advanced diffractometer with monochromatic CuK α radiation ($\lambda=1.54\text{\AA}$) to identify the crystalline nature of the proposed nanocomposites. The XRD patterns of the synthesized ZnO@fMWCNTs nanocomposite are shown in **Figure III.2 (a)**. The obtained results are compared with the JCPDS card (36–1451) of pure ZnO. As can be seen from **Figure III.2 (a)**, the diffraction peak at 25.6° corresponds to the functionalized MWCNTs at (002) plane. The crystal structure characterization of the ZnO@fMWCNTs nanocomposite exhibits highly defined diffraction peaks at 31.95° , 34.65° , 36.35° , and 47.7° , indicating the various diffraction planes of (100), (002), (101) and (100), respectively. These resulting diffraction peaks confirm the pure crystalline features of the synthesized ZnO NPs without any impurities as confirmed by XRF in **Figure III.2 (b)** [1]. According to the results presented above, it is shown that fMWCNTs-based nanocomposites gradually make the transition from an amorphous to a crystalline phase with the presence of ZnO nanoparticles. Thus, ZnO NPs have interacted with fMWCNTs [4].

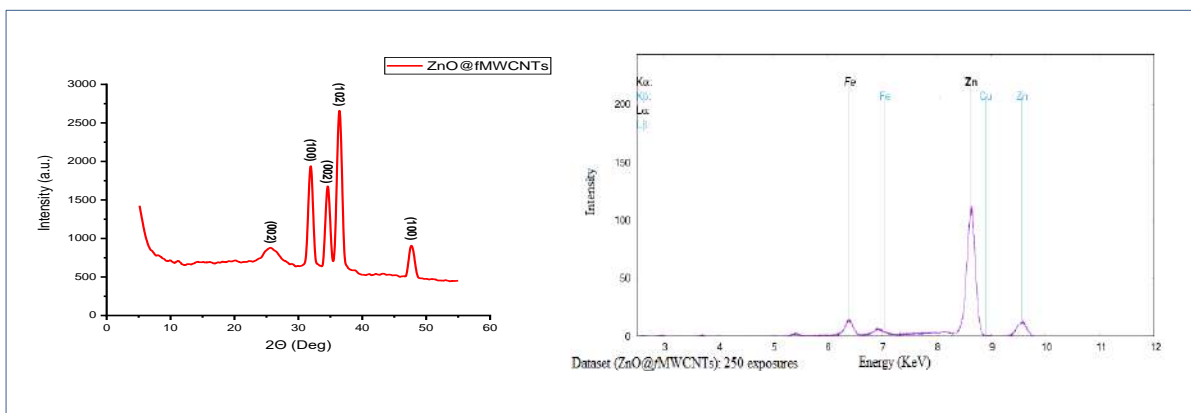


Figure III.2. XRD fragments and (b) XRF of synthesized nanocomposites ZnO@fMWCNTs.

The morphological characterization of the synthesized ZnO, *fMWCNTs*, and ZnO@*fMWCNTs* nanocomposites was examined by SEM technique. As shown in **Figure III.3 (A)**, the synthesized ZnO NPs have a porous surface texture like a sea sponge, while forming a random distribution of smaller agglomerated ZnONPs inside bigger particles. On the other hand, the SEM analysis confirmed that exposure of MWCNTs to nitric acid and sulfuric acid HNO₃:H₂SO₄ (1:3) created deformation in the morphology of the treated MWCNTs. The *fMWCNTs* shrank and created a perforated structure as seen in **Figure III.3 (B)**. After ultrasonication of *fMWCNTs* with ZnO NPs, this area was shrunken again and surface became more porous. The formed walls were shaped as large honeycomb-like structures as shown in **Figure III.3 (C)**.

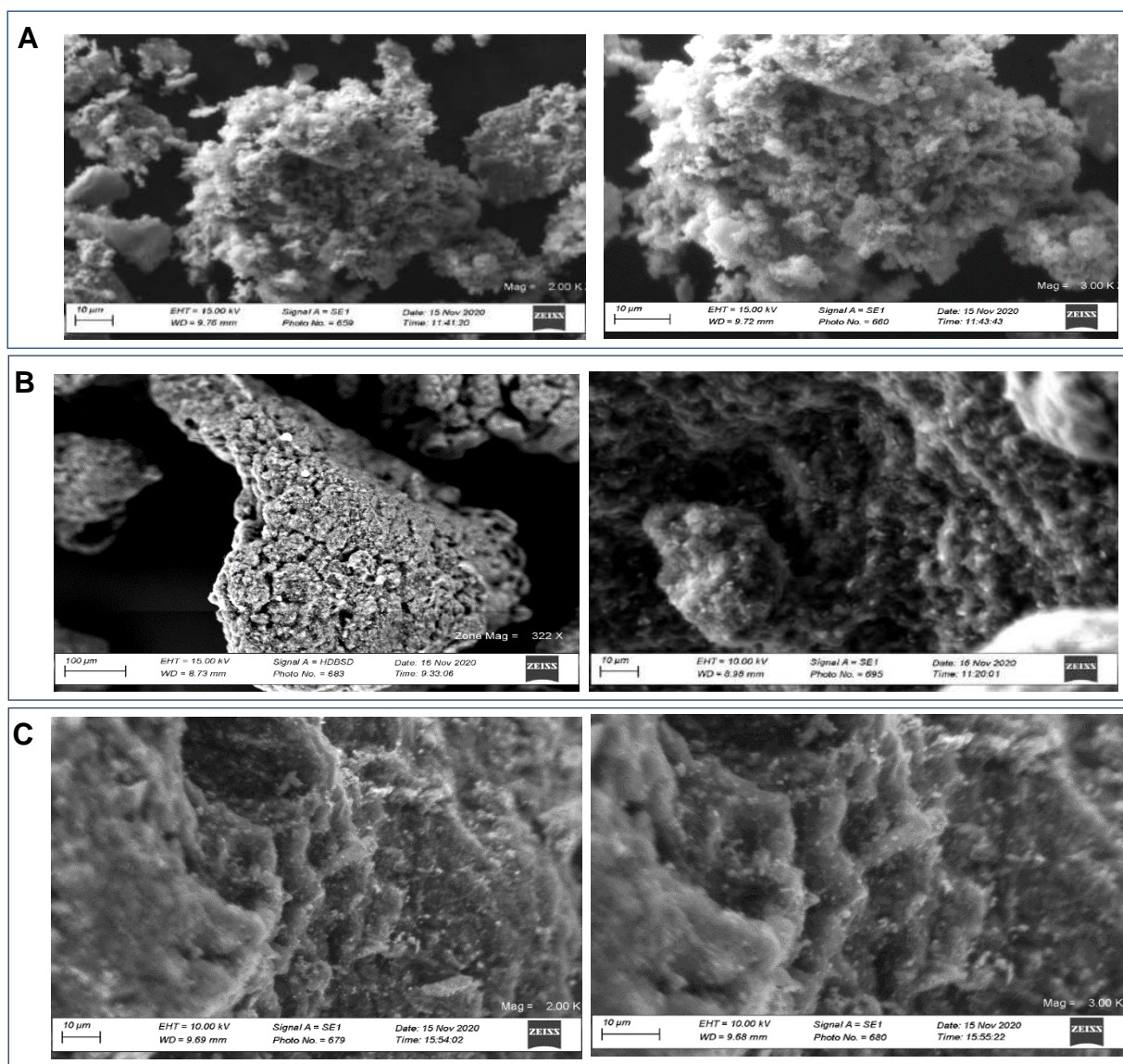


Figure III.3. SEM analysis of A) ZnO NPs, B) *fMWCNTs*, and C) ZnO@*fMWCNTs*.

III.1.2. Physico-chemical analysis of MWCNTs, rGO, and NiO/rGO/fMWCNTs nano-hybrid

The influence of the new synthesis approach, the doping effectiveness of reduced graphene, and the nanostructure of the as-synthesized nanocomposite were all investigated. The NiO/rGO/MWCNTs nano-hybrid was characterized by Fourier transform infrared spectroscopy (FT-IR), field emission scanning electron microscopy (SEM), X-ray diffraction (XRD), and X-ray fluorescence (XRF).

The morphologies of MWCNTs, rGO, and NiO/rGO/MWCNTs were observed by a scanning electron microscope (SEM). As shown in **Figure III.4a**, *fMWCNTs* are agglomerated in a flaky porous structure like rock shapes due to the acidification treatment. The porous and interconnected integrated surface of *fMWCNTs* exhibits a large specific surface area and contributes to strong adsorption and rapid diffusion of CC and HQ molecules. rGO has a leaf structure like grapes as shown in **Figure III.4b**. As can be seen in **Figure III.4c**, rGO is relatively uniformly dispersed on the surface of the functionalized MWCNTs. In addition, it has a white-colored curvy silk-like structure, indicating the presence of metal oxides, which is NiO NPs, in the synthesized nano-hybrid.

Figure III.5 shows infra-red (IR) spectra of (a) NiO/rGO/*fMWCNTs*, (b) rGO/*fMWCNTs*, and (c) *fMWCNTs*. The figure shows a C=C absorption peak at 1646 cm^{-1} . The bands from 1520 cm^{-1} to 1650 cm^{-1} are due to the C=C–C bending vibrational modes. The vibrational mode of C–H stretching corresponds to the band around 3000 cm^{-1} . The long band between 3560 cm^{-1} and 3750 cm^{-1} is attributed to the O–H stretch mode from the carboxylic groups attached to the carbon nanotubes during the functionalization process. The sharp band at 3800 cm^{-1} refers to the O–H stretch mode of nickel oxide [19]. These functional groups increase the number of bands at the Fermi level, enabling electron transfer between carbon atoms. No absorption peak near 1750 cm^{-1} corresponds to the tensile exercise of C=O for curves “a” and “b” in **Figure III.5**, indicating that graphene oxide is successfully reduced [20].

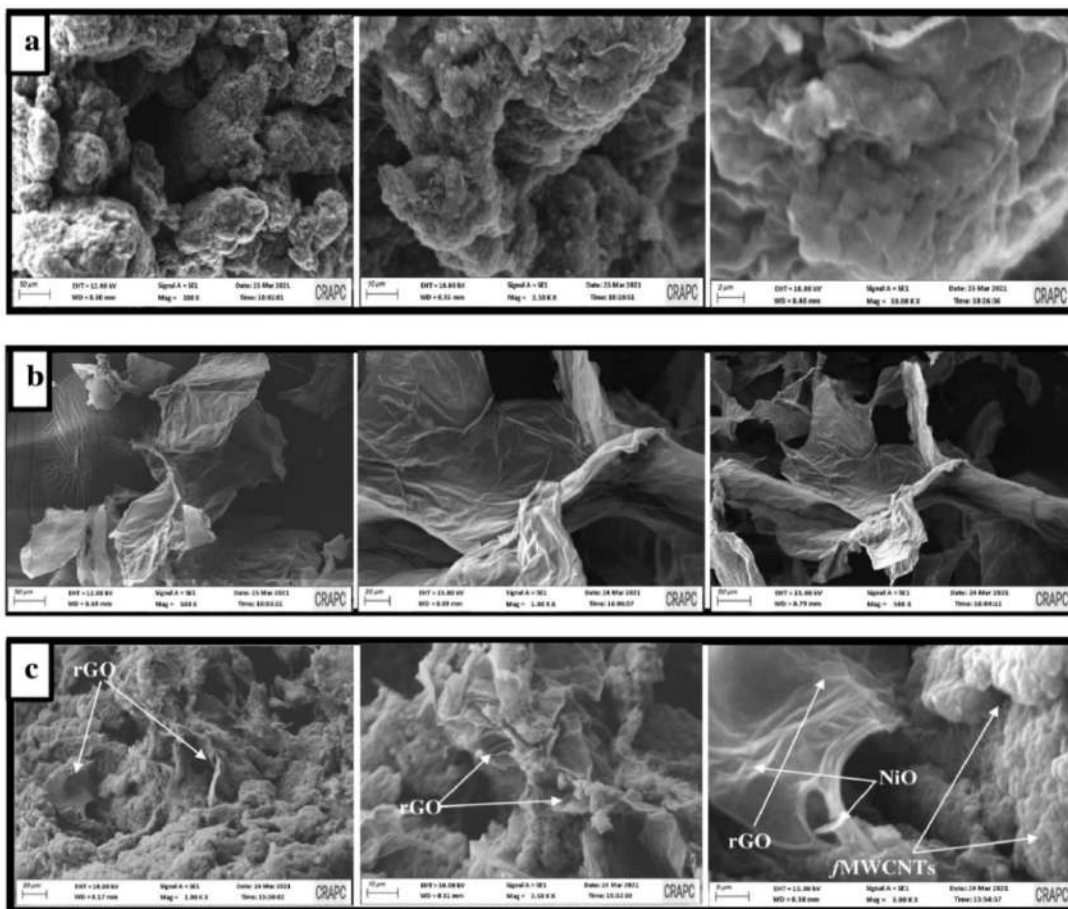


Figure III.4. SEM analysis of (a) fMWCNTs, (b) rGO and, (c) NiO/rGO/fMWCNTs.

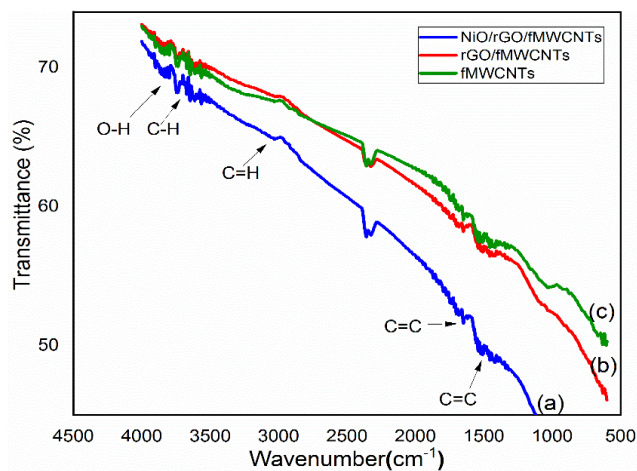


Figure III.5. Fourier transform infrared spectroscopy spectra of fMWCNTs, rGO/fMWCNTs and NiO/rGO/fMWCNTs nanocomposites.

To understand more deeply the structure and constitution of the NiO/rGO/MWCNTs nano-hybrid, an X-ray diffraction experiment was performed and the results are shown in **figure III.6a**. As shown, the (002) plane of MWCNTs corresponds to the diffraction peak at 25.86° , and the (002)

plane of rGO corresponds to the diffraction peak at 25.85° . As can be seen from the figure III.6a we can clearly note that rGO and MCNTs are the dominant part in the synthesized hybrid compared to NiO NPs that appeared at 14.5° , 29.5° , 34.75° , and 43.45° correspond to the crystal orientations of nickel at (002), (220), (311), and (200) planes, respectively. An X-ray fluorescence analysis (FRX) was also undertaken to investigate the presence of pure nickel in the synthesized nano-hybrid (**figure III.6b**). Pure nickel incurs a rather strong peak with an energy of 6.5 KeV, while the other peak at 8 KeV is attributed to the copper electrode of the instrument. Another less intense iron peak at 8.2 KeV was discovered as well as the presence of extremely low-intensity peaks of other metals such as iron (Fe) and copper (Cu), validating that the nickel oxide NPs were purely synthesized in the nano-hybrid.

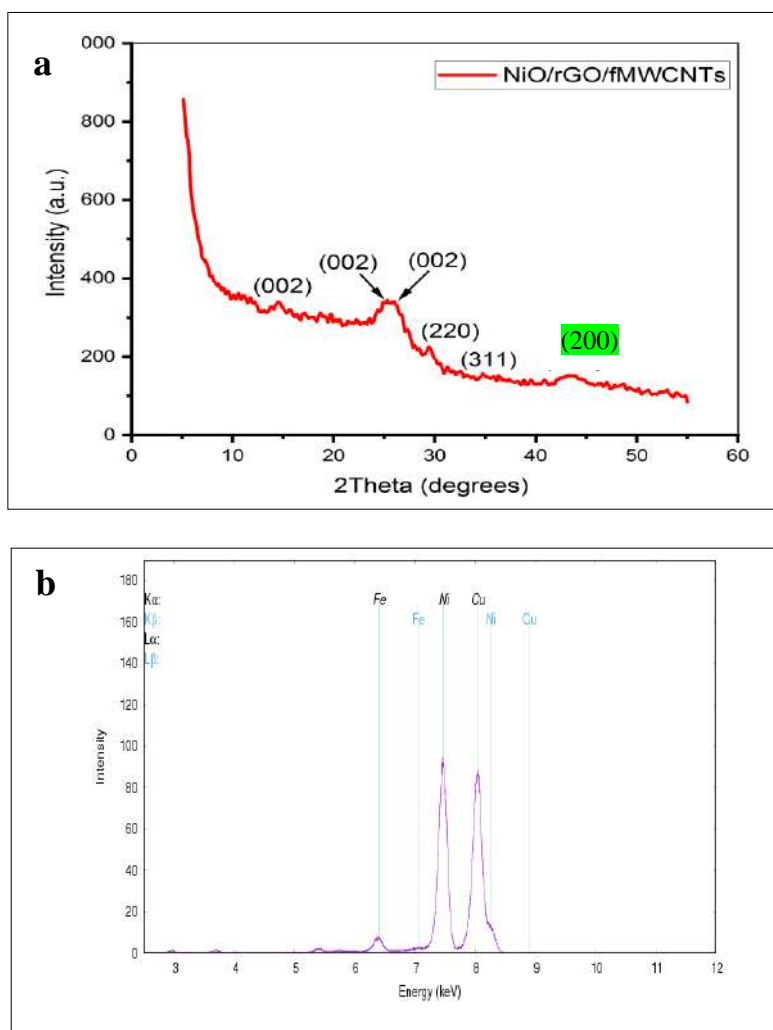


Figure III.6. XRD fragments and (b) XRF of the synthesized nanocomposites.

In conclusion, these analysis data demonstrate that the NiO/rGO/fMWCNTs nano-hybrid was purely produced through the proposed single-step synthesis method presented in this work. Compared with previous synthesis methods, our method is considered environmentally safe, facile, rapid, and cheap to fabricate (**Table III.1**).

Table III.1. Comparison with state-of-the-art synthesis methods of NiO, rGO, and fMWCNTs.

Nano-composite	Synthesis method	Synthesis duration	Toxic chemicals	Cost	Simplicity	Reference	
Ni/NiO-Gr	Chemical	Slow	<i>Yes</i>	Cheap	No	[21]	
MWCNTs/rGO	Hydrothermal	Average	<i>Yes</i>	Expensive		[22]	
NiO/Fe ₃ O ₄ /rGO	Solvothermal		<i>No</i>	Expensive		[23]	
NiO/CNTs	Atomic Layer deposition		<i>No</i>	Average		[24]	
CNTs/NiO	Chemical		<i>No</i>	Cheap		Yes	[25]
AuNP-rGO-MWCNTs	Chemical		<i>No</i>	Average		No	[26]
CNCs-rGO/GCE	Hydrothermal		<i>No</i>	Average		Yes	[27]
NiO/rGO/fMWCNTs	Chemical	Rapid	<i>No</i>	Cheap	Yes	This work	

III.1.3. Physico-chemical analysis of monometallic Fe-MOF nanosheets

This section characterizes the novel synthesis method, including the reduced efficacy of reduced graphene, and the nanostructure of as-synthesized MOF nanosheets. SEM, XRD, and XRF were used to analyze rGO and Fe-MOF nanohybrids.

Powder XRD patterns of the synthesized Fe-MOF nanosheets (NSs) are seen in **figure III.7**. The major peaks are located at 9.3°, 15.6°, 18.3°, and 19.1°, which are in excellent accordance with those of the iron oxide phase [37], demonstrating that Fe-MOF nanosheets were successfully synthesized. XRF measurements were also undertaken to investigate the presence of pure iron in the synthesized framework. As shown in **figure III.8**, pure iron appears in a rather strong peak of 300 Å° with an energy of 6.5 KeV. Another less intense iron peak at 7 KeV was discovered. In addition, the presence of extremely low-intensity peaks of other metals is shown such as chromium (Cr), copper (Cu), and cobalt (Co), revealing that the organometallic complex synthesized in this work is primarily based on iron oxide. As a result, the XRD and XRF data revealed that the synthesized composite was produced purely from the Fe-MOF framework.

SEM was next used to analyze the morphology of Fe-MOF nanosheets (NSs) and rGO, revealing the leaf-like structure of rGO as shown in **figures III.9** (A, B, C). **Figures III.9** (D, E, F) presents the 3D sphere-like cluster structure of Fe-MOF NSs. The clusters are a few microns in size and are made up of ultrathin 3D spherical nanosheets that have been assembled.

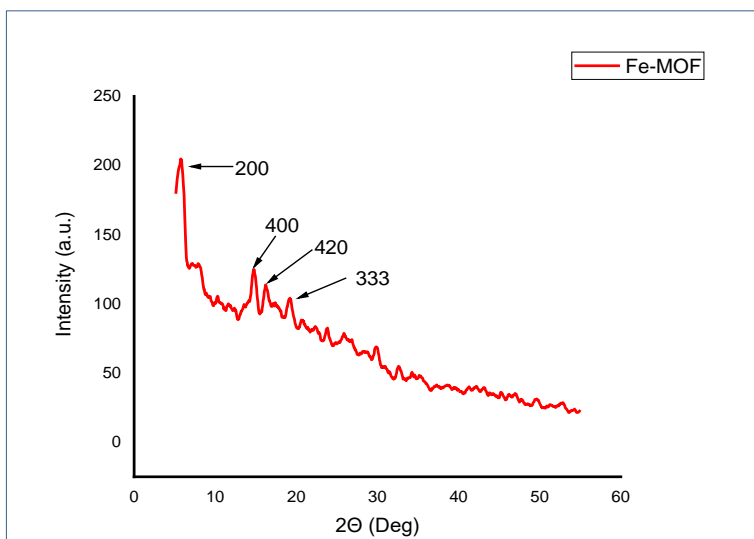


Figure III.7. XRD fragments of the synthesized Fe-MOF.

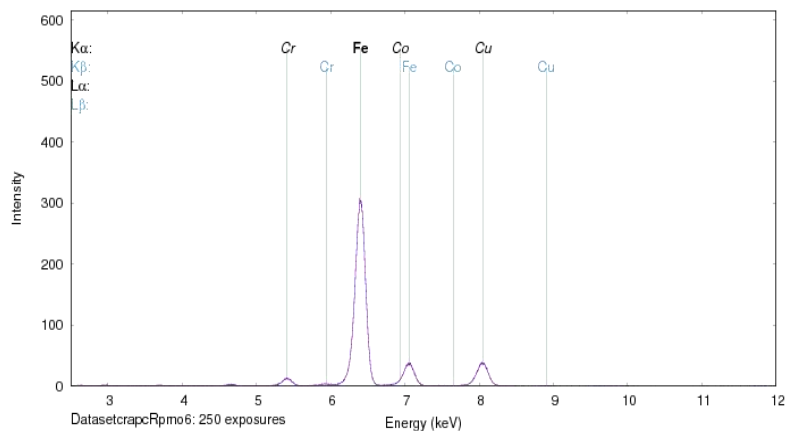


Figure III.8. XRF patterns of the synthesized Fe-MOF.

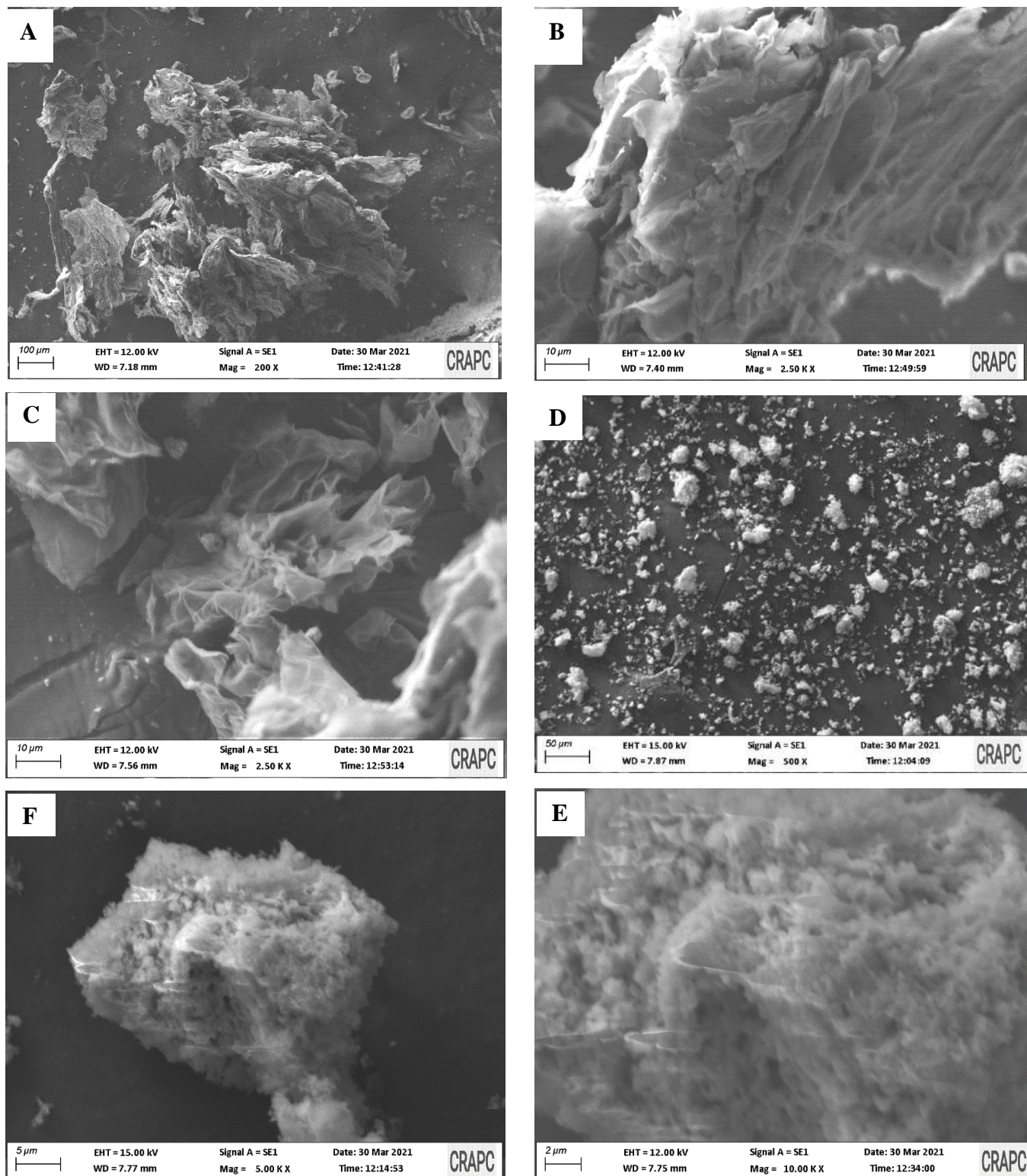


Figure III.9. The SEM images of rGO (A), (B), (C), homogeneous distribution of the organometallic particles in the synthesized framework (D), three-dimensional shape of the MOF (E), and porous structure of the synthesized MOF (F).

III.1.4. Physico-chemical analysis of Ni-Co-LDH and rGO-Cu

Fourier transform infrared (FT-IR) spectra of the synthesized GO, rGO-CuO, and Ni-Co-LDH were obtained to determine the different functional groups, and they are displayed in **figure III.10**. **Figure III.10a** depicts a comparison between the spectrums of GO and rGO-CuO. GO exhibits absorption peaks at 3300, 1695, and 1110 cm^{-1} in these spectra [42] due to hydroxyl, carboxyl, and epoxy functionalities presented in the composite. The intensity of OH stretching in the rGO-CuO spectra was dramatically lowered, indicating that GO was reduced during the doping process [43,44], while the CuO stretching vibrations cause the absorption peak at 515 cm^{-1} in rGO-CuO. The present findings match those reported values [45] which confirm the successful synthesis of the rGO-CuO hybrid. The Ni-Co-LDH FTIR spectra (**figure III.10b**) were characteristic of layer double hydroxide [46,47]. The stretching of vibration of O-H (ν O-H) was linked to the broad band at 3437 cm^{-1} . Water molecules (H-O-H) vibration was ascribed to the band at 1629 cm^{-1} . The vibration of carbonate species was linked to the strong band at 1356 cm^{-1} . The band at 1356 cm^{-1} can be assigned to the vibration of interlayer CO_3^{2-} and NO_3^- anions. CO_3^{2-} participated to form the nickel cobalt carbonate hydroxide hydrate with Ni_2^+ and Co_2^+ ions via coordinate bonds while NO_3^- retained in the interlayer of LDH. The broad peak at 634 cm^{-1} can be assigned to the M-O, O-M-O, and M-O-M (M=Co and Ni) vibrations [48]. The bands in the 500–800 cm^{-1} range were attributed to metal–oxygen bond stretching, specifically Ni–O and Co–O.

Figure III.11 shows the results of a scanning electron microscope (SEM) investigation of the current catalytic system. The photos above depict the surface coverage and the minimal characteristics of the Ni-Co-LDH (**figure III.11a** and **figure III.11b**). The surface morphology of the produced Ni-Co-LDH revealed rough surfaces that make it more porous and appear to be agglomerated in sphere-like shapes. As a result, the produced LDH has a porous surface that allows it to be combined with other materials while also providing a good indicator of its affinity for the 5-CP molecule. Also, SEM was used to describe the surface morphologies of rGO-CuO. (**figure III.11c** and **figure III.11d**). Apart from the wrinkled layers, distribution of CuO particles on the basal planes of graphene is also evident in the SEM micrograph of rGO-CuO displaying the magnetic properties of rGO-CuO along with the dispersion and agglomeration processes of rGO.

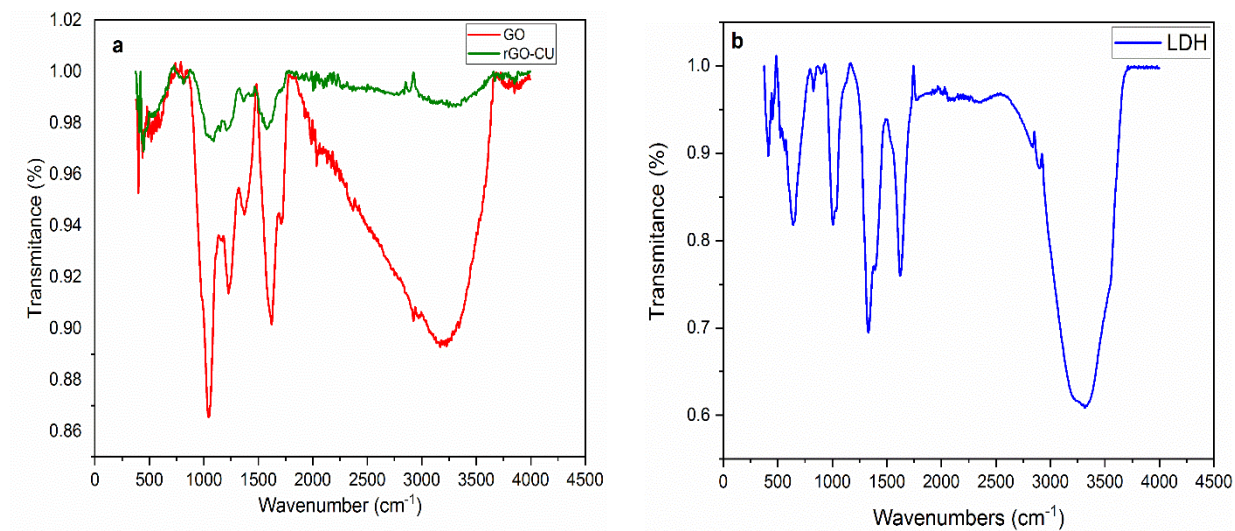


Figure III.10. ATR spectra of (a) GO and rGO-CuO and, (b) Ni-Co-LDH composites

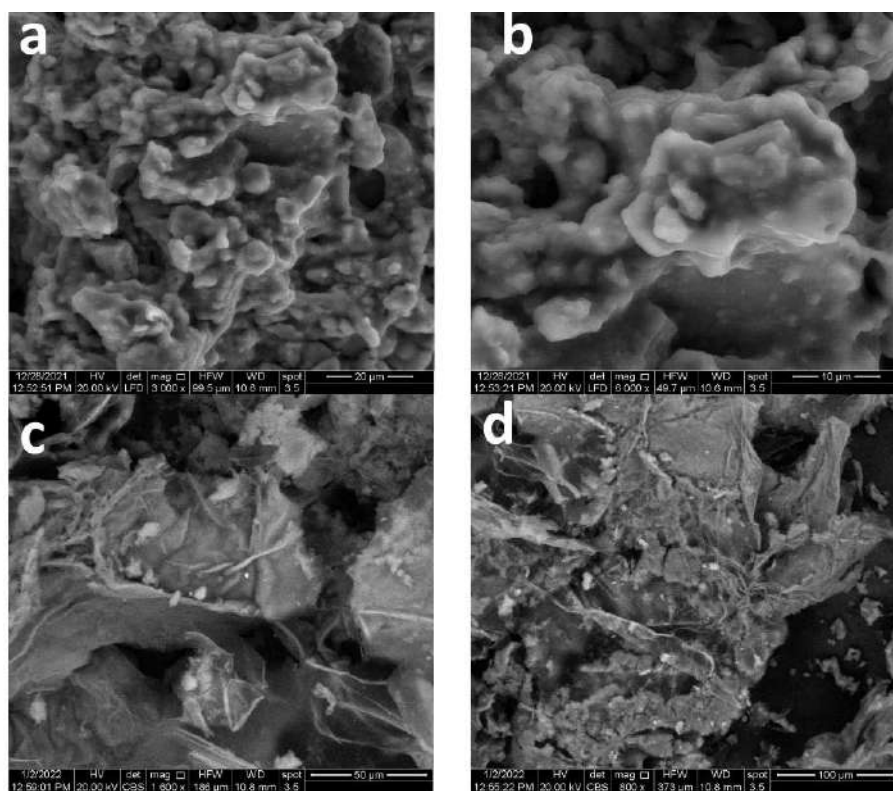


Figure III.11. SEM analysis of (a, b) Ni-Co-LDH and (c, d) rGO-CuO nanocomposites.

III.2. Characterization of the electrode matrix

III.2.1. Electrochemical behavior of *f*MWCNTs, ZnO NPs, and ZnO@*f*MWCNTs to catechol (CC) detection

To assess the electrochemical behavior of the synthesized nanomaterials for catechol detection, the glassy carbon electrode (GCE) was modified using *f*MWCNTs, ZnO NPs, and ZnO@*f*MWCNTs nanocomposites. **Figure III.12** presents the cyclic voltammetry (CV) responses of the bare GCE, ZnO/GCE, *f*MWCNTs/GCE, and *f*MWCNTs/ZnO@*f*MWCNTs/GCE at a scan rate of 100 mV/s in a 0.1 M PBS solution contains 1 mM of CC. As shown, minimal redox peaks appear on the curves of the bare GCE and ZnO/GCE, indicating that both the bare GCE and ZnO/GCE can't detect CC effectively. However, much larger redox peaks exist on the curves of *f*MWCNTs/GCE, ZnO@*f*MWCNTs/GCE, and *f*MWCNTs/ZnO@*f*MWCNTs/GCE, confirming better detection of CC. The CV curve of *f*MWCNTs/ZnO@*f*MWCNTs/ GCE exhibits the largest redox peak, providing higher sensitivity compared to *f*MWCNTs/GCE and ZnO@*f*MWCNTs/GCE.

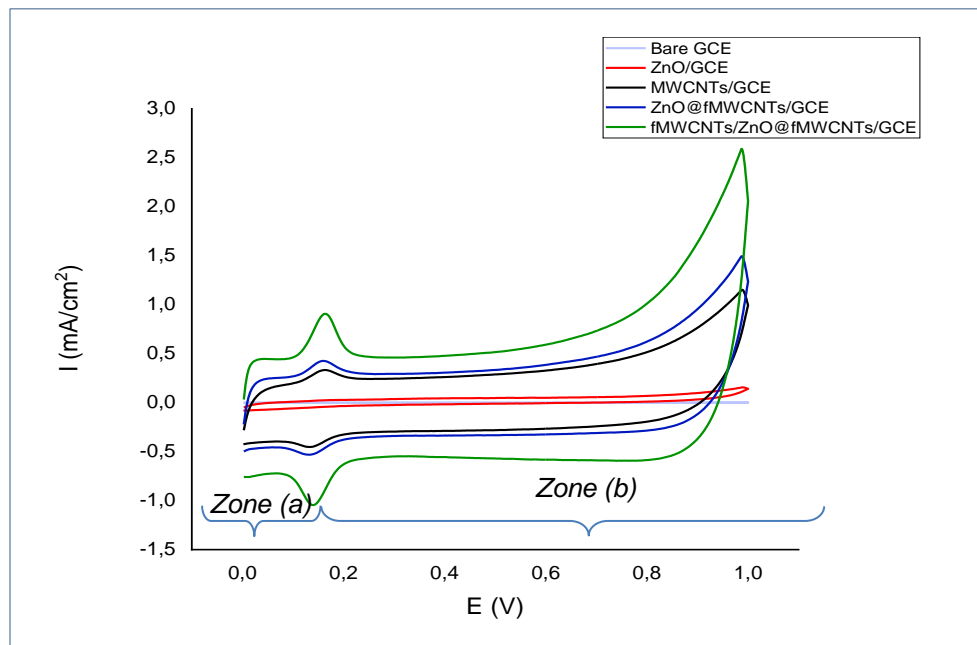


Figure III.12. CV responses of the bare GCE and the modified electrodes.

On the CV curve of *f*MWCNTs/ZnO@*f*MWCNTs/GCE, the potential difference (DE_p) of the redox peaks is around 60 mV which manifests the reversibility of CC redox reactions at the double-layered *f*MWCNTs electrode [5]. This good electrochemical performance of *f*MWCNTs/ZnO@*f*MWCNTs can be attributed to the excellent electronic conductivity of the

synthesized *fMWCNTs* and the affinity reaction on the engineered-interface-based carboxyl groups in both *fMWCNTs* and *ZnO@fMWCNTs* which are likely to have high interaction with CC.[6] Such interactions in the synthesized hybrid *fMWCNTs/ZnO@fMWCNTs* further increase the redox peaks compared to the cases using *fMWCNTs* or *ZnO@fMWCNTs* alone. In addition, the peaks of *ZnO@fMWCNTs/GCE* are larger than those of *fMWCNTs/GCE*, indicating that the ZnO NPs may promote the redox reaction of CC on the modified GCE due to the high electrochemical activity of ZnO NPs and their ultra-high electron transfer which may improve the stability of the modified electrode.

It can be noted that two major phenomena appeared in the CV plots denoted as Zone (a) and (b) as can be seen in **Figure III.12**. In zone (a), the redox current mainly depends on the electron transfer rate of the redox reaction of CC and the applied scan rate [7]. Contrary to zone (b) where the redox current depends on the diffusion constant. Here, the adsorbed layer of *fMWCNTs* above *ZnO@fMWCNTs* enhances the electron transfer rate (zone (a)) and also minimizes the mass-transport limitations (zone (b)) at the electrochemical sensing interface. These enhancements are possibly attributed to the boosted mass-transfer of the antifouling synthesized hybrid. The second layer (*fMWCNTs*) of the hybrid acts as a conductive layer, while preventing the working electrode from any fouling drawbacks due to the absorbance feature of *fMWCNTs* hybrid and its mechanical strength. To sum up, the large surface area, good conductivity, and biocompatibility of the synthesized *fMWCNTs/ ZnO@fMWCNTs* provide an excellent catalytic activity for CC detection with good sensitivity and stability.

III.2.1.1. Dosage optimization of *fMWCNTs/ZnO@fMWCNTs*

The relationship between different dosages of *fMWCNTs/ ZnO@fMWCNTs* nanohybrids and the anodic peak current in 0.1 M PBS containing 1 mM of CC is presented in **Figure III.13**. As shown, 2 mL of *fMWCNTs/ZnO@fMWCNTs* in (1:1) ratio was chosen as the optimal volume to be used in the next sections of this work.

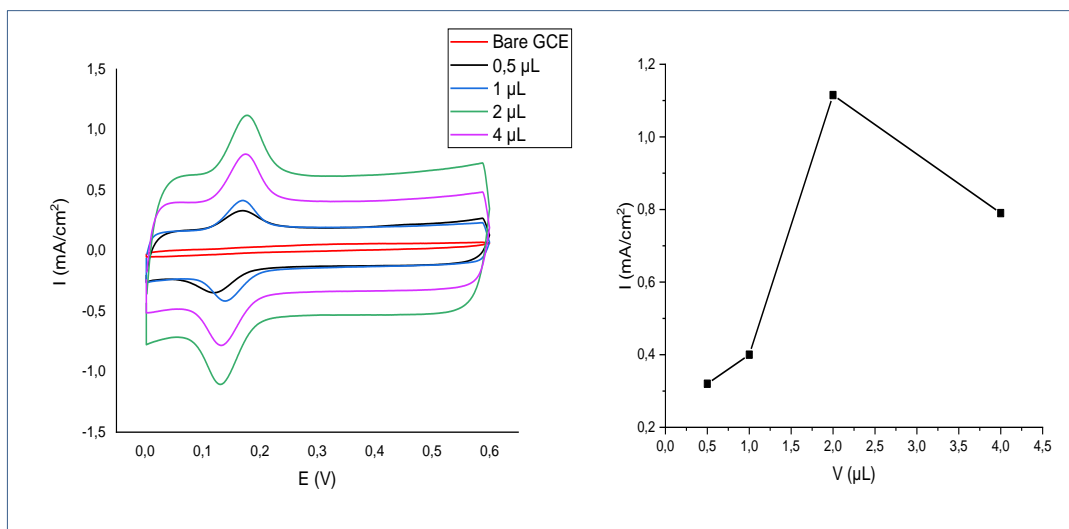


Figure III.13. Dosage effect of $fMWCNTs/ZnO@fMWCNTs$ (μL) in presence of 1 mM CC in 0.1M PBS at Sweep rate 100 mV/s.

III.2.1.2. Electrochemical behavior of CC at $fMWCNTs/ZnO@fMWCNTs/GCE$

The electrochemical activity of $fMWCNTs/ZnO@fMWCNTs/GCE$ was further investigated using a redox phase of 100 μM of CC. **Figure III.14(A)** shows Cyclic Voltammograms (CVs) of the bare GCE and $fMWCNTs/ZnO@fMWCNTs/GCE$ using 0.1 M PBS with a scan rate of 100 mV/s. As shown in **Figure III.14(A)**, the modified electrode exhibited a higher peak current than the bare GCE, indicating a boost of the electron and mass transfer rates due to the good electrical conductivity and catalytic activity of $fMWCNTs$, and the high electron transfer of ZnO NPs presented in the hybrids. The surface area of the electroactive interface can be calculated using Randles–Sevick’s equation as follows [8].

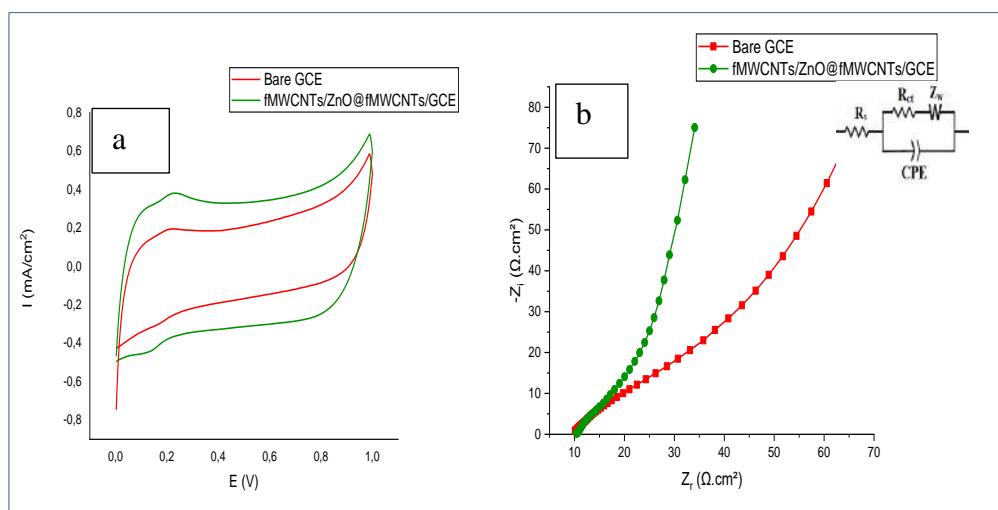


Figure III.14. (a) CVs and (b) EIS for the bare GCE (blue curve) and $fMWCNTs/ZnO@fMWCNTs/GCE$ (red curve) in a 0.1 M PBS solution (pH 7.5) with 100 mM CC at a sweep rate of 0.1 V/s.

$$I_p = 2.69 \times 10^5 \cdot n^{3/2} \cdot A \cdot D^{1/2} \cdot C_0 \cdot V^{1/2}$$

where I_p is the peak current in Ampere, V the scan rate (V/s), n the number of changed electrons, A the electroactive surface area (cm^2), D the diffusion coefficient (cm^2/s), and C_0 the concentration of the electroactive species (mol/cm^3). According to the calculation, the manufactured electrode has a larger surface area (0.14 cm^2) than the GCE (0.07 cm^2)

The Nyquist plot of electrochemical impedance spectroscopy (EIS) typically comes in two segments; the first one is the semicircular segment at higher frequencies expressing the load transfer resistance (R_{ct}), and the other one is the linear portion at lower frequencies expressing the diffusion capacity. EIS measurements of *fMWCNTs/ZnO@fMWCNTs/GCE* were carried out in the presence of 100 mM of CC in a 0.1M PBS solution, over a frequency range between 10^{-1} and 10^5 Hz with a signal amplitude of 10 mV and 10 data points per frequency decade. The diameter of the semicircle of the Nyquist plot is proportional to the charge transfer resistance (R_{ct} value), which was obtained by the electrochemical circle fit option of Voltalab software using the equivalent circuit consisting of R_{ct} , solution resistance ($R_s \approx 10 \Omega \cdot \text{cm}^2$), and Warburg impedance (Z_w). **Figure III.14 (B)** shows the Nyquist plots of the bare GCE and *fMWCNTs/ZnO@fMWCNTs/GCE*. The obtained Nyquist plots were fitted with Randles equivalent circuit model [R_s , R_{ct} , C_{PE} , and Z_w]. The R_{ct} value of the bare GCE ($118,2 \Omega \cdot \text{cm}^2$) seems to be much higher than the R_{ct} value of *fMWCNTs/ZnO@fMWCNTs/GCE* ($28,46 \Omega \cdot \text{cm}^2$), suggesting a lower electron transfer rate of bare GCE. The *fMWCNTs/ZnO@fMWCNTs/GCE* has a significantly decreased semi-circular segment, indicating a reduced charge transfer resistance and improved electron transfer rate due to the conductive nature of the *fMWCNTs* and the high electron transfer rate of ZnO NPs. These results show that the proposed sensor has a lower load transfer resistance and a higher electron transfer rate on the sensing interface compared to the bare electrode. This may be attributed to the existence of ZnO NPs decorated on *fMWCNTs* and the synergistic effect of the *fMWCNTs* and *ZnO@fMWCNTs* nanocomposites, which promotes the electron transfer rate between the electrolytic solution and the electrode surface.

III.2.2. Electrochemical characterization of NiO/rGO/*fMWCNTs*, rGO/*fMWCNTs*, and *fMWCNTs*

In this work, the modified electrodes of the above materials were prepared by a simple dropping method. Firstly, a Pt electrode was pretreated by the method described in the previous section. Subsequently, 3 μL dispersion solutions of the aforementioned NiO/rGO/*fMWCNTs*, rGO/*fMWCNTs*, and *fMWCNTs* materials were dropped on Pt electrodes, respectively. Lastly, these modified electrodes were dried at room temperature. These modified Pt electrodes are denoted as NiO/rGO/*fMWCNTs*/Pt, rGO/*fMWCNTs*/Pt, and *fMWCNTs*/Pt, respectively, in this paper.

Cyclic voltammetry (CV) analysis was performed with the three modified and one bare Pt electrodes (as shown in **figure III.15**). 5 mM CC was inserted in a 0.1 M PBS solution (pH 7.5), and the scan rate was 100 mV/s. As shown in the CV curves (**Figure III.15**), the redox peaks of CC are present at 151.5 mV on the *fMWCNTs*/Pt's curve, 149.07 mV on the rGO/*fMWCNTs*/Pt's curve, 147 mV on the NiO/rGO/*fMWCNTs*/Pt's curve. No redox peak appears on the bare electrode's curve. The potential differences (D_{Ep}) between the oxidation and reduction potentials increases for the modified electrodes. The slight shift of peak potential and the change of D_{Ep} indicates that NiO/rGO/*fMWCNTs*/Pt is more conducive in the RedOx process of CC. The addition of NiO made this process easier to occur, exactly as rGO did, when it was added to the carboxylated *fMWCNTs*. This phenomenon occurs because of the synergetic effect of NiO and rGO and the high catalytic activity of *fMWCNTs*.

On the other hand, the oxidation peak current of NiO/rGO/*fMWCNTs*/Pt is extremely superior compared to the bare electrode. Compared to rGO/*fMWCNTs*/Pt and *fMWCNTs*/Pt, the CC redox peak current of NiO/rGO/*fMWCNTs*/Pt is increased by 1.5 and 3 times, respectively. These results indicate that the electrochemical signals of CC are amplified by the high conductivity of the synthesized nano-hybrid (NiO/rGO/*fMWCNTs*) thanks to the electron transfer ability of NiO, and the synergic catalytic activity of rGO and *fMWCNTs*.

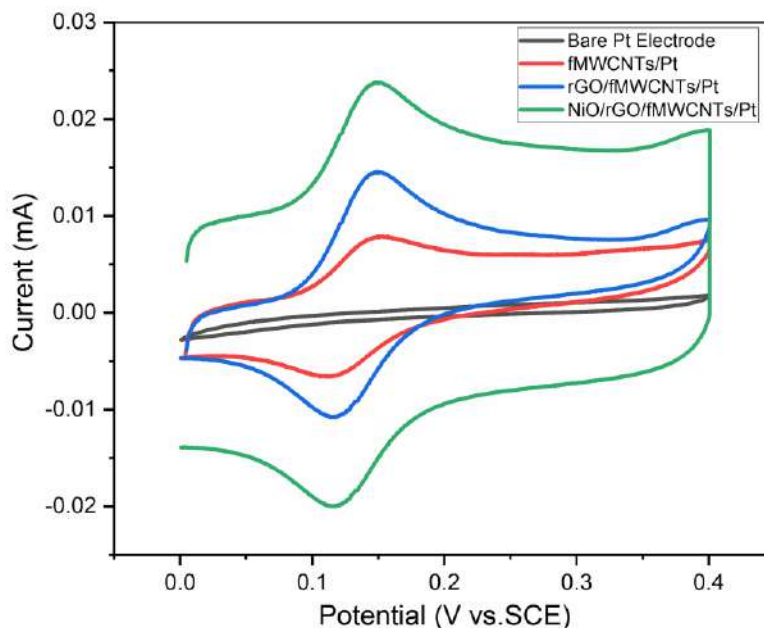


Figure III.15 CV responses of three different modified and bare Pt electrodes in the presence of 5 mM CC in 0.1 M PBS (pH 7.5) at a scan rate of 100 mV/s.

III.2.2.1. Optimization of NiO/rGO/fMWCNTs modification amount

The relationship between different dosages of NiO/rGO/fMWCNTs and the anodic peak current is shown in **Figure III.16**. Here the PBS solution includes 5 mM of CC. As the dosage of NiO/rGO/fMWCNTs increases, the anodic peak current increases firstly, then reaches the maximum at a volume of 3 mL of NiO/rGO/fMWCNTs, and finally decreases afterwards. When the dosage gets larger than 3 mL, the film thickness of NiO/rGO/fMWCNTs increases, degrading the conductivity of the modified electrode. Therefore, 3 mL of NiO/rGO/fMWCNTs was chosen for the best volume in this work.

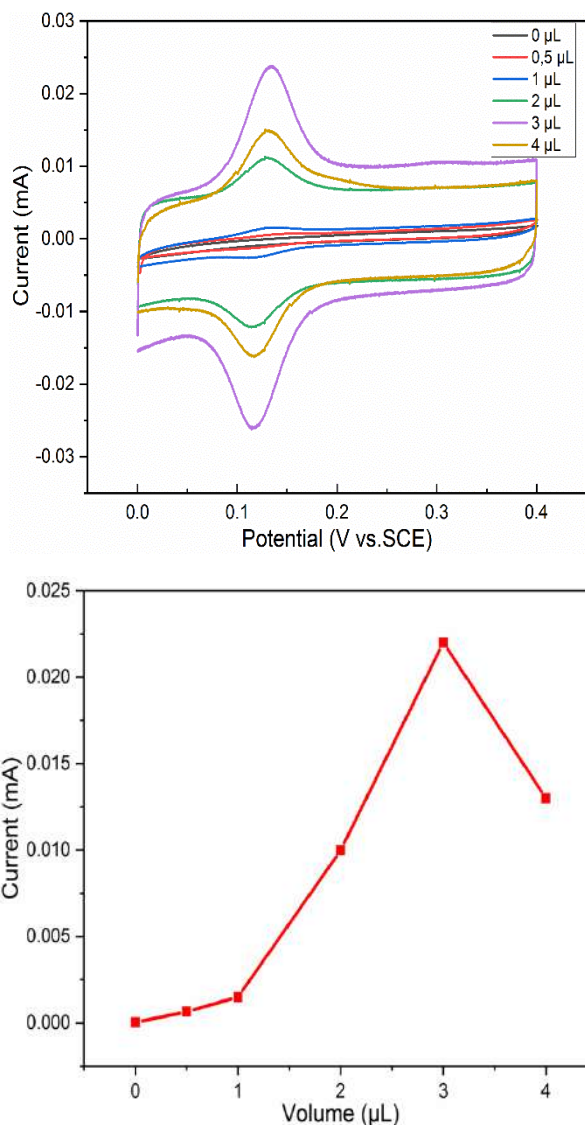


Figure III.16. Effect of dosage of NiO/rGO/fMWCNTs (3 mg/ml) in 0.1 M PBS (pH 7) contains 5 mM catechol with sweep rate of 0.1 V/s.

III.2.2.2. Simultaneous electrochemical behavior of NiO/rGO/fMWCNTs/Pt toward CC and HQ

To explore the electrocatalytic activity of NiO/rGO/fMWCNTs/Pt to CC and HQ oxidation and reduction, cyclic voltammetry (CV) was performed in a PBS (0.1 M, pH 7) including 100 μM CC and HQ. **Figure III.17(a)** shows CV results of a bare Pt and the modified electrode (NiO/rGO/fMWCNTs/Pt). No redox peaks appear when the bare Pt is used to detect CC and HQ. In contrast, NiO/rGO/fMWCNTs/Pt incurs a pair of significant redox peaks. It can be seen that the peak current of the CC and HQ oxidation for NiO/rGO/fMWCNTs/Pt is about 10 times higher than that of the bare electrode. Apparently, NiO/rGO/fMWCNTs/Pt exhibits much better electrocatalytic activity than bare electrodes toward CC and HQ. This result is attributed to the high synergic effects

of the matrix components in high electron transfer rate, high conductivity, and low electron transfer resistance.

To evaluate the electrical parameters (resistances and capacitances) of the modified electrode (NiO/rGO/*fMWCNTs*), electrochemical impedance spectroscopy (EIS) was carried out in a PBS (0.1 M) containing 100 μ M of CC and HQ over a frequency range from 0.1 Hz to 100 kHz with a signal amplitude of 10 mV and 10 data points per frequency decade. **Figure III.17(b)** shows that the impedance of the bare Pt is extremely high. The impedance of the modified electrode, on the other hand, is greatly reduced thanks to the nanocomposite (NiO/rGO/*fMWCNTs*) doped on the Pt surface. This is because *fMWCNTs* and rGO improves the conductivity of the electrode surface. Furthermore, the presence of NiO in the matrix boosts the electron transfer rate on the electrode surface. This EIS results also confirmed that NiO/rGO/*fMWCNTs* are effectively fixed on the Pt electrode's active surface.

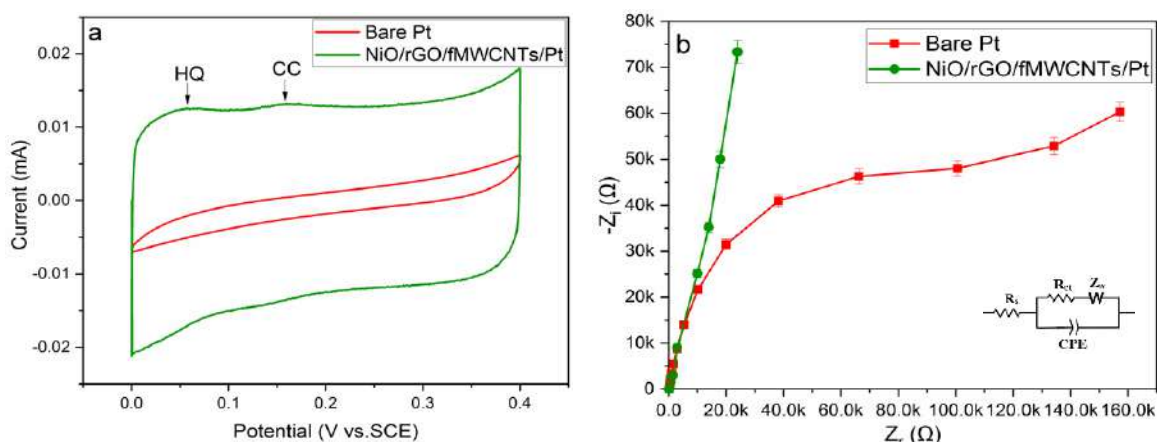


Figure III.17. (a) CV and (b) EIS results of NiO/rGO/*fMWCNTs*/Pt and a bare Pt electrode. A 0.1-M PBS (pH 7) with 100- μ M CC and 100- μ M of HQ, and a scan rate of 100 mV/s are used.

III.2.3. Electrochemical behavior of rGO, Fe-MOF and rGO/Fe-MOF to 5-chlorophenol (5-CP) detection

The conformation and structure of the synthesized nanomaterials have a substantial influence on their electrocatalytic activity and electron transportability. To disclose the interfacial characteristics of the nanocatalyst-modified electrodes, CV experiments were initially performed in a phosphate-based buffer solution (PBS) with a pH of 7 at a scan rate of 100 mV/s containing 5 mM of 5-CP, as shown in **figure III.18**. The bare AuE (a) and Fe-MOF/AuE (b) are displayed minor oxidation peak currents. In comparison, the oxidation peaks at rGO/AuE (c) is drastically larger. It can be attributed to rGO's high conductivity, which promotes the electron transport. Furthermore, the CV

response at rGO/Fe-MOF/AuE was even greater (d). This occurrence was caused by the synergy effect of Fe-MOF and rGO, where Fe-MOF provided a large specific surface area and rGO boosted the electronic conductivity.

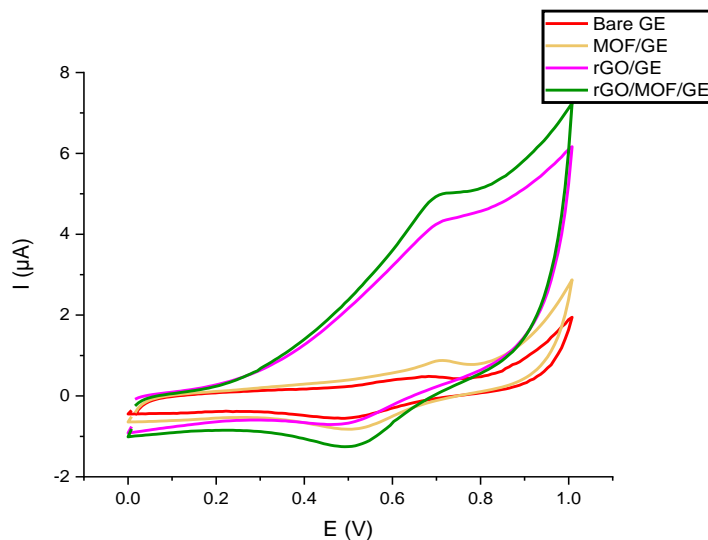


Figure III.18. CVs of 5 mM 5-CP at different modified gold electrodes (AuEs) in the 0.1-M PBS at scan rate of 50 mV/s.

III.2.4. Electrochemical characterization of Ni-Co-LDH, rGO-CuO and Ni-Co-LDH/rGO-CuO

Different electrodes of bare AuE, Ni-Co-LDH/AuE, rGO-CuO/AuE and Ni-Co-LDH/rGO-CuO/AuE were characterized using CV measurements in 5 mM of potassium ferri-ferrocyanide solution containing 0.1 M KCl. As shown in **figure III.19**, it can be clearly observed that both the Ni-Co-LDH/AuE and rGO-CuO/AuE show an increasing current intensity compared with the bare AuE. However, compared to Ni-Co-LDH/AuE, rGO-CuO/AuE boosted more the signal due the excellent conductivity of rGO, the good transfer rate of copper and to the synergic effect between CuO and rGO. On the other hand, to improve the sensitivity of the Ni-Co-LDH/AuE sensing system, Ni-Co-LDH materials then were combined with the organic-inorganic hybrid namely rGO-CuO in 1/1 ratio (3 mg/ml). As can be seen in the **figure III.19**, Ni-Co-LDH/rGO-CuO/AuE network sensing system showed good electrochemical performance compared to the bare AuE, Ni-Co-LDH/AuE and even to rGO-CuO/AuE. This good electrochemical performance of Ni-Co-LDH/rGO-CuO/AuE can be attributed to the excellent electronic conductivity of the synthesized rGO-CuO and the affinity reaction on the engineered-interface-based carboxyl groups in Ni-Co-

LDH and the dual task combination between Ni-Co-LDH and rGO-CuO on AuE surface which is likely to have high interaction with 5-CP.

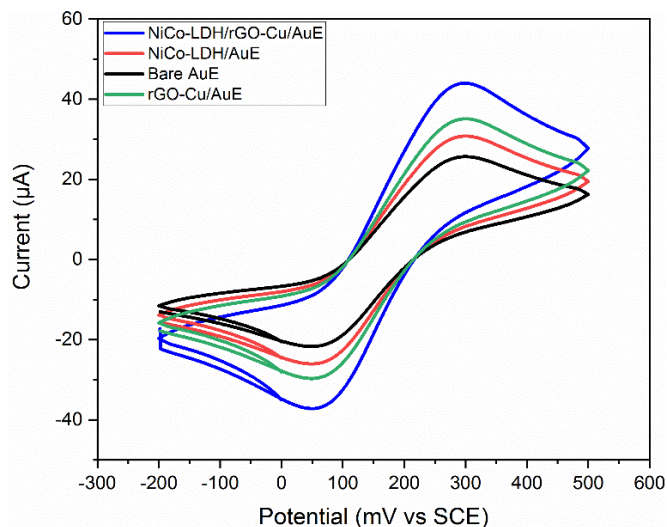


Figure III.19. CVs of 5 mM ferri-ferrocyanide at different modified AuE in the presence of 0.1 M PBS (pH 7) at sweep rate of 0.1 V/s.

III.3. Effect of scan rate and pH value

III.3.1. Effect of scan rate and pH on fMWCNTs/ZnO@fMWCNTs/GCE

The effect of pH value on the electrochemical behavior of 100 mM CC at fMWCNTs/ZnO@fMWCNTs/GCE was studied over a pH range of 5.0–8.0 by CV in PBS 0.1M.

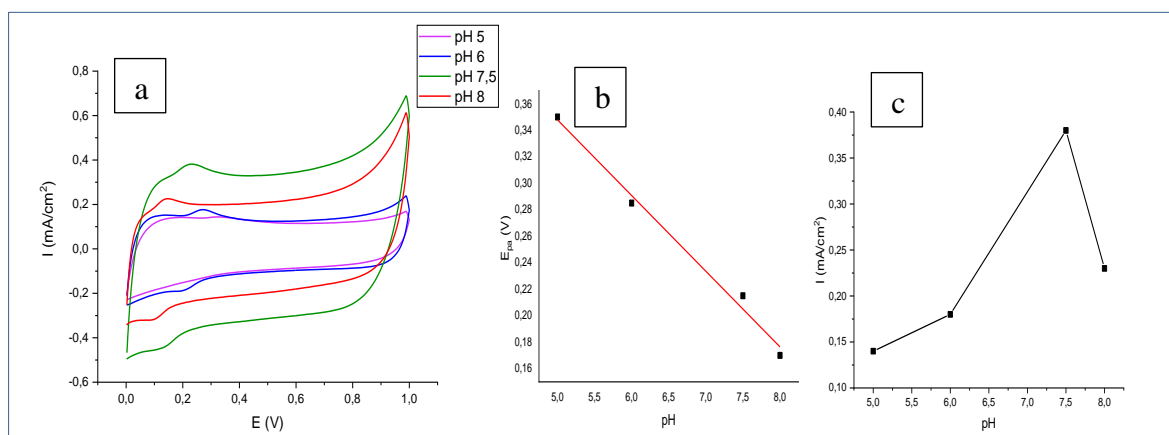


Figure III.20. (a) CVs obtained for CC at fMWCNTs/ZnO@fMWCNTs/GCE in the presence of varied pH; (b) Plot of E_{pa} versus pH; (c) Graph of I_{pa} versus pH.

As shown in **Figure III.20 (A)**, it can be noticed that the anodic peak currents of CC increase with the increase of pH value from 5.0 to 7.5 where the anodic peak current reaches the maximum. Then, with further increase of pH values from 7.5 and above, the peak current of CC gradually decreases. This decrease may be made by the transformation of CC to anions at high pH [8]. Therefore, a PBS of pH 7.5 was chosen for the detection of CC in this work. **Figure III.20 (B)** shows the correlation

between the anodic peak potentials (E_{pa}) and the pH values of PBS. It is clear that as the pH value rises, E_{pa} of CC is driven linearly to more negative potential values. This indicates the involvement of protons in the redox reaction of CC on the surface of GCE. The linear regression equation of CC is E_{pa} (mV) = 633–57.pH ($R^2 = 0.99$). The rate of the regression equation is quite identical to the theoretical Nernstian value of 59 mV (the slope here is 57 mV), demonstrating that the electrochemical redox of CC involves two electrons and two protons ($2e^-/2H^+$) [9]. The scan rate effect on *fMWCNTs/ZnO@fMWCNTs/GCE* was studied by cyclic voltammetry for different scan rates (10–400 mV/s) in 0.1 M PBS containing 100 mM of CC. By increasing the scan rate, a steady enhancement of anode and cathode current peaks was observed as shown in **Figure III.21 (a)**. In addition, the potential peaks are changed negligibly toward positive and negative sides, respectively. **Figure III.21 (b)** shows the relation between the peak current (I_p) and the scan rate (v). The redox peak currents of CC are directly related to the scan rate values. Superior linearity with the correlation coefficient value (R^2) was found to be 0.996 in the obtained result. **Figure III.21 (c)** shows the I_p plot versus the square root scan rate ($v^{1/2}$). Here the correlation coefficient value (R^2) is found to be 0.981. Consequently, the results indicate that the electron transfer mechanism is dominated by CC adsorption. The experimental disparity in the peak potential (ΔE_p) heterogeneous rate constant (k) is obtained using **Eq. (1)**. The corresponding parameters are shown in **Table III.2** [10].

$$\Delta E_p = 201.39 \cdot \log\left(\frac{v}{k^0}\right) - 301.78 \quad (1)$$

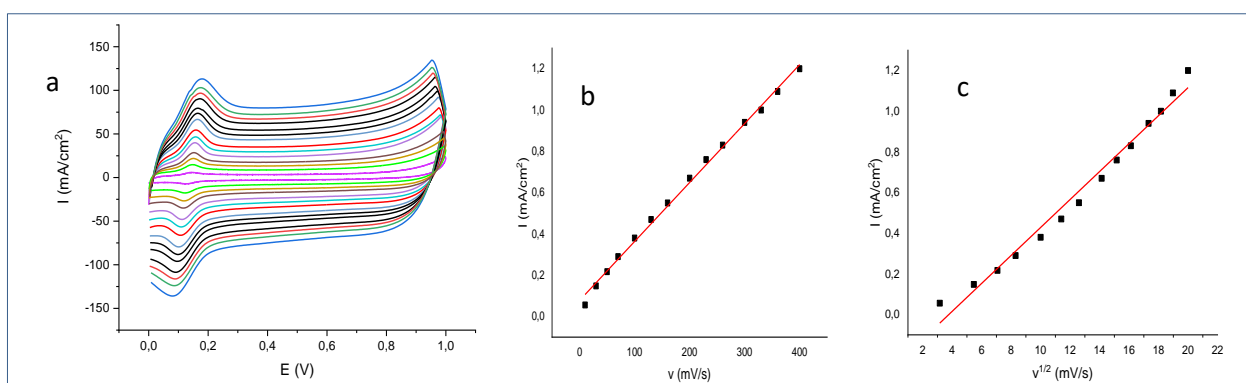


Figure III.21. Effect of (a) scan rate of 100 μ M CC at *fMWCNTs/ZnO@fMWCNTs/GCE*, plots of peak current versus (b) scan rates and (c) (scan rates)^{1/2} for CC in 0.1M PBS.

Table III.2. Heterogeneous rate constant for CC at fMWCNTs/ZnO@fMWCNTs/GCE.

Scan rate (mV/s)	Difference in peak potential (ΔE_p)	Heterogeneous rate constant (k^0) in s^{-1}
10	17.8	0.26
30	30.7	0.67
50	43.7	0.96
100	51.9	1.75
130	63.7	1.99
160	70.84	2.25
200	79.08	2.45
230	92.56	2.53
260	102.2	2.56
300	106.78	2.61
330	123.3	2.65
360	124.4	2.75
400	129.6	2.88

III.3.2. Effect of scan rate and pH on NiO/rGO/fMWCNTs/Pt

Effects of the acidity on the redox activity of NiO/rGO/fMWCNTs/Pt on CC and HQ was investigated. The experiments were examined in 0.1 M PBS for a pH range from 4 to 8. The results are shown in **figure III.22**. As seen, between 4 and 7 of pH, the peak oxidation currents of CC and HQ increase as the pH increases. When the pH is 7, the peak currents of CC and HQ reach the maximum. When the alkalinity increases further, the peak currents begin to diminish (**figure III.22(b)**). This is because the catalytic reaction of CC and HQ on NiO/rGO/fMWCNTs/Pt is a process involving protons. CC and HQ ionizes protons, and the acidity of PBS affects their ionization balance. The acidity promotes the ionization, but the alkalinity hinders the ionization. Therefore, a pH 7 of PBS was selected to detect both CC and HQ in further studies of this work.

To evaluate how many protons are involved in the redox reactions of CC and HQ, the oxidation potential (E_{pa}) is drawn over the pH in **figure III.22(c)**. The linear relation between E_{pa} and pH is $E_{pa}(\text{mV}) = -56 \times \text{pH} + 585$ for CC, and $E_{pa}(\text{mV}) = -57 \times \text{pH} + 456$ for HQ with correlation factors R^2 of 0.9981 and 0.9869, respectively. The slopes of the two regression equations (56 and 57 mV/pH) are quite identical to the theoretical Nernstian value of 59 mV/pH, indicating that the

electrochemical redox processes of CC and HQ involve a transfer of two electrons and two protons ($2\text{H}^+/2\text{e}^-$) [28].

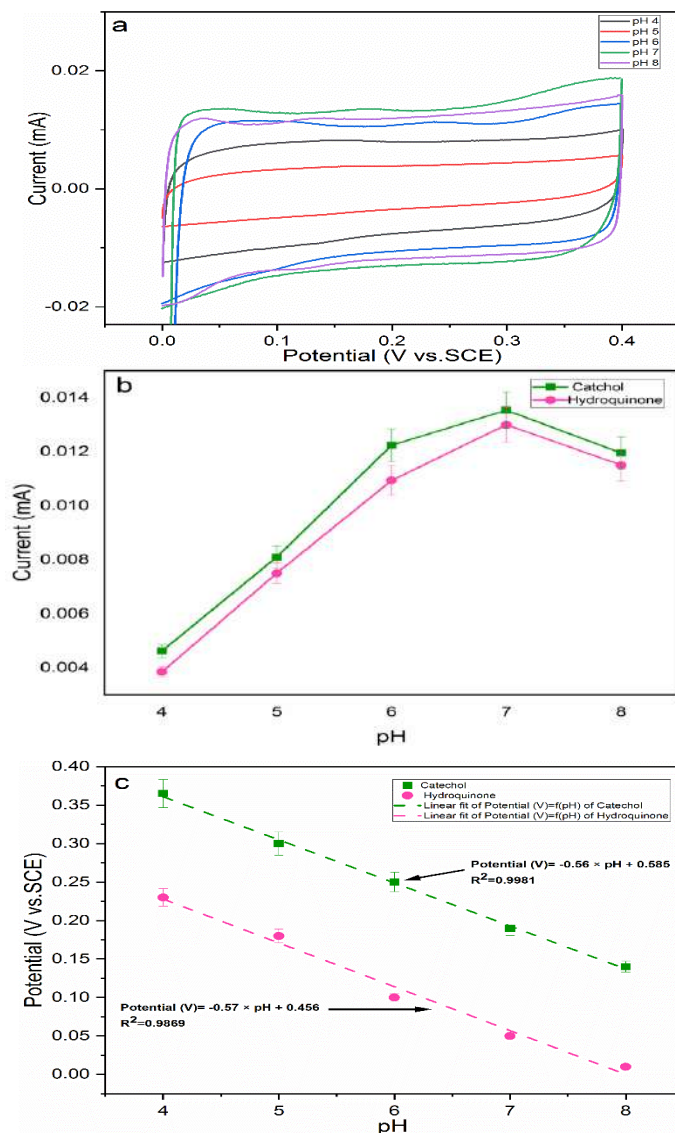


Figure III.22. (a) Cyclic voltammograms obtained for catechol and hydroquinone ($100 \mu\text{M}$) at NiO/rGO/fMWCNTs/Pt in the presence of varied pH; (b) Graph of oxidation current versus pH; (c) Plot of oxidation potential versus pH.

To investigate dynamic behavior of CC and HQ at NiO/rGO/fMWCNTs, the scanning rate v (mV/s) effect on the peak oxidation currents of CC and HQ was studied. The cyclic voltammograms of CC and HQ at NiO/rGO/fMWCNTs with various scan rates are shown in **Figure III.23 (a)**. As shown,

the peak oxidation currents of CC and HQ were proportional to square root of the scan rate. By linear regression, the following fitted equations are obtained:

$$I_{CC} \text{ (mA)} = 0.003 \times v \text{ (mV/s)} - 0.0163 \text{ (R}^2 = 0.967\text{)};$$

$$I_{HQ} \text{ (mA)} = 0.0032 \times v \text{ (mV/s)} - 0.0181 \text{ (R} = 0.9781\text{)}.$$

These relations show that both the electrode reaction processes of CC and HQ at NiO/rGO/fMWCNTs are dominated by diffusion.

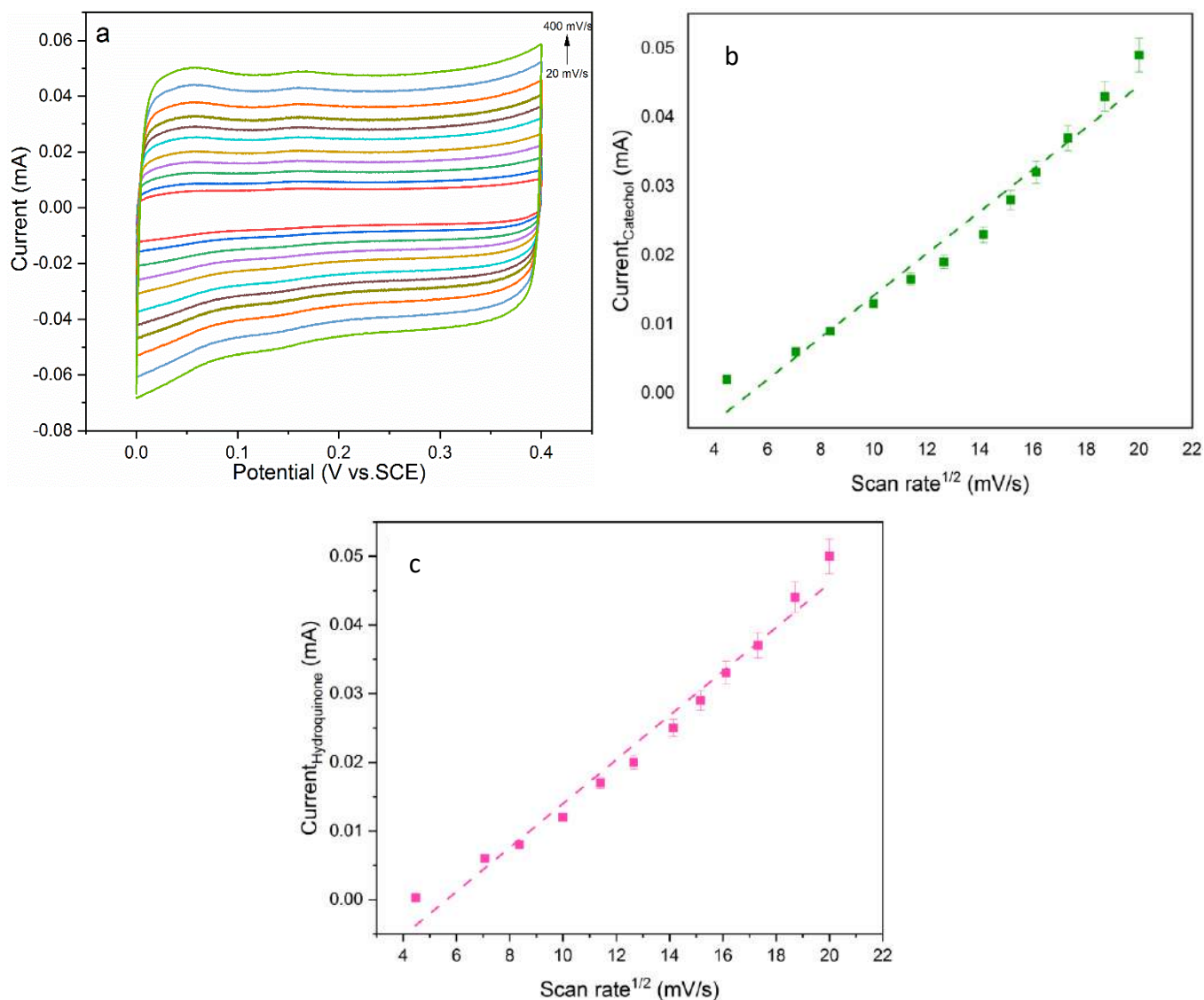


Figure III.23. (a) Cyclic voltammograms obtained for catechol and hydroquinone (100 μM) in 0.1 M PBS (pH 7) at NiO/rGO/fMWCNTs/Pt in the presence of varied scan rate; c) Plot of oxidation current (Catechol) (b) and oxidation current (hydroquinone) (c) versus scan rate $1/2$.

III.3.3. Effect of scan rate on rGO/Fe-MOF/AuE

As indicated in **figure III.24**, the CV response of rGO/Fe-MOF/AuE to 5-CP (100 μ M) was examined by varying the scan rate (ν) from 10 to 100 mV/s to investigate the electrochemical reaction kinetics. According to **figure III.25.b**, the oxidation peak currents of 5-CP gradually rose linearly with the increase of the scan rate (ν) in the 10-100 mV/s range.

The fitted linear equation was $I_{pa} = 0.097 \nu - 0.368$ ($R^2 = 0.991$), **figures III.25** (A and B). It indicated that the electro-oxidation of 5-CP on rGO/Fe-MOF/AuE was controlled by the adsorption process.

Moreover, the anodic peak potential (E_{pa}) of 5-CP has a linear relationship with $\ln \nu$, and the equation is $E_{pa} = 0.78 + 0.02 \ln \nu$ ($R^2 = 0.9986$, **figure III.25 C**). Based on Laviron equation [38]: $E_{pa} = E^0 + (RT/\alpha nF) \ln (RTk_s) + (RT/\alpha nF) \ln V$ wherein E^0 is standard potential; n is the transferred electron number; α refers to the charge transfer coefficient; k_s is the standard rate coefficient. Since α was equal to 0.5, n was calculated as 1.

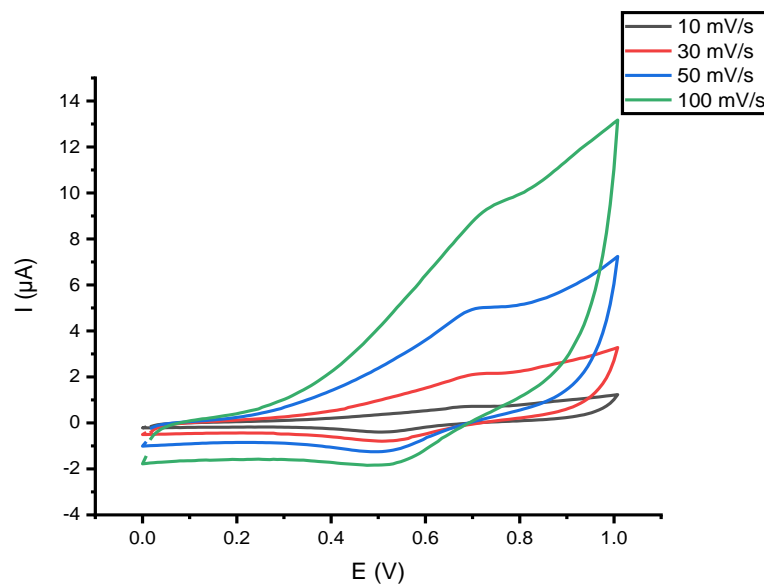


Figure III.24. Effect of CV scan rate on 100 μ M 5-CP in 0.1 M PBS at rGO/Fe-MOF/AuE. The scan rates: 10, 30, 50, and 100 mV/s.

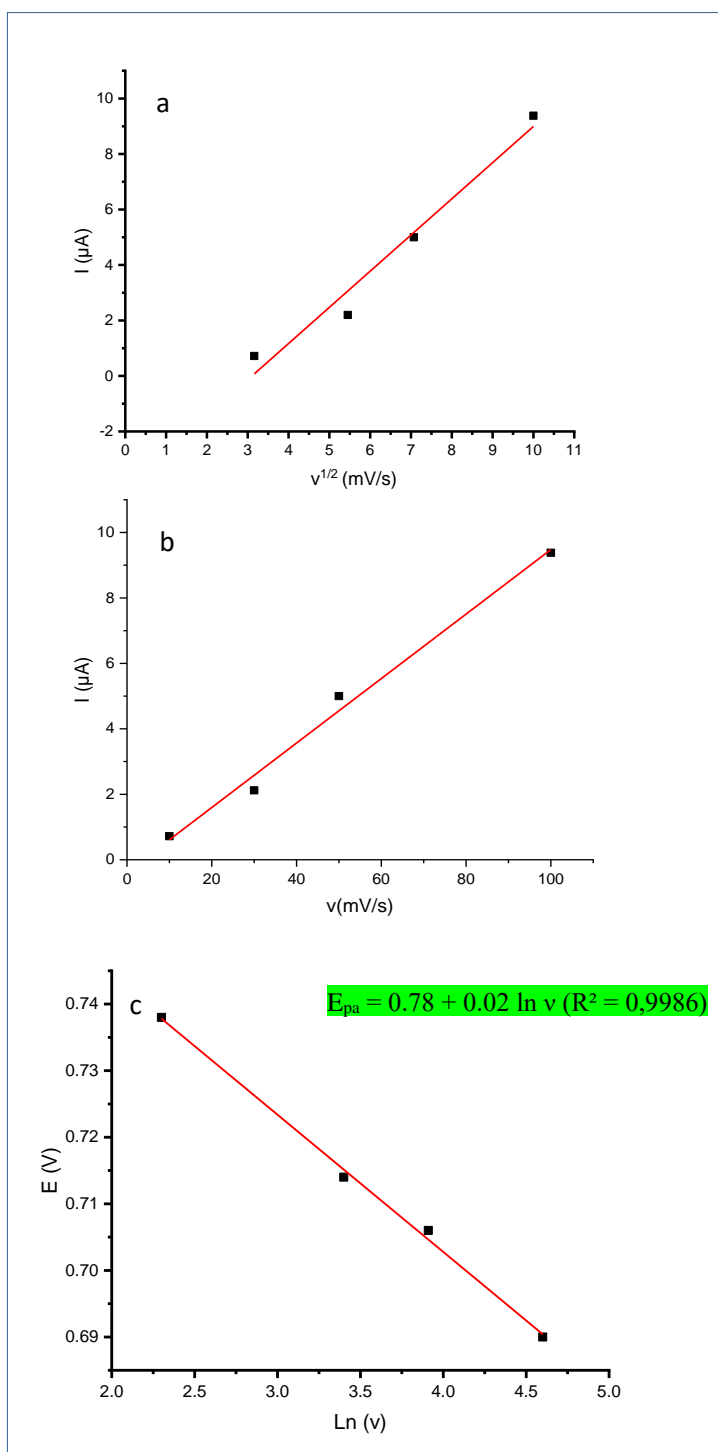


Figure III.25. Plots of peak current versus scan rates (a), (scan rates)^{1/2} (b) (10–100 mV/s), and relationship between E and $\ln(v)$ (c) for 100 μM 5-CP.

III.3.4. Effect of scan rate on Ni-Co-LDH/rGO-CuO/AuE

As shown in **figure III.26a**, the influence of varied scan rates ranging from 20–80 mV/s on the electrochemical performance of the Ni-Co-LDH/rGO-CuO/AuE was also investigated. The magnitudes of the current intensity responses illustrated in **figure III.26a** demonstrate a progressive rise as the scan rate increases. As a result, it was discovered that the size of the current response is linearly dependent on the scan rate, as shown in **figure III.26b** by the equations below: $I(\mu\text{A})=0.45.SR^{1/2}(\text{mV/s})-0.71$ ($R^2=0.9987$). **Figure III.26b** shows well-defined 5-CP redox peaks, indicating surface-controlled electrochemistry, and the redox peak current value ratio was near to one, indicating no side reaction. The active surface area of the Ni-Co-LDH/rGO-CuO/AuE was estimated based on Randles–Sevick equation [48] as presented below:

$$I_p = 2.69 \times 10^5 \cdot n^{3/2} \cdot A \cdot D^{1/2} \cdot C_0 \cdot V^{1/2} \quad (1)$$

where I_p is the peak current in Ampere, V the scan rate (V/s), n the number of changed electrons, A the electroactive surface area (cm^2), D the diffusion coefficient (cm^2/s), and C_0 the concentration of the electroactive species (mol/cm^3).

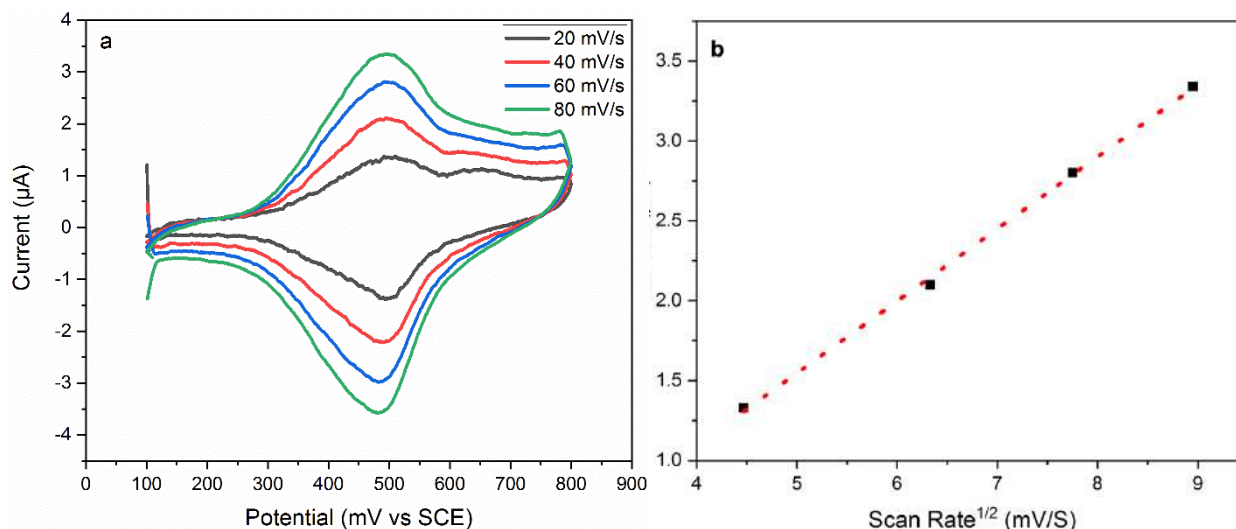


Figure III.26. (a) Effect of scan rate range from 20 to 80 mV/s of 50 µM 5-CP in 0.1 M PBS at Ni-Co-LDH/rGO-CuO/AuE. (b) Current (µA) versus Scan rate^{1/2} (mV/s).

III.4. Electrochemical detection of the organic pollutant

III.4.1. Electrochemical detection of CC using *fMWCNTs/ZnO@fMWCNTs/GCE*

Catechol (CC) detection was performed by cyclic voltammetry measurements with *fMWCNTs/ZnO@fMWCNTs/GCE* for various CC concentrations from 10 μM to 1000 μM (**Figure III.27 (a)**) using a typical addition process in 0.1 M PBS with a scan rate of 100 mV/s. As seen in **Figure III.27 (b)**, the increase of I_{pa} fits the linear equation of $I_{pa} (\text{A}/\text{cm}^2) = 2,2 \cdot C (\mu\text{M}) + 220,3$ ($R^2 = 0.995$) where the concentrations of CC were in the range of 10–200 μM . Using the **equations (3), (4), and (5)**, [11] the detection limit (LOD) of the developed sensor was obtained around 0.027 mM while the quantification limit (LOQ) was about 0.092 mM. In addition, the fabricated sensor responds to a wide linear range of CC concentrations from 10 μM to 200 μM and a sensitivity of 0.0022 mA/cm².mM.

$$\text{LOD} = 3 \cdot \text{SD} / \text{M}. \quad (3)$$

$$\text{LOQ} = 10 \cdot \text{SD} / \text{M}. \quad (4)$$

$$\text{SD} = (\sqrt{N}) \cdot \text{SE}. \quad (5)$$

Where: SD: Standard deviation; SE: standard error; N: number of essays (here N=6) and; M: slope (here M=2). As shown in **Table III.3**, compared with other carbon-nanotubes-based electrochemical catechol sensors, the presented *fMWCNTs/ZnO@fMWCNTs/GCE* has a wider linear range and a lower limit of detection due to the antifouling characteristic by the double layers of *fMWCNTs*, the electron transfer enhancement, and high conductivity of ZnO and *fMWCNTs*.

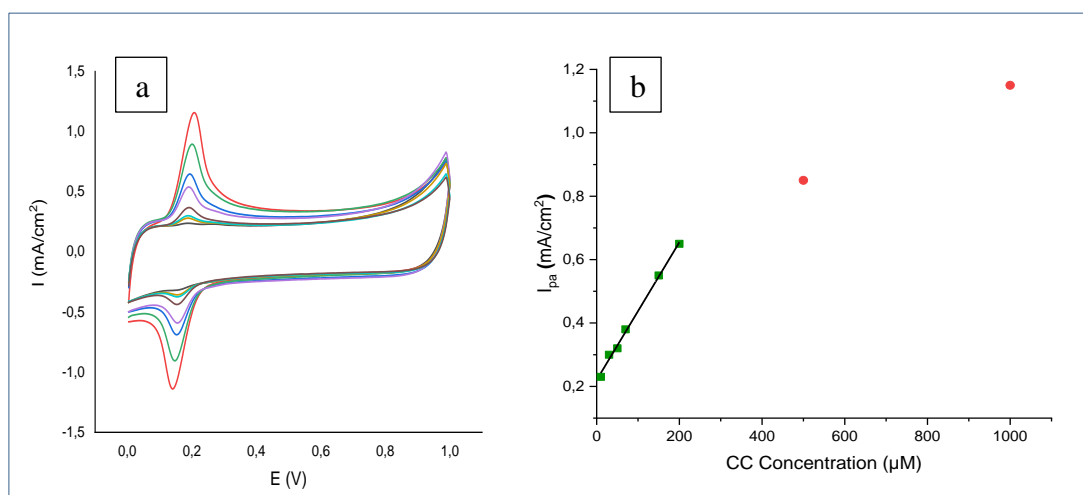


Figure III.27. (a) CVs of *fMWCNTs/ZnO@fMWCNTs/GCE* for various concentrations (10–1000 μM CC) in a 0.1 M PBS at a sweep rate of 0.1 V/s. (b) I_{pa} versus CC concentration.

Table III.3. Comparison with state-of-the-art catechol sensors based on carbon nanotubes.

Sensing interface	Linear range (μM)	LOD (μM)	Reference
Lac/MWCNTsCOOH/AuNPsSDBS/PEDOT/GCE	11.99 – 94.11	12.26	[12]
GCE/MWCNT@CADE	0 – 1000	-	[13]
Co ₃ O ₄ /MWCNTs/GCE	10 – 700	8.5	[1]
MWCNTs@reduced graphene oxide nanoribbon/GCE	15 – 1101	1.73	[14]
PDEA-PS/C ₆₀ MWCNT/GCE	4 – 135	1.45	[2]
c-MWCNTs/PDAd(b-CDe)/c-MWCNT/GCE	0.25 – 4000	0.04	[3]
Gr-CDP-MWCNTs/GCE	0.1 – 27.2	0.03	[15]
<i>f</i> MWCNTs/ZnO@ <i>f</i> MWCNTs/GCE	10 – 200	0.027	This work

III.4.2. Simultaneous detection of CC and HQ using NiO/rGO/*f*MWCNTs/Pt

The CV method was used here to determine the linearity of the electrochemical sensor. NiO/rGO/*f*MWCNTs/Pt was used to detect CC and HQ in a 0.1 M PBS containing different concentrations of CC (10~400 μM) and HQ (10~400 μM). **Figure III.28 (a)** shows the resulting CV curves. It can be known that the peak currents of oxidation and reduction increase as the concentration of CC and HQ increases. **Figures III.28 (b) and III.28 (c)** show the peak current of CC and HQ over their concentrations, respectively.

As shown in **Figure III.28b**, the linear range of the CC detection is from 10 to 300 μM , with a linear fitted equation of $I_{\text{CC}} (\mu\text{A}) = 0.05 \times C (\mu\text{M}) + 3.8$ ($R^2 = 0.9987$), a detection limit (LOD) of 19.86 nM, and a quantification limit (LOQ) of 60.25 nM ($S/N = 3$). Similarly, the linear range of the HQ detection is also from 10 to 300 μM with a linear fitted equation of $I_{\text{CC}} (\mu\text{A}) = 0.04 \times C (\mu\text{M}) + 3.6$ ($R^2 = 0.9965$), a LOD of 40.18 nM, and a LOQ of 121.76 nM ($S/N = 3$). In addition, the measured sensitivity of NiO/rGO/*f*MWCNTs/Pt is 55.7 $\text{nA}/\text{cm}^2 \cdot \mu\text{M}$ and 38.77 $\text{nA}/\text{cm}^2 \cdot \mu\text{M}$ for CC and HQ, respectively. Table III.4 provides a comparison of the proposed NiO/rGO/*f*MWCNTs/Pt sensor with other related modified electrodes for detecting CC and HQ. As shown, our proposed sensor has a lower detection limit and a high sensitivity.

Table III.4. Comparison with state-of-the-art CC and HQ sensors based on rGO.

Electrode matrix	Linear range (μM)		Detection limit (μM)		Ref.
	CC	HQ	CC	HQ	
CNCs-rGO	1-400	1-300	0.4	0.87	[27]
Au-PdNF/rGO	2.5-100	1.6-10	0.8	0.5	[29]
P-rGO	5-120	5-90	0.18	0.08	[30]
MIL-101(Cr)-rGO	4-1000	10-1400	0.66	4.1	[31]
rGO-CS	1-400	1-300	75	75	[32]
rGO	1-200	6-200	0.1	0.2	[33]
rGO-MWCNTs	5.5-540	8-391	1.8	2.6	[34]
rGO/Fe ₃ O ₄ /AuNPs	0.05-550	0.1-500	0.02	0.17	[35]
NiO/rGO/fMWCNTs	10-300	10-300	0.019	0.040	This work

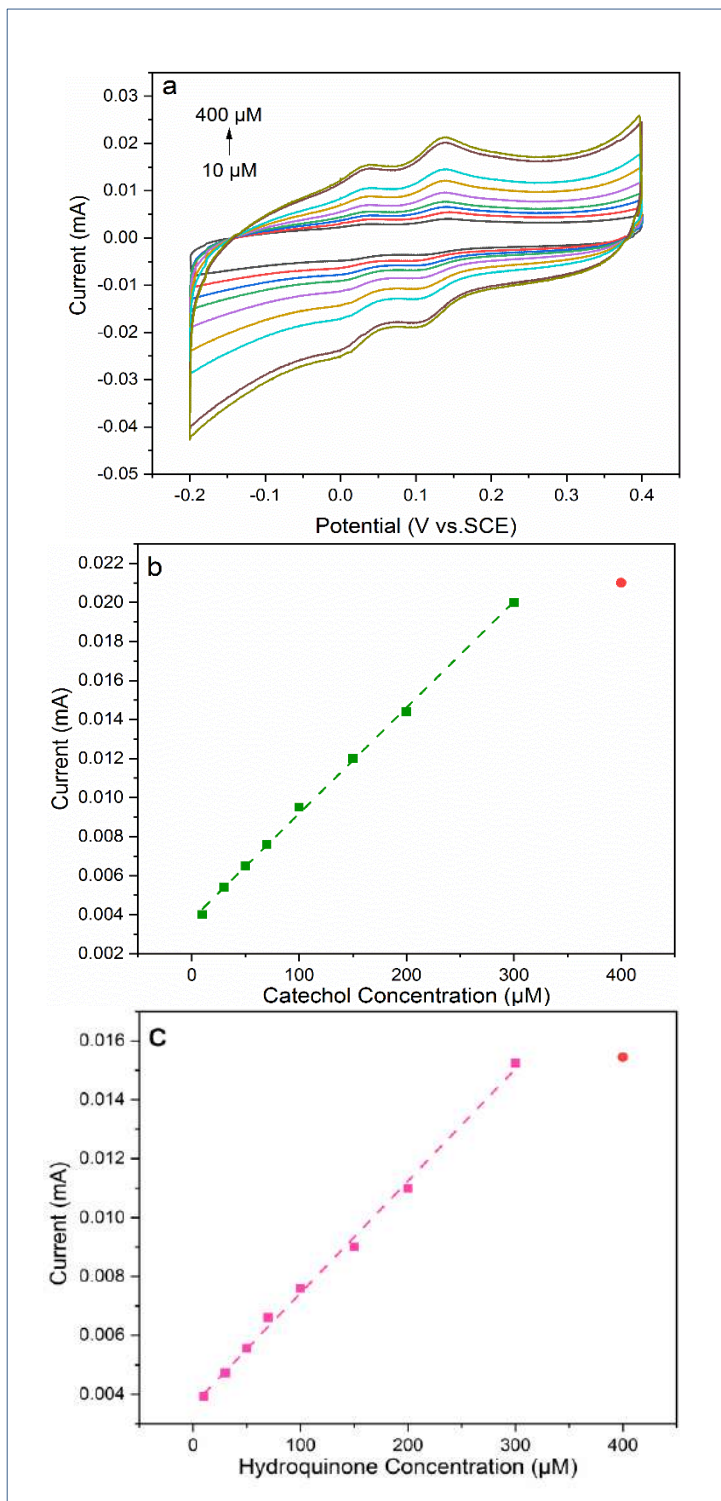


Figure III.28. (a) CVs obtained for various concentrations of CC and HQ in 0.1 M PBS (pH 7) at NiO/rGO/fMWCNTs/Pt; (b) I_{pa} versus CC concentration; (c) I_{pa} versus HQ concentration.

III.4.3. Electrochemical detection of 5-CP using rGO/Fe-MOF/AuE

Square wave voltammetry (SWV) measurements with rGO/Fe-MOF/AuE were done for various 5-CP concentrations ranging from 50 μM to 200 μM (**figure III.29** (A)) using a standard addition operation in 0.1 M PBS with a scan rate of 100 mV/s. As can be seen in **figure III.29** (B), the increase of I_{pa} fits the linear equation of $I_{\text{pa}} (\text{A}/\text{cm}^2) = 0.003 \times C (\mu\text{M}) + 2.025$ ($R^2 = 0.982$) where the concentrations of 5-CP were in the range of 50–200 μM . The detection limit (LOD) of the developed sensor was obtained around 75.63 nM, while the quantification limit (LOQ) was about 254.54 nM. In addition, the fabricated sensor responds to a wide linear range of 5-CP concentrations from 50 μM to 200 μM and sensitivity of 3.4 nA/nM

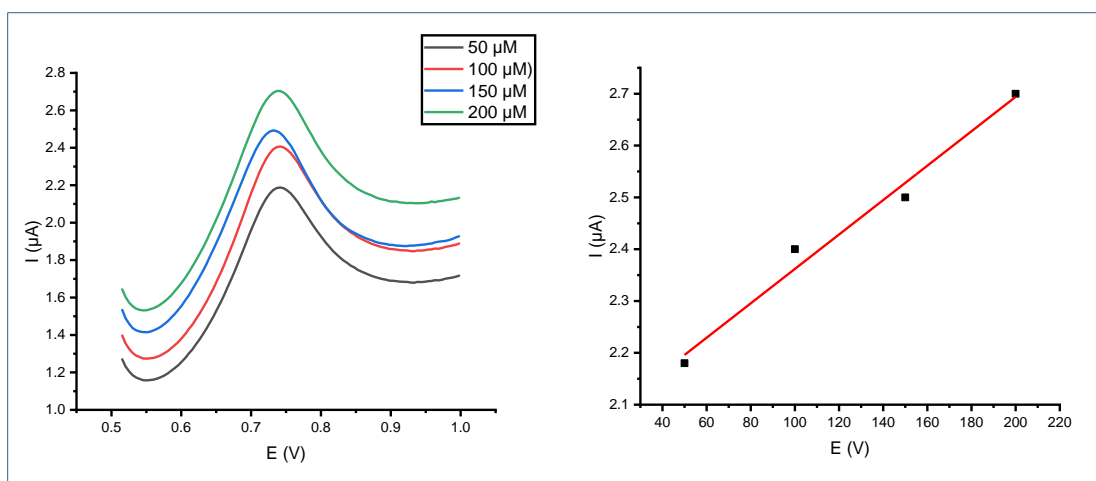


Figure III.29. (A) SWV of rGO/Fe-MOF/AuE for various concentrations (50–200 μM 5-CP) in a 0.1M PBS at a sweep rate of 0.05 V/s. (B) I_{pa} versus 5-CP concentration.

Compared to other MOF-based electrochemical 5-CP sensors, the presented rGO/Fe-MOF/AuE has a wider linear range and lower limit of detection (as shown in **Table III.5**) due to the unique characteristics of the recognition matrix, including electron transfer enhancement and high conductivity of rGO, and large specific surface area of Fe-MOF.

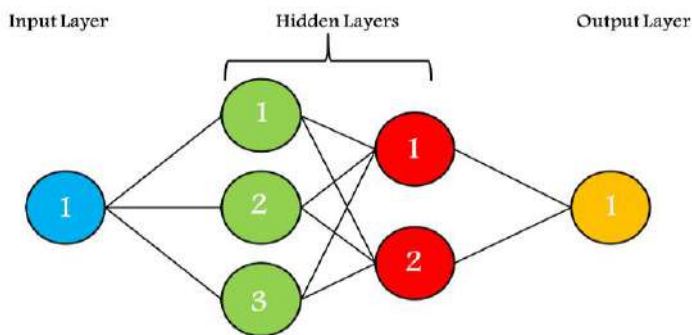
Table III.5. Comparison with state-of-the-art phenol-compound sensors based on MOFs.

MOFs-based sensors	Linear range (μM)	LOD (μM) S/N=3	Reference
1.1.1 FeO _x /TiO ₂ @Mc	5 – 310	0.18	[39]
Zr-based UiO-66	0.0 – 1.0	0.18	[40]
1.1.2 Zn-MOF	0.2 – 12	0.12	[41]
rGO/Fe-MOF	50 – 200	0.075	This work

III.4.3.1. ANN modeling of the sensor

III.4.3.1.1. Data analysis of 5-CP using ANN

The usage of an artificial neural network (ANN) algorithm created in MATLAB 6.1 (Mathworks, Natick, MA) utilizing the Neural Network Toolbox, version 4.0, resulted in far more accurate pollutant detection. The ANN model, depicted in **figure III.30**, is composed of three layers: (i) the input layer of analyte responses; (ii) two hidden layers, the first of which contains three neurons and the second of which contains two neurons; and (iii) the output layer, which represents a three-digit value that identifies the concentration of 5-CP. **Table III.6** depicts the ANN's detailed structure and architecture. The developed ANN algorithm was trained to identify 5-CP and provide an approximate estimate of the concentration by rounding the output to the nearest quantized concentration number, ranging from LOD 75 nM to 200 μM .

**Figure III.30.** ANN architecture for estimation of 5-CP concentrations.

The ANN was trained by repeatedly inputting the experimental findings, such as the sensor channel responses to 5-CP at four concentrations (50 μM , 100 μM , 150 μM , and 200 μM). The Levenberg-Marquardt approach was used in the ANN training method to maximize the neurons' weights in the

hidden layers. Using the limited experimental results of this research, this algorithm appears to be the fastest way for network training. The activation function for the hidden neurons was a log-sigmoid, while the activation function for the output neurons was a log-purelin function. The training was performed for 8,000 epochs (e.g., 8,000 repetitions of data feeding) with a mean square error (MSE) goal set to 10^{-20} and a learning rate set to 0.1 (10%). However, 1358 epochs were enough to reach ESM saturation at $9.4744 \cdot 10^{-12}$, as shown in **figure III.31**.

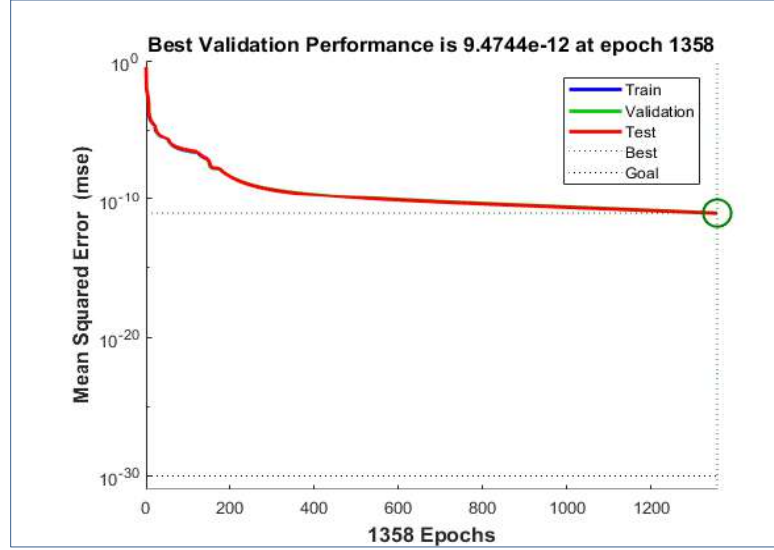


Figure III.31. Mean squared error (MSE) over the trained epochs of the ANN. The learning rate (LR) was set to 10%.

Table III.6. Structure, architecture and settings of the best-found model for the 5-CP prediction.

5-CP ANN	
<i>Inputs</i>	5-CP concentrations (μM)
<i>Output</i>	Current response (μA)
<i>Layers</i>	4
<i>Hidden Layer</i>	2
<i>Hidden Neurons</i>	5
<i>Transfer functions</i>	Logsig/Logsig/purelin
<i>Train function</i>	Traingdm (batch gradient descent with momentum algorithm)
<i>Learning rate</i>	0.1 (10%)
<i>Train epochs</i>	8000
<i>Mean Squad Error (MSE)</i>	10^{-30}
<i>Number of Training Data</i>	100%
<i>MSE Saturation (Best)</i>	9.4744×10^{-12}
<i>Performance Epochs (Best)</i>	1358

Figure III.32 presents graphs showing the training, validation, and testing data. The solid line holds the best fit regression analysis line between the outputs and targets in each plot, while the dashed line represents the perfect result for the case that outputs = targets. The correlation factor R-value presents the relationship between the outputs and targets for 5-CP concentrations and relative responses. The training data show that the ANN model fits the response of 5-CP sensor well. The validation and test data reveal a high R-value as well. The scatter plots demonstrate that great fitting is achieved with the constructed ANN in this work. Following the training, the ANN algorithm was put to the test by feeding it with data from the proposed sensor for PBS solutions spiked with a specific concentration of pollutants chosen randomly from the LOD (75 nM) to 200 μM . **Table III.7** summarizes the outcomes of each test.

The ANN result is a three-digit code that indicates the concentration of 5-CP rounded to the closest quantized concentration value. In spite of having a limited quantity of data for ANN training, the program was able to accurately estimate the pollutant concentration, even with a tiny inaccuracy, as shown in **figure III.33**. The comparison of values in the last two columns indicating the obtained and actual concentrations of pollutants reveals that the concentration was appropriately assessed. For instance, a sample spiked with 200 μM of 5-CP was detected using the ANN at a concentration of 199 μM , whereas a sample injected with 50 μM of 5-CP was detected using the ANN at a concentration of 50.15 μM . In comparison, as demonstrated in **Figure III.33 B**, the software properly anticipated the 5-CP concentrations.

The results are quite encouraging since simple electrochemical measurements of the anodic current at +0.7 V combined with the ANN-based data processing allow for identification of the contaminants and a reasonable estimate of their quantities.

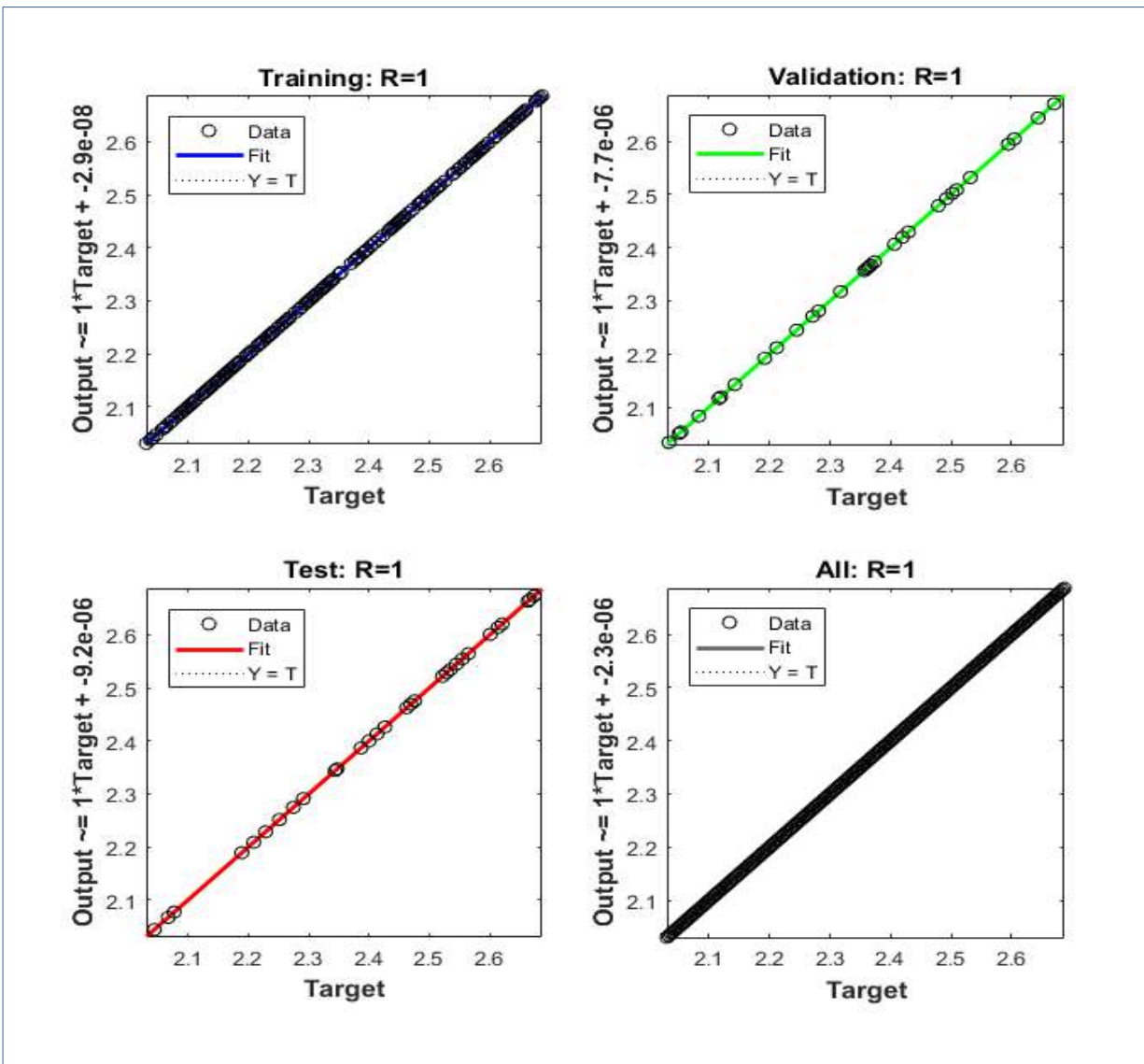


Figure III.32. Correlation factor (R) for the training, validation, testing, and all data of the developed ANN.

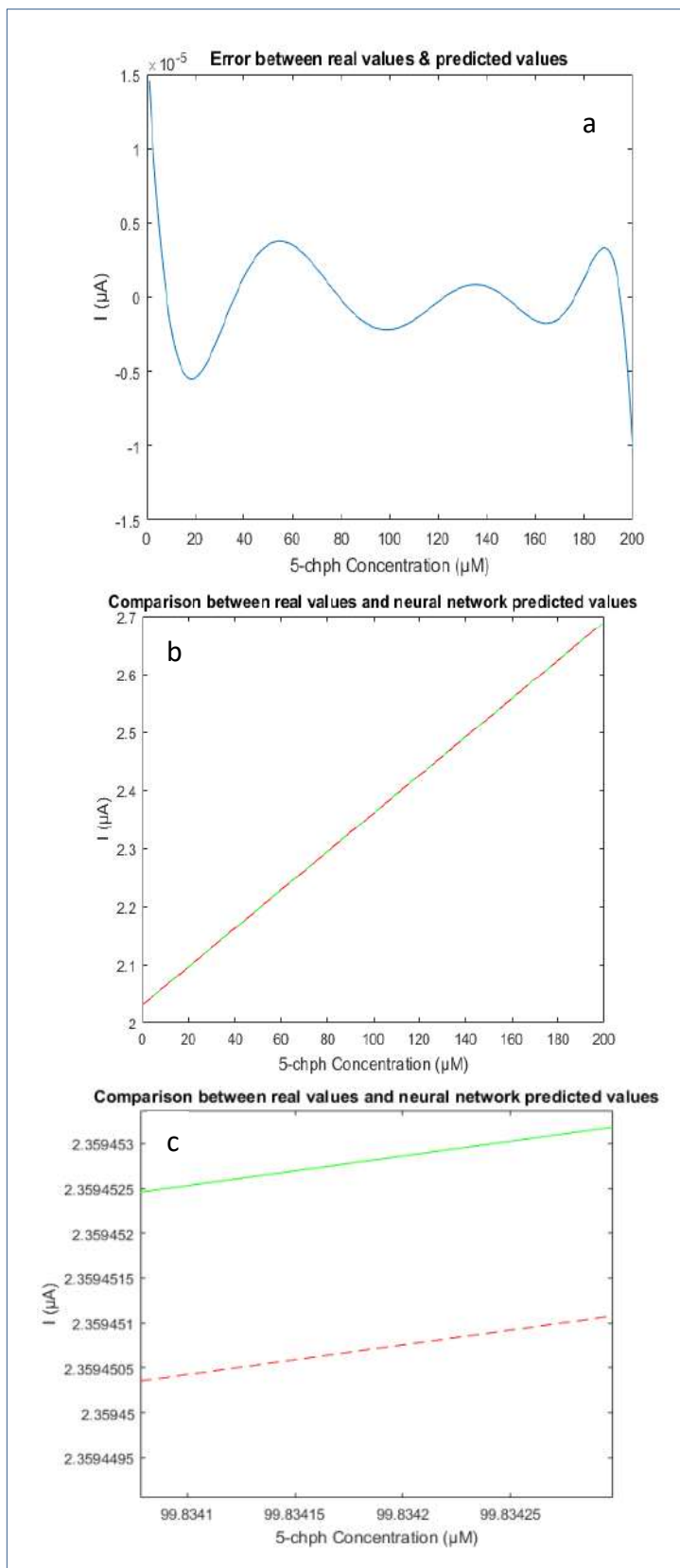


Figure III.33. (a) ANN prediction error; (b), (c) Comparison between the real values (green color) and the predicted ones (red color) obtained by the developed ANN.

Table III.7. Comparison between the real and estimated 5-CP concentrations using the developed ANN

Real 5-CP Concentration (μM)	5-CP oxidation Current (μA)	Estimated 5-CP Concentration (μM)	5-CP oxidation Current (μA)
0.075	Not Applicable (NA) at the lab.	0.075	2.0303
0.25	NA	0.25	2.0308
0.50	NA	0.50	2.0317
0.75	NA	0.75	2.0325
1.00	NA	1.00	2.0333
5.00	NA	5.00	2.0465
10.0	NA	10.0	2.0630
20.0	NA	20.0	2.0960
30.0	NA	30.0	2.1290
40.0	NA	40.0	2.1620
50.0	2.187	50.0	2.1950
65.0	NA	65.0	2.2445
80.0	NA	80.0	2.2940
93.0	NA	93.0	2.3369
100	2.400	100	2.3600
110	NA	110	2.3930
130	NA	130	2.4590
140	NA	140	2.4920
150	2.500	150	2.5250
160	NA	160	2.5580
170	NA	170	2.5910
190	NA	190	2.6570
200	2.702	200	2.6900

III.4.4. Electrochemical detection of 5-CP using Ni-Co-LDH/rGO-Cu/AuE

The electrochemical response of the Ni-Co-LDH/rGO-CuO/AuE has been studied as a function of 5-CP concentrations (from 1 to 50 μM) as shown in Fig. 5a using CV with a scan rate of 100 mV/s in 0.1 M PBS solution (pH 7).

It can be seen from the inset of **figure III.34a** that the magnitude of the electrochemical response current of the Ni-Co-LDH/rGO-CuO/AuE was observed to increase with an increase in the 5-CP concentrations. This was attributed to the successful interaction between the present catalyst and 5-CP molecule due to the synergic effect between the organic-inorganic hybrid (rGO-CuO) and Ni-Co-LDH. A linear plot was drawn between changes in current and the concentrations of CC and is almost linear (**figure III.34b**), which is expressed in the following equation $I (\mu\text{A})=0.0125 C(\mu\text{M})+0.7796$ ($R^2=0.98876$). The cyclic voltammetry results show that the prepared sensor showed a wide linear response to 5-CP concentrations ranging from 1 to 50 μM with a correlation coefficient of 0.98876. The detection limit (LOD) of the developed sensor has been estimated as 12.64 μM while the quantification limit (LOQ) was estimated to be 38.32 μM . In terms of limit of detection, we are on par with most of the recent reports but as per our knowledge, this is not only the first report using such combination of an LDH with an organic-inorganic composite based on green synthesis to detect 5-CP, but also the present study reports the first use of Ni-Co-LDH based electrochemical sensor matrix to detect 5-CP.

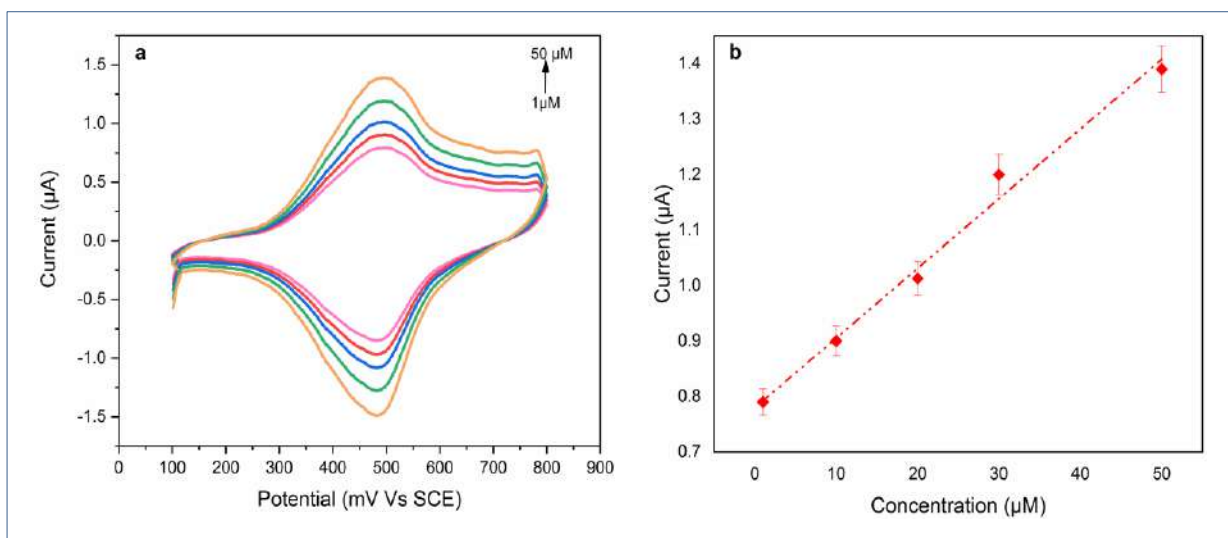


Figure III.34. (a) CVs of Ni-Co-LDH/rGO-Cu/AuE for various concentrations (1–50 μM 5-CP) in a 0.1 M PBS at a sweep rate of 0.1 V/s. b) I_{pa} versus 5-CP concentration.

III.5. Analytical performance of the fabricated sensors

III.5.1. Analytical performance of fMWCNTs/ZnO@fMWCNTs/GCE

III.5.1.1. Selectivity, stability, repeatability, and reproducibility of fMWCNTs/ZnO@fMWCNTs/GCE

To assess the electroanalytical characteristics of the fabricated sensor; several studies including selectivity, stability, repeatability, and reproducibility were investigated. The selectivity was evaluated by an interference experiment carried out by using cyclic voltammetry measurements for fMWCNTs/ZnO@fMWCNTs/GCE in the presence of 0.1 M PBS at a scan rate of 100 mV/s as can be seen in **Figure III.35 (A)**. Here, CC concentrations were changed whilst hydroquinone (HQ), penta-chlorophenol (p-Ch-ph), and phenol (ph) concentrations were kept constant. From **Figure III.35 (B)**, HQ, p-Ch-ph, and ph concentrations were kept constant (50 mM) and the concentration of CC was increased from 50 to 200 mM. As shown in **Figure III.35**, there were no changes or negligible changes in the potentials and peak current of CC. Hence, the results validate that the fabricated sensor based on an antifouling double layered of fMWCNTs possess exceptional selectivity toward catechol, and it can monitor CC even in a phenolic compounds mixed solution.

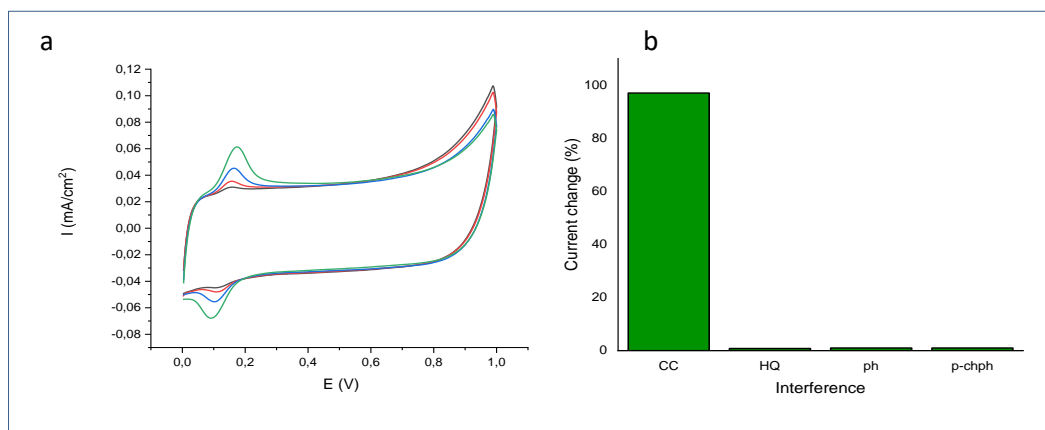


Figure III.35. (a) CV results at a scan rate of 100 mV/s for fMWCNTs/ZnO@fMWCNTs/GCE in 0.1 M PBS solution with hydroquinone (HQ), penta-chlorophenol (p-Ch-ph) and phenol (ph). The CC concentration is varied from 50 to 200 μ M while concentrations of the others are kept at 50 mM. (b) The percentage current change (%) of each interference.

The stability of the fabricated catechol sensor was investigated by performing continuous CV for 50 cycles at 100 μM CC. As shown in **Figure III.36**, the redox current and potential remain unchanged. The deterioration rate of the developed sensor was measured by the percentage degradation using the equation (I_{pn}/I_{p1}) , [16] where I_{pn} and I_{p1} are the n^{th} and 1st cycle anodic peak current, respectively. The stability of *fMWCNTs*/ZnO@*fMWCNTs*/GCE was measured at 94.5% after 50 cycles. These results indicate that the fabricated sensor retained its performance even after 50 cycles, demonstrating its excellent stability due to its antifouling character obtained by the synergic effect of the double layers of *fMWCNTs* and physicochemical stability of ZnO NPs.

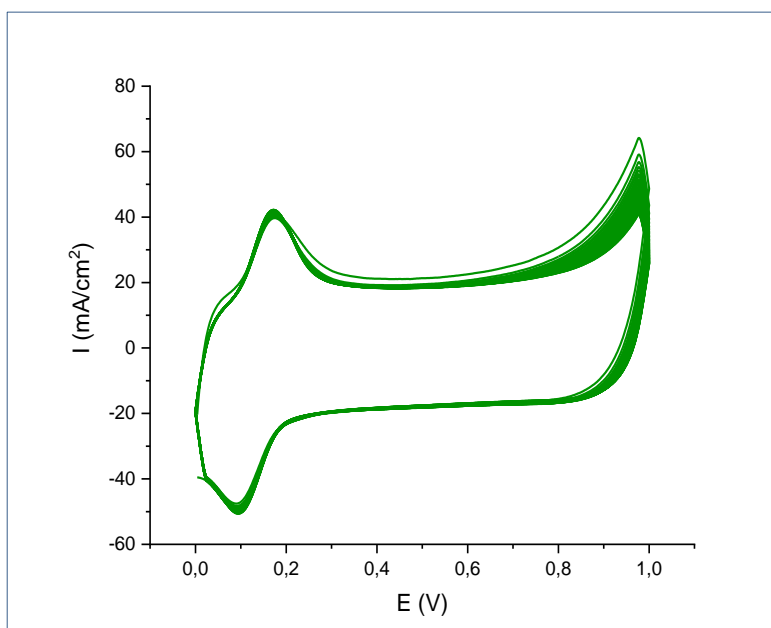


Figure III.36. Stability of 50 CVs gotten for 100 μM CC at *fMWCNTs*/ ZnO@*fMWCNTs*/GCE with sweep rate of 0.1 V/s, respectively.

The reproducibility of the sensor was also investigated using 8 different modified electrodes as can be shown in **Figure III.37 (a)**. The relative standard deviation (RSD) of the studied electrodes was around 3.93%, indicating good reproducibility of the sensor (**Figure III.37 (b)**).

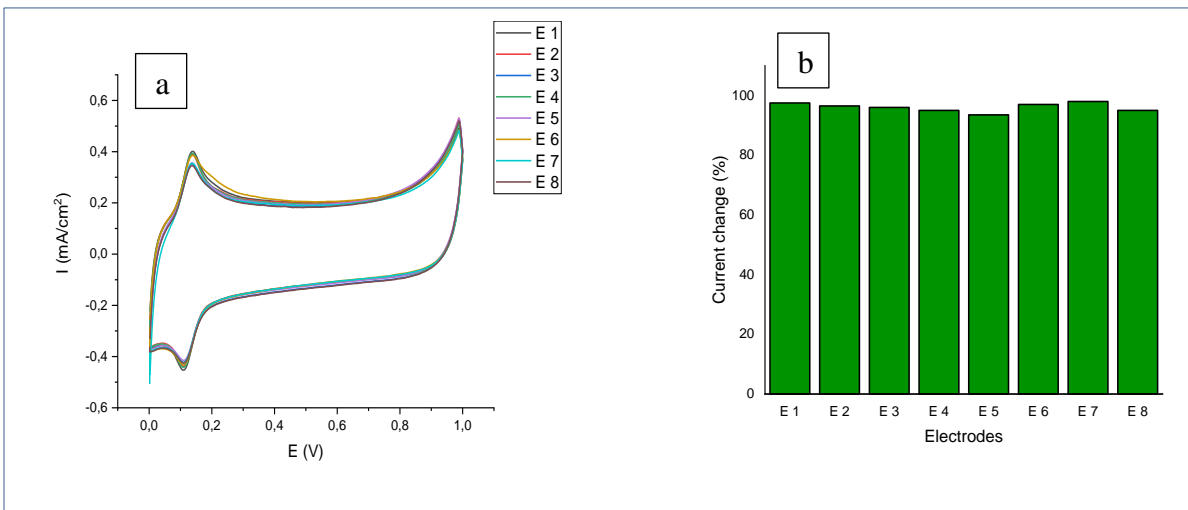


Figure III.37. (a) CVs gotten for 100 μ M CC at 8 different fMWCNTs/ZnO@fMWCNTs/GCE with sweep rate of 0.1 V/s. (b) The percentage current change (%) of each modified GCE.

The repeatability of the developed catechol sensor was investigated by analyzing the response of 10 successive measurements using the same modified GCE in PBS containing 100 mM CC. The results obtained are presented in **Figure 38**. The RSD was 2.15% for CC, thereby exhibiting appreciable repeatability indicating the important role of the fMWCNTs/ZnO@fMWCNTs hybrid's antifouling character to prevent the fabricated sensor from any fouling films while redox reactions of CC.

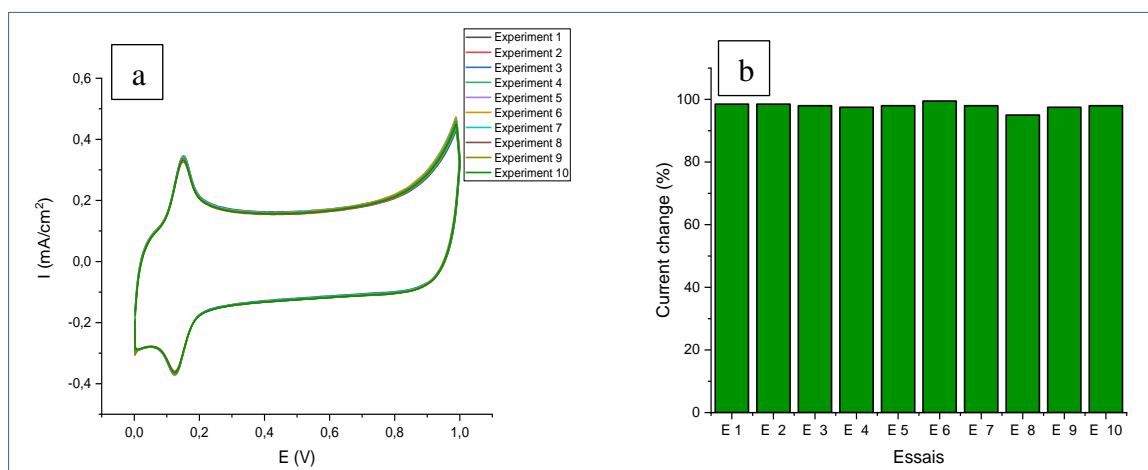


Figure III.38. (a) 10 repeated CVs gotten for 100 μ M CC at fMWCNTs/ZnO@fMWCNTs/GCE with sweep rate of 0.1 V/s. (b) The percentage current change (%) of each experiment.

III.5.1.2. Practicality of fMWCNTs/ZnO@fMWCNTs/GCE

The practicality of the developed sensor was assessed by detecting CC in a local tap water, which was tested without any treatment (**Figure III.39**). The concentrations of CC were

tested with *fMWCNTs/ZnO@fMWCNTs/GCE* using a typical addition process. Good recoveries from 93 to 99% for CC were obtained indicating the significant practicality and reliability of the sensor for practical use **Table III.8**.

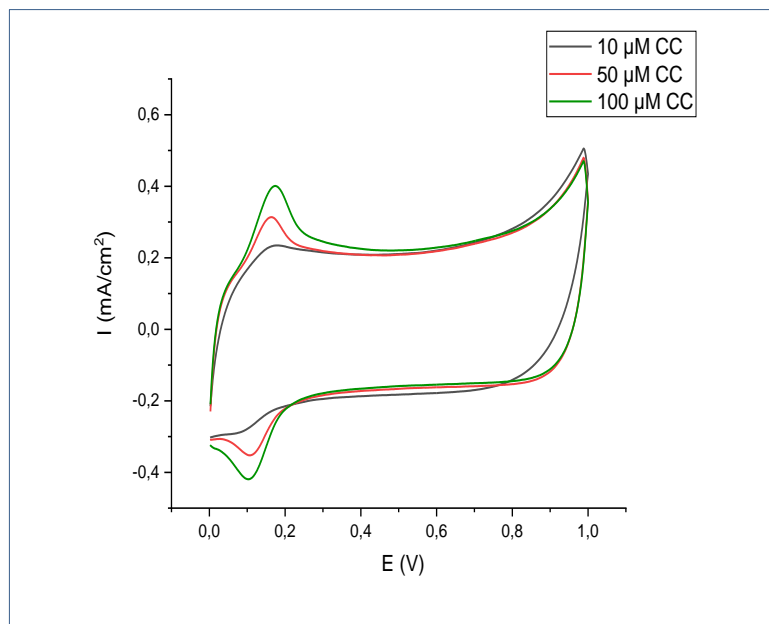


Figure III.1.39. CV curves at a sweep rate of 0.1 V/s for CC for tap water samples with three different CC concentrations (10, 50, and 100 μM).

Table III.8. Recoveries of CC in a local tap water sample at *fMWCNTs/ZnO@fMWCNTs/GCE*.

Sample	Compound	Added (μM)	Founded (μM)	Recovery (%)
Tap Water	Catechol	00	00	-
		10	9.5	95
		50	46.5	93
		100	99	99

III.5.2. Electroanalytical performance of NiO/rGO/*fMWCNTs*/Pt

III.5.2.1. Stability Anti-interference and reproducibility of NiO/rGO/*fMWCNTs*/Pt

A NiO/rGO/*fMWCNTs*/Pt was continuously scanned for 30 times in a 0.1-M PBS (pH = 7) containing 100 μM CC and HQ. It was found that the peak currents of CC and HQ remained the almost same. The current change rate ($I_{30}/I_1 = \text{current change} (\%)$) is 92.3% and 91.6% for CC and HQ, respectively, as shown in **figure III.40**.

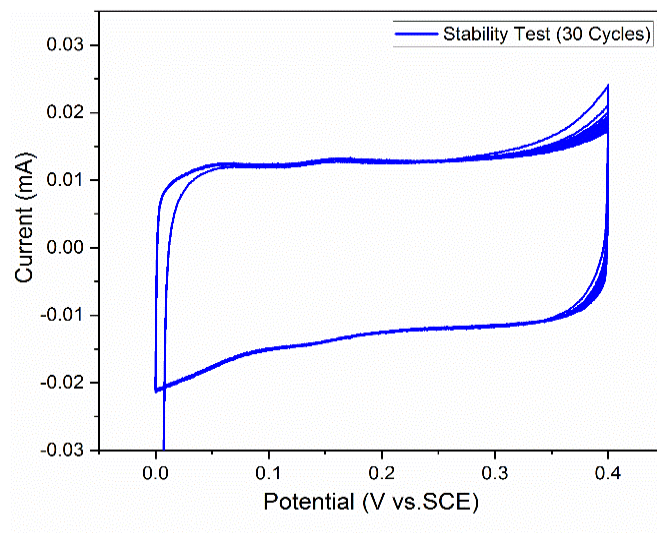


Figure III.40. Stability of 50 cyclic voltammety curves gotten for 100 μM catechol and 10 μM hydroquinone at NiO/rGO/fMWCNTs/Pt with sweep rate of 0.1 V/s.

In the determination of CC and HQ using the proposed sensor, the interference between CC and HQ detections was evaluated quantitatively. Here, the concentration of HQ was fixed at 50 μM and that of CC was varied as 50, 100, 200, 400, and 1000 μM . As shown in **Figure III.41**, the HQ oxidation current remains practically constant in all the different CC concentrations. On the contrary, the CC oxidation current increases as the CC concentration increases. The results suggest that each addition of CC does not affect the detection of HQ. This validates a good anti-interference ability of the fabricated sensor and a good selective detection of CC and HQ.

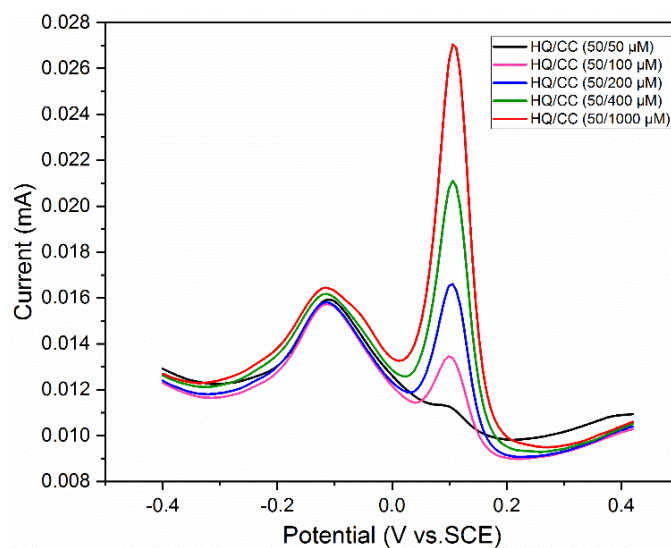


Figure III.41. DPV curves at NiO/rGO/fMWCNTs/Pt with constant HQ concentration and varied CC concentrations in 0.1 M PBS ($\text{pH} = 7.0$).

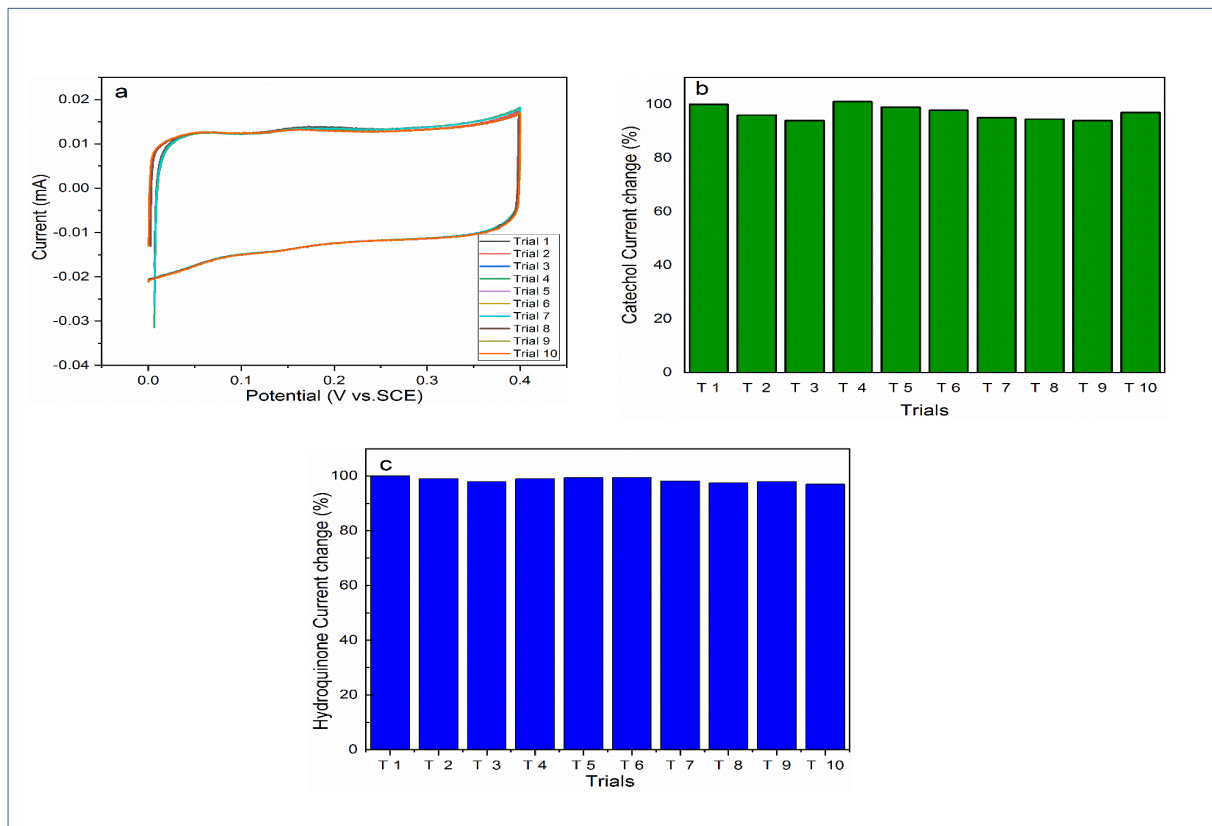


Figure III.42. (a) 10 repeated cyclic voltammety curves gotten for 100 μM catechol at fMWCNTs/ZnO@fMWCNTs/Pt with sweep rate of 0.1 V/s. (b) and (c) the percentage of current change (%) of catechol and hydroquinone, respectively.

10 samples of NiO/rGO/fMWCNTs/Pt were also tested to determine CC and HQ in parallel, as shown in **Figure III.42(a)**. The relative standard deviations (RSDs) of CC and HQ are 3.27% and 1.44%, respectively. These results demonstrate that the proposed sensor has good stability and reproducibility.

III.5.2.2. Practicality of NiO/rGO/fMWCNTs/Pt

To verify its practicality, the fabricated sensor was tested in a tap water containing CC and HQ. **Figure III.43** shows the CV results for the recovery of CC and HQ by NiO/rGO/fMWCNTs/Pt, and **Table III.9** summarizes the results. The measured recovery rates of CC and HQ were 90~106.66 % and 88~98.66 %, respectively. The results confirm that the proposed method has a good reliability and accuracy even in real-life cases.

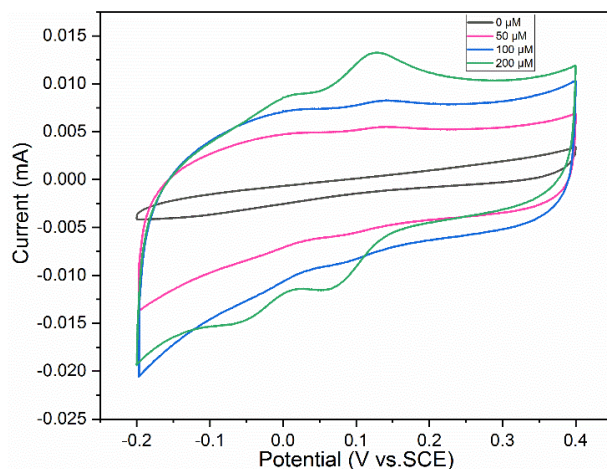


Figure III.43. CV curves at a sweep rate of 0.1 V/s for CC and HQ in tap water samples with three different concentrations of CC and HQ (10, 50, and 100 μM).

Table III.9. Recoveries of CC and HQ in a local tap water sample at NiO/rGO/fMWCNTs/Pt.

<i>Sample</i>	<i>Compound</i>	<i>Added (μM)</i>	<i>Founded (μM)</i>	<i>Recovery (%)</i>
<i>Tap water</i>	CC	00	00	-
		50	45	90
		100	96	96
		150	160	106.66
<i>Tap water</i>	HQ	00	00	-
		50	44	88
		100	90	90
		150	148	98.66

III.5.3. Electroanalytical performance of rGO/MOF/AuE

III.5.3.1. Reproducibility and repeatability of the rGO/MOF/AuE

As shown in figure III.44a, reproducibility of the sensor was also investigated using 5 different modified electrodes. The relative standard deviation (RSD) of the electrodes was 3.858%, indicating good reproducibility of the sensor. In addition, repeatability of the developed 5-CP sensor was investigated by analyzing the response of 5 successive measurements using the same modified AuE in PBS containing 200 μM of 5-CP. The results are presented in figure III.44b. The RSD was 5.1% for 5-CP, thereby exhibiting appreciable repeatability of the produced sensor.

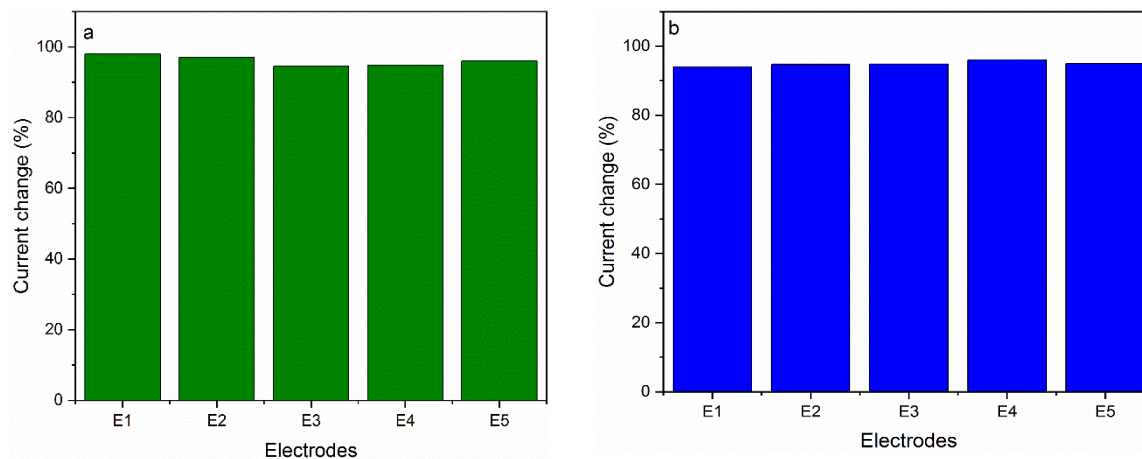


Figure III.44. (a) Reproducibility test for 5 rGO/MOF/AuE in the presence of 200 μM of 5-CP. (b) Repeatability test for 5 rGO/MOF/AuE in the presence of 200 μM of 5-CP.

III.5.4. Electroanalytical performance of Ni-Co-LDH/rGO-CuO/AuE

III.5.4.1. Stability of Ni-Co-LDH/rGO-CuO/AuE

The device's stability is a critical stage in any sensor system and must be correctly calibrated. The electrochemical scanning stability of Ni-Co-LDH/rGO-CuO/AuE was investigated by measuring the current response of the sensing system for 20 cycles in 50 μM of 5-CP using CV, as shown in **figure III.45**. The relative standard deviation (RSD) values were estimated from the current responses of Ni-Co-LDH/rGO-CuO/AuE to be equal 3.6%, indicating that the electrode was stable. Thus, even after 20 cycles of applied voltage, the electrode has no bias stability concerns and continues to function effectively in 5-CP detection.

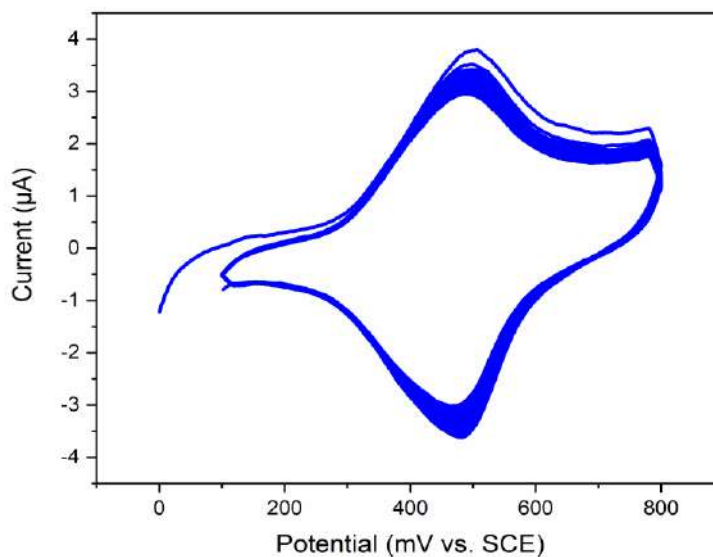


Figure III.45. Stability of 20 CVs gotten for 50 μM 5-CP at Ni-Co-LDH/rGO-CuO/AuE with sweep rate of 0.1 V/s.

III.6. Conclusion

The ultimate goal of this Ph.D. research programme was to develop a simple, cheap, highly sensitive and selective CC, HQ and 5-CP sensors. Several nanomaterials have been synthesized to modify electrodes' active surface to try and accomplish this aim. The primary goal of this chapter is to investigate the electrocatalytic behavior of carbon nanomaterials such as carbon nanotubes (CNTs) and reduced graphene oxide (rGO) in conjunction with metal oxide nanoparticles (NPs) such as copper oxide (CuO), zinc oxide, and nickel oxide (NiO). Metal organic framework (MOF) and Layer double hydroxide (LDH) have been investigated as newly manufactured nanocomposites also. Several physicochemical analysis techniques including FTIR, XRF, XRD, and SEM have been examined to characterize the synthesized nanomaterials.

Simultaneously, this work aims to build innovative electrochemical sensors based on changes of electrode surfaces with these nanomaterials, using various alternatives of these nanomaterials and nanocomposites integration into sensing systems for organic pollution detection. The work related to organic pollution detection such as catechol (CC), hydroquinone (HQ) and penta-chlorophenol (5-CP) detection. In this purpose, four different sensors have been prepared to detect CC, HQ and 5-CP. fMWCNTs/ZnO@fMWCNTs/GCE to detect CC and NiO/rGO/fMWCNTs/Pt to detect HQ and CC simultaneously, while Fe-MOF/rGO/AuE and Ni-Co-LDH/rGO-CuO/AuE have been used to detect 5-CP.

The detailed particular results are

- The first sensor, fMWCNTs/ZnO@fMWCNTs/GCE, provided very interesting analytical parameters including wide linear range ranging from 10 to 200 μM CC and low limit of detection around 0.027 μM CC. The developed catechol sensor exhibited high stability, repeatability, reproducibility, and selectivity against other phenolic compounds. In addition, the proposed sensor can successfully detect CC in real water samples with great recovery performance.
- Through a facile, green, and cost-effective procedure, the NiO/rGO/fMWCNTs/Pt have been fabricated to detect HQ and CC simultaneously. The sensor's performances were validated to be appropriate for application to the determination of phenolic compounds (CC and HQ in this case) in water samples with a wide linear range and a low LOD of 19.86 nM

and 40.18 nM for CC and HQ, respectively. In addition, the sensor was proven to have a high anti-interference ability and a good stability.

- Another electrochemical sensor based on Fe-MOF/rGO for 5-CP measurements was developed. The Fe-MOF/rGO hybrid offered sufficient reactive sites and electrocatalytic activity toward 5-CP as a sensor matrix. For the detection of 5-chlorophenol, the suggested sensor performed well with excellent sensitivity and a low detection limit around 0.075 μM 5-CP. Then, based on this composite, an electrochemical sensing platform with excellent sensitivity and potential applicability was built. On the other hand, the current study reported the usage of artificial neural networks to tackle the sensor's problem of detecting low 5-CP concentrations near the LOD. The difficulty of monitoring and identifying 5-CP in aqueous systems were solved using neural networks. Using the experimental findings of the suggested sensor toward 5-CP, the analysis and control procedure was carried out. The use of ANN software for data processing allows for more accurate detection of low-concentration 5-CP instantaneously, allowing for real-time monitoring of the pollutant from LOD to 200 μM .
- For the first time, we described the green synthesis of the organic-inorganic hybrid rGO-CuO decorated Ni-Co-LDH and its use in the construction of a new sensitive electrochemical sensor for 5-CP detection. The suggested sensor was described and employed for the electrochemical measurement of 5-CP with a limit of detection around 12.64 μM while the linear range has been determined to be from 1 to 50 μM . The sensing system demonstrated ease of setup, acceptable measurement reusability, and high stability towards the 5-CP analyte.

General conclusion and future prospective

Several sensors design that integrate metals, metal oxides nanoparticles and carbon materials such as multi-walled carbon nanotubes and graphene with the electrochemical transducers via several other compounds have been studied. The glassy carbon electrode (GCE) modified with a double layer of *f*MWNTs doped with ZnO NPs, has demonstrated to be an interesting alternative for amperometric sensing of catechol (CC). *f*MWCNTs/ZnO@*f*MWCNTs/GCE sensor has showed a higher detection sensitivity compared to the bare GCE; promotes electronic transference and facilitates the amperometric determination of CC starting at a well determined potential. In addition, the results obtained indicate a good stability of the measurements. The potential shift gained due to the use of a CNTs double layered matrix of MWCNTs brings advantages providing relatively lower working potentials in future (bio)sensor applications.

The simultaneous detection of catechol (CC) and hydroquinone (HQ) has been concluded that the NiO/rGO/*f*MWCNTs/Pt exhibits highly electrocatalytic activity. The modified electrode provides a higher selectivity in voltametric measurements of CC and HQ. The verification of this enhanced response of the MWCNTs in the presence of NiO and rGO may point out the way toward the use of other supramolecules for the chemical manipulation and processing of MWCNTs for sensor applications. As a result, it is essential to achieve a true understanding of the response enhancement as well as of the nature of such interactions linked with the unique properties of MWCNTs in the presence of other carbon nanomaterial and metals NPs. The use of a combination of host-guest electrostatic interactions with an electron enhancer is a novel aspect allowing a more rational design of analytical strategies that could find application in neuroscience. Studies in this direction are currently underway.

The Fe-MOF/rGO hybrid offered sufficient reactive sites and electrocatalytic activity toward 5-CP as a sensor matrix. For the detection of 5-CP, the suggested sensor performed well with excellent sensitivity and a low detection limit. Then, based on this composite, an electrochemical sensing platform with excellent sensitivity and potential applicability was built. As a result of the research, the suggested sensing element may open up new avenues for the design and production of other very sensitive sensing systems for various applications in the future.

On the other hand, the current study reported the usage of artificial neural networks to tackle the sensor's problem of detecting low 5-CP concentrations near the LOD. The difficulty of monitoring and identifying 5-CP in aqueous systems were solved using neural networks. Using the experimental findings of the suggested sensor toward 5-CP, the analysis and control procedure was carried out. The use of ANN software for data processing allows for more accurate detection of low-concentration 5-CP instantaneously, allowing for real-time monitoring of the pollutant from LOD to 200 μM .

The usage of ANN is capable of increasing the sensor sensitivity and evaluating real-world data. The ANN program should be able to identify contaminants in complicated samples with a combination of contaminants. Pollutant concentration evaluation should also be more exact, so more ANN algorithms implementing a polynomial approximation of concentration dependence of sensor responses should be constructed.

Modifications of conventional electrodes with the synthesized nanomaterials have showed in most cases lower over potentials and higher oxidation currents for the detection of CC, HQ and 5-CP comparing to modifications performed with unmodified electrodes. The shown ability of the materials studied in this thesis to promote the electron transfer between these pollutants and the electrode surface suggests an attractive electrocatalytic nanomaterial for development of new electrochemical sensors.

Future Perspectives

The exploitation of carbon materials and metal oxide nanoparticles in the design of electrochemical sensors is still in its beginnings. Future efforts should aim at better understanding the structural- electrochemical reactivity of these nanomaterials-modified electrodes and the factors that govern the electron-transfer kinetics. It was shown that in some cases the electrocatalytic effect of carbon nanomaterials is similar to effect of metal oxide nanoparticles while in other cases there is a huge difference between carbon nanomaterials and metal oxide nanoparticles.

The future applications of the developed nanomaterials including CNTs, graphene and metal oxides NPs based electrochemical sensors require further developments in the following directions:

a) It is highly recommended to improve the electrochemical response (sensitivity, detection limit, stability etc.) toward CC, HQ and 5-CP as well as to other phenolic compounds and work more on the applicability of the sensors in real samples.

b) Development of carbon-based electrochemical sensors. These devices will offer several advantages such as cost efficiency, fast response and simple preparation beside improvements of the reproducibility. Novel alternatives for dispersing CNTs into other polymeric matrixes and solvents to develop novel CNTs-inks with interest for screen-printing technology of CNTs based conducting electrodes will be studied.

c) Focus on the nearest future on the application of the prepared sensors mentioned in the work in a lab-on-a-chip system to evaluate the electrochemical response so as to improve the sensitivity and operational stability using a minimum volume of sample for future applications in medicine and environmental studies.

References

- [1] He, X.; Wang, T.; Pan, Z.; Dayo, A. Q.; Wang, J.; Liu, W. Curing Characteristics, Kinetics, and Thermal Properties of Multifunctional Fluorene Benzoxazines Containing Hydroxyl Groups. *J. Appl. Polym. Sci.* 2021, 138, 50131. DOI: 10.1002/app.50131.
- [2] Scheibe, B.; Borowiak-Palen, E.; Kalenczuk, R. J. Oxidation and Reduction of Multiwalled Carbon Nanotubes — Preparation and Characterization. *Mater. Charact.* 2010, 61, 185–191. DOI: 10.1016/j.matchar.2009.11.008.
- [3] Jiang, Y.; Wang, H.; Li, B.; Zhang, Y.; Xie, C.; Zhang, J.; Chen, G.; Niu, C. Interfacial Engineering of Si/Multi-Walled Carbon Nanotube Nanocomposites towards Enhanced Lithium Storage Performance. *Carbon* 2016, 107, 600–606. DOI: 10.1016/j.carbon.2016.06.068.
- [4] Li, S.; Thomas, A. Emerged Carbon Nanomaterials from MetalOrganic Precursors for Electrochemical Catalysis in Energy Conversion. In *Advanced Nanomaterials for ElectrochemicalBased Energy Conversion and Storage*; Elsevier: USA, 2020; pp 393–423. DOI: 10.1016/B978-0-12-814558-6.00012-5.
- [5] Yao, D.; Feng, J.; Wang, J.; Deng, Y.; Wang, C. Synthesis of Silicon Anode Binders with Ultra-High Content of Catechol Groups and the Effect of Molecular Weight on Battery Performance. *J. Power Sources* 2020, 463, 228188. DOI: 10.1016/j.jpowsour.2020.228188.
- [6] Chen, Q.; Yang, S. Quantifying the Kinetics of Electron Transfer on Commercial Porous Carbon Electrodes. *Meet. Abstr.* 2020, MA2020-02, 2684–2684. DOI: 10.1149/MA2020-02412684mtgabs.
- [7] Wu, F.; Zhao, J.; Han, D.; Zhao, S.; Zhu, R.; Cui, G. A Three Electrode Integrated Electrochemical Platform Based on Nanoporous Gold for the Simultaneous Determination of Hydroquinone and Catechol with High Selectivity. *Analyst* 2021, 146, 232–243. DOI: 10.1039/D0AN01746A.
- [8] Huang, R.; Liao, D.; Chen, S.; Yu, J.; Jiang, X. A Strategy for Effective Electrochemical Detection of Hydroquinone and Catechol: Decoration of Alkalization-Intercalated Ti₃C₂ with MOF-Derived N-Doped Porous Carbon. *Sens. Actuators, B.* 2020, 320, 128386. DOI: 10.1016/j.snb.2020.128386.
- [9] Chetankumar, K.; Swamy, B. E. K.; Sharma, S. C. Poly (Benzoguanamine) Modified Sensor for Catechol in Presence of Hydroquinone: A Voltammetric Study. *Electroanal. Chem.* 2019, 849, 113365. DOI: 10.1016/j.jelechem.2019.113365.
- [10] Chetankumar, K.; Swamy, B. E. K.; Naik, T. S. S. K. A Reliable Electrochemical Sensor for Detection of Catechol and Hydroquinone at MgO/GO Modified Carbon Paste Electrode. *J Mater Sci: Mater Electron* 2020, 31, 19728–19740. DOI: 10.1007/s10854-020-04498-x.
- [11] Jiaojiao, X.; Pengyun, W.; Bin, Z.; Onyinye, A. I. Enhancing Electrochemical Sensing for Catechol by Biomimetic Oxidase Covalently Functionalized Graphene Oxide. *Bioprocess Biosyst. Eng.* 2021, 44, 343–353. DOI: 10.1007/s00449-020-02446-x.
- [12] Huang, D.-L.; Wang, J.; Cheng, F.; Ali, A.; Guo, H.-S.; Ying, X.; Si, L.-P.; Liu, H.-Y. Synergistic Effect of a Cobalt Fluoroporphyrin and Graphene Oxide on the Simultaneous Voltammetric Determination of Catechol and Hydroquinone. *Microchim Acta* 2019, 186, 381. DOI: 10.1007/s00604-019-3417-6.
- [13] Balram, D.; Lian, K.-Y.; Sebastian, N. Ultrasound-Assisted Synthesis of 3D Flower-like Zinc Oxide Decorated FMWCNTs for Sensitive Detection of Toxic Environmental Pollutant 4-Nitrophenol. *Ultrason. Sonochem.* 2020, 60, 104798. DOI: 10.1016/j.ultsonch.2019.104798.
- [14] Shaikshavali, P.; Madhusudana Reddy, T.; Venu Gopal, T.; Venkataprasad, G.; Kotakadi, V. S.; Palakollu, V. N.; Karpoomath, R. A Simple Sonochemical Assisted Synthesis of Nanocomposite (ZnO/MWCNTs) for Electrochemical

Sensing of Epinephrine in Human Serum and Pharmaceutical Formulation. *Colloids Surf, A*. 2020, 584, 124038. DOI: 10.1016/j.colsurfa.2019.124038.

[15] Yola, M. L.; Atar, N. Novel Voltammetric Tumor Necrosis Factor-Alpha (TNF- α) Immunosensor Based on Gold Nanoparticles Involved in Thiol-Functionalized Multi-Walled Carbon Nanotubes and Bimetallic Ni/Cu-MOFs. *Anal. Bioanal. Chem.* 2021, 413, 2481–2492. DOI: 10.1007/s00216-021-03203-z.

[16] Charithra, M. M.; Manjunatha, J. G. Poly (l-Proline) Modified Carbon Paste Electrode as the Voltammetric Sensor for the Detection of Estriol and Its Simultaneous Determination with Folic and Ascorbic Acid. *Mater. Sci. Energy Technol.* 2019, 2, 365–371. DOI: 10.1016/j.mset.2019.05.002.

[17] C. Wang, L. Zhang, H. Yuan, Y. Fu, Z. Zeng, and J. Lu, “Preparation of a PES/PFSA- g -MWCNT ultrafiltration membrane with improved permeation and antifouling properties,” *New J. Chem.*, vol. 45, no. 11, pp. 4950–4962, 2021, doi: 10.1039/D0NJ05322H.

[18] A. Nisar, M. Saeed, M. Muneer, M. Usman, and I. Khan, “Synthesis and characterization of ZnO decorated reduced graphene oxide (ZnO-rGO) and evaluation of its photocatalytic activity toward photodegradation of methylene blue,” *Environ. Sci. Pollut. Res.*, Mar. 2021, doi: 10.1007/s11356-021-13520-6.

[19] X.-Q. Chen, B. Zhang, L. Xie, and F. Wang, “MWCNTs polyurethane sponges with enhanced super-hydrophobicity for selective oil–water separation,” *Surf. Eng.*, vol. 36, no. 6, pp. 651–659, Jun. 2020, doi: 10.1080/02670844.2019.1711303.

[20] N. Dou and J. Qu, “Rapid synthesis of a hybrid of rGO/AuNPs/MWCNTs for sensitive sensing of 4-aminophenol and acetaminophen simultaneously,” *Anal. Bioanal. Chem.*, vol. 413, no. 3, pp. 813–820, Jan. 2021, doi: 10.1007/s00216-020-02856-6.

[21] X. Zhang, Z. Zhang, Q. Liao, S. Liu, Z. Kang, and Y. Zhang, “Nonenzymatic Glucose Sensor Based on In Situ Reduction of Ni/NiO-Graphene Nanocomposite,” *Sensors*, vol. 16, no. 11, p. 1791, Oct. 2016, doi: 10.3390/s16111791.

[22] S. Yang *et al.*, “An Ultrasensitive Electrochemical Sensor Based on Multiwalled Carbon Nanotube@Reduced Graphene Oxide Nanoribbon Composite for Simultaneous Determination of Hydroquinone, Catechol and Resorcinol,” *J. Electrochem. Soc.*, vol. 166, no. 6, pp. B547–B553, 2019, doi: 10.1149/2.0011908jes.

[23] M. Pei, Y. Wu, Z. Qi, and D. Mei, “Synthesis and electrochemical performance of NiO/Fe₃O₄/rGO as anode material for lithium ion battery,” *Ionics*, vol. 26, no. 8, pp. 3831–3840, Aug. 2020, doi: 10.1007/s11581-020-03545-1.

[24] L. Zhao *et al.*, “Nickel oxide/carbon nanotube nanocomposites prepared by atomic layer deposition for electrochemical sensing of hydroquinone and catechol,” *J. Electroanal. Chem.*, vol. 808, pp. 245–251, Jan. 2018, doi: 10.1016/j.jelechem.2017.12.019.

[25] R. Prasad and B. R. Bhat, “Multi-wall carbon nanotube–NiO nanoparticle composite as enzyme-free electrochemical glucose sensor,” *Sens. Actuators B Chem.*, vol. 220, pp. 81–90, Dec. 2015, doi: 10.1016/j.snb.2015.05.065.

[26] H. Yu, R. Li, and K. Song, “Amperometric determination of nitrite by using a nanocomposite prepared from gold nanoparticles, reduced graphene oxide and multi-walled carbon nanotubes,” *Microchim. Acta*, vol. 186, no. 9, p. 624, Sep. 2019, doi: 10.1007/s00604-019-3735-8.

[27] Y. H. Huang *et al.*, “One-pot hydrothermal synthesis carbon nanocages-reduced graphene oxide composites for simultaneous electrochemical detection of catechol and hydroquinone,” *Sens. Actuators B Chem.*, vol. 212, pp. 165–173, Jun. 2015, doi: 10.1016/j.snb.2015.02.013.

[28] A. A. Avan and H. Filik, “Simultaneous electrochemical sensing of dihydroxybenzene isomers at multi-walled carbon nanotubes aerogel/gold nanoparticles modified graphene screen-printed electrode,” *J. Electroanal. Chem.*, vol. 878, p. 114682, Dec. 2020, doi: 10.1016/j.jelechem.2020.114682.

- [29] Z. Li, Y. Liu, Y. Jia, G. Zhou, C. Ye, and L. Zhang, "Electrochemical Discrimination of Dihydroxybenzene Isomer at Different Thiols Self-Assembled Monolayers on Gold and Simultaneous Determination of Catechol and Hydroquinone," *J. Electrochem. Soc.*, vol. 167, no. 13, p. 136511, Oct. 2020, doi: 10.1149/1945-7111/abbcdf.
- [30] H. Zhang, X. Bo, and L. Guo, "Electrochemical preparation of porous graphene and its electrochemical application in the simultaneous determination of hydroquinone, catechol, and resorcinol," *Sens. Actuators B Chem.*, vol. 220, pp. 919–926, Dec. 2015, doi: 10.1016/j.snb.2015.06.035.
- [31] L. A. Goulart, R. Gonçalves, A. A. Correa, E. C. Pereira, and L. H. Mascaro, "Synergic effect of silver nanoparticles and carbon nanotubes on the simultaneous voltammetric determination of hydroquinone, catechol, bisphenol A and phenol," *Microchim. Acta*, vol. 185, no. 1, p. 12, Jan. 2018, doi: 10.1007/s00604-017-2540-5.
- [32] H. Yin *et al.*, "Electrochemical behavior of catechol, resorcinol and hydroquinone at graphene–chitosan composite film modified glassy carbon electrode and their simultaneous determination in water samples," *Electrochimica Acta*, vol. 56, no. 6, pp. 2748–2753, Feb. 2011, doi: 10.1016/j.electacta.2010.12.060.
- [33] L. Chen, Y. Tang, K. Wang, C. Liu, and S. Luo, "Direct electrodeposition of reduced graphene oxide on glassy carbon electrode and its electrochemical application," *Electrochem. Commun.*, vol. 13, no. 2, pp. 133–137, Feb. 2011, doi: 10.1016/j.elecom.2010.11.033.
- [34] F. Hu, S. Chen, C. Wang, R. Yuan, D. Yuan, and C. Wang, "Study on the application of reduced graphene oxide and multiwall carbon nanotubes hybrid materials for simultaneous determination of catechol, hydroquinone, p-cresol and nitrite," *Anal. Chim. Acta*, vol. 724, pp. 40–46, Apr. 2012, doi: 10.1016/j.aca.2012.02.037.
- [35] F.-Y. Kong *et al.*, "Voltammetric simultaneous determination of catechol and hydroquinone using a glassy carbon electrode modified with a ternary hybrid material composed of reduced graphene oxide, magnetite nanoparticles and gold nanoparticles," *Microchim. Acta*, vol. 186, no. 3, p. 177, Mar. 2019, doi: 10.1007/s00604-019-3273-4.
- [36] M. Hicham, A. Fethi, S. Ha, and B. Khaldoun, "Antifouling double layers of functionalized-multi-walled carbon nanotubes coated ZnO for sensitive and selective electrochemical detection of catechol," *Fuller. Nanotub. Carbon Nanostructures*, pp. 1–14, Jun. 2021, doi: 10.1080/1536383X.2021.1940150.
- [37] S. Bhattacharjee, J.-S. Choi, S.-T. Yang, S. B. Choi, J. Kim, and W.-S. Ahn, "Solvothetical Synthesis of Fe-MOF-74 and Its Catalytic Properties in Phenol Hydroxylation," *J. Nanosci. Nanotechnol.*, vol. 10, no. 1, pp. 135–141, Jan. 2010, doi: 10.1166/jnn.2010.1493.
- [38] K. Li, Y. Li, L. Wang, L. Yang and B. Ye, "Study the voltammetric behavior of 10-Hydroxycamptothecin and its sensitive determination at electrochemically reduced graphene oxide modified glassy carbon electrode," *Ara. Jour Chem*, vol. 12, no. 1, pp. 2732–2739, Jun. 2015, doi: 10.1016/j.arabjc.2015.05.014
- [39] M. Wang *et al.*, "Bimetallic metal–organic framework derived FeO /TiO₂ embedded in mesoporous carbon nanocomposite for the sensitive electrochemical detection of 4-nitrophenol," *Sens. Actuators B Chem.*, vol. 281, pp. 1063–1072, Feb. 2019, doi: 10.1016/j.snb.2018.11.083.
- [40] A. Shahat, H. M. A. Hassan, and H. M. E. Azzazy, "Optical metal-organic framework sensor for selective discrimination of some toxic metal ions in water," *Anal. Chim. Acta*, vol. 793, pp. 90–98, Sep. 2013, doi: 10.1016/j.aca.2013.07.012.
- [41] Y. Pan, J. Wang, X. Guo, X. Liu, X. Tang, and H. Zhang, "A new three-dimensional zinc-based metal-organic framework as a fluorescent sensor for detection of cadmium ion and nitrobenzene," *J. Colloid Interface Sci.*, vol. 513, pp. 418–426, Mar. 2018, doi: 10.1016/j.jcis.2017.11.034.
- [42] R. Jamatia, A. Gupta, B. Dam, M. Saha, and A. K. Pal, "Graphite oxide: a metal free highly efficient carbocatalyst for the synthesis of 1,5-benzodiazepines under room temperature and solvent free heating conditions," *Green Chem.*, vol. 19, no. 6, pp. 1576–1585, 2017, doi: 10.1039/C6GC03110B.
- [43] A. Gupta, R. Jamatia, R. A. Patil, Y.-R. Ma, and A. K. Pal, "Copper Oxide/Reduced Graphene Oxide Nanocomposite-Catalyzed Synthesis of Flavanones and Flavanones with Triazole Hybrid Molecules in One Pot: A

Green and Sustainable Approach,” *ACS Omega*, vol. 3, no. 7, pp. 7288–7299, Jul. 2018, doi: 10.1021/acsomega.8b00334.

[44] A. Maria Jastrzębska, A. Roman Olszyna, J. Jureczko, and A. Kunicki, “New Reduced Graphene Oxide/Alumina (RGO/Al₂O₃) Nanocomposite: Innovative Method of Synthesis and Characterization,” *Int. J. Appl. Ceram. Technol.*, vol. 12, no. 3, pp. 522–528, May 2015, doi: 10.1111/ijac.12183.

[45] Y. Zhao, X. Song, Q. Song, and Z. Yin, “A facile route to the synthesis copper oxide/reduced graphene oxide nanocomposites and electrochemical detection of catechol organic pollutant,” *CrystEngComm*, vol. 14, no. 20, p. 6710, 2012, doi: 10.1039/c2ce25509j.

[46] R. Benhiti *et al.*, “Kinetic, isotherm, thermodynamic and mechanism investigations of dihydrogen phosphate removal by MgAl-LDH,” *Nanotechnol. Environ. Eng.*, vol. 6, no. 1, p. 16, May 2021, doi: 10.1007/s41204-021-00110-7.

[47] C. Novillo, D. Guaya, A. Allen-Perkins Avendaño, C. Armijos, J. L. Cortina, and I. Cota, “Evaluation of phosphate removal capacity of Mg/Al layered double hydroxides from aqueous solutions,” *Fuel*, vol. 138, pp. 72–79, Dec. 2014, doi: 10.1016/j.fuel.2014.07.010.

[48] R. Li *et al.*, “Large Scale Synthesis of Ni-Co Layered Double Hydroxides for Superior Asymmetric Electrochemical Capacitor,” *Sci. Rep.*, vol. 6, no. 1, p. 18737, May 2016, doi: 10.1038/srep18737.